Optimization of radio resource allocation in uplink green LTE networks

Fatima Zohra Kaddour

ParisTech
INSTITUT DES SCIENCES ET TECHNOLOGIES
PARIS INSTITUTE OF TECHNOLOGY

TELECOM ParisTech

2014-ENST-0012

EDITE - ED 130

Doctorat ParisTech

T H È S E

pour obtenir le grade de docteur délivré par

TELECOM ParisTech

Spécialité Informatique et Réseaux

présentée et soutenue publiquement par

Fatima Zohra KADDOUR

le 4 mars 2014

Optimisation de l'allocation des ressources radio sur le lien montant d'un réseau OFDMA sous contraintes de consommation d'énergie

Directeur de thèse: **Prof. Philippe MARTINS**
Co-encadrement de la thèse: **Dr. Emmanuelle VIVIER**

Jury

Prof. Luc VANDENDORPE, Professeur, UCL, Belgique	Rapporteur
Prof. Xavier LAGRANGE, Professeur, TELECOM Bretagne, France	Rapporteur
Prof. Michel TERRE, Professeur, CNAM, France	Examinateur
Dr. Jérôme BROUEH, Ingénieur, Alcatel-lucent, France	Examinateur
Dr. Lina MROUEH, Enseignant Chercheur, ISEP, FRANCE	Invité
Dr. Mylene PISCHELLA, Enseignant Chercheur, CNAM, France	Invité

TELECOM ParisTech
Ecole de l'Institut Mines-Télécom - membre de ParisTech
46 rue Barrault 75013 Paris - (+33) 1 45 81 77 77 - www.telecom-paristech.fr

T H È S E

To the memory of my dad

Acknowledgment

My deep gratitude goes first to my advisers Dr. Emmanuelle VIVIER at ISEP (Institut Supérieur d'Electronique de Paris), and Prof. Philippe MARTINS at Telecom ParisTech. This work would not have been completed without their unlimited encouragement, continuous support, and all their suggestions during the development of my thesis.

I would like to thank very much the thesis reviewers Prof. Luc VANDENDORPE at ULC (Université Catholique du Louvain) and Prof. Xavier LAGRANGE at Telecom Bretagne for their time devoted to carefully reading the manuscript. The same gratitude goes to the examiners Dr. Jérôme BROUEH at Alcatel-Lucent and Prof. Michel TERRE at CNAM (Conservatoir National des Arts et Métiers) who gave me the honor for presiding over the jury. Their advice and detailed comments were very helpful to significantly improving the quality of the final report.

My deepest gratitude goes also to Dr. Lina MROUEH at ISEP and Mylene PISCHELLA at CNAM for their availability, recommandations, continuous support and valuable advice. It was a great fortune for me to collaborate with them and I really enjoyed it.

I am really grateful to ISEP for financing my research and providing me the opportunity to do teaching assistance of signal processing and telecommunications lectures in the school. This experience could not happen without the help of ISEP teachers and the SITe team members.

Great thanks to all my friends and my colleagues in SITe team. I would like to thank particularly Itebeddine, Ujjwal, Mario, Louis, Marthe and Yacine for their friendship and their invaluable support.

I am deeply grateful to my family, specially my mother and brother for their unlimited support that help me to move forward in life, and giving me the opportunity to come to Paris to complete my Master degree at Telecom ParisTech.

Finally, I dedicate my thesis to my beloved father, who unfortunately passed away few moths after my arrival to France. He was a such devoted father, always dreaming for a better future for us and working hard for that. Without his encouragements and his wise vision, I would have never gone that far in life.

Abstract

ACTUALLY, 3^{rd} Generation Partnership Project (3GPP) Long Term Evolution (LTE) networks present a major advance in cellular technology. They offer significant improvements in terms of spectrum efficiency, delay and bandwidth scalability, thanks to the simple architecture design and the use of the Orthogonal Frequency Division Multiplexing (OFDM) based access techniques in the physical layer. In LTE architecture, the evolved Node B (eNB) is considered as the single node between the User Equipment (UE) and the Evolved Packet Core (EPC). Consequently, the eNB is responsible of the mobility and the Radio Resource Management (RRM).

This thesis studies the uplink RRM in green LTE networks, using the Single Carrier Frequency Division Multiple Access (SC-FDMA) technique. The objective is the throughput maximization in a distributed radio resource allocation architecture. Hence, a channel dependent RRM is studied. First, to evaluate the channel condition metrics, a new Inter-Cell Interference (ICI) estimation model is proposed, when a power control process is applied to the UEs transmission power. The ICI estimation model validation and robustness against environment variations are established analytically and with simulations.

Then, the LTE networks dimensioning is investigated. The adequate 3GPP standardized bandwidth that can be allocated to each cell in order to satisfy the UEs Quality of Service (QoS) is evaluated in random networks, by considering the statistical behavior of the networks configuration, and depending on the used RRM policy: fair or opportunistic Resource Block (RB) allocations, for Single Input Single Output (SISO) and Multiple Input and Multiple Output (MIMO) systems. In addition, the MIMO diversity and multiplexing gains are discussed.

As a standardized bandwidth is allocated to a cell, the RRM of the limited number of available RBs is investigated. Therefore, a new radio resource allocation algorithm, respecting the SC-FDMA constraints, is proposed in SISO systems. It efficiently allocates the RBs and the UE transmission power to the users. The proposed RB allocation algorithm is adapted to the QoS differentiation. The proposed channel dependent power control considers a minimum guaranteed bit rate that the UE should reach. The performances of the proposed RRM are compared with the performances of other well known schedulers, respecting the SC-FDMA constraints, found in the literature. Finally, the proposed RB allocation algorithms are also extended to the Multi-User MIMO (MU-MIMO) systems where a new transceiver is proposed. It combines the Zero Forcing (ZF) and the Maximum Likelihood (ML) decoders at the receiver side.

Contents

List of Figures

List of Tables

Notation

Sets and numbers

$\mathbb{C}$	Set of complex numbers
$\mathbb{R}$	Set of reals.
$\lvert\mathcal{A}\rvert$	Cardinality of a set $\mathcal{A}$
$\lceil x \rceil$	Closest integer $\lceil x \rceil \geq x$
x^*	Conjugate of a complex number
$\lvert z \rvert$	Absolute value of a complex number $z \in \mathbb{C}$.

Probability and statistics

X	Random variable
$p_X(x)$	Probability distribution function (pdf) of X
$F_X(x)$	Cumulative distribution function (cdf) $F_X(x) = \text{Prob}\{X \leq x\}$
$\mathcal{CN}(0, \sigma^2)$	Complex Gaussian random variable with zero mean and variance σ^2
$\mathbb{E}[x]$	Expectation of x

Matrices and vectors

$\mathbf{A}$	Matrix
$\mathbf{v}$	Vector
$\mathbf{I}_N$	Identity matrix with $N \times N$ size
$\det(\mathbf{A})$	Determinant of square matrix $\mathbf{A}$
$\text{Tr}(\mathbf{A})$	Trace of a square matrix $\mathbf{A}$
$\lVert\mathbf{v}\rVert$	Euclidian norm of vector $\mathbf{v}$
$\mathbf{A}^\dagger$	Transpose-conjugate of matrix $\mathbf{A}$
$\mathbf{V}^{[T]}$	Transpose of vector $\mathbf{v}$
$\text{diag}(\mathbf{a})$	Diagonal matrix whose diagonal entries are the elements of vector a_i
ker	Kernel of a matrix

Thesis specific notations

$\mathcal{A}$	Set of semi-orthogonal users
$\mathcal{A}_k$	Set of allocated RBs of UE k
$\mathcal{C}$	Set of available RBs
$\mathcal{K}$	Set of users
$\mathcal{M}_x$	Matrix of metrics
$\mathcal{S}$	Set of simultaneously active UEs in MU-MIMO systems
A_s	Shadowing coefficient
A_f	Fast fading coefficient
C_k	Theoretical Shannon capacity of user k
$C_{.I.O}^{(m,n)}$	Theoretical Shannon capacity of the .I.O system (SISO, MIMO, SIMO, MISO) in the resource element (m, n)
f_c	Frequency carrier
G_M	Mobile antenna gain
G_A	eNB antenna gain
$I_{l,s}$	Inter-cell interference generated by the interfering sector l and received at the concerned sector s
K	Path loss constant
K_f	Frequency reuse factor
N	Thermal noise in the considered bandwidth
N_{RB}	Number of RBs
N_s	Number of simultaneously transmitting UEs in a MU-MIMO systems
N_{UE}	Number of users in the concerned sector
$P_{eNB_{max}}$	eNB maximum transmission power
$P_{e,k}$	Transmission power of UE k on one RB considering the standardized MCS, after power control
P_{mean}	Mean power
P_{med}	Median power
$P_{k_{Tx}}$	Transmission power of UE k on one RB
$P_{k_{Tx}}^{c}$	Transmission power of UE k on RB c, after power control
$P_{k_{Tx}}^{m}$	Transmission power of UE k on subcarrier m
$P_{k,eNB}^{(m,n)}$	Received power at the eNB level
P_L	Path loss
P_{max}	UE maximum transmission power
$P_{RB_{Alg}}$	Average transmission power per RB in function of the used algorithm
R_r	Total individual throughput of UE k

r_k	Instantaneous rate of user k in one RB
S_{RB}	Solution of the RB allocation problem
β	Path loss exponent
δ_k^c	Number of bits per resource element
Δ_γ	Signal to interference plus noise ratio margin
γ	Signal to Interference plus Noise Ratio
$\gamma_{(k,c)}^{\text{eff}}$	Effective signal to interference plus noise ratio of UE k in the resource block c
$\frac{1}{\nu}$	Mean service time
ρ	Surface density
$(.)^{(m,n)}$	Specific value of a resource element (m, n)

Abreviations and acronyms

3GPP	Third Generation Partnership Project
4G	Fourth Generation
CA	Carrier Aggregation
CCU	Cell Center Users
CDF	Cumulative Distribution Function
CDMA	Code Division Multiple Access
CEU	Cell Edge Users
CQI	Channel Quality Identifier
CP	Cyclic Prefix
CSI	Channel State Information
DAST	Diagonal Algebraic Space Time Block
eNB	evolved NodeBs
EPC	Evolved Packet Core
EPS	Evolved Packet System
E-UTRAN	Evolved-Universal terrestrial Radio Access Network
FDD	Frequency Division Duplexing
FDPS	Frequency Domain Packet Scheduling
FFR	Fractional Frequency Reuse
FFT	Fast Fourier Transform
GBR	Guaranteed Bit Rate
HSPA	High Speed Packet Access
ICI	Inter-Cell Interference
ICT	Information Communities and Telecommunications
IFFT	Inverse Fast Fourier Transform
IP	Internet protocol
ISI	Inter-Symbol Interference
I-SC-FDMA	Interleaved Single carrier Frequency Division Multiple Access

LTE	Long Term Evolution
L-SC-FDMA	Localized Single Carrier Frequency Division Multiple Access
MAI	Multiple Access Interference
MCS	Modulation and Coding Scheme
ML	Maximum Likelihood
MIMO	Multiple Input Multiple Output
MMSE	Minimum Mean Square Error
MSC	Mobile Switching Controller
MU-MIMO	Multi-user MIMO
OFDM	Orthogonal Frequency Division Multiplexe
OFDMA	Orthogonal Frequency Division Multiple Access
PAPR	Peak to Average Power Ratio
PC	Power Control
PCC	Policy and Charging Control
PCN	Packet Core Network
PDN	Packet Data network
PDP	Power Delay Profile
PS	Packet Scheduler
QCI	Quality of Service Class Identifier
QoS	Quality of Service
RAC	Radio Admission Controller
RAN	Radio Access Network
RE	Resource Element
RNC	Radio Access Controller
RRM	Radio Resource Management
SC-FDMA	Single Carrier Frequency Division Multiple Access
SDMA	Space Division Multiple Access
SFR	Soft Frequency Reuse
SISO	Single Input Single Output
SVD	Singular Value Decomposition
TDPS	Time Domain Packet Scheduling
TTI	Transmission Time Interval
UE	User Equipement
UMTS	Universal Mobile Telecommunication System
ZF	Zero Forcing

Résumé Détaillé de la Thèse

DE nos jours, avec la popularité des terminaux mobiles intelligents (smartphones), offrant des fonctionnalités et applications gourmandes en débit, la communauté des technologies de l'information et de la communication est face à de grands défis pour répondre à une hausse continue du débit à offrir aux possesseur de ces terminaux. Le réseau 3GPP (Third Generation Partnership Project) LTE (Long Term Evolution) représente une grande avancée dans les réseaux cellulaires. Grâce à son interface radio basée sur l'OFDM (Orthogonal Frequency Division Multiplex) qui transmet les signaux numériques sur des fréquences orthogonales et son architecture simplifiée, le réseau 3GPP LTE permet en particulier d'atteindre des débits élevés et un temps de latence relativement réduit (10 ms).

La technologie LTE utilise des techniques d'accès multiples basées sur l'OFDM : l'OFDMA (Orthogonal Frequency Division Multiple Access) sur le lien descendant et le SC-FDMA (Single Carrier-Frequency Division Multiple Access) sur le lien montant. Ces techniques permettent une allocation de bande de fréquences flexible, allant de 1.4 MHz à 20 MHz, et une efficacité spectrale trois fois plus élevée que celle obtenue par le réseau HSPA (High Speed Packet Access). Lorsque une bande passante de 20 MHz est allouée à une cellule, on obtient un débit agrégé de 75 Mbps sur le lien descendant (réseau vers abonné) et 50 Mbps sur le lien montant dans le cas d'un système SISO (Single Input Single Output), et 350 Mbps sur le lien descendant dans le cas d'un système 4x4 MIMO (Multiple Input Multiple Output).

Dans cette thèse, nous étudions l'optimisation de l'allocation des ressources radio sur le lien montant d'un réseau LTE, utilisant la technique d'accès SC-FDMA, sous des contraintes de consommation d'énergie. Nos études se concentrent sur l'allocation des ressources radio, incluant l'allocation des blocs de ressources (Resource Block (RB))[1] sur lesquels le mobile transmet ses données ainsi que l'allocation de la puissance de transmission de ce dernier. Notre objectif étant de maximiser le débit agrégé dans la cellule, nous optons pour une politique d'allocation opportuniste se basant sur les conditions radio de chaque utilisateur dans la cellule.

Nous nous intéressons dans un premier temps à l'estimation des conditions radio de l'utilisateur,

[1] la plus petite granularité défini dans le standard qu'on peut alloué à un utilisateur

et plus précisément à l'estimation du niveau d'interférence inter-cellulaires (IIC) reçu au niveau de la station de base (Base Station (BS)), causé par l'utilisation d'un même RB dans les cellules voisines. Les détails relatifs au nouveau modèle d'estimation du niveau d'interférence proposé dans cette thèse sont présentés dans le Chapitre 3. En LTE, la station de base est l'entité responsable de l'allocation des ressources radio aux utilisateurs. Une étude de planification est établie au préalable pour définir la bande de fréquences allouée à chaque cellule. Afin de minimiser la probabilité de dépassement de dimensionnement, une bande de fréquences adéquate doit être définie en fonction de la charge du réseau, de la Qualité de Service (QdS) offerte aux utilisateurs ainsi que de la politique d'allocation utilisée. Un modèle analytique, permettant d'évaluer la borne supérieure de la probabilité de dépassement de dimensionnement, est proposé dans le Chapitre 4. Ce modèle a été developpé lorsqu'une ou plusieurs QdS sont offertes aux utilisateurs en considérant deux politiques d'allocation des blocs de ressources, une opportuniste et une autre équitable. Le nombre de RBs dans une bande de fréquences étant limité, la station de base doit allouer ses ressources judicieusement. Nous proposons donc dans le Chapitre 5 un algorithme opportuniste et efficace, qui maximise le débit total de la cellule, tout en minimisant la puissance de transmission des mobiles, sans affecter la QdS des utilisateurs. Dans le Chapitre 6, l'étude des performances de l'algorithme d'allocation de ressources radio proposé a été étendue au cas d'un système multi-utilisateurs (Multi-User MIMO) où un nouveau décodeur a été proposé.

Chapitre 3 - Estimation du niveau d'interférences intercellulaires

Le niveau d'interférence inter-cellulaires, subi par un utilisateur sur sa liaison montante et reçu au niveau de la station de base, est causé par l'utilisation du même bloc de ressource par d'autres utilisateurs dans les cellules voisines. Puisque l'emplacement de l'utilisateur interférent n'est pas fixe, l'estimation du niveau d'interférence inter-cellulaires sur le lien montant est plus complexe que sur le lien descendant. Il est égale à la puissance reçue au niveau de la station de base centrale, de la part des utilisateurs interférents. Ainsi, le contrôle de puissance, en réduisant la puissance d'émission des mobiles et donc des interférents, réduit le niveau de l'interférence inter-cellulaire.

Le contrôle de puissance adopté dans cette thèse est basé sur la QdS désirée, traduit par le niveau du rapport signal à bruit plus interférence (Signal to Interference plus Noise Ratio (SINR)) et les conditions radio.
Nous pourrons décrire la puissance d'émission $P^c_{k_{Tx}}$ d'un mobile k émettant des données sur le RB c, désirant une QdS correspondant à un niveau de SINR γ_{tg}, comme suit:

$$P^c_{k_{Tx}} = \min\left\{\frac{\gamma_{\text{tg}}.(N + I^c_{eNB})}{\Lambda^c_k \|h\|^2}, P_{max}\right\} \tag{1}$$

Où:

- P_{max} est la puissance de transmission maximale du mobile,
- h est le coefficient de l'évanouissement rapide (fading de Rayleigh),
- N est le niveau de bruit thermique reçu,

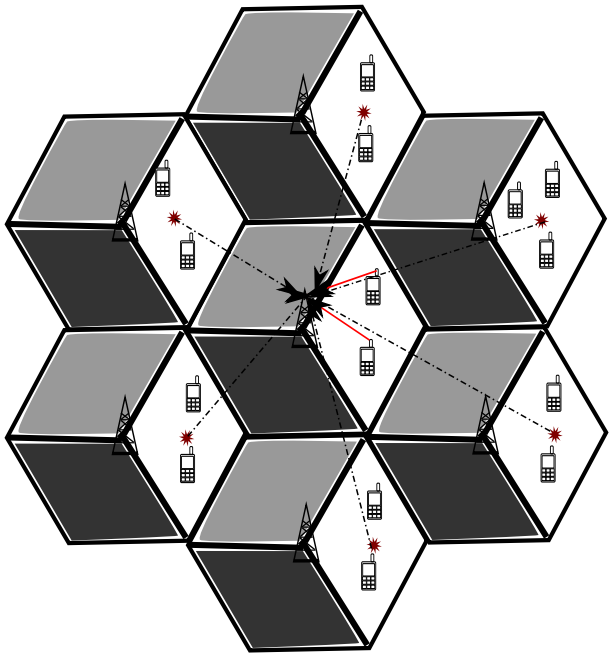

Figure 1: Modèle d'estimation des interférences inter-cellulaires

- I^c_{eNB} est le niveau des interférences reçues au niveau de la station de base sur le ressource bloc c,
- Λ^c_k traduit les conditions radio de l'utilisateur k sur le bloc de ressource c définie par :

$$\Lambda^c_k = P_L(r)G_A(\theta)G_M A_s \tag{2}$$

avec :

- G_M : gain d'émission du mobile équivalent à 1.
- $G_A(\theta)$: gain de réception de l'antenne (BS) en fonction de θ, l'angle entre le mobile k et l'axe principal du rayonnement de l'antenne de la station de base centrale (equation 2.3).
- $P_L(r)$: gain canal en fonction de r, la distance séparant le mobile k et la station de base centrale, obtenu par le modèle d'Okumura Hata [5],
- A_s : coefficient du shadowing généré par une loi log-normal.

La méthode d'estimation du niveau des interférences inter-cellulaires présentée dans cette thèse est applicable sur le lien montant. Nous considérons que le niveau d'interférence $I^c_{s,eNB}$ causé par un secteur voisin s, utilisant la même bande de fréquences, est équivalent à la puissance reçue de la part d'un point virtuel v situé au barycentre géographique des N_{UE} utilisateurs actifs dans le secteur s, et émettant à une puissance médiane P_m (comme illustré sur la Figure 1).
Ainsi, le niveau des interférences inter-cellulaires total I^c_{eNB} est estimé par :

$$I^c_{eNB} = \sum_{s=2}^{19} I^c_{s,eNB} \tag{3}$$

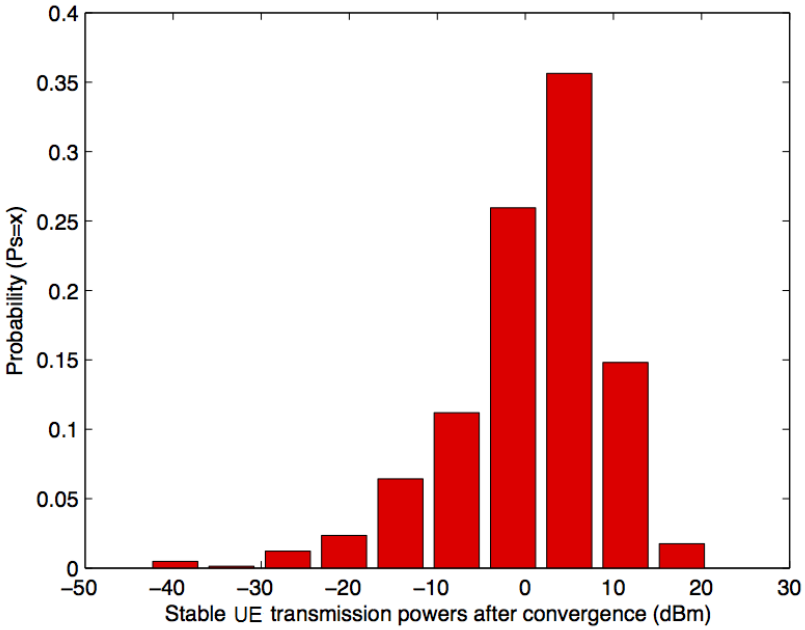

Figure 2: Histogramme des puissances de transmission des mobiles après contrôle de puissance

Où :

$$I^{c}_{s,eNB} = P_m.\Lambda^{c}_{v}\|h\|^2 \tag{4}$$

Nous avons choisi la puissance médiane P_m plutôt que la puissance moyenne car en statistique, celle-ci est plus fiable pour représenter la tendance centrale d'une distribution asymétrique [6] [7] [8]. La Figure 2, représentant l'histogramme des puissances de transmission des mobiles avec un tirage aléatoire des interférents dans les secteurs voisins, confirme l'asymétrie de la distribution des puissances de transmission.

Pour valider la méthode proposée, nous comparons ses performances avec celles générées par des tirages de Monte Carlo. Pour ce faire, nous comparons la distribution des puissances de transmission des mobiles après contrôle de puissance en estimant le niveau des interférences inter-cellulaires avec la méthode proposée, avec la distribution des puissances de transmission après contrôle de puissance lorsqu'on tire aléatoirement un interférent dans chaque secteur voisin. Afin de comparer les deux distributions, nous utilisons deux tests probabilistes :

1. **Le test Log Ratio** : défini par le logarithme du rapport entre deux distributions. Dans notre cas le rapport entre la densité de probabilité des puissances de transmission après contrôle de puissance en estimant le niveau des interférences inter-cellulaires par le modèle proposé et la densité de probabilité des puissances de transmission après contrôle de puissance en calculant le niveau des interférences inter-cellulaires avec la méthode de Monte Carlo. On note ce rapport

$\Delta(x)$ et on le calcule par la formule suivante :

$$\Delta(x) = \log \frac{Prob(d_M \leq x)}{Prob(d_{MC} \leq x)} \tag{5}$$

Nous considérons que le modèle d'estimation d'IIC est valide si le logarithme du rapport des deux distributions $\Delta(x)$ est inférieur à 1 ou idéalement tant vers 0.

2. **Le test de divergence de Kullback-Leibler** : plus utilisé dans le domaine de la théorie de l'information, il est considéré comme un test Log Ratio pondéré. Ce test est une mesure non-symétrique de la différence entre deux distributions. On le note $KL(x)$ et définit comme suit :

$$KL(x) = Prob(d_M \leq x).\Delta(x) \tag{6}$$

Pour ces deux tests, d_M et d_{MC} représentent les puissances de transmission stables des mobiles (puissance de transmission après convergence du contrôle de puissance) obtenues en estimant le niveau des interférences inter-cellulaires par le modèle proposé "Modèle d'estimation des IIC" (Algorithme 1) et par la méthode de "Monte Carlo" (Algorithme 2) respectivement.

Pour des raisons d'équité, nous considérons dans nos simulations que tous les utilisateurs cherchent à atteindre le même débit (le même γ_{tg}), et nous n'allouons qu'un seul bloc de ressource à chaque utilisateur.

Algorithm 1 Modèle d'estimation des IIC

Init : $I_c = 0$
Placer aléatoirement N_{UE} utilisateurs actifs,
Déterminer leur barycentre,
for $It = 1$ to S **do**
  for $k = 1$ to M_S **do**
    $P^c_{k_{Tx}}(It) = \min\left[\frac{\gamma_{\text{tg}}*(N+I^c_{eNB})}{\Lambda^c_k|h|^2}, P_{max}\right]$
  end for
  $P_m = \textbf{median}[P^c_{k_{Tx}}]$
  $I^c_{eNB} = \sum_{k=2}^{19} P_m \Lambda^c_k |h|^2$: IIC générée par les 18 secteurs interférents
end for
for $k = 1$ to M_S **do**
  $P_{S_k} = P^c_{k_{Tx}}(S)$: puissance de transmission stable de l'utilisateur k
end for
$V_S(i) = [P_{S_1} P_{S_2} ... P_{S_{M_S}}]$: sauvegarde des puissances d'émission après contrôle de puissance.

L'algorithme 1 résume les étapes proposées pour l'estimation du niveau des interferences inter-cellulaires, avec S le nombre d'itérations nécessaires pour la convergence de la puissance d'émission.

La Figure 3 représente la densité de probabilité des puissances de transmission stables des mobiles dans la cellule centrale en estimant le niveau des interférences par le modèle proposé et la densité de probabilité des puissances de transmission stables des mobiles dans la cellule centrale en calculant

Algorithm 2 Simulation de Monte Carlo

Init : $P^c_{k_{Tx}} = P_{max}$ $k = 1, ..., N_{UE}$
for $i = 1$ to M **do**
  Tirer aléatoirement N_{UE} utilisateurs actifs
  Pour chaque utilisateur actif
  for $m = 1$ to MT **do**
    Tirer aléatoirement un utilisateur interférent k_s dans chaque secteur voisin s avec une puissance de transmission $P^c_{k_{Tx},s}$
    for $It = 1$ to S **do**
      for $s = 2$ to 19 **do**
        $I^c_{eNB} = \sum_{s=2}^{19} P^c_{k_{Tx}} \Lambda^c_k |h|^2$.
      end for
      $P^c_{k_{Tx}}(It) = min[\frac{\gamma_{\text{tg}} * (N + I^c_{eNB})}{\Lambda^c_k |h|^2}, P_{max}]$, mise à jour de $P^c_{k_{Tx}}$ pour $k = 1, ..., N_{UE}$.
    end for
    $P_{S_k} = P^c_{k_{Tx}}(S)$, Puissance de transmission stable
    $V_S(m) = [P_{S_1}, P_{S_2}, ..., P_{S_{MT}}]$
  end for
  Sauvegarder $V_S(m)$ dans la matrice Mat P(i) $M \times N_{UE}$
end for
Sauvegarder Mat P (i) dans la table de résultats (Taille finale : $(MT * M) \times N_{UE}$).

le niveau des interférences par la méthode de Monte Carlo. Nous remarquons la similitude des deux courbes obtenues par les deux approches. La puissance de transmission stable des mobiles varie entre -48 dBm et 21 dBm. Cette plage de variation respecte l'intervalle exigé par la norme [9]. Le tableau 1 représente les résultats de simulation obtenues par le test Log Ratio dans le cas :

- PL : Atténuation de parcours (Path Loss) uniquement en utilisant le modèle d'Okmura Hata.
- PL+Fad : Atténuation de parcours avec un fading de Rayleigh d'écart-type $\sigma_f = 1$.
- PL+Fad+Shad : Atténuation de parcours avec un fading de Rayleigh d'écart-type $\sigma_f = 1$ et un Shadowing d'écart-type $\sigma_s = 4\ dB$.

Les valeurs résumées dans le tableau sont très inférieures à 1. La plus grande valeur de $\Delta(x)$ est égale à 0.14, ce qui nous permet de valider notre modèle.

La Figure 4 représente le résultat obtenu par le test de divergence de Kullback-Leibler. La courbe représentant $KL(x)$ dans le cas considérant le modèle d'Okumura Hata uniquement présente un maximum de 0.03. Pour tester la robustesse du modèle nous avons ajouté du fading de Rayleigh et du shadowing avec différents écart-types. Nous avons fait varier l'écart-type du fading de Rayleigh (σ_f) de 1 à 3, et l'écart-type du shadowing (σ_s) de 4 dB à 7 dB. Les courbes représentant le test Kullback-Leibler avec ces variations de paramètres sont plus lisses et avec une dynamique plus importante. Mais dans tous les cas de figures, les valeurs respectent la condition de validité du test Log Ratio (le maximum atteint est 0.1 avec un fading de Rayleigh d'écart-type $\sigma_f = 1$ et un shadowing d'écart-type de $\sigma_s = 7$ dB).

Puissance (dBm)	$\Delta(x)$ σ_f =1, σ_s = 4 dB		
	PL	PL + Fad	PL+Fad+Shad
≤ -30	0.14	0.11	0.122
[-30;-25]	0.048	0.063	0.11
[-25;-20]	0.04	0.009	0.099
[-20;-15]	0.024	0.026	0.09
[-15;-10]	0.022	0.033	0.078
[-1;-5]	0.02	0.024	0.068
[-5;0]	0.03	0.042	0.06
[0;5]	0.043	0.042	0.049
[5;10]	0.026	0.031	0.037
[10;15]	0.014	0.018	0.0 28
[15;21]	0.003	0.0042	0.015

Table 1: Le test Log Ratio $\Delta(x)$

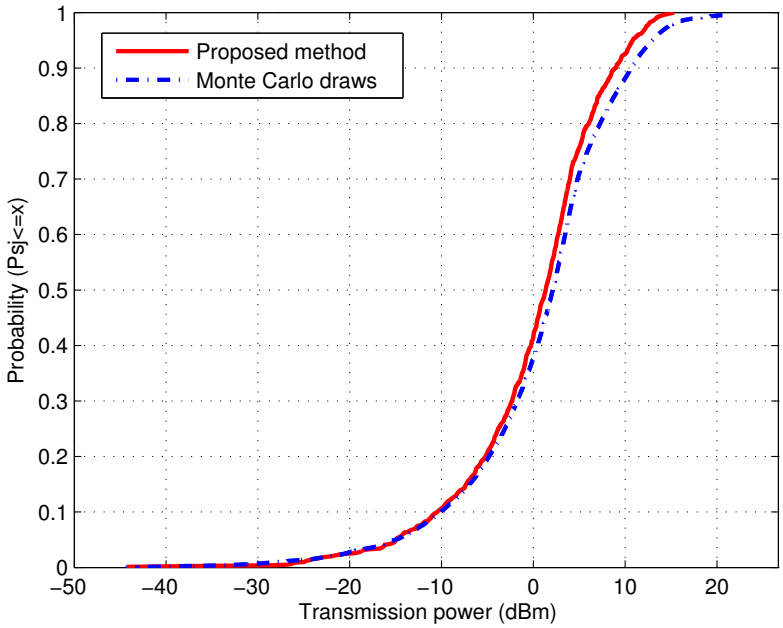

Figure 3: Densité de probabilité des puissances de transmission des mobiles après convergence

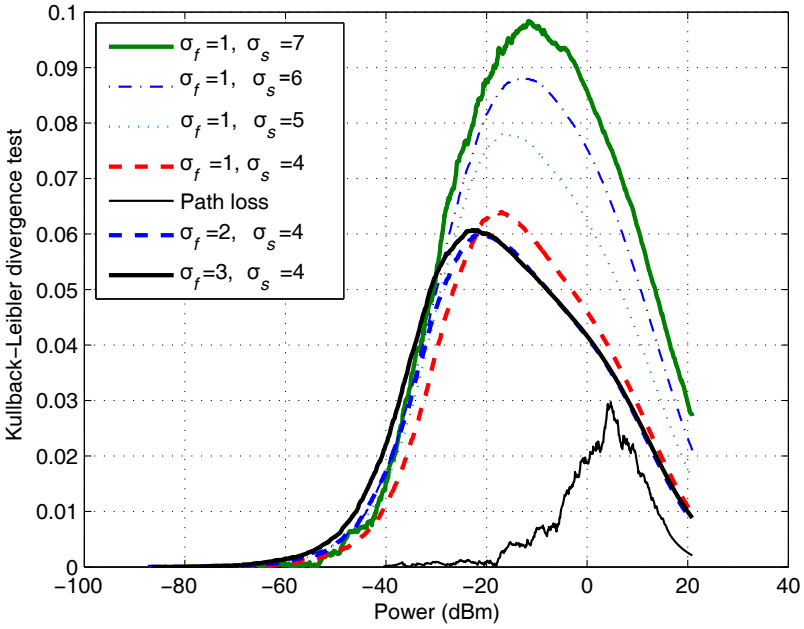

Figure 4: Le test de divergeance de Kullback-Leibler

Afin de valider le modèle analytiquement et tester la fiabilité de la puissance médiane P_{med} par rapport à la puissance moyenne P_{mean}, nous avons développé l'expression analytique de P_{med} et P_{mean}. La validité du modèle analytique a été prouvée grâce aux tests statistiques utilisés lors de la simulation. De la Figure 5, nous constatons la validité du modèle puisque les valeurs du test de Kullback-Leibler obtenues sont faibles, et la meilleure performance est obtenue par le modèle utilisant la puissance médiane.

Chapitre 4 - Modèle analytique de la borne supérieure de la probabilité de dépassement de dimensionnement

Sachant que le nombre de blocs de ressources dans une bande de fréquences est limité, l'entité responsable de l'allocation des ressources radio cherche à maximiser les performances du réseau en allouant efficacement les RBs aux utilisateurs. Cet objectif ne peut être atteint que lorsque la bande de fréquences allouée à une cellule est adaptée à sa charge ainsi qu'à la QdS offerte aux utilisateurs. Dans cette thèse, nous avons développé un modèle analytique qui permet d'évaluer la borne supérieure de la probabilité de dépassement de dimensionnement et ce, en fonction de la charge du réseau, de la QdS offerte aux utilisateurs et de la politique d'allocation de RB appliquée. Nous avons considéré une politique d'allocation équitable et opportuniste dans un système SISO et un système MIMO, lorsqu'une ou plusieurs QdS sont offertes aux utilisateurs.

Nous considérons qu'une cellule est en dépassement de dimensionnement, lorsque cette dernière n'a pas assez de blocs de ressources pour les allouer aux utilisateurs qui lui sont rattachés en satis-

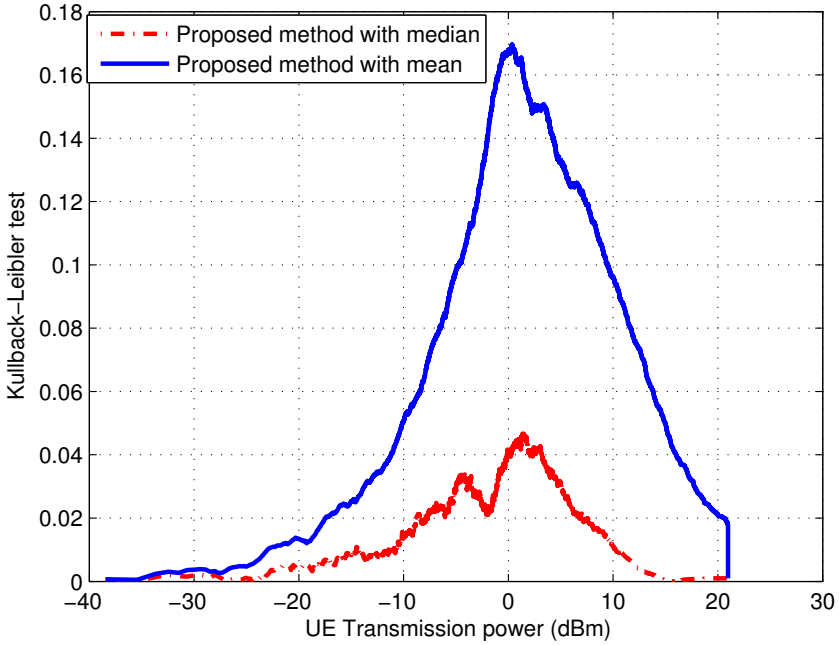

Figure 5: Test de divergence de Kullback-Leibler entre le modèle analytique de la méthode proposée et le tirage de Monte Carlo

.

faisant leur QdS. Afin de développer le modèle analytique de la borne supérieure de la la probabilité de dépassement de dimensionnement, nous utilisons la géométrie stochastique et son large arsenal d'outils mathématiques.

On considère $N_{UE} = |\varphi_{UE}|$ le nombre d'utilisateurs présents dans la cellule C et φ_{UE} l'ensemble de ces utilisateurs. Le débit correspondant à la QdS requise par l'utilisateur est noté C_0. Le nombre total de RBs $\mathbb{N}$ nécessaires pour servir et satisfaire la QdS de tous les utilisateurs présents dans la cellule C est donc:

$$\mathbb{N} = \sum_{k \in \varphi_{UE}} N_k(x) \tag{7}$$

avec $N_k(x)$ le nombre total de RBs nécessaires pour satisfaire la QdS de l'utilisateur k.
Nous considérons que le système est en dépassement de dimensionnement, si le nombre total de RB nécessaires pour servir et satisfaire la QdS de tous les utilisateurs de la cellule $\mathbb{N}$ est supérieur au nombre de RBs disponibles au niveau de la station de base.

Lors de l'établissement du modèle analytique de la borne supérieure de la probabilité de dépassement de dimensionnement, nous avons calculé les débit en fonction de la capacité de Shannon. Ainsi, le

nombre de RB nécessaires pour satisfaire la QdS de l'utilisateur k est :

$$N_k = \left\lceil \frac{C_0}{\bar{C}_k} \right\rceil \tag{8}$$

avec $\bar{C}_k = W \log_2(1+\gamma_k)$ la capacité de Shannon moyenne, W la largeur de bande de fréquences d'un RB et γ_k le niveau du SINR permettant d'atteindre la QdS requise par l'utilisateur k.

Afin de simplifier les calculs, nous avons posé les hypothèses suivantes:

1. La cellule C est ronde, d'un rayon R, avec une station de base munie d'une antenne omnidirectionnelle située au centre de la cellule
2. On n'autorise un utilisateur à transmettre que si :
   - le niveau de SINR de l'utilisateur est supérieur à γ_{min}, ce qui implique un nombre maximum de RBs N_{max} à allouer à un utilisateur, donné par :

$$N_{\max} = \left\lceil \frac{C_0}{W \log_2(1+\gamma_{\min})} \right\rceil \tag{9}$$

   - l'utilisateur est sélectionné par l'ordonnanceur (i.e. $z = 1$ ou $z = 0$ indique respectivement si l'utilisateur est sélectionné ou pas par l'ordonnanceur). Deux types de politique d'allocation de ressources radio sont considérés :
     (a) une politique équitable : tous les utilisateurs ont la même chance d'être sélectionnés par l'ordonnaceur,
     (b) une politique opportuniste : l'ordonnanceur sélectionne en premier l'utilisateur ayant les meilleures conditions radio.
3. Le contrôle de puissance de transmission des utilisateurs n'est pas pris en compte. Ainsi, la puissance de transmission moyenne d'un utilisateur par RB est $P_{k_{Tx}} = \frac{P_{max}}{N_{max}}$.

En se basant sur ces hypothèses, nous développons un modèle analytique de la borne supérieure de la probabilité de dépassement de dimensionnement en considérant une politique d'allocation équitable et opportuniste dans un système SISO et MIMO avec une et plusieurs QdS.

Borne supérieure de la probabilité de dépassement de dimensionnement dans un système SISO

La probabilité de dépassement de dimensionnement est donnée par :

$$P_{\text{out}} = Prob\left(\int N d\varphi \geq N_{\text{RB}} \right) \tag{10}$$

En se basant sur la géométrie stochastique, où les utilisateurs sont générés par un processus de Poisson ponctuel d'intensité $\Lambda(x)$ (donné en fonction de la densité surfacique des utilisateurs ρ et leur temps moyen de service ν, $\Lambda(x) = \frac{\rho}{\nu}$), nous utilisons le théorème de la limite centrale (théorème 2.3) pour calculer la borne supérieure de la probabilité de dépassement de dimensionnement. Lorsque αN_{RB}

blocs de ressources sont alloués à la cellule, la borne supérieure de la probabilité de dépassement de dimensionnement P_{sup} est exprimée par:

$$Prob\left(\int N d\varphi \geq \alpha N_{\mathrm{RB}}\right) \leq \quad P_{\mathrm{sup}}$$

où,

$$P_{\mathrm{sup}} = \quad \exp\left(-\frac{v_N}{N_{\max}^2} g\left(\frac{(\alpha-1)m_N N_{\max}}{v_N}\right)\right) \tag{11}$$

avec $g(t) = (1+t)\ln(1+t) - t$.

Pour obtenir P_{sup}, nous devons calculer les deux premiers moment m_N et v_N de notre processus.

Le nombre de RB nécessaires pour satisfaire la QdS de chaque utilisateur k est :

$$N_k(x,y,z) \quad = \left\lceil \frac{C_0}{W\log_2\left(1+\frac{P_t P_L(x)}{\tilde{\eta} y}\right)} \right\rceil z \tag{12}$$

$$= \left\lceil \frac{C_0}{W\log_2\left(1+\frac{P_t K}{\tilde{\eta} y \|x\|^{\beta}}\right)} \right\rceil z \tag{13}$$

Le processus de Poisson ponctuel est donc marqué par la marque du shadowing noté y et la marque de la décision de l'ordonnanceur z. Ces marques étant indépendantes, le processus de Poisson marqué devient un processus de Poisson ponctuel dans $\mathbb{R}^3$ d'intensité $\Lambda(x) \otimes p_s(y)dy \otimes p(z)dz$.
Grâce à la formule de Campbell (Formule 2.1) nous pouvons calculer m_N et v_N comme suit:

$$m_N = \int N(x,y,z)\ p_s(y)dy\ p(z)dz\ d\Lambda(x) \tag{14}$$

et

$$v_N = \int N^2(x,y,z)\ p_s(y)dy\ p(z)dz\ d\Lambda(x) \tag{15}$$

Les deux premiers moments du processus N peuvent aussi être exprimés en fonction des aires A_j contenant les utilisateurs ayant besoin au plus de j RBs pour satisfaire leur QdS :

$$m_N = \frac{\rho}{\nu}\sum_{j=1}^{N_{\max}-1} j(A_j - A_{j-1}) + \frac{\rho}{\nu} N_{\max}(\pi R^2 - A_{N_{\max}-1}) \tag{16}$$

et

$$v_N = \frac{\rho}{\nu}\sum_{j=1}^{N_{\max}-1} j^2(A_j - A_{j-1}) + \frac{\rho}{\nu} N_{\max}^2(\pi R^2 - A_{N_{\max}-1}) \tag{17}$$

On considère γ_j le seuil du niveau du SINR, j le nombre de RBs nécessaires à l'utilisateur pour atteindre sa QdS définie par son débit cible C_0, avec :

$$\gamma_j = 2^{C_0/(jW)} - 1 \quad \text{pour } j = 1, \cdots, N_{\max} - 1 \quad \text{et } \gamma_0 = \infty$$

Les surfaces A_j peuvent être déterminés par :

$$\begin{aligned} A_j &= \int_{C\times\mathbb{R}^+\times Z} \mathbb{1}_{\{y\|x\|^\beta \le P_t K/\tilde{\eta}\gamma_j\}}\, p_s(y)dy\; p(z)dz\; dx \\ &= \int_{C\times\mathbb{R}^+\times Z} p\left(y\|x\|^\beta \le \tilde{\gamma}_j\right) p(z)dz\; dy\; dx \end{aligned} \tag{18}$$

avec $\tilde{\gamma}_j = \frac{P_t K}{\tilde{\eta}\gamma_j}$.
Dans le cas d'une allocation équitable de RBs, nous obtenons :

$$\boxed{A_j = \tfrac{\nu}{\rho R^2} \exp\left(2/\zeta + 2\alpha_j/\zeta\right)\Phi(\zeta \ln R - 2/\zeta - \alpha_j) + \tfrac{\nu}{\rho}\Phi(\alpha_j - \zeta \ln R)} \tag{19}$$

Lorsqu'une allocation opportuniste de RB est utilisée, nous obtenons :

$$\boxed{A_j = 2\pi \int_0^R \left[1 - \left(1 - \Phi\Big(\frac{\frac{\tilde{\gamma}_j}{r^\beta} - \mu_s}{\sigma_s}\Big)\right)^{\breve{N}_{\mathrm{UE}}}\right] r\; dr} \tag{20}$$

Lorsque plusieurs QdS sont offertes aux utilisateurs, nous considérons chaque classe d'utilisateurs demandant une QdS définie comme étant un processus de Poisson ponctuel marqué par sa classe de QdS l, avec $l \in \mathbb{L}$. Le développement du modèle analytique de la borne supérieure de la probabilité de dépassement de dimensionnement de tout le système, considérant les différentes QdS offertes reste inchangé. La différence réside dans le calcul des deux premiers moments du processus global qui peuvent être décrits comme suit :

$$\boxed{\hat{m}_N = \textstyle\sum_{l=1}^{\mathbb{L}} m_{N,l}} \tag{21}$$

$$\boxed{\hat{v}_N = \textstyle\sum_{l=1}^{\mathbb{L}} v_{N,l},} \tag{22}$$

et la valeur du nombre maximum de RBs alloués à un utilisateur est définie par :

$$\hat{N}_{\max} = \max_l\; N_{l,\max} \tag{23}$$

Ainsi, la borne supérieure de la probabilité de dépassement de dimensionnement $P^{\mathrm{SISO}}_{\mathrm{sup,QoS}}$ est donnée par :

$$\boxed{P^{\mathrm{SISO}}_{\mathrm{sup,QoS}} = \exp\left(-\tfrac{\hat{v}_N}{\hat{N}^2_{\max}} g\left(\tfrac{(\alpha-1)\hat{m}_N \hat{N}_{\max}}{\hat{v}_F}\right)\right)} \tag{24}$$

Borne supérieure de la probabilité de dépassement de dimensionnement dans un système MIMO

Dans le cas d'un système MIMO, pour des raisons de complexité de calcul, nous ne considérons que l'effet du fading. Le signal venant d'un même utilisateur subit la même atténuation de parcours et le même shadowing. Ce qui différencie la qualité du signal venant des différentes antennes d'émission d'un même mobile sont les différentes coefficients du fading subi sur chacun des chemins. Dans ce système, nous avons étudié le gain de diversité et le gain de multiplexage.

1- Gain de diversité

Il consiste à choisir le meilleur chemin pour envoyer l'information. Lorsque une politique d'allocation équitable est considérée, cela revient à une sélection aléatoire de l'utilisateur qui transmet, mais le choix de l'antenne de transmission se fait sur la base des coefficients des fading qu'il subit sur les différents chemins. Considérons n_t antennes de transmission et n_r antennes de reception, le chemin choisi est $|h^*|^2$, qui maximise le gain de fading sur $n_t n_r$ chemins.

$$|h^*|^2 = \max_{1\leq i\leq n_t, 1\leq j\leq n_r} |h_{i,j}|^2.$$

En appliquant les même étapes de développement utilisées dans le cas d'un système SISO, nous obtenons la borne supérieure de la probabilité de dépassement de dimensionnement en fonction des deux premiers moments du processus. Ces derniers se calculent en fonction des aires A_j dont l'expression dans le cas d'un système MIMO avec gain de diversité utilisant une politique d'allocation de RB équitable est :

$$\boxed{A_j = \frac{1}{N_{\mathrm{UE}}}\left[\pi R^2 - 2\pi \int_0^R r\left(1 - e^{-\frac{r^\beta}{\tilde{\gamma}_j}}\right)^{n_t n_r} dr\right]} \tag{25}$$

Lorsque une politique d'allocation de RB opportuniste est utilisée, l'utilisateur sélectionné par l'ordonnanceur est celui qui a les meilleurs conditions radio, et la transmission se fait sur le meilleur chemin. Ceci revient à choisir l'utilisateur ayant le meilleur gain de fading parmi N_{UE} utilisateurs et le meilleur coefficient de fading parmi $n_t n_r$ chemins :

$$k^* = \arg \max_{1\leq k\leq N_{UE}} \left[\max_{1\leq i\leq n_t, 1\leq j\leq n_r} | h_{i,j}^{(k)} |^2 \right].$$

L'expression de A_j dans ce cas là est donnée par :

$$\boxed{A_j = \pi R^2 - 2\pi \int_0^R r\left(1 - e^{-\frac{r^\beta}{\tilde{\gamma}_j}}\right)^{N_{\mathrm{UE}} n_t n_r} dr} \tag{26}$$

2- Gain de multiplexage

Cette technique consiste à transmettre l'information sur les n_t antennes de transmission. On suppose que les conditions canal ne sont pas connues de l'émetteur. La puissance de transmission est répartie équitablement sur ses n_t antennes. La capacité du canal dépend donc des valeurs propres de la matrice $\mathbf{HH}^\dagger = \mathbf{UDU}^\dagger$. D est la matrice diagonale contenant les valeurs propres $\mu_1, \mu_2, \ldots, \mu_m$ de la decomposition de $\mathbf{HH}^\dagger$ avec $m = \min(n_t, n_r)$. Dans ce cas, la capacité du MIMO est décrite comme suit,

$$C = \log_2 \det\left(\mathbf{I}_{n_t} + \frac{P_t K}{n_t \tilde{\eta} \|x\|^\beta} \mathbf{HH}^\dagger\right) \tag{27}$$

$$= C \log_2 \prod_{i=1}^{m} \left(1 + \frac{P_t K \mu_i}{n_t \tilde{\eta} \|x\|^\beta}\right) \tag{28}$$

En considérant C_{tot} le débit total exigé par un utilisateur afin qu'il puisse transmettre les flux de données sur les n_t antennes, le nombre de RB nécessaires afin de satisfaire la QdS de cet utilisateur est donc :

$$N_k(x, \mu, z) = \left\lceil \frac{C_{tot}}{W \log_2(\prod_{i=1}^{m}(1 + \frac{P_t K \mu_i}{n_t \tilde{\eta} \|x\|^\beta}))} \right\rceil z \tag{29}$$

Les valeurs propres n'étant pas indépendantes, nous avons été contraints de faire le dimensionnement sur une seule antenne. Pour des raisons évidentes nous avons préféré un sur-dimensionnement du réseau prenant en compte l'antenne nécessitant le plus de RBs (i.e. ayant la plus petite valeur propre). Puisque les valeurs propres sont ordonnées, le nombre nécessaire de RBs pour satisfaire la QdS de l'utilisateur k est :

$$N_k(x, \mu, z) \geq \left\lceil \frac{C_{tot}}{W m \log_2\left(1 + \frac{P_t K \mu_1}{n_t \tilde{\eta} \|x\|^\beta}\right)} \right\rceil z \tag{30}$$

Lorsqu'une politique d'allocation de RB équitable est utilisée, l'utilisateur sélectionné par l'ordonnanceur est choisi aléatoirement. En revanche, le dimensionnement se fait sur la plus petite valeur propre μ_1 comme décrit précédemment. Les deux premier moments du processus sont calculés en fonction des aires A_j, dont l'expression dans un système MIMO 2x2 est donnée par :

$$\boxed{A_j = \frac{1}{N_{\text{UE}}} \left[\pi R^2 - 2\pi \int_0^R \left(1 - e^{-2\frac{r^\beta}{\tilde{\gamma}_j^{\text{MIMO}}}}\right) r dr\right]} \tag{31}$$

Dans le cas d'une politique d'allocation opportuniste, l'utilisateur choisi est celui bénéficiant des meilleures conditions radio et le dimensionnement se fait toujours sur la plus petite valeur propre. L'expression de A_j est donc donnée par :

$$\boxed{A_j = \pi R^2 - 2\pi \int_0^R \left(1 - e^{-2\frac{r^\beta}{\tilde{\gamma}_j^{\text{MIMO}}}}\right)^{N_{\text{UE}}} r dr,} \tag{32}$$

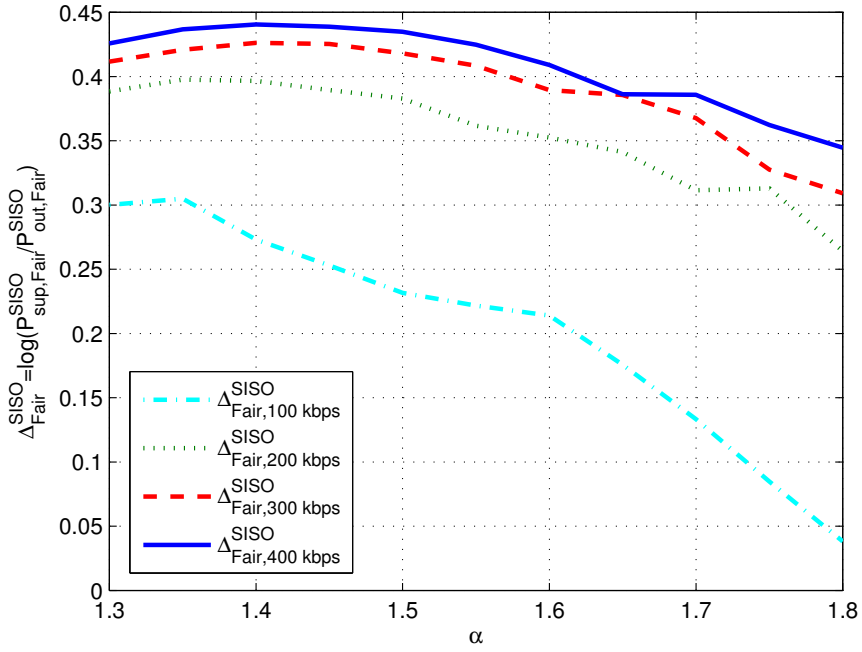

Figure 6: Test Log Ratio de la borne supérieure de la probabilité de dépassement de dimensionnement dans un système SISO avec une politique équitable d'allocation de RB

Afin de valider le modèle, nous avons utilisé le test Log Ratio défini précédement. Ce test permet de mesurer l'écart entre la borne supérieure de la probabilité de dépassement de dimensionnement obtenue par le modèle analytique proposé, et la probabilité de dépassement de dimensionnement obtenue par simulation par des tirages de Monte Carlo. Les résultats obtenus (Figure 6 dans le cas d'un système SISO et Figure 7 dans le cas d'un système MIMO) nous ont permis de valider le modèle dans le cas de systèmes SISO et MIMO avec gain de multiplexage et gain de diversité, tout en considérant les deux types de politique d'allocation de RB.

La borne supérieure de la probabilité de dépassement de dimensionnement nous a permis de juger si la bande de fréquences allouée est adéquate ou non au réseau tout en considèrant la charge du réseau, la QdS offerte, la politique d'allocation de RB adoptée et le système utilisé. Dans le cas où la bande de fréquences est non adéquate (probabilité de dépassement élevée), nous proposons d'accroître le nombre de RBs disponibles en augmentant la bande allouée au réseau avec la technique d'aggrégation de porteuse (Carrier Aggregtion). Ceci nous permet d'augmenter le nombre total de RBs dans la cellule et de diminuer par la même occasion la probabilité de dépassement de dimensionnement.

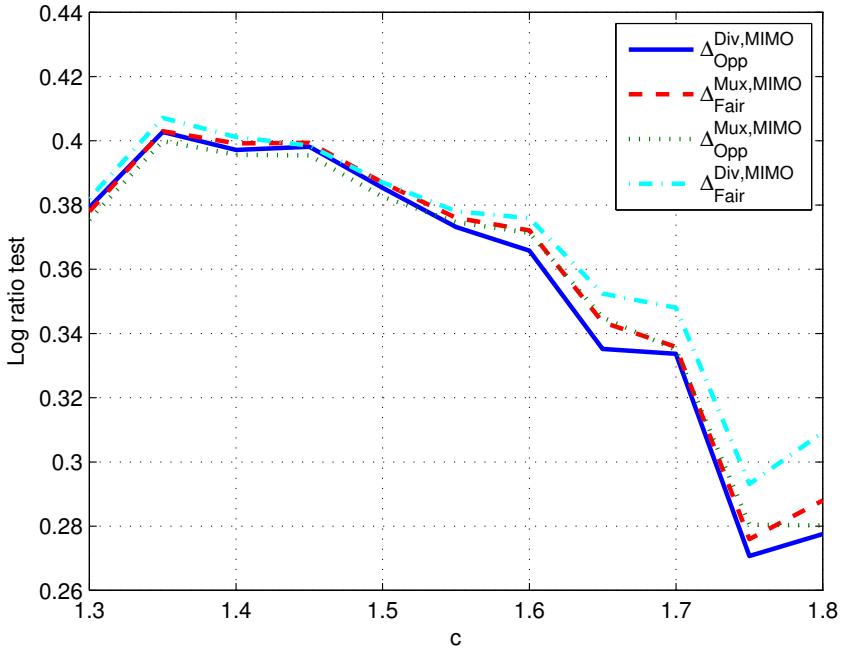

Figure 7: Test Log Ratio de la borne supérieure de la probabilité de dépassement de dimensionnement dans un système MIMO

Chapitre 5 - Allocation des ressources radio

Après avoir défini la bande de fréquences adéquate à allouer à une cellule, nous nous intéressons ensuite à la politique d'allocation des ressources radio, en nombre limité, aux utilisateurs. Notre objectif est de maximiser le débit total de la cellule. Nous proposons un nouvel algorithme, Opportunistic and Efficient RB allocation algorithm (OEA), basé sur une politique opportuniste, tout en allouant efficacement les ressources radio (blocs de ressources et puissance de transmission des mobiles) aux utilisateurs. La solution de l'allocation des ressources radio sur le lien montant est $S_{RB} \in S$ qui maximise la somme des débits individuels des utilisateurs $R_k \; \forall \; k \; = 1, \cdots, N_{UE}$, avec S l'ensemble des allocations possibles de RB aux utilisateurs. Le problème d'allocation des ressources radio sur le lien montant est donc exprimé par:

$$S_{RB} = \arg \max_{S_{RB} \in S} \left\{ \sum_{k=1}^{N_{UE}} R_k \right\}$$

sous les contraintes suivantes :

- Chaque RB est alloué exclusivement à un utilisateur,

$$\sum_{k \in \mathcal{K}} w_k^c(t) = 1 \quad \forall c \in \mathcal{C}$$

avec $\mathcal{K}$ l'ensemble des utilisateurs dans la cellule, $\mathcal{C}$ l'ensemble des RBs et $w_k^c(t) = 0$ ou $w_k^c(t) = 1$ indique si le RB c est alloué à l'utilisateur k à l'instant t.

- Contrainte de contiguïté : les RBs alloués à un même utilisateur doivent être contigus dans le domaine fréquentiel,

$$\forall\ k \in \mathcal{K},\ w_k^c(t) = 0\ \forall\ c \geq j+2 \text{ si } w_k^j(t) = 1 \text{ and } w_k^{j+1}(t) = 0$$

- Contrainte du MCS robuste : un utilisateur doit utiliser le même schéma de codage et de modulation (MCS : Modulation and Coding Scheme) sur l'ensemble des RBs qui lui sont allouées

$$R_k(t) = r_k(t)|\mathcal{A}_k| \tag{33}$$

avec $R_k(t)$ le débit total de l'utilisateur k à l'instant t, $r_k(t)$ le débit instantané de l'utilisateur k sur un RB en considérant la contrainte du MCS robuste, et $\mathcal{A}_k$ l'ensemble des RB alloués à l'utilisateur k.

- Prise en compte de la limite de la puissance de transmission du mobile, puisque la somme des puissances de transmission d'un même utilisateur sur les différents RBs qui lui sont alloués ne doit pas excéder P_{max}.

Vu la complexité de l'allocation conjointe (allouer conjointement les RBs et la puissance de transmission), nous avons opté pour une allocation séparée. Sachant que le SINR dépend de la puissance de transmission des mobiles, nous avons donc choisi d'allouer dans un premier temps les RBs aux utilisateurs, puis d'ajuster la puissance de transmission des mobiles en fonction des conditions radio de chaque l'utilisateur sur les RBs qui lui sont alloués.

L'allocation des RBs prend en considération les contraintes imposées par la technique SC-FDMA (i.e. contrainte de contiguïté des RBs et la contrainte du MCS robuste).

L'efficacité de l'algorithme résulte des conditions supplémentaires imposées lors de l'allocation d'un RB supplémentaire. L'algorithme proposé n'alloue un RB supplémentaire à l'utilisateur k que si l'allocation de ce dernier améliore le débit total de l'utilisateur tout en respectant la contrainte du MCS robuste.
En SC-FDMA la puissance de transmission du mobile est équitablement répartie sur l'ensemble des RBs alloués à un utilisateur. Puisque le SINR efficace sur un RB dépend de la puissance de transmission du mobile sur ce même RB, une mise à jour de la métrique (i.e. SINR) est donc appliquée avant chaque nouvelle allocation, telle que :

$$\overline{\gamma_{(k,c)}^{\text{eff}}} = \overline{\gamma_{(k,c)}^{\text{eff}}} - 10\log(|\mathcal{A}_k| + 1) \quad \forall c \in \mathcal{A}_k \tag{34}$$

avec $\overline{\gamma_{(k,c)}^{\text{eff}}}$ le SINR efficace moyen de l'utilisateur k sur RB c, et $|.|$ la cardinalité d'un ensemble.

Une condition supplémentaire est vérifiée lors de l'extension de l'allocation. Cette dernière impose

un nombre maximum de RB alloués à un utilisateur $\alpha_{k_{max}}$. Dans le cas opportuniste, un nombre maximum égal au nombre maximum de RBs dans la cellule, est autorisé (i.e. la station de base peut allouer à un même utilisateur tous les RBs dont elle dispose $\alpha_{k_{max}} = N_{RB}$).

Afin d'adapter cet algorithme à la QdS des utilisateurs, une variante de l'algorithme, nommée QoS based OEA, est proposée. Cette variante fixe le nombre maximum de RBs à allouer à un utilisateur en fonction de sa QdS demandée (définie par $R_{target,k}$ le débit cible de l'utilisateur k) et ses conditions radio tel que :

$$\alpha_{k_{max}} = \left\lceil \frac{R_{target,k}}{r_k(t)} \right\rceil \tag{35}$$

L'allocation des RBs aux utilisateurs considère que la puissance de transmission des mobiles est fixée à P_{max}. A la fin du processus d'allocation de RB, l'utilisateur k atteint un débit $R_k(t)$. Notre objectif est de diminuer la puissance de transmission $P_{e,k}$ du mobile k en appliquant un contrôle de puissance, sans affecter son débit atteint avant le contrôle de puissance. Pour atteindre cet objectif, le contrôle de puissance doit prendre en compte le niveau minimum du SINR, atteint sur l'ensemble des RBs allouées, afin de garantir l'utilisation du même MCS qu'avant le contrôle de puissance. Ainsi le contrôle de puissance est défini dans ce cas par :

$$P_{e,k} = \frac{P_{\max}}{|\mathcal{A}_k|} \frac{\gamma_{\text{tg}}}{\gamma^{\text{eff}}_{(k,\min)}} \tag{36}$$

où, γ_{tg} le débit cible est exprimé en dB comme suit :

$$(\gamma_{\text{tg}})_{dB} = (\gamma_{\text{MCS},k})_{dB} + (\Delta_\gamma)_{dB} \tag{37}$$

avec $\gamma_{MCS,k}$ le niveau minimum du SINR requis pour pouvoir utiliser le même MCS, Δ_γ une marge de SINR, et $\gamma^{\text{eff}}_{(k,min)}$ le SINR minimum effectivement atteint par l'utilisateur k sur l'ensemble des RBs qui lui sont alloués :

$$\gamma^{\text{eff}}_{(k,\min)} = \min_{c \in \mathcal{A}_k} \gamma^{\text{eff}}_{(k,c)} \tag{38}$$

Les performances de l'algorithme proposé sont étudiées dans un réseau régulier (i.e. composé de cellules hexagonales, chacune munie d'une station de base au centre de la cellule) et un réseau aléatoire (i.e. un réseau généré par la superposition de deux processus de Poisson d'intensité λ_{eNB} et λ_{UE} représentant respectivement les stations de base et les utilisateurs) en termes de complexité, débit agrégé, efficacité énergétique, nombre d'utilisateurs servis, taux de RBs alloués et équité de débit entre les utilisateurs.

Les performances du OEA sont comparées avec les performances de la méthode optimale obtenue par la programmation entière [10], connue pour sa complexité, et d'autres algorithmes référencés

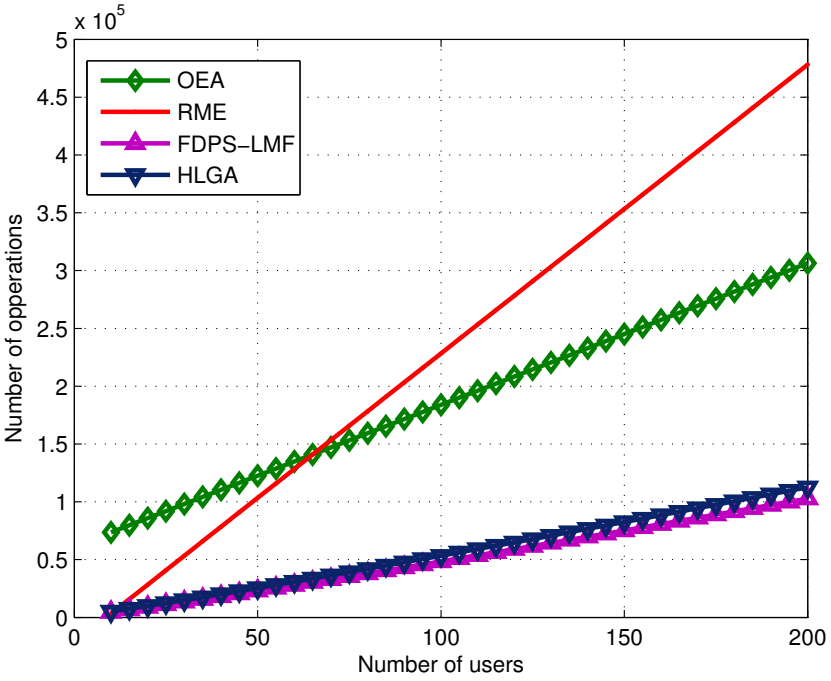

Figure 8: Nombre d'opáerations nécessaires pour l'allocation des ressources radio

dans le domaine tels que : Frequency Domain Packet Scheduling- Largest Mertic First (FDPS-LMF), Recursive Maximum Expansion (RME), Heuristic Localized Gradian Algorithm (HLGA), proposés respectivement dans [11], [12] et [13].

La complexité étant polynomiale pour les algorithmes OEA, FDPS-LMF, HLGA et RME, nous avons calculé et comparé le nombre nécessaire d'opérations à effectuer par chacun des algorithmes pour allouer les RBs aux utilisateurs de la cellule, et ce pour différentes charges du réseau. La Figure 8 montre que le nombre d'opérations nécessaires pour l'algorithme OEA est inférieur à celui de l'algorithme RME lorsque le nombre d'utilisateurs dans la cellule dépasse 70 utilisateurs. Le nombre d'opérations nécessaires pour allouer les RBs aux utilisateurs, lorsqu'une bande de 10 MHz est allouée à la cellule et que le nombre d'utilisateurs N_{UE} est égal à 100, est inférieur à 0.2 million opérations. Ceci prouve que l'algorithme peut être exécuté en moins de 0.5 ms (la période d'ordonnancement) avec une station de base munie d'un processeur à deux corps qui opèrent à 2 x 34 k millions d'instructions par seconde (disponible dans le marché).

La Figure 9 illustre les débits agrégés obtenus par les différents algorithmes. Le débit agrégé obtenu par l'OEA est proche de celui obtenu par la méthode optimale. L'algorithme QoS based OEA atteint un débit agrégé un peu plus faible. Ceci est dû au débit cible exigé par les utilisateurs fixé à 600 kbps. Les algorithmes HLGA, FDPS-LMF et RME atteignent le plus faible débit agrégé car leur métrique cherchant une équité en débit entre les utilisateurs, ils allouent les RBs aux utilisateurs qui

ont un faible débit et probablement des conditions radio qui ne leur permettent finalement même pas d'employer le plus robuste des MCS.

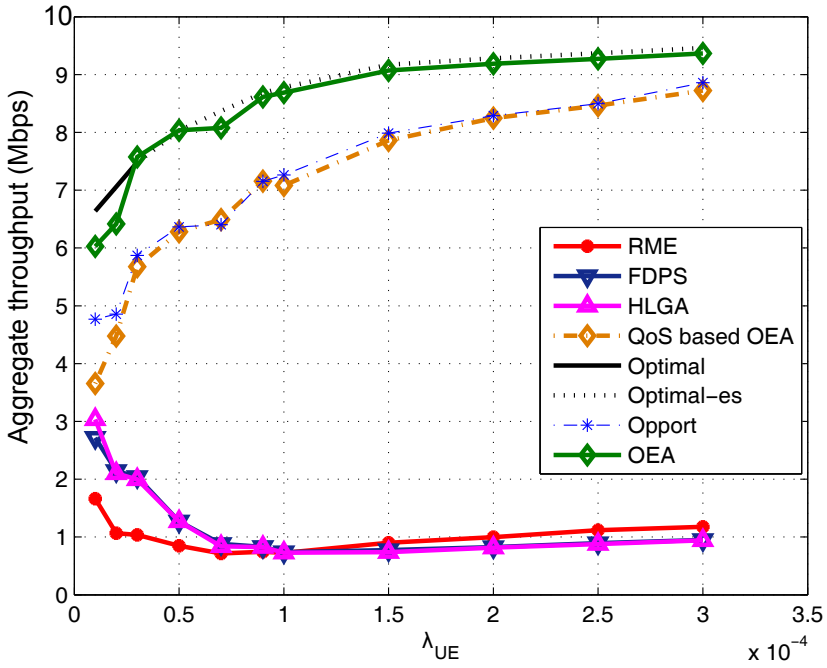

Figure 9: Débit agrégé dans un secteur d'un réseau aléatoire

La Figure 10 représente la proportion d'utilisateurs servis par chaque algorithme. L'algorithme QoS based OEA, avec ses conditions de débit amélioré et de nombre maximum de RBs alloués par utilisateur, permet de maximiser la proportion d'utilisateurs servis. Les algorithmes HLGA et FDPS-LMF atteignent une proportion d'utilisateurs servis élevée. Ceci est dû à leur politique d'allocation qui considère qu'un utilisateur est servi lorsque l'expansion de l'allocation est interrompue à cause de la contrainte de contiguité non satisfaite entre les RBs où l'utilisateur en question maximise la métrique.

Les algorithmes RME, FDPS-LMF et HLGA, allouant des RBs à des utilisateurs ne pouvant pas employer le plus robuste des MCS, atteignent un débit nul quelque soit le nombre de RBs qui leur est alloué. Ils maximisent donc le taux de RBs gaspillés (i.e. allouer des RBs à des utilisateurs ayant un débit nul). La Figure 11 présentant le taux moyen de RBs gaspillés montre que les algorithmes OEA et QoS based OEA annulent le gaspillage des RBs grâce à la mise à jour de la métrique avant chaque nouvelle allocation et leur condition d'amélioration de débit.

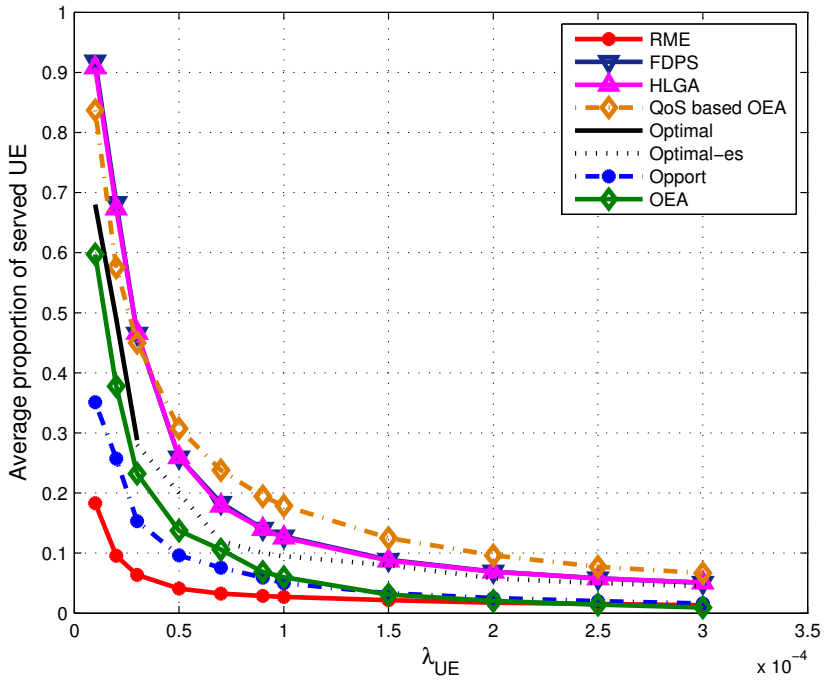

Figure 10: Proportion moyenne d'utilisateurs servis dans un réseau aléatoire

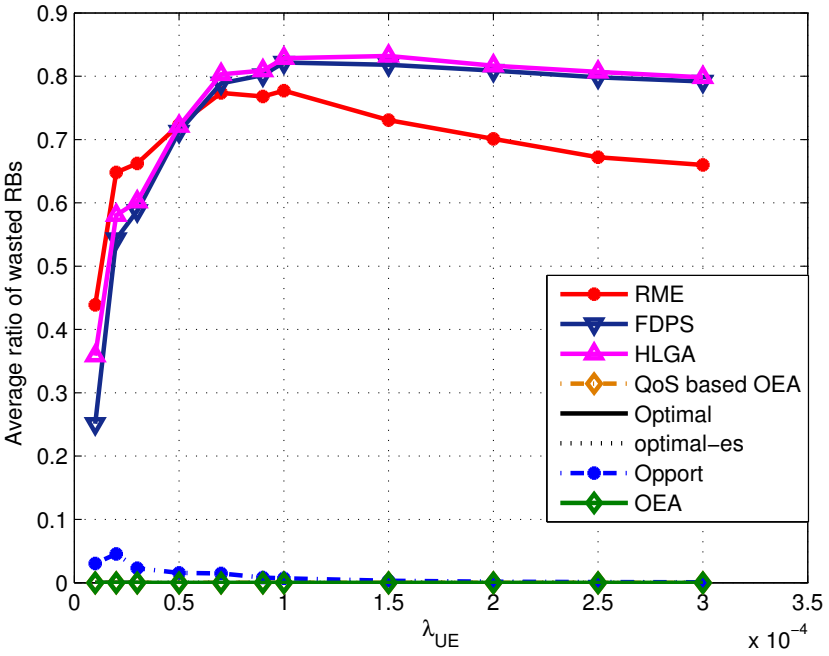

Figure 11: Taux moyen de RB gaspillés dans un réseau aléatoire

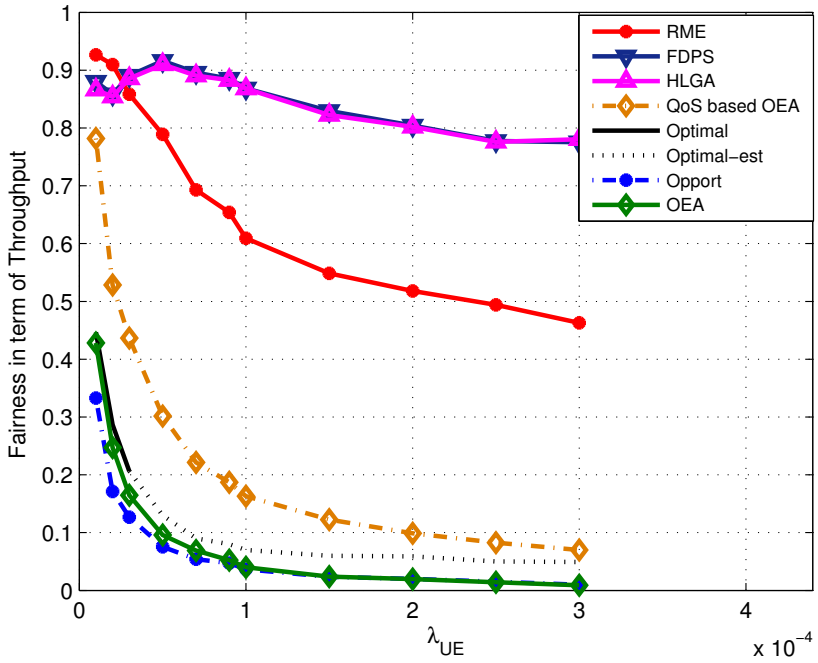

Figure 12: Equité en terme de débit entre les utilisateurs dans un réseau aléatoire

Nous avons calculé l'équité en terme de débit comme définie dans [14], et donnée par :

$$F_{Alg} = \frac{\left(\sum_{k=1}^{N_{UE}} R_k(\Delta T)\right)^2}{\left(N_{UE} \sum_{k=1}^{N_{UE}} R_k(\Delta T)^2\right)} \tag{39}$$

La Figure 12 illustrant cette équité montre que les algorithmes RME, FDPS-LMF et HLGA maximisent l'équité en terme de débit entre les utilisateurs. Le calcul d'équité de ces algorithmes prend cependant en compte les utilisateurs ayant un débit nul. Vu le taux de gaspillage de RB observé pour ces algorithmes, nous soupçonnons que ce niveau élevé d'équité est aussi dû au taux élevé de RB gaspillés.

En terme d'efficacité énergétique, nous avons comparé le niveau moyen de puissance de transmission des utilisateurs après le contrôle de puissance. La Figure 13 montre que la puissance de transmission moyenne atteinte par les algorithmes proposés, à forte charge, est de 13 dBm. Cette réduction de puissance de transmission des mobiles permet de maximiser l'efficacité énergétique et de maximiser la duré de vie de la batterie des mobiles.

Chapitre 6 - Allocation des RBs dans une système multi-utilisateurs

Vu les performances de l'algorithme proposé OEA, nous avons étendu l'étude de ce dernier dans un système multi-utilisateurs MIMO (MU-MIMO), où plusieurs utilisateurs potentiels $N_{u,p}$ peuvent transmettre leurs données dans un même RB, grâce à un codeur/ décodeur adapté. Pour cela, nous

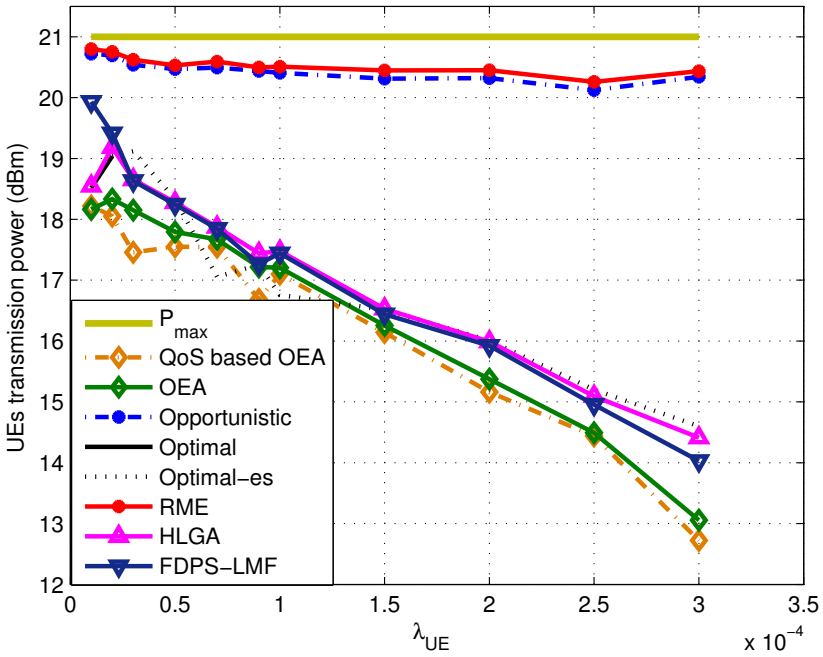

Figure 13: Puissance de transmission moyenne des utilisateurs sur un TTI, dans un réseau aléatoire

proposons un nouveau décodeur (Figure 14) qui combine un décodeur zero forcing (ZF) et un décodeur à maximum de vraisemblance (ML) afin d'annuler le niveau d'interférence entre utilisateurs partageant le même RB et décoder les données envoyées par chacun.

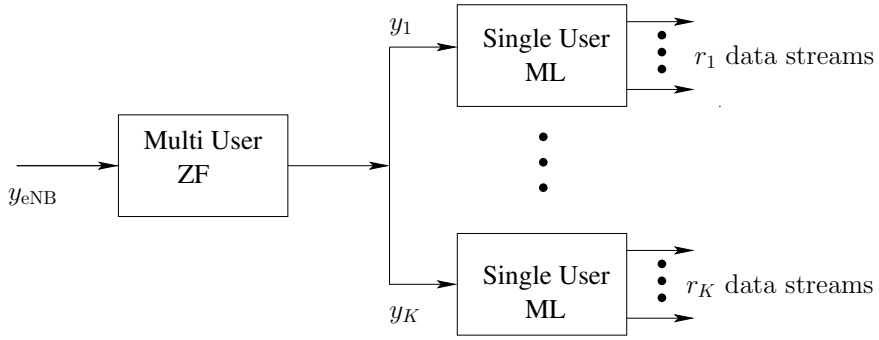

Figure 14: Décoder combiné ZF et ML

Nous avons étudié l'impact de la métrique sur l'algorithme dans un contexte multi-utilisateurs, en étudiant les performances suivant deux métriques :

- $\mathcal{M}_{rate}$: maximise le débit par RB. Le nombre d'utilisateurs partageant un RB est $N_s \leq \min(n_r, N_{u,p})$.
- $\mathcal{M}_{UE}$: maximise le nombre d'utilisateurs transmettant des données par RB, $N_s = \min(n_r, N_{u,p})$.

Ces deux métriques nous permettent de sélectionner les utilisateurs partageant le même RB. L'extension de l'allocation des RBs pour chaque utilisateur se fait en fonction de l'algorithme Cen-

tral Opportunistic Scheduling (COS) qui est une adaptation de l'algorithme OEA dans le cas multi-utilisateurs. Nous avons considéré la condition d'amélioration de débit comme une condition additionnelle pour étudier l'effet de cette dernière sur le comportement de l'algorithme. Une stratégie d'orthogonalité est prise en compte lors de la sélection des utilisateurs.

La Figure 15 représente le débit agrégé dans la cellule utilisant l'algorithme COS lorsque les métriques $\mathcal{M}_{rate}$ et $\mathcal{M}_{UE}$ sont utilisées avec ou sans les conditions : amélioration de débit et la stratégie d'orthogonalité. Les performances sont comparées aux performances de l'algorithme Random Matching Scheduling (RMS) qui sélectionne aléatoirement les utilisateurs partageant le même RB.

Nous constatons un écart entre les courbes représentant le débit agrégé obtenu par les algorithmes RMS, COS utilisant la métrique $\mathcal{M}_{rate}$ et COS utilisant la métrique $\mathcal{M}_{UE}$. Cet écart est réduit lorsque les conditions d'amélioration de débit et stratégie d'orthogonalité sont considérées.

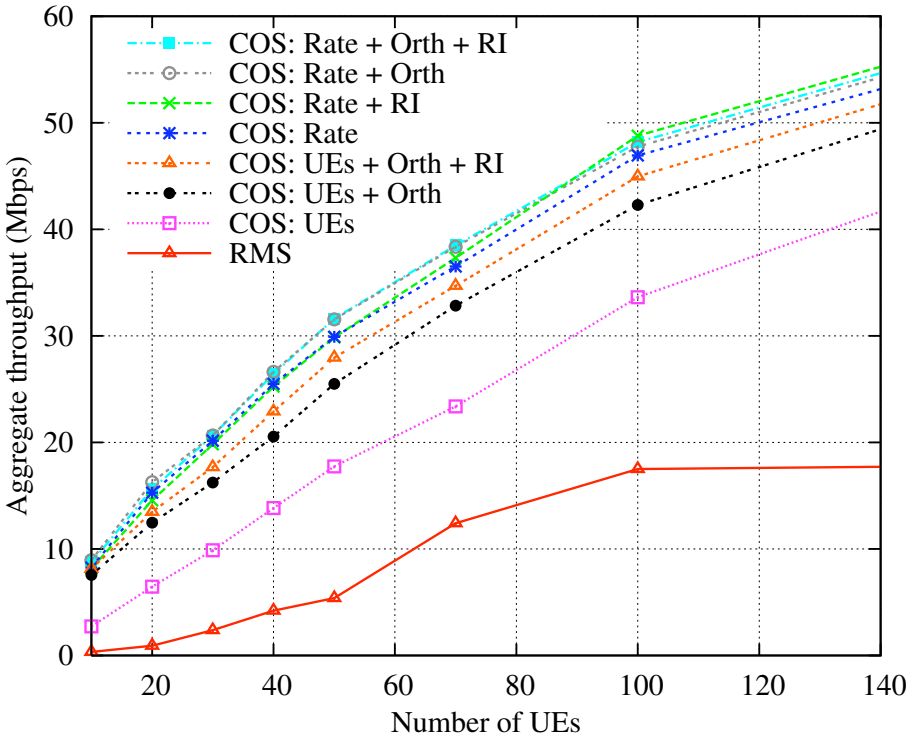

Figure 15: Débit agrégé dans un secteur de la cellule considérée

Les performances en terme de nombre d'utilisateurs servis sont illustrées dans la Figure 16. En utilisant la métrique $\mathcal{M}_{UE}$, l'algorithme COS sert plus d'utilisateurs que lorsque la métrique $\mathcal{M}_{rate}$ est utilisée. En rajoutant des conditions telles que l'amélioration de débit et la stratégie d'orthogonalité, le taux d'utilisateurs servis augmente. Un compromis entre le débit agrégé de la cellule et le pourcentage d'utilisateurs servis est donc obtenu avec l'algorithme COS utilisant la métrique maximisant le

nombre d'utilisateurs servis $\mathcal{M}_{UE}$ avec condition d'amélioration de débit et stratégie d'orthogonalité.

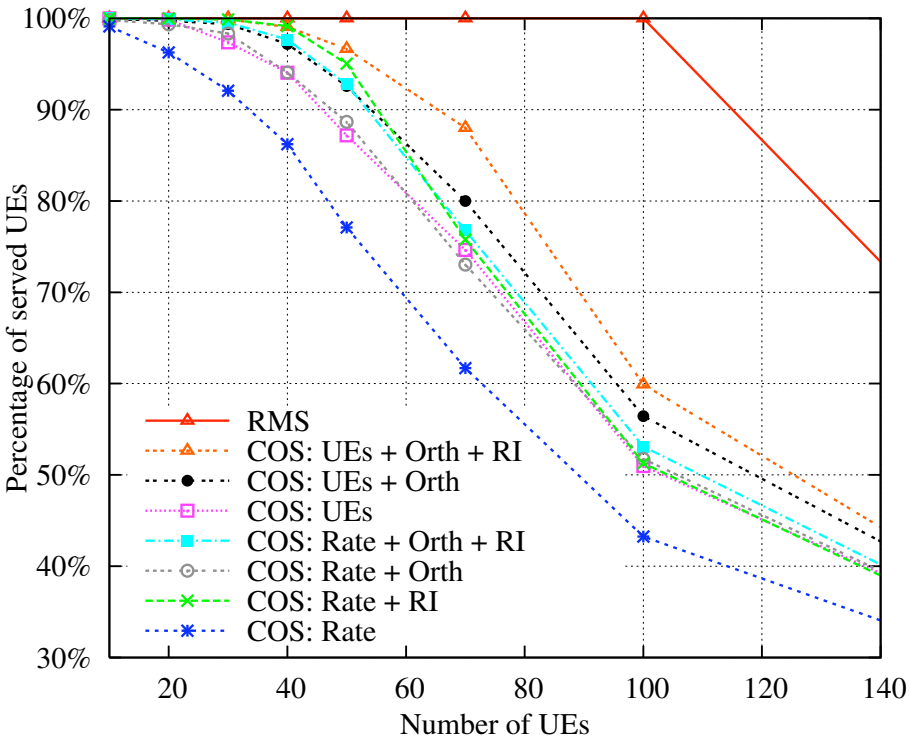

Figure 16: Pourcentage des utilisateurs servis dans la cellule

Conclusion

Dans cette thèse nous avons étudié l'allocation des ressources radio sur le lien montant d'un réseau OFDMA, et plus précisément dans un réseau LTE, sous des contraintes de consommation d'énergie. Nous nous sommes intéressés dans un premier temps à l'estimation du niveau d'interférences auquel sont soumis les utilisateurs. Nous avons donc développé un nouveau modèle d'estimation du niveau d'interférence inter-cellulaire sur le lien montant d'un réseau LTE. Ce modèle peu complexe a relevé le défit de l'estimation des niveaux des interférences inter-cellulaires sur le lien montant qui devait considérer l'emplacement variable des utilisateurs interférents et la puissance de transmission non uniforme des mobiles interférents non uniforme. Notre modèle considère que la contribution d'un secteur en terme d'interférence équivaut à la puissance reçue au niveau de la station de base centrale de la part d'un utilisateur virtuel situé au barycentre géographique du secteur interférent et émettant à une puissance médiane. Ce nouveau modèle d'estimation des interférences inter-cellulaires a été validé par simulation et analytiquement en considérant les deux tests statistiques suivants : test Log Ratio et le test de divergence de Kullback-Leibler. Ensuite, nous avons abordé le problème de planification fréquentielle des réseaux cellulaires. Nous avons développé un modèle analytique permettant, à nombre de RBs par cellule fixé, d'évaluer la borne supérieure de la probabilité de dépassement de dimensionnement. Cette borne supérieure permet de juger si la bande de fréquences allouée à la

cellule est adéquate ou non, tout en prenant en compte la charge du réseau, le comportement de l'environnement radio, la QdS offerte aux utilisateurs et la politique d'allocation de ressources radio utilisée. Le modèle analytique de la borne supérieure de la probabilité de dépassement de dimensionnement a été développé pour un système SISO et un système MIMO en considérant le gain de diversité et le gain de multiplexage. En fonction de la probabilité de dépassement de dimensionnement obtenue, nous avons évalué la bande de fréquences à allouer à une cellule et ajusté cette dernière en agrégeant une porteuse adéquate afin de diminuer la probabilité de dépassement de dimensionnement. Lorsque la bande de fréquences adéquate est allouée à une cellule, nous avons proposé un nouvel algorithme basé sur une politique opportuniste, qui alloue efficacement les RBs aux utilisateurs et permet de maximiser le débit total de la cellule. Les performances de cet algorithme ont été étudiées dans un réseau régulier et dans un réseau aléatoire, en les comparant aux algorithmes les plus référencés trouvés dans la littérature. Vu les résultats encourageants que nous avons obtenus, nous avons étendu l'application de cet algorithme à un système multi-utilisateurs MIMO. Nous avons proposé un nouveau décodeur qui combine un décodeur zero forcing (ZF) et un maximum de vraisemblance (ML) pour annuler l'interférence entre les utilisateurs partageant le même RB. Cette étude a été faite pour différentes métriques (métrique maximisant le débit par RB, et métrique maximisant le nombre d'utilisateurs par RB) et un compromis a été trouvé en terme de maximisation de débit total de la cellule, en utilisant la métrique de maximisation de nombre d'utilisateurs servis par RB, et en imposant des conditions d'orthogonalité et d'amélioration de débit dans l'algorithme d'allocation de RBs aux utilisateurs.

Chapter 1

Introduction and Outline

1.1 Motivations

NOWADAYS, popularity of smart terminals, with their enhanced functionalities and applications, makes the Information and Communication Technologies (ICT) face more and more serious challenges. The third Generation Partnership Project (3GPP) Long Term Evolution (LTE) networks represent a major advance in cellular technology and their performances accommodate the wireless broadband constantly increasing demand. LTE offers significant improvements over previous technologies. Among them we can note that it provides a higher data throughput. Actually, the system supports, within 20 MHz bandwidth, 75 Mbps in downlink and 50 Mbps in uplink in Single Input Single Output (SISO) and up to 350 Mbps in downlink with 4×4 Multiple Input Multiple Output (MIMO) [15]. In addition, the simple system access architecture decreases the system latency: only 10 ms of latency is needed to transmit data between users and the network [16].

Indeed, the Mobile Switching Controller (MSC) and Radio Access Controller (RNC), that are placed respectively in the core network and the 2G and 3G Radio Access Network (RAN), do not exist in LTE architecture. The LTE base station, commonly termed evolved NodeB (eNB), inherited of some high level of RNC and MSC functionalities, such as mobility management and Radio Resource Management (RRM). The remaining functionalities have been removed up to the Packet Core Network (PCN) [17]. The RRM has a crucial role because a best use of radio resources can greatly improve the system performances. The limited radio resources place the RRM as the main interest on researchers to fully exploit LTE potentialities. The RRM is responsible of managing multi-user radio access and determines the strategies and algorithms for allocating the radio resources to the users depending on their individual Quality of Service (QoS) requirements and channel conditions.

In LTE, new multiple access techniques to the radio air interface, based on Orthogonal Frequency Division Multiplex (OFDM) method, are introduced: Orthogonal Frequency Division Multiple Access (OFDMA) in the downlink and Single Carrier Frequency Division Multiple Access (SC-FDMA) in the uplink [18]. These access techniques allow a flexible bandwidth allocation (from 1.4 MHz to 20 MHz) [15], and an increase of the spectral efficiency (three or four times higher than the spectral efficiency of High Speed Packet Access (HSPA) Release 6) [19]. In OFDMA, the available bandwidth is divided into orthogonal subcarriers, whose narrowness is such that fading is considered as flat over each of them. Consequently, their allocation to the users can be done according to the users channel conditions over each subcarrier. Since the users are orthogonally multiplexed, the intra-cell interference is cancelled. The drawback of OFDMA is a high generated Peak to Average Power Ratio (PAPR), which makes it irrelevant on uplink due to the User Equipment (UE) battery life. Unlike OFDMA, SC-FDMA generates a low PAPR, by considering the whole allocated subcarriers as a single carrier and sharing equally the UE transmission power over it [20] [21] [22]. The LTE release 8 standards impose on each UE to be allocated contiguous subcarriers and to use the same Modulation and Coding Scheme (MCS) over its whole allocated subcarriers [23]. Due to these two SC-FDMA specific constraints, the RRM algorithms proposed for the downlink can not be directly applied to the uplink.

Radio resource allocation process occurs each Transmission Time Interval (TTI) of 1 ms duration, it is performed throughout the allocation of Resource Blocks (RB), which are the smallest grid that can be allocated to one UE. Each user can be allocated more than one RB to guarantee its required QoS. The LTE standardized bandwidth contains a fixed number of RBs [3]. To benefit from the full performances of the system, we should efficiently allocate the limited number of RBs in order to increase the cell's capacity, to serve more users and to prevent from wasting radio resources. In addition, radio resource allocation should be processed with low computational complexity, as it occurs recursively every 1 ms and potentially concerns a large number of heterogenous users in highly loaded networks.

1.2 Contributions

The main purpose of this dissertation is to show how we can efficiently allocate the flexible bandwidth to each cell (or sector) regarding the QoS required by the users and minimizing their dimensioning outage probability due to insufficient resources. Once the frequency planning is performed, the allocation of radio resources in uplink LTE networks is discussed. We consider a distributed resource allocation architecture, where each eNB allocates radio resources independently of the radio resources allocation decision of the other eNBs of the network. In this context, radio resources allocation includes both the allocation of RBs to the users and the determination of the UEs transmission power. In addition, the RB allocation entity respects the SC-FDMA technique constraints and aims at maximizing the system satisfaction level. It is then extended to the Multi-User MIMO (MU-MIMO) case, where one RB can be shared by several users. Green power allocation is also studied, where the UE transmission power is

established according to the user's QoS requirements and the radio channel conditions experienced by the concerned user over its whole allocated RBs. UE transmission power reduction leads to decrease the Inter-Cell Interference (ICI). Consequently, a new model of ICI estimation is proposed for the uplink, adapted to the Power Control (PC) applied on the UE transmission powers.
The main objectives of the studies performed in this thesis are:

- to estimate the inter-cell interference in uplink green LTE networks. Since ICI is caused by the use of the same resources by other users in the neighboring cells, then the ICI level, in uplink, depends of the transmission power of these interfering users. However, in case of UE power control application, the ICI level is different from the one used while the UE transmission powers are set at their maximum. For that purpose, we propose a low computational complexity model of ICI level estimation received at the eNB over each RB when UE power control is applied.

- to propose an analytical model for the dimensioning outage probability evaluation, which helps the radio dimensioning of uplink LTE networks. To allocate an adequate bandwidth to each cell (or sector) according to the network's load and the user's QoS, an analytical model of the dimensioning outage probability is developed. This model evaluates analytically the upper bound of the probability that users are in outage because of insufficient resources. The upper bound of the dimensioning outage probability, by considering the network's configuration, helps us to determine the required number of RBs that should be allocated to the cell (or sector), with the corresponding maximum dimensioning outage probability. An average number of RBs needed to serve the users, by considering the RB allocation policy and the users QoS requirements, is computed. The fair RB allocation algorithm and the opportunistic RB allocation algorithm are investigated. The dimensioning outage probability upper bound is evaluated for one and multiple users QoS classes. This study is also extended to the MIMO systems.

- to determine a low computational complexity radio resource allocation scheme, which aims at maximizing the aggregate throughput of the network with a low UE transmission power. Our aim is an efficient allocation of the radio resources to users, with respect to the release 8 SC-FDMA constraints. The RBs are efficiently allocated to the users according to their individual channel conditions and QoS requirements. Then, an adjustment of UE transmission power is performed without affecting the throughput achieved by the concerned user before the transmission power reduction. The performances of the proposed radio resource allocation scheme are given in regular and random networks. The RB allocation algorithm performance analysis is extended to the MU-MIMO systems, where the spectrum efficiency is improved. An adaptation of the RB allocation algorithm for the LTE-Advanced (LTE-A) networks is also investigated.

1.3 Assumptions

Throughout this thesis, we make some assumptions that are given in the following:

- *Distributed radio resource allocation architecture*:
  Each eNB is responsible of the radio resource allocation over its served users, without considering the resource allocation decision made by the neighboring eNBs. The radio resource allocation is based on the radio channel conditions given by the Channel State Information (CSI).

- *Network topology*:
  Except Chapter 4, tri-sectored antennas are used. To manage ICI, we allocate different frequency bandwidths at each sector and adopt a $1 \times 3 \times 3$ frequency reuse pattern. Two topologies are used: a regular topology and a random topology. The regular one is a grid of hexagonal cells where users are classified into each sector regarding to their geographical positions. The random topology is a superposition of Poisson point processes of intensity λ_{eNB} and λ_{UE} that represent respectively the eNBs and the UEs. The sector selection, in random networks, is given with respect to the Reference Signal Received Power (RSRP), where a comparison of the downlink received power from each sector is performed.

- *Knowledge of the channel conditions*:
  We assume a full knowledge of the channel conditions at the receiver. This knowledge is due to the CSI that estimates the propagation of the signal including the shadowing and fading effects with help of the Reference Signals (RS). These RS are sent both in uplink and downlink in a specific resource element (RE) of each RB.

- *Frequency Division Duplexing (FDD) mode*:
  We consider a LTE FDD mode, where the uplink and the downlink transmissions operate in two different bandwidths. The FDD LTE frame structure of 10 ms duration is considered. Each frame is divided into ten subframes and each subframe consists of two time slots.

- *Resource allocation*:
  The resource allocation process occurs each TTI which corresponds at one subframe of 1 ms duration. As the allocated resources are of 0.5 ms duration, the allocated resources in the first slot of one subframe are maintained for the second slot. Since the resource allocation is based on the channel state information on each resource, then the metric used to allocate the radio resources is averaged over the two slots. We consider a perfect synchronization between UEs and eNB, with the standardized Cyclic Prefix (CP). Thus, the Inter-Symbol Interference (ISI) is assumed to be null.

- *Users Traffic*:
  The users are drawn uniformly in the area. We assume that each active user has an infinite backlog of data to send. Our objective is to maximize the aggregate throughput of the network; therefore we allocate to the users the radio resources that maximize their individual throughput, except in Chapter 4, where the upper bound of the dimensioning outage probability is established considering a target throughput of each user, and in Chapter 5, when QoS differentiation RB allocation algorithm is proposed.

1.4 Thesis outline

The optimization of radio resource allocation is investigated. In Chapter 2 the technical and mathematical necessary background is given. Since it is based on the channel state information of each UE on each radio resource, the ICI level is first estimated in green LTE network (Chapter 3). Then, we aim at determining the adequate allocated bandwidth to each cell (or sector) according to a given maximum dimensioning outage probability. The analytical model of the dimensioning outage probability upper bound is developed, for SISO and MIMO systems, in Chapter 4. Once the allocated bandwidth is performed, the algorithms and strategies for radio resource allocation are studied in Chapter 5. They include the allocation of resource blocks and the UE transmission power. Then, the RB allocation study is expanded to MU-MIMO system in Chapter 6.

- **Chapter 2 - Preliminaries**
  Chapter 2 provides the technical and mathematical background needed in this thesis. The technical background concerns the LTE system technical specificities: radio resource management, modulation and coding scheme, QoS, MIMO and MU-MIMO techniques, and the main simulation parameter considered in this thesis. The mathematical background consists of the Poisson point process and the marked Poisson point process which are used in Chapter 4 to evaluate the dimensioning outage probability upper bound.
- **Chapter 3 - Inter-cell interference estimation in green LTE networks**
  This chapter investigates the inter-cell interference estimation in the uplink of green LTE networks. We propose a new model of inter-cell interference estimation when the UE transmission power control is applied. The proposed model is given in a regular network where the location and the controlled power of each user is assumed known. This model has low computational complexity and it avoids Monte Carlo simulations. The ICI estimation model is validated both analytically and by simulations.
- **Chapter 4 - dimensioning Outage probability upper bound depending on RRM**
  Chapter 4 focuses on dimensioning uplink LTE networks. We propose an analytical model to evaluate an upper bound of the probability that users are blocked because of an insufficient number of resources. This upper bound helps cell planners to estimate the network configuration and the necessary allocated bandwidth to each cell. The number of RBs allocated to each UE is established as a function of its required QoS. The study is expanded to the multiple QoS class

in SISO system. The diversity and multiplexing gains in MIMO systems are also investigated.

- **Chapter 5 - Radio resource allocation scheme for green LTE networks**
  In this chapter, we focus on the uplink radio resource allocation. It includes algorithms and strategies to allocate RBs to the UEs and to adjust their transmission power. Two algorithms are proposed: the Opportunistic and Efficient RB Allocation (OEA) algorithm and the Quality of Service based Opportunistic and Efficient RB Allocation (QoS based OEA) algorithm. These algorithms allocate efficiently the RBs, while respecting the LTE release 8 SC-FDMA constraints. An adaptation of these two algorithms for LTE-A networks is investigated. The UE power allocation consists of allocating the lowest possible power to each UE without affecting its individual throughput. The simulation performances are given in regular and random networks, which allow us to analyze the RB allocation algorithms stability.
- **Chapter 6 - Radio resource management in MU-MIMO**
  In this chapter, the proposed OEA algorithm discussed in Chapter 5 is extended to MU-MIMO networks. For this, we first propose a new transceiver structure that gives the possibility to spatially multiplex different UEs data streams and offers to each UE a reliable individual throughput by exploiting the transmit and receive diversity. Then, we show, using this transceiver structure, how to extend the OEA algorithm in the MU-MIMO context.

1.5 List of publications

International journals

- **F.Z. Kaddour**, E. Vivier, L. Mroueh, M. Pischella and P. Martins, "Green Opportunistic and Efficient Resource Block Allocation Algorithm for LTE Uplink Networks", submitted to IEEE Transaction on Vehicular Technology.

International conferences

- **F.Z. Kaddour**, E. Vivier, M. Pischella, L. Mroueh and P. Martins, "Green Opportunistic and Efficient Resource Block Allocation Algorithm for LTE Uplink Networks ", in proceedings of 3rd IEEE GreenComm online conference, Oct. 2013.
- M.V.V. Reddy, E. Vivier, **F. Z. Kaddour**, "Joint benefits of Fractional Frequency Reuse and Relays in LTE Networks ", in proceedings of 3rd IEEE GreenComm online conference, Oct. 2013.
- L. Mroueh, E. Vivier, **F.Z. Kaddour**, M. Pischella and P. Martins, "Combined ZF and ML Decoder for Uplink Scheduling in Multi-User MIMO LTE Networks ", in proceedings to IEEE International Symposium on Personal, Indoor and Mobile Radio Communications (PIMRC), London, UK, Sept. 2013.
- **F.Z. Kaddour**, P. Martins, L. Decreusefond, E. Vivier and L. Mroueh, "Outage probability upper's bound in uplink Long Term Evolution networks with multi QoS users classes ", in proceedings of IEEE Global Communications conference (GLOBECOM), Atlanta, USA, Dec. 2013.
- **F.Z. Kaddour**, M. Pischella, P. Martins, E. Vivier and L. Mroueh, "Opportunistic and Efficient Resource Block Allocation Algorithms for LTE Uplink Networks", in proceedings of IEEE Wireless Communications and Networking Conference (WCNC), Shanghai, China, Apr. 2013.
- **F.Z. Kaddour**, E. Vivier, M. Pischella and P. Martins, "A New Method for Inter-Cell Interference Estimation in Uplink SC-FDMA Networks", in proceedings of IEEE Vehicular Technology Conference (VTC) Spring 2012, Yokohama, Japan, May. 2012.
- A. Kessab, **F.Z. Kaddour**, E. Vivier, L. Mroueh, M. Pischella and P. Martins, "Gain of Multi-Resource Block Allocation and Tuning in the Uplink of LTE Networks", in proceedings of IEEE International Symposium of Wireless Communication System (ISWCS), Aug. 2012.

Chapter 2

Preliminaries

AS A STARTING point of this thesis, this chapter provides a background on the technical and the mathematical tools that will be relevant to further developments. Some technical preliminaries on various aspects of LTE systems are introduced with a special focus on the uplink of radio resource management. Both physical and Medium Access Control (MAC) layers are also detailed. Then, we provide a unified system model for wireless transmission taking into account Single Input Single Output (SISO), Multiple Input Multiple Output (MIMO) and Multi-User MIMO (MU-MIMO) systems. Finally, we provide some mathematical background on the Poisson point process. These tools will be later used in Chapter 4 to compute the dimensioning outage probability due to the lack of resources in LTE networks.

2.1 LTE system technical specificities

In this section, we review from [24] [9] the main specificities of the LTE system covering its performance targets and the physical and medium access layers. We also provide a comparative study of the advantage in terms of PAPR[1] of the use of SC-FDMA technique rather than OFDMA one.

2.1.1 LTE performance targets

The goal of LTE standards aim at creating a new technology providing higher data rates, larger coverage area, lower latency and higher spectral efficiency. These objectives are largely reached due to a new architecture and a new air interface. LTE is a simplified architecture which refers to a reduced number of access nodes between the UEs and the core network. Only the eNB is considered as an

[1] PAPR is a ratio between the peak amplitude squared and the average power squared.

access component in the Evolved-Universal Terrestrial Radio Access Network (E-UTRAN), between UE and the Evolved Packet Core (EPC) network. It is considered as the terminal point of the RAN. LTE realize on OFDMA modulation. It supports a flexible bandwidth which can be 1.4, 3, 5, 10, 15 and 20 MHz [9]. It is useful for mobile operators that can not guarantee a contiguous 20 MHz bandwidth on account of the fragmentation of spectrum allocation. The flexible bandwidth allows several combinations of Carrier Aggregation (CA), that are added in LTE-A (Release 10). Actually, each component carrier has one of the standard bandwidths cited above, and the maximum number of carrier components that can be aggregated, is set to five. Thereby, the maximum allocated bandwidth reaches 100 MHz [25]. Within a 20 MHz bandwidth, the LTE peak data rate reaches 75 Mbps in downlink and 50 Mbps for SISO uplink, and up to 350 Mbps in uplink with 4×4 MIMO antennas. In the SISO case, the peak data rate corresponds to 5 bps/Hz in downlink and 2.5 bps/Hz in uplink, which is higher than the spectral efficiency reached with the HSPA networks [19].

2.1.2 Orthogonal Frequency Division Multiplexing

The wireless local area networks IEEE 802.11a and wireless metropolitan area networks IEEE 802.16-2004 standards are the first technologies which introduce the multi-carrier technique by using OFDM/TDMA mode, in the communication networks. OFDMA was first adopted in 2005 by the mobile services of WiMAX [26]. But it was revealed by the 3GPP LTE which adopted it in downlink and adapted it for the uplink by introducing the SC-FDMA. OFDM divides the available bandwidth into orthogonal narrowband subcarriers. This results in a flat fading channel in each subcarrier. The subcarriers can then be allocated in an opportunistic way. Each UE will be allocated subcarriers where it experiences good radio channel conditions. The techniques based on OFDM modulation are efficient in opportunistic allocation. Increasing the number of subcarriers introduces a multi-user diversity. Consequently, the probability that all the users are in a deep fade in all subcarriers decreases. The data symbols are transmitted over orthogonal subcarriers which leads to an inter-symbol interference cancellation. The orthogonality is obtained with an Inverse Fast Fourier Transform (IFFT) at transmission, and a Fast Fourier Transform (FFT) at reception with an adequate regular spacing frequency [21]. The robustness of the OFDM technique in case of multi-path is reached with the insertion of the Cyclic Prefix (CP). The CP is a duplication of the last temporal information of each OFDM symbol at the beginning of this symbol (Figure 2.1). Then, even in case of delay in radio transmission, all the symbols will be recovered.

Figure 2.1: Cyclic Prefix of an OFDM symbol

2.1.3 OFDM based LTE multiple access techniques

In the following, two access technique based on OFDM are presented: the OFDMA and the SC-FDMA.

Orthogonal Frequency Division Multiple Access - OFDMA

OFDMA is a multiple access technique based on OFDM physical layer. It allows a multiple access and shares simultaneously the available frequency bandwidth over multiple users. The drawback of the OFDMA technique is the high generated PAPR, which relates on the power amplifier efficiency at the transmitter. The power amplifier should operate in very large linear region to overcome the distortion of the signal peaks into non-linear region. This leads to an increase of the power amplifier complexity design and an expensive UEs.

Single Carrier Frequency Division Multiple Access - SC-FDMA

Due to a high PAPR, OFDMA use in uplink is not adapted to mobile terminal constraint (because of the battery autonomy). Then, its variant SC-FDMA, termed also DFTS-OFDM (for Discrete Fourier Transform Spread-OFDM), was adopted for the uplink of the LTE networks. This technique consists in adding a FFT at the beginning of the transmission (before the subcarrier mapping) and an IFFT at the end of the reception (after the subcarrier remapping and equalization). With FFT/ IFFT a large number of zeros symbols are added to obtain a power 2 number of subcarriers. This aims at reducing the PAPR [21]. Both OFDMA and SC-FDMA techniques block diagrams are given in Figure 2.2.

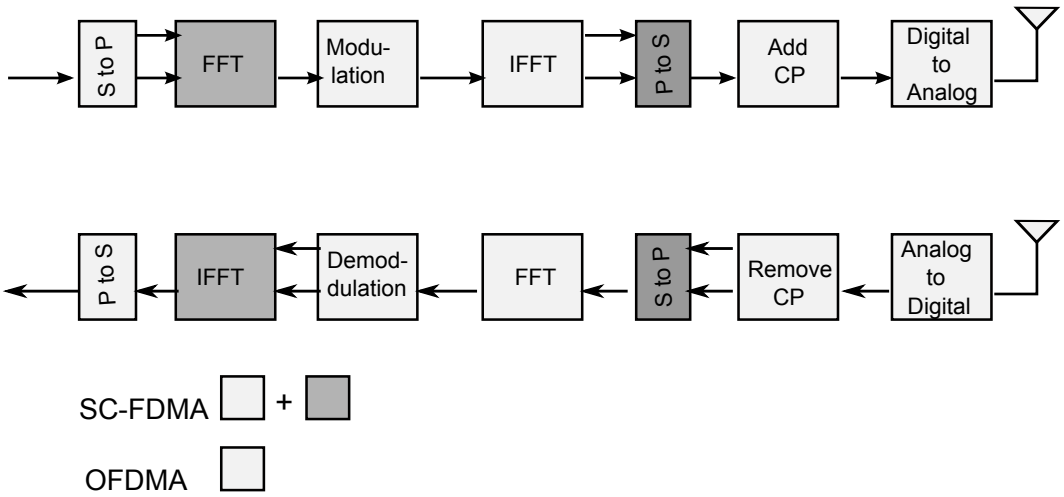

Figure 2.2: OFDMA and SC-FDMA technique block diagrams for LTE

SC-FDMA advantages

Thanks to the FFT mapper block added by the SC-FDMA technique, which spreads the information over multiple subcarriers, the SC-FDMA inherits of the OFDM frequency diversity gain. Two

SC-FDMA types were proposed: Interleaved SC-FDMA (I-SC-FDMA) and Localized SC-FDMA (L-SC-FDMA). In I-SC-FDMA, the symbols are spread over subcarriers and complete the N points of FFT with zeros symbols in-between. L-SC-FDMA centralizes the data symbols in a portion of adjacent subcarriers and complete the N FFT points with zero symbols as shown in figure 2.3.

Since the information are spread over the entire bandwidth, the I-SC-FDMA is more robust to the

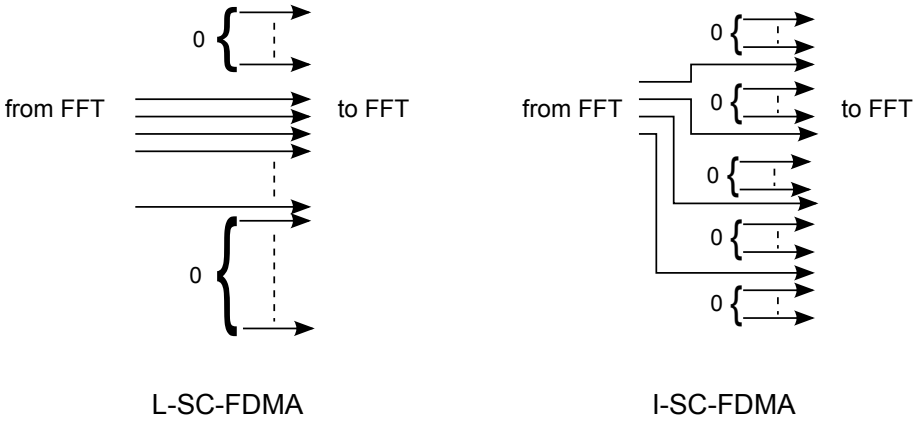

Figure 2.3: Interleaved and Localized SC-FDMA

frequency selective fading and offers an additional frequency diversity gain compared to the classical OFDMA. The L-SC-FDMA, in combination with a channel dependent scheduling, can potentially offer multi-user diversity in frequency channel conditions [20].

The major advantage of SC-FDMA over OFDMA is the low generated PAPR while transmitting the signal. Authors of [22] compare the generated PAPR between OFDMA and the two SC-FDMA types: I-SC-FDMA and L-SC-FDMA. The study reveals that the I-SC-FDMA gives better performances than the L-SC-FDMA. Actually, I-SC-FDMA generates a PAPR, in case of QPSK modulation, which is about 10 dB lower than the one generated by OFDMA. Whereas, the PAPR generated by the L-SC-FDMA is only about 3 dB lower. However, the SC-FDMA modulated signal can be viewed as a single carrier signal. A pulse shaping filter can be applied to the transmitted signal. As a result, the PAPR performances of I-SC-FDMA are degraded, while the L-SC-FDMA performances are unchanged [20] [22]. Consequently, the overall PAPR performances of L-SC-FDMA are better than the I-SC-FDMA ones. Therefore, L-SC-FDMA was finally adopted for the uplink of LTE release 8 networks.

As a consequence for our thesis, the subcarriers adjacency constraint will be considered for radio resource allocation to UEs. This constraint will not be taken into account in LTE-A networks. Actually, since carrier aggregation was adopted by the standards in LTE-A in order to increase the data rate, the component carriers can belong to different operating bandwidth. Then, in order to support the carrier aggregation in the uplink, as well in downlink, the I-SC-FDMA was adopted which enables frequency selective scheduling within carrier components [27].

2.1.4 LTE RB allocation constraints

By adopting L-SC-FDMA in LTE release 8, the RB allocation in our thesis should consider the following constraints:

1. **Contiguity constraint**: the L-SC-FDMA technique requires contiguous subcarriers for each UE. Then to obtain an optimal PAPR, the RBs allocated to each UE should also be contiguous in the frequency domain.
2. **Modulation and Coding Scheme (MCS) robustness**: the MCS summarizes the modulation type and the coding rate that are possible for data transmission. The MCS configuration depends on the radio channel conditions, expressed by the Signal to Interference plus Noise Ratio (SINR) experienced by each UE on each RB. The SINR level translates the received signal and the receiver ability to decode correctly the sent information. The SINR level required for each modulation and coding scheme is given in Table 2.1, taken from [2] and restricted to the MCS considered in this thesis: QPSK, 16 QAM and 64 QAM modulations with $\frac{1}{2}$, $\frac{2}{3}$ and $\frac{3}{4}$ coding rates. The high order modulation is more sensitive to bad channel conditions than the low order modulations, due to higher density constellation that the receiver should decode. Thereby, the adapted coding rate should be chosen in order to allow error correction. To keep the control information overhead small, the same MCS is used by each UE over its whole allocated bandwidth [28]. This constraint is called the MCS robustness.

SINR range (dB)	Modulation	Code rate
$-7 < SINR \leq -5$	QPSK	0.07
$-5 < SINR \leq -3$	QPSK	0.11
$-3 < SINR \leq -1$	QPSK	0.18
$-1 < SINR \leq 1$	QPSK	0.30
$1 < SINR \leq 3$	QPSK	0.43
$3 < SINR \leq 5$	QPSK	0.58
$5 < SINR \leq 7$	16QAM	0.36
$7 < SINR \leq 8.5$	16QAM	0.47
$8.5 < SINR \leq 10$	16QAM	0.60
$10 < SINR \leq 11.5$	64QAM	0.45
$11.5 < SINR \leq 13.5$	64QAM	0.55
$13.5 < SINR \leq 15$	64QAM	0.65
$15 < SINR \leq 17$	64QAM	0.75
$17 < SINR \leq 19.5$	64QAM	0.85
$SINR \geq 19.5$	64QAM	0.92

Table 2.1: SINR to Code rate mapping [2]

The contiguity constraint makes the RB allocation less flexible and adds more challenges to the RRM entity. Thus, most RRM strategies proposed for LTE downlink can not be directly used for the uplink. For this purpose, new RB allocation algorithms, respecting the LTE release 8 SC-FDMA constraints, are proposed in Chapter 5. Since the I-SC-FDMA technique is used for LTE-A networks,

the contiguity constraint is cancelled, while maintaining the MCS robustness constraint. Thus, we prove that with small modifications, our proposed RB allocation algorithms, can also be applied to LTE-A networks.

2.1.5 Uplink LTE frame structure

Considering LTE FDD, the same frame structure is applied in both uplink and downlink. Each frame consists of ten subframes of 1 ms each. One subframe is defined as two consecutive slots, where the time slot duration is 0.5 ms. In case of SC-FDMA technique, the signal transmitted in each slot is described with a grid of N_{RB}^{UL} contiguous RBs. One RB is the smallest grid that can be allocated to one UE. It consists of N_{sc}^{RB} equal to 12 consecutive subcarriers and N_{symb}^{UL} equal to 6 or 7 SC-FDMA symbols according to the prefix cyclic type [24]. The frame structure described in Figure 2.4 considers a normal cyclic prefix.
Different number of RBs are available according to the flexible standardized LTE bandwidths, as detailed in Table 2.2.

Channel bandwidth (MHz) B	1.4	3	5	10	15	20
FFT size	128	256	512	1024	1536	2048
Number of subcarriers	72	180	300	600	900	1200
Number of available RBs	6	15	25	50	75	100

Table 2.2: Bandwidth vs number of available RBs [3]

2.1.6 QoS in LTE

Unlike previous cellular systems, LTE has been designed to support only packet-switched services. It aims at providing seamless IP connectivity between UEs and the Packet Data Network (PDN), without disturbing the user's applications during mobility. QoS support in LTE is provided through an Evolved Packet System (EPS) bearer. An EPS bearer is established when a UE connects to the PDN and is categorized into either a Guaranteed Bit Rate (GBR), or a non Guaranteed Bit rate (non-GBR) bearer, depending on whether the user has a minimum guaranteed bit rate requirement or not. The QoS parameters that are set and controlled by a Policy and Charging Control (PCC) architecture within the EPC network are: the Allocation Retention Priority (ARP) which helps the network to decide which RBs are kept in congestion case, the Maximum Bit Rate (i.e. a limit on data rates: no radio bearer exhausts the network resources), the GBR, and the QoS Class Identifier (QCI). The QCI defines a set of characteristics that describe the packet forwarding treatment between the UE and the EPC. These characteristic are: the bearer type, the packet delay budget (between the UE and the EPC), and the Packet Loss Rate. They are summarized in the 3GPP standards [29].

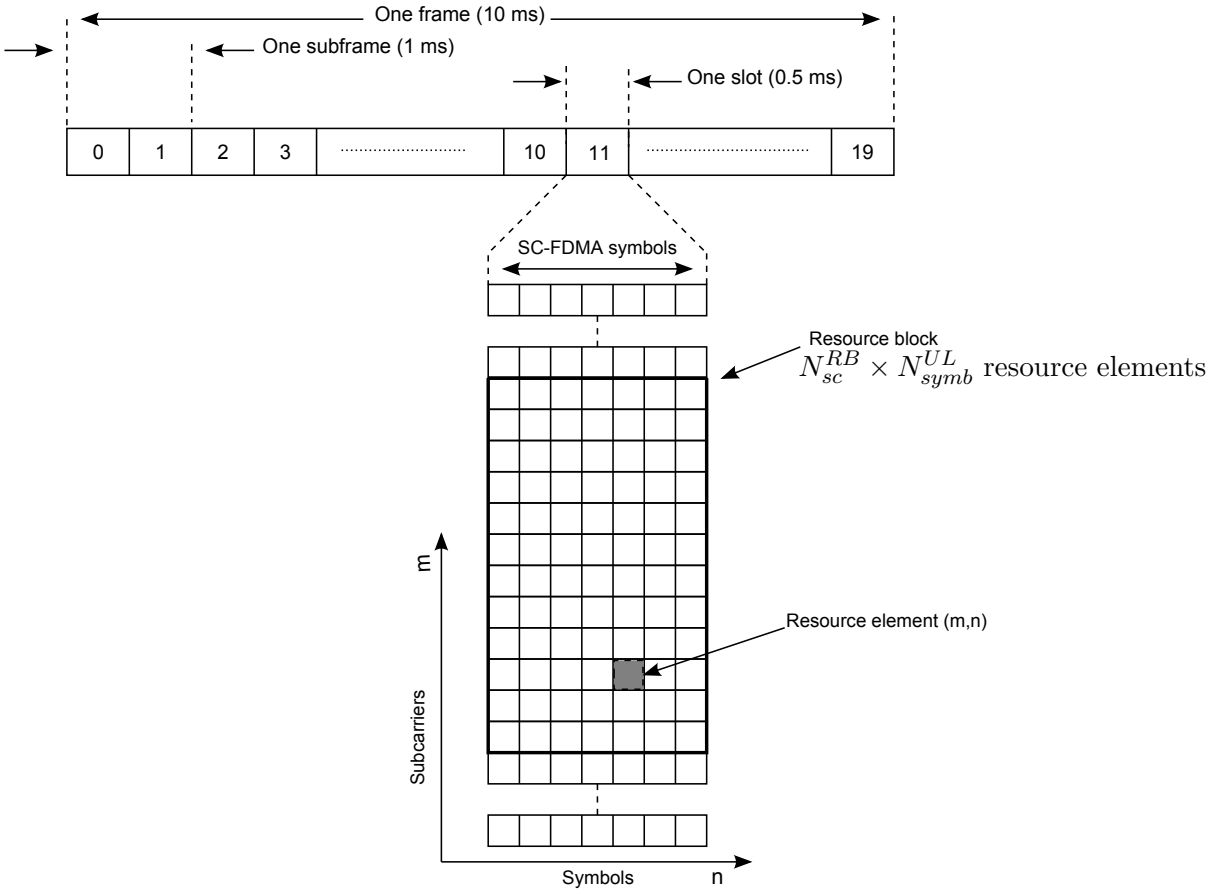

Figure 2.4: LTE FDD frame structure

2.1.7 Radio resource management

The parameters cited above are considered by the Radio Resource Management (RRM) which plays a crucial role in LTE networks by managing the limited radio resources in such a way that the radio transmission is as efficient as possible. In E-UTRAN, the role of RRM focuses on two major tasks:

1. **Radio Admission Controller (RAC)**: which is responsible for examining UEs admission requests for new connections. The admission control is performed considering the available resources, the current network's load and the QoS required by the UEs [28].
2. **Packet Scheduler (PS)**: which refers to the allocation of RBs to the UEs considering the link adaptation. According to [30], the PS can be uncoupled into two entities : (i) Time Domain Packet Scheduling (TDPS) which establishes the priority between the users selected by the RAC, and (ii) Frequency Domain Packet Scheduling (FDPS) which searches the pair (RB,UE) that maximizes the utility function. These two entities are illustrated on Figure 2.5.

Adapted management of radio resources optimizes the system performance and also reduces the cost per bit transmitted over the radio interface. In SISO, the number of users that can be served during one TTI is limited by the number of available RBs in the allocated bandwidth (the number of served

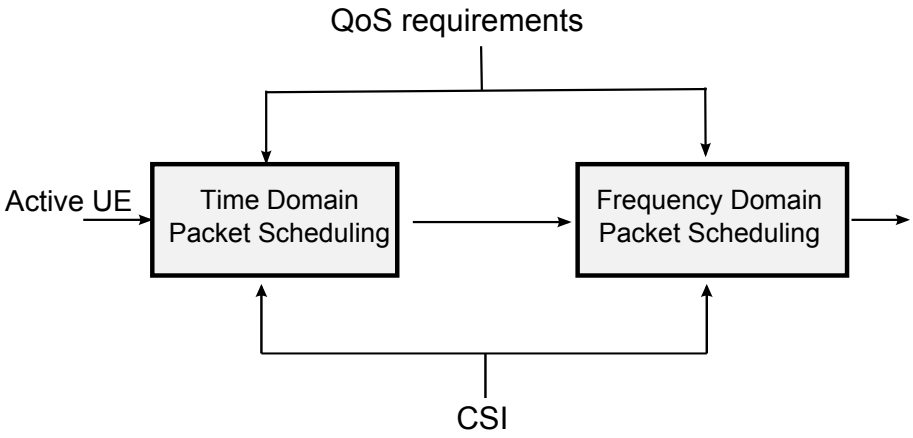

Figure 2.5: Packet Scheduler design

users will not exceed the number of available RBs within the allocated bandwidth Table 2.2). The uplink scheduler must map efficiently the RBs among users considering the limited UE transmission power. LTE uplink scheduling can be addressed as an optimization problem, where the desired solution is the mapping between the schedulable UEs and the RBs, that maximizes the desired performance target. Solving the scheduling problem can be very complex due to the high number of factors to take into account, as well as the virtually unlimited number of scheduling patterns to examine. In addition, the packet scheduler faces the hard-time constraints where the scheduling is done at the frequency of subframes which corresponds to one TTI. As the TTI duration is equal to 1 ms, the scheduler has only few milliseconds to come up with the optimal allocation scheme. We can divide the scheduling problem in two subproblems :

1. **Utility function**: a mathematical function that translates into a metric the satisfaction of the system related to its target. These target requirements can refer to performance metrics such as data throughput (total throughput of the system or throughput per UE), fairness (in terms of throughput or resources), minimization of transmission power, or minimization of the dimensioning outage probability. The utility function depends on the metrics used in the time domain (M^{TD}) and the frequency domain (M^{FD}) packet scheduling respectively. The utility function that user k experiences in the resource block c can be computed as :

$$U_k \rightarrow M^{TD}(k).M^{FD}(k,c) \tag{2.1}$$

   Usually, M^{TD} and M^{FD} measure the quality of the radio channel. In this case, the scheduler is called *channel-dependent*.
2. **Allocation policy**: the allocation policy involves the strategies and algorithms that the network adopts to allocate the radio resources to the users. These strategies are defined by the operators. Dynamic resource allocations are applied. They take the users QoS requirements into consideration in order to satisfy the served users. The allocation policy aims at limiting the network's congestion and enhancing the service quality [31].

In this thesis, only the frequency domain packet scheduling is considered. Since the metric used is the SINR experienced by each UE over each RB at each TTI, and the allocations of RBs performed at each TTI are independents, we prefer to use for the algorithm we propose the term *RB allocation* instead of *scheduling*.
Chapter 4 focuses on fair and opportunistic RB allocation algorithms to evaluate the dimensioning outage probability upper bound. These two algorithms are the extreme cases. The dimensioning outage probability of other RB allocation algorithms will be lower bounded and upper bounded by opportunistic and fair RB allocations. In Chapter 5, other RB allocation algorithms are investigated, such as the OEA and the QoS based OEA algorithms. The proposed algorithms are compared with the most cited RB allocation algorithms for LTE uplink networks, in the literature. An extension of the algorithm is proposed in MU-MIMO context (Chapter 6).

2.2 Wireless channel model

In this section, we provide a unified model for the propagation over the wireless channel when communicating over the uplink channel, from the UE towards the eNB. We first review the modeling of the transmission of SISO system when using OFDM technique and, taking into account the eNB and UE transmission power's and antenna's gains, the path loss propagation model, the fading and the shadowing parameters. Then, we define for this channel model the effective SINR computation. We give then a brief overview on the MIMO systems and the diversity and spatial division multiplexing techniques. Then, we show how to compute the MIMO effective SINR using optimal and sub-optimal decoders. Finally, we recall the system model of multi-user MIMO uplink systems, focusing on the capacity region and the Spatial Division Multiple Access (SDMA) techniques.

2.2.1 Cell types

There are four types of cells in LTE networks: macrocells, microcells, picocells, and femtocells. For urban areas, the cells used are macrocells, which cover areas in kilometers and serve a hundreds of users. Microcells cover smaller areas, and are added to improve the coverage in dense urban areas. In this thesis, we consider only macrocells, where the maximum inter-site distance in the regular network is set to 1.7 km. We assume that the eNBs are installed at a 30 m height and radiate with a maximum power P_{eNB} equal to 20 W (equivalent to 43 dBm).

2.2.2 User Equipment class

The user equipment is the device used directly by the end user to communicate. It can be a handheld telephone, a laptop computer equipped with a mobile broadband adapter, or any other device. Whatever the device, the UE specifications are given by the LTE standards. In [32], four UE classes are defined. Each class of UE has its specific transmission power and its tolerance. In this thesis, a UE

class 3 is used, implying a maximum transmission power P_{max} equal to 125 mW which is equivalent to 21 dBm.

2.2.3 Propagation model

Unlike wired media, the wireless medium is unreliable due to its broadcast nature and the propagation environment effects. The transmitted signal from the UE to the eNB which are separated with a distance r undergoes an attenuation due to the radio waves propagation, called path loss. To predict the signal attenuation and the coverage by the same way, many statistical models are proposed according the used frequency band, the type of deployment (urban, suburban, rural, etc), and the type of used technology. The most widely used propagation models are summarized in [33]. In LTE, there are three models that can be used: Okumura Hata, COoperation in Science and Technology (COST-231) and International Mobile Telecommunication (IMT-2000). In this dissertation, the Okumura Hata propagation model for urban area is used [5], where the path loss is expressed as:

$$P_L(r) = Kr^{-\beta} \tag{2.2}$$

with, K the path loss constant equal to $10^{\frac{-a}{10}}$, and β is the path loss exponent equal to $\frac{b}{10}$. The parameters a and b are computed according to the frequency carrier f_c and the UE and eNB heights set respectively to 1.5 m and 30 m. Table 2.3 summarizes the obtained Okumura Hata propagation model parameters according to the used frequency carrier.

$f_c(MHz)$	a	b
2600	137.7	34.4
800	117.85	34.4

Table 2.3: Okumura Hata propagation model parameters

2.2.4 eNB and UE antennas gains

Gains of antennas used for transmission and reception aim at improving the signal strength. Except in Chapter 4 where the eNB antenna is considered as omnidirectional with 0 dBi gain, in the rest of the thesis, tri-sectored eNB antennas are considered, whatever the network topology: regular networks or random networks. The antenna's radiation pattern used at each sector, taken from the LTE radio frequency system scenarii given in the standards [34], is expressed in dB as:

$$(G_A(\theta))_{dB} = (G_{eNB})_{dB} - \min\left\{12\left(\frac{\theta}{\theta_{3dB}}\right)^2, A_m\right\}, \qquad -180^\circ \leq \theta \leq 180^\circ \tag{2.3}$$

where G_{eNB} is the eNB antenna gain set to 17 dBi in the boresight direction, θ_{3dB} is the 3 dB beam width equal to 70°, and A_m is the maximum attenuation set to 20 dB.
In regular networks equipped with tri-sectored antennas, the angle between the users of each sector

and the antenna boresight does not exceed 60°. In this case, the antenna radiation pattern can be written as:

$$(G_A(\theta))_{dB} = (G_{eNB})_{dB} - 12\left(\frac{\theta}{\theta_{3dB}}\right)^2, \qquad -60° \leq \theta \leq 60° \tag{2.4}$$

This simplified antenna radiation pattern will be used in Chapter 3 for the ICI estimation analytical model.

The UE is equipped with an omnidirectional antenna with a transmission gain $G_M = 0$ dBi [32]. To be able to use the MIMO technique in Chapter 4 and 6, the UE will have four omnidirectional antennas.

2.2.5 Shadowing and fading effects

In addition to the path loss, the radio waves can encountered some obstacles that are present on the path. Then, the transmitted signal can be scattered, reflected or diffracted, which leads to additional attenuations. Each path can have a different amount of attenuation and delay. Two major effects are considered in this thesis:

a)- **Shadowing**
Shadowing is considered as a large-scale fading which results of attenuations due to signal diffraction around large objects in the propagation path. In our dissertation, we note the shadowing attenuation parameter A_s, which is modeled with a log-normal distribution.

b)- **Fast fading**
Fast fading coefficients, noted h, refer to rapid variations of the signal levels, due to multi-path scattering effects, time dispersion, and Doppler shifts that arise from relative motion between the transmitter and the receiver. Fast fading is called Rayleigh fading or Rician fading because when a large number of reflective paths is encountered, the received signal envelope is described by a Rayleigh or Rician probability density function (PDF)[2]. Considering, in this thesis, an urban area with multiple reflective paths with No-dominant Line-Of-Sight (NLOS) propagation path, Rayleigh fading is used.

1. **Uncorrelated Rayleigh fading**
Assuming uncorrelated fast fading, we consider the fading coefficients h as random variables following a Rayleigh distribution : $h \sim \text{Rayleigh}(\sigma)$, if $h = \sqrt{X^2 + Y^2}$, where the variables X and Y, following a normal distribution, i.e. $X \sim N(0, \sigma^2)$ and $Y \sim N(0, \sigma^2)$, are considered as independent. The uncorrelated fading coefficients are used for: 1) the robustness analysis of the ICI estimation model over fading effects (Chapter 3), and 2) the dimensioning study in MIMO systems (Chapter 4).
2. **Frequency correlated Rayleigh fading**
In the case of frequency correlated Rayleigh fading, the fading coefficients h^m with $1 \leq m \leq N_{sc}^{RB}$, are considered to be correlated in the frequency domain. So, each user expe-

[2]The Rice distribution is a generalization of the Rayleigh distribution.

riences a correlated fading over the subcarriers, with respect to the coherence bandwidth B_c. To generate a frequency correlated Rayleigh fading, a Fourier Transform of the Power Delay Profile (PDP) is used [1] [35]. Pedestrian users are considered in our simulation. The corresponding PDP value for six paths, taken from [4], are given in Table 2.4. The resulting frequency correlated fading coefficients are illustrated in Figure 2.6 for a bandwidth of 10 MHz and an FFT size of 1024. The frequency correlated Rayleigh fading is

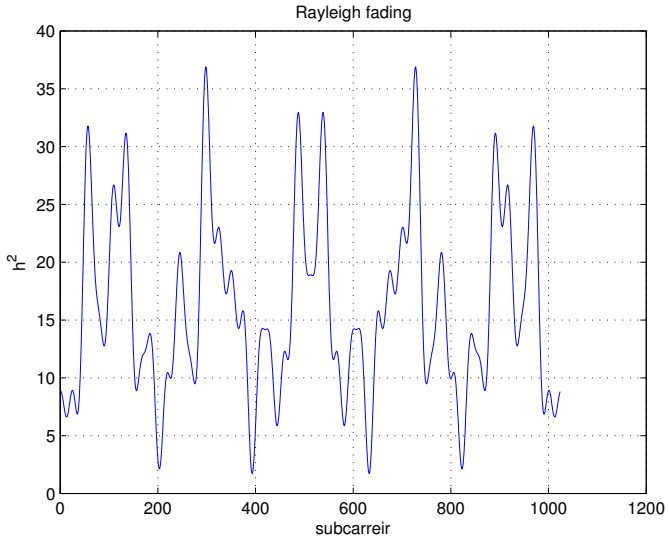

Figure 2.6: Correlated Rayleigh Fading-FFT based approach

used in instantaneous simulations such as in our thesis, for the performance study over one TTI of the RB allocation algorithm in MU-MIMO systems (Chapter 6).

Power of path (p_k) [dB]	0	-1	-9	-10	-15	-20
Path delay (τ_k) [μs]	0	0.3	0.7	1.1	1.7	2.5

Table 2.4: Multi-tap channel: power delay profile [4]

3. **Time-frequency correlated Rayleigh fading**
   Here, we consider that each UE experiences different fast fading coefficient $h^{(m,n)}$ over the different resource elements of one RB (i.e. $1 \leq m \leq N_{sc}^{RB}$ and $1 \leq n \leq N_{symb}^{UL}$). The fast fading coefficients are assumed to be correlated in time and frequency, with a correlation factor of $\alpha_{cor} = 0.5$. The used method to generate a time-frequency correlated fast fading coefficients is presented in Appendix A.2.
   Figure 2.7 shows the variation of the fast fading coefficients over: 1) subcarriers: 1024 subcarriers corresponding to 10 MHz bandwidth, and 2) symbols: in 140 symbols which constitute one LTE FDD frame of 10 ms. This kind of fading coefficients is used in Chapter 5, where the proposed RB allocation algorithms performance analysis is given through 1000 TTI simulations.

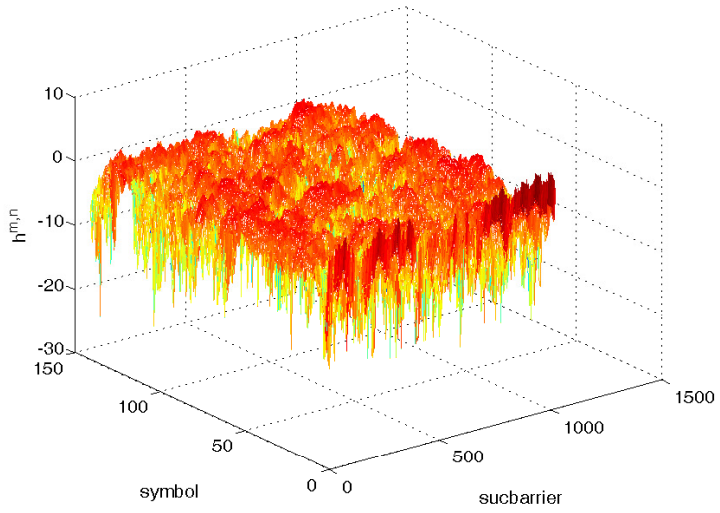

Figure 2.7: Time-Frequency correlated Rayleigh fading

After an overview of the wireless channel propagation signal, we give in the following section how can we use these parameters to compute the effective SINR of each UE over each RB in SISO, MIMO and MU-MIMO systems.

2.3 Effective SINR computation in point-to-point and multi-user systems

Before transmitting their data, the UEs need information about their channel conditions, which are measured thanks to the SINR. While the RB is the smallest grid to be allocated to one UE, the SINR computation smallest grid is one Resource Element (RE). The SINR that each UE k experiences on each RE (m, n) is expressed as:

$$\gamma_k^{(m,n)} = \frac{P_{k,eNB}^{(m,n)}}{N + I_{eNB}^{(m,n)}} \tag{2.5}$$

where $P_{k,eNB}^{(m,n)}$ is the received power of the transmitted signal from UE k at the eNB level. N is the noise in the frequency bandwidth (i.e. the subcarrier m). In practice, the noise is predominantly thermal and it can be calculated with the following formula:

$$N = k_B T B \tag{2.6}$$

with $k_B = 1.38\ 10^{-23}$ the Boltzmann constant, $T = 290\ K^\circ$ the receiver ambient temperature and B the frequency bandwidth, corresponding, in this case, to the subcarrier spacing (15 kHz).
Since orthogonal modulation is used, the intra-cell interference are cancelled and only the inter-cell interferences are considered. Thus, $I_{eNB}^{(m,n)}$ represents the ICI level received at the eNB level on the RE

(m, n), and results from the frequency reuse pattern strategy.
Over the whole RB c, the effective SINR of UE k can be deduced from the grid SINRs $\gamma_k^{(m,n)}$, using the mean instantaneous capacity method, defined in [34], such that,

$$\gamma_{(k,c)}^{\text{eff}} = 2^{C_k / N_{symb}^{UL}} - 1 \tag{2.7}$$

where C_k is the normalized capacity computed as:

$$C_k = \frac{1}{N_{sc}^{RB}} \cdot \sum_{i=1}^{N_{symb}^{UL}} \sum_{j=1}^{N_{sc}^{RB}} \log_2 \left(1 + \gamma_k^{(m,n)}\right) \tag{2.8}$$

The power $P_{k,eNB}^{(m,n)}$ received at the eNB level from UE k depends on the UE transmission power per RB, the channel propagation parameters, and the system used as detailed in the following subsections.

2.3.1 Single Input Single Output (SISO) systems

In point-to-point transmission, only one antenna is used at the transmitter side and at the receiver side, as illustrated in Figure 2.8. The UE data transmission is ensured by a SISO channel, and the total UE transmission power is used on this channel. Then, the power of the signal received at the

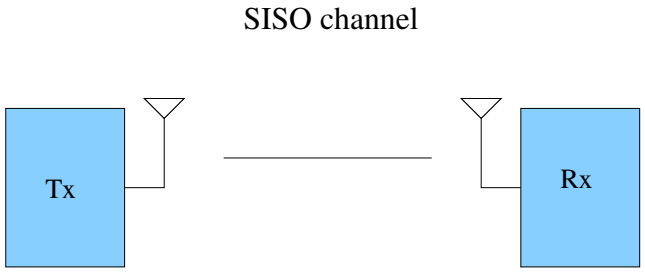

Figure 2.8: Point-to-point transmission

eNB level from UE k is expressed as:

$$P_{k,eNB}^{(m,n)} = P_{k_{Tx}}^{(m)} \ \Lambda \mid A_f \mid^2 \tag{2.9}$$

where $P_{k_{Tx}}^{(m)}$, the UE k transmission power over subcarrier m, is given as a function of the UE transmission power per RB $P_{k_{Tx}}$ as:

$$P_{k_{Tx}}^{(m)} = \frac{P_{k_{Tx}}}{N_{sc}^{RB}}$$

Λ groups the antennas gains, the path loss and the shadowing coefficient as follows:

$$\Lambda = P_L(r) \ G_A(\theta) \ G_M \ A_s \tag{2.10}$$

where r and θ are respectively, the distance between UE k and the eNB and the angle between the UE and the eNB boresight antenna.
The fast fading coefficient A_f is equal to h, h^m or $h^{(m,n)}$ according to the considered fast fading type: uncorrelated, frequency correlated or time-frequency correlated.

2.3.2 Multiple Input Multiple Output (MIMO) systems

In MIMO systems, multiple antennas are used at both the transmitter and the receiver sides. This has the advantage of generating a diversity between UE antennas and eNB antennas, which is represented by a channel matrix having the fading coefficients as elements. One of the main advantage of using MIMO system is the possibility to multiplex different data streams on the different antennas. The number of separable data streams is equal to the rank of the channel matrix. Moreover, when using adequate space time coding, these different schemes can benefit from the different channel paths and hence increase the communication robustness by exploiting the diversity gain. This latest sends the same data coded informations over multiple paths with independent uncorrelated fading paths. Then, if one or more paths are in deep fading, the data can be successfully transmitted over an other path. When the channel is perfectly known at the transmitter side, waterfilling algorithm is used to distribute efficiently the power among the different eigen modes by allocating low power to the low eigen modes and high power to the highest ones [36]. When the total power is very low, this corresponds to allocating the whole power to the strongest eigen mode. However, for high SINR, this corresponds to an uniform power allocation. The full channel knowledge at the transmitter side is not always feasible in a practical system. The power is uniformly distributed among all the antennas without penalizing the maximal number of data streams that can be transmitted. Unless clearly mentioned, we assume in this thesis that the wireless channel is only known at the receiver side, without any knowledge of the channel at the transmitter side, even in MIMO systems.

In the following, we consider the transmission over a MIMO system as depicted in Figure 2.9, when

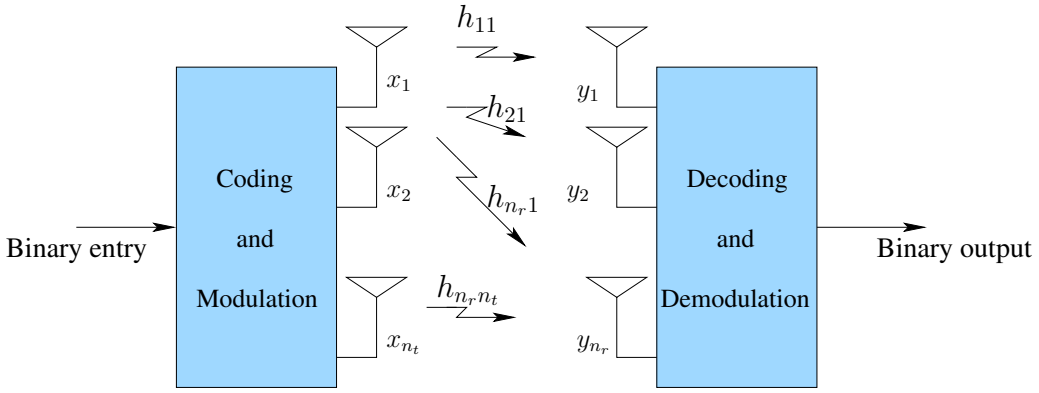

Figure 2.9: Multiple Input Multiple Output system

having n_t antennas at the transmitter side (the UE) and n_r antennas at the receiver side (the eNB). In the uplink of LTE release 8, there are up to 4 antennas at the eNB side and only one antenna is used

for transmission at the UE side. In LTE-A, there are up to 8 antennas at the eNB and 4 antennas at the UE, and four layers are allowed in uplink (4×4 MIMO). We assume that this MIMO system is studied in a LTE context using an OFDM system. The transmission with MIMO is characterized by the fading coefficients $h_{i,j}$ between the antenna j of the UE and the antenna i of the eNB. Notice that if two antennas are separated with a distance more than $\lambda/2$, the fading coefficients are then uncorrelated. The channel matrix $\mathbf{H}$ contains the fading coefficients $h_{i,j}$.
Let $\mathbf{x} \in \mathbb{C}^{n_t \times 1}$ denote the transmitted vector at each UE and at a given time-frequency slot. Then, the received signal $\mathbf{y} \in \mathbb{C}^{n_r \times 1}$ at the eNB and at this time-frequency slot[3] is,

$$\mathbf{y} = \sqrt{\frac{P_{k_{Tx}}^{(m)} \Lambda}{n_t}}\, \mathbf{H}\mathbf{x} + (\mathbf{z} + \mathbf{i})$$

where $\mathbf{z}$ is the additive noise vector with variance $\mathbb{E}[\mathbf{z}\mathbf{z}^\dagger] = N_0 \mathbf{I}_{n_r}$ and $\mathbf{i}$ is the interference that will be considered as Gaussian noise with mean $\mathbb{E}[\mathbf{i}\mathbf{i}^\dagger] = I_{\text{mean}}$. We assume that, in MIMO systems, the interference is treated as a noise at the eNB. The transmitted signal $\mathbf{x}$ is such that $\mathbb{E}[\mathbf{x}\mathbf{x}^\dagger] = 1$. When using a maximum likelihood decoder, the capacity of this MIMO system at a given time-frequency grid or resource element has been derived in [37] and is such that,

$$C_{\text{MIMO}}^{(\text{m,n})} = \log_2 \det \left(\mathbf{I}_{n_r} + \frac{P_{k_{Tx}}^{(m)} \Lambda}{n_t (N_0 + I_{\text{mean}})}\, \mathbf{H}\mathbf{H}^\dagger \right) = \min(n_t, n_r) \log_2 (1 + \gamma_k^{(m,n)}) \tag{2.11}$$

The effective SISO SINR over one RE required to decode one data stream can be then computed as,

$$\gamma_{\text{k}}^{(\text{m,n})} = 2^{\frac{C_{\text{MIMO}}^{(m,n)}}{\min(n_t, n_r)}} - 1 \tag{2.12}$$

and the effective SISO SINR over the whole RB can be deduced from Equation (2.8). Using the mapping between the SINR and the MCS, the SISO spectral efficiency per-stream can be deduced and the MIMO spectral efficiency corresponds to the SISO spectral efficiency multiplied by $\min(n_t, n_r)$.

2.3.3 Multi-User MIMO (MU-MIMO) system

We consider a multi-user MIMO uplink channel where we denote by $\mathcal{S}$ the set of simultaneously active UEs and $N_s = |\mathcal{S}|$ its cardinality. The UEs having n_t antennas each want to communicate simultaneously with a common eNB equipped with n_r receive antennas. Multi-user MIMO technique allows the eNB to transmit or receive a signal to or from multiple users on the same time-frequency grid. Then, in uplink, the eNB can receive multiple signals transmitted from different users, carried on the same resource blocks (see figure 2.10).

We note $\mathbf{H}_k$ the channel matrix that contains the uncorrelated fading coefficients $h_{i,j}^{(k)}$ between the antenna j of UE k and the antenna i of the eNB. Let $\mathbf{x}_n \in \mathbb{C}^{n_t \times 1}$ denote the transmitted vector at

[3] Note that the time-frequency index is dropped here to simplify the notation.

each UE. Then, the received signal $\mathbf{y} \in \mathbb{C}^{n_r \times 1}$ at the eNB is,

$$\mathbf{y} = \sum_{k=1}^{N_s} \sqrt{P_{k_{Tx}}^{(m)} \ \Lambda_k} \ \mathbf{H}_k \mathbf{x_k} + (\mathbf{z} + \mathbf{i}) \tag{2.13}$$

where

$$\Lambda_k = P_L(r_k) \ G_A(\theta_k) \ G_M \ A_{s_k}, \tag{2.14}$$

$\mathbf{z}$ is the additive noise vector with variance $\mathbb{E}[\mathbf{z}\mathbf{z}^\dagger] = N_0 \mathbf{I}_{n_r}$, and $\mathbf{i}$ is the interference that will be considered as Gaussian noise with mean $\mathbb{E}[\mathbf{i}\mathbf{i}^\dagger] = I_{\text{mean}}$. We assume that the interference is treated as a noise at the eNB. The transmitted signal $\mathbf{x}_k$ is such that $\mathbb{E}[\mathbf{x}_k \mathbf{x}_k^\dagger] = 1$.
In LTE-A, the MU-MIMO techniques are implemented both in uplink and downlink as they improve the spectral efficiency and the system performances. The use of the same resource grid by different users simultaneously results in a co-channel interference, referred as: Multiple Access Interference (MAI) in the uplink, and Multi-User Interference (MUI) in downlink. Due to the multiple receive antennas, the MAI can be deleted at the receiver side using linear or non linear decoding which allow the detection of the transmitted signals from different UEs, even in case of a non perfect knowledge of the channel. The computation of the effective SINR in function of the transceiver will be detailed in Chapter 6.
We define the multi-user group $\mathcal{S}$ as a group of users that share the same RB. The users within a multi-user group are selected according to the multi-user group selection criteria specified by the RRM entity. When the number of users in a multi-user group increases, the system requires a more precise CSI, that we can not always predict precisely, and the scheduling algorithm complexity increases.

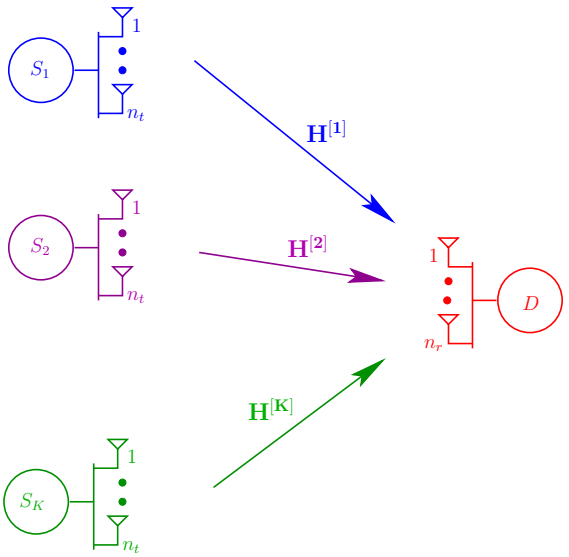

Figure 2.10: Multi-user Multiple Access Channel: N_s UEs with n_t antennas each and an eNB equipped with n_r antennas

2.3.4 Capacity region and Multiplexing gain

For $\mathcal{J} \in \mathcal{S}$ simultaneously transmitting UEs at a given RB, the capacity region contains the set of all feasible J-tuple $(R_1, \ldots, R_J)$ such that,

$$\sum_{k \in \mathcal{J}} R_k \leq \log_2 \left| \mathbf{I}_4 + \frac{P_{k_{Tx}}^{(m)}}{n_t} \frac{1}{N_0 + I_{\text{mean}}} \sum_{k \in \mathcal{J}} \Lambda_k \mathbf{H}_k \mathbf{H}_k^{\dagger} \right| \tag{2.15}$$

for all the possible sets $\mathcal{J} \subseteq \{1, \ldots, N_s\}$. The multiplexing region defines the maximal number of streams that can be decoded simultaneously at the eNB. Over one RB, let $N_{u,p}$ be the number of potential UEs among the total number N_{UE} of UEs in the cell, and r_l with $1 \leq l \leq N_{\text{UE}}$ be the number of streams submitted by UE l over one RE. Then, the multiplexing region $\mathcal{R}$ is defined as

$$\mathcal{R} = \{r_k \in \mathbb{N} : r_k \leq \min(n_t, n_r) \text{ and } \sum_k r_k \leq \min(n_r, N_{u,p} n_t)\}.$$

The $\min(n_r, N_{u,p} n_t)$ transmitted streams can be simultaneously decoded at the eNB side using suboptimal linear decoders (such as Zero Forcing (ZF) or Minimum Mean Square Error (MMSE) decoder) or other optimal decoders such as the Maximum Likelihood (ML) decoder. Although the ML decoder improves the theoretical total throughput compared to linear precoding schemes, this comes at the expense of an increased complexity at the eNB side.
In case of two UEs having $n_t = 3$ antennas and an eNB with $n_r = 4$ antennas, and as it can be seen from Figure 2.11, the number of streams per UE is limited to 3 and the total number of streams for both UE is limited to 4. The possible combinations are: $(1, 3); (2, 2); (3, 1)$.

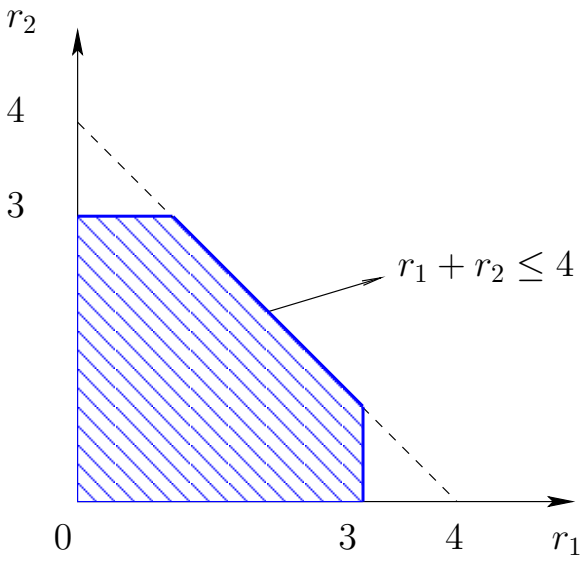

Figure 2.11: Multiplexing gain region for the case of two UEs having $n_t = 3$ antennas each and an eNB equipped with $n_r = 4$ antennas.

2.4 Mathematical basics

In this section, we review the main mathematical tools used in this thesis. We discuss about the use of the stochastic geometry and Poisson point processes in wireless communication systems modeling.

2.4.1 Stochastic geometry in wireless network

Considering the cellular networks as a regular network with hexagonal cells leads to intractable results unless a massive Monte Carlo simulations are run. In addition, the regular network is an unrealistic assumption, since the eNBs do not follow a hexagonal grid and specially in dense urban area where the inter-site distance are small and UE cell selection is determined by the channel conditions experienced by each UE. In this thesis, stochastic geometry is used to model the LTE networks. This leads to a random location of the networks components and also to model the system statistically with more tractable results. Among the point processes, the Poisson point process (PPP) are the most tractable [38]. In fact, it was studied first in wireless networks modeling by Bacceli [39]. The characterization of the interference distribution, the dimensioning outage probability, the transport capacity and connectivity or the delay in large ad hoc networks were studied in [40] [41] [42] [43] [44]. It was also used for modeling the time varying configuration of nodes and mobility in [45].

2.4.2 Poisson Point Process

The configuration $\varkappa$ in $\mathbb{R}^k$ is the set $\{x_n, n \geq 1\}$, where for each $n \geq 1$, $x_n \in \mathbb{R}^k$, $x_n \neq x_m$ for $n \neq m$ and each compact subset of $\mathbb{R}^k$ contains only a finite subset of $\varkappa$. A point process φ is a random variable with values in $\Omega_{\mathbb{R}^k}$, i.e. $\varphi(\omega) = \{X_n(\omega), n \geq 1\} \in \mathbb{R}^k$, where $\Omega_{\mathbb{R}^k}$ is a set of configurations in $\mathbb{R}^k$. For $A \subset \mathbb{R}^k$, we denote by φ_A the random variable which counts the number of atoms of $\varphi(\omega)$ in A:

$$\varphi_A(\omega) = \sum_{n \geq 1} 1_{X_n(\omega) \in A} \in N \cup \{+\infty\}$$

Poisson point processes are particular instances of point processes such that:

Definition 2.1 *Let Λ be a σ-finite measure on $\mathbb{R}^k$. A point process φ is a Poisson point process of intensity Λ in $\mathbb{R}^k$ whenever the following two properties hold:*

1. *For any compact subset $A \in \mathbb{R}^k$, φ_A follows a Poisson distribution of intensity $\Lambda(A)$ as:*

$$\mathbf{P}(\varphi_A = k) = \exp\left(\Lambda(A)\frac{\Lambda(A)^k}{k!}\right)$$

2. *For any disjoint subset A and B, the random variables φ_A and φ_B are independent.*

Assuming that the positions of the users are independent and identically distributed, the time between two consecutive users demands for service is exponentially distributed with surface density $\rho(x)$ and their service time follows an exponential distribution with mean $\frac{1}{\nu}$; then the point process of active

users positions is, in equilibrium, a Poisson point process with intensity $d\Lambda(x) = \frac{\rho(x)}{\nu}dx$.

Proof: For a region H, and respecting the assumption above, the number of active UEs is similar than the number of customers in a $M/M/\infty$ queue with input rate h and mean service time $\frac{1}{\nu}$. From [46], it is known that the number of UE U in equilibrium is:

$$\mathbf{P}(U = u) = \frac{(h/\nu)^n}{n!} exp^{\frac{-h}{\nu}}$$

Then, the number of active UEs follows the condition 1 of definition 2.1 is satisfied with intensity $\lambda(H)$ as:

$$\Lambda(H) = \frac{h}{\nu} = \int_H \frac{\rho(x)}{\nu} dx$$

Since the positions of the active UEs $x_n, n \geq 1$ are independent and identically distributed and their number follows a Poisson distribution, then $\varphi = \{x_n, n \geq 1\}$ is a Poisson point process. □

In the following, we describe some operations on the point process that preserve the Poisson point process law:

- *Superposition*: for n Poisson point processes $\varphi_1, \varphi_2, \cdots, \varphi_n$ of intensities $\lambda_1, \lambda_2, \cdots, \lambda_n$, with $n < \infty$, the superposition $\varphi = \sum_{i=1}^{n} \varphi_i$ is known to be a Poisson point process with intensity $\lambda = \sum_{i=1}^{n} \lambda_i$.
- *Thinning*: the thinning is the inverse of the superposition operation. Considering a Poisson point process φ of intensity λ and a function $p : \mathbf{E} \to [0, 1]$, the thinning of φ with retention function p is given by $\varphi^p = \sum \sigma_i \epsilon_{z_i}$, where the random variables $\{\sigma_i\}_i$ are independent given φ and $\mathbf{P}(\sigma_i = 1 \mid \varphi) = p(z_i) = 1 - \mathbf{P}(\sigma_i = 0 \mid \varphi)$. If p is λ measurable, then φ^p is a Poisson point process of intensity $p\lambda$ with $p\lambda(A) = \int_A p(z) d\lambda(z)$.
- *Transformation*: known also as a displacement theorem. We consider another σ-compact metric space $\mathbf{E}'$ and a probability kernel $p(z, .)$, i.e. for all $z \in \mathbf{E}$, $p(z, .)$ is a probability measure in $\mathbf{E}'$. The transformation of a Poisson point process φ by p with intensity λ in $\mathbf{E}$ is defined as $\varphi_p = \sum \epsilon_{z'_i}$, where $z'_1, z'_2, \cdots$ are independent given φ and has the probability $\mathbf{P}(z'_i \in A' \mid \varphi) = p(z_i, A')$. It is shown that φ^p is a Poisson point process of intensity $\lambda'(A') = \int_{\mathbf{E}} p(z, A') d\lambda(z)$.

2.4.3 Definition of a marked Poisson point process

If, to each point $x_n \in \mathbb{R}^k$ of the Poisson point process φ (i.e. the measurable space), is attached some information $y_n \in \mathbb{R}^l$, so-called marks, then we obtain $\tilde{\varphi}$ a marked point process.

Assuming that the law of Y_n depends only on the position x_n through a probability kernel $\mathcal{K}_r$, by the displacement theorem, we can prove that $\tilde{\varphi} = \{(x_n, y_n), n \geq 1\}$ is a Poisson point process of intensity $\mathcal{K}_r(x, dy) d\Lambda(x)$ on $\mathbb{R}^k \times \mathbb{R}^l$.

Proof: Let define the configuration of the form as $\{(x_n, y_n), n \geq 1\}$ where for each $n \geq 1, x_n \in \mathbf{R}^k$ and $y_n \in X$. Then, the couple (x_n, y_n) is defined on $\mathbf{R}^{k+m}$. Considering a Poisson point process $\varphi = \{x_n, n \geq 1\}$ with position dependent marking as a marked point process for which the law of the

marks y_n, the mark associated to the point located at x_n, depend only on x_n through a kernel $\mathcal{K}_r$:

$$\mathbf{P}(y_n \in B \mid \varphi) = \mathcal{K}_r(x_n, B), \qquad \text{for any } B \subset X \tag{2.16}$$

If $\mathcal{K}_r$ is a probability kernel, i.e., if $\mathcal{K}_r(x, X) = 1$ for any $x \in \mathbf{R}^k$ then, it is well known that $\tilde{\varphi}$ is a Poisson point process of intensity $\mathcal{K}_r(x, dy)d\Lambda(x)$ on $\mathbf{R}^k \times \mathbf{R}^{\mathbf{m}}$ $\square$.

2.4.4 Useful formulas

In the following, we introduce the well known and useful theorems and formulas, relevant in the Poisson point process domain [39] and references therein: the Campbell formula and the concentration inequality.

Theorem 2.1 (Campbell Formula) *Let X be a point process on φ and let $f :\to \mathbb{R}$ be a measurable function. Then the random sum*

$$F = \sum_{x \in X} f(x)$$

is a random variable, with expected value

$$\mathbb{E}\left[\sum_{x \in X} f(x)\right] = \int_{\varphi} f(x)\ \lambda(dx) \tag{2.17}$$

In the special case where X is a point process on $\mathbb{R}^d$ with an intensity function β, Campbell formula becomes:

$$\mathbb{E}\left[\sum_{x \in X} f(x)\right] = \int_{\varphi} f(x)\beta(x)dx \tag{2.18}$$

Theorem 2.2 (Marked Poisson point process - First moment) *Let $\tilde{\varphi}$ be a marked Poisson point process on $\mathbb{R}^k \times \mathbb{R}^l$. Let Λ be the intensity of the underlying Poisson point process and $\mathcal{K}_r$ the kernel of the position dependent marking. For $f : \mathbb{R}^k \times \mathbb{R}^l \to \mathbb{R}$ a measurable non negative function, let F be the sum of the realizations of f over $\tilde{\varphi}$*

$$F = \int f d\tilde{\varphi} = \sum_{n \geq 1} f(X_n, Y_n)$$

Using the Campbell formula, the first moment $\mathbf{E}(F)$ of F is obtained such that:

$$\mathbf{E}(F) = \int_{\mathbb{R}^k \times \mathbb{R}^l} f(x, y)\mathcal{K}_r(x, dy)d\Lambda(x)$$

To describe the variations of the Poisson point process when we add a new atom x at the configuration, we define the discrete gradient $D_x F(\omega)$.

Definition 2.2 *For $F : \Omega_{\mathbb{R}^k} \to \mathbb{R}$, for any $x \in \mathbb{R}^k$, the discrete gradient of F is:*

$$D_x F(\omega) = F(\omega \cup x) - F(\omega)$$

We notice that for $F = \int f d\varphi, \quad D_x F = f(x), \quad \forall x \in \mathbb{R}^k$.

From [47] [48] we consider the following theorem on which our results are based:

Theorem 2.3 (Concentration inequality [49]) *Assume that φ is a Poisson point process on $\mathbb{R}^k$ of intensity Λ. Let $f : \mathbb{R}^k \to \mathbb{R}^+$ a measurable non-negative function and:*

$$F(\omega) = \int f d\varphi = \sum_{n \geq 1} f(X_n(\omega))$$

be the sum of the realizations of the function f over the Poisson point process. Assume that $\mid D_x F(\omega) \mid \leq s$ for any $x \in \mathbb{R}^k$; therefore the two first moments of F, m_F and v_F, are expressed as:

$$m_F = \mathbf{E}[F] = \int f(x) d\Lambda(x) \tag{2.19}$$

and

$$v_F = \int \mid D_x F(\omega) \mid^2 d\Lambda(x) = \int f^2(x) d\Lambda(x) \tag{2.20}$$

Then, for any $\tau \in R^+$, the probability that $(F - m_F)$ exceeds τ is bounded by:

$$\mathbf{P}(F - m_F \geq \tau) \leq \exp\left(-\frac{v_F}{s^2} g\left(\frac{\tau \times s}{v_F}\right)\right) \tag{2.21}$$

with $g(t) = (1+t)\ln(1+t) - t$.

Introducing $\tau = (\alpha - 1) m_F$, the probability that the Poisson point process F exceeds αm_F can be upper bounded by P_{sup} as follows:

$$P_{\text{sup}} = \exp\left(-\frac{v_F}{s^2} g\left(\frac{(\alpha - 1) m_F s}{v_F}\right)\right) \tag{2.22}$$

This mathematical background is used in Chapter 4 to develop an analytical model of the upper bound of the dimensioning outage probability.

2.5 Conclusion

In this chapter, we reviewed some basic notions on LTE systems where we focus on the uplink radio access and the physical layer of this network. Then, we gave a unified system model for SISO, MIMO and MU-MIMO systems where we emphasize on the effective SINR of each system studied in a LTE context. These concepts will be useful in Chapter 3 for interference estimation and in Chapter 5 and Chapter 6 for the conception of radio resource allocation in SISO and MU-MIMO systems. Finally, some mathematical tools on Poisson point processes and the marked poisson processes were introduced and they will be reused in Chapter 4 for radio resource planning.

Chapter 3

Inter-Cell Interference estimation for green uplink LTE networks

Part of this chapter was published in IEEE VTC Spring 2012[1]

THIS chapter proposes an estimation method for inter-cell interference in a green uplink LTE networks. The proposed model takes into account the UE transmission power control. To the best of our knowledge, few works in the literature consider the inter-cell interference estimation in such conditions. The proposed model of ICI estimation results in a low computational complexity, where several iterations of Monte Carlo simulations are replaced by one operation. This model considers that the contribution of the interferers located in a sector is equivalent to the contribution of a virtual UE located at the barycenter of the considered interfering active users and radiating at their median power. The model is validated analytically and also by simulations. Its robustness against the environment variations such as the fading and the shadowing effects is also considered.

[1] F.Z. Kaddour, E. Vivier, M. Pischella and P. Martins, "A New Method for Inter-Cell Interference Estimation in Uplink SC-FDMA Networks", in proceedings of IEEE Vehicular Technology Conference (VTC) Spring 2012 , Yokohama, Japan, May. 2012.

3.1 Introduction

Radio resource management aims at maximizing the system utility function and improving the system performances. The RRM is based on a metric which translates the objective of the radio resource management. Usually, the main objective of the operators is the network's capacity maximization. This capacity can be expressed in terms of aggregate throughput, maximization of the individual throughput, number of served subscribers per cell, etc. To achieve this goal, the metric should take into account the users channel conditions, such as the signal to interference plus noise ratio that each user experiences over each resource block. The SINR depends on the UE transmission power, its channel conditions over the RB used for transmission and the interference level. Since the intra-cell interference is cancelled in LTE, the major challenge is the estimation of the inter-cell interference level. The ICI has always been the center of interest of researchers, especially on the uplink. Unlike downlink, where the interfering eNBs locations are known, the ICI on the uplink is caused by UEs in the neighboring cells that share simultaneously the same resource block. Their location is random and their transmission power, especially in green network, is not fixed. Hence, the estimation is more difficult. To mitigate the ICI, a proper frequency planning is performed. The reduction of the UE transmission power can also greatly reduce the ICI level, but increases the complexity of its estimation. Consequently, we aim at developing a new ICI estimation model for green LTE networks, where the UE transmission power is controlled. The proposed ICI estimation model is less complex and overcome the Monte Carlo simulations. The validation of the model is given by simulations, using the log ratio test and the Kullback-Leibler divergence test. An analytical validation is also investigated where the user's median and mean transmission power analytical model is developed.
In Section 3.2.1, the existing ICI mitigation methods are discussed. The adopted method of ICI mitigation is given in Section 3.2.2. The existing ICI estimation models, as well as the one we proposed, in LTE networks are developed in Section 3.3. The simulation results and analytical validation of the proposed model are respectively given in Section 3.4 and Section 3.5.

3.2 Inter-cell interference mitigation

3.2.1 ICI mitigation state of the art

When the frequency reuse is 1, the same frequency bandwidth is allocated to each cell of the network. If no power control is adopted, the resulting user's SINR becomes weak, especially for cell edge users which are more interfered by users served by the neighboring cells and using the same resource blocks. Hence, the network performances are degraded. To mitigate this inter-cell interference, we try to allocate different frequency bandwidths to adjacent cells (i.e. frequency reuse factor $K_f \geq 1$), and to reduce the transmission power of the interfering users, or a combination of these two techniques.
Many works were proposed in these topics. Authors of [50] present the effect of the frequency reuse factor on the downlink. A frequency reuse factor of 1 ($K_f = 1$) in downlink gives good performances in low loaded networks. These performances are degraded when the network's load increases. The

traditional frequency reuse factor of $K_f = 3$ uses three frequency bandwidths, where each one is allocated to one cell in a three cell pattern. Then, the inter-site distance between each interfering eNB is increased and the interference between them decreases by the same way. This observation is also valid in uplink: since the interfering UEs are further, the strength of the interfering signals decreases. With $K_f = 3$, good system performances are obtained, even in high loaded networks. However, such a frequency reuse factor decreases the spectrum efficiency, since only a third proportion of the spectrum is used for transmission in each cell. The study given by the authors of [51] and [52] exploits the advantages of $K_f = 1$ by managing the radio resource allocation. When the interference is high on one RB, the eNBs cooperate and agree on an allocation policy that decreases ICI level by allocating an other free RB to the most interfering UEs. A cooperative eNB network is detailed in [53]. The drawback of this method is a high signaling message load exchanged between the eNBs of the network. An open-loop fractional power control has been considered in [54] and inter-cell power control in [55]. In [56], the authors propose to decrease or increase the UE transmission power by 1 dB if needed. A power control depending on the bandwidth frequency was proposed in [57]. This method is usually known as a Soft Frequency Reuse (SFR). It combines frequency planning and power control, where a power level is allocated for each portion of the frequency bandwidth. Many combination schemes are proposed, while the main idea is to allocate three different power levels to each third portion of the bandwidth. A classification of the users in Cell Center Users (CCU) and Cell Edge Users (CEU) is proposed in [50] and [57], known as a Fractional Frequency Reuse (FFR). As the CEUs are the most interfered users, the authors propose to allocate them different frequency bandwidths with different power transmission levels (see [57] for downlink and [58] for uplink).
In order to mitigate ICI without considering frequency planning, a power control technique was proposed for the uplink, based on the power spectral density and a compensation of the path loss [59].

3.2.2 Adopted ICI mitigation

In our study, to mitigate the inter-cell interference we combine frequency planning and the control of the UE transmission power, as follows:

Frequency planning

For system performances reasons cited before, a frequency reuse factor $K_f = 3$ is adopted. The network is divided in patterns, where each pattern consists of N_c cells. There are N_s sectors per cell and N_f different frequency bandwidths per pattern. According to [60], we define a frequency reuse pattern by $N_c \times N_s \times N_f$. Excepted in Chapter 4, we choose to use tri-sectored antennas. Hence, the possible frequency reuse patterns that can be used are illustrated in Figure 3.1, and defined as follows:

(a) Frequency reuse pattern $(3 \times 1 \times 3)$: consists of three adjacent cells. Each cell is served by an antenna and is allocated a distinct bandwidth.
and
Frequency reuse pattern $(1 \times 3 \times 3)$: consists of one cell divided in three sectors, where each

sector is served by an antenna and is allocated a distinct bandwidth:

(b) The antenna boresight is equal to 0° and is radiating towards the further point of the sector.

(c) The antenna boresight is equal to 30°.

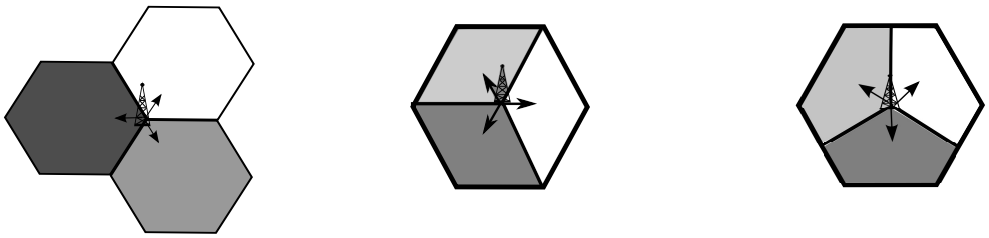

(a) (3x1x3) pattern (b) (1x3x3) pattern with boresight=0° (c) (1x3x3) pattern with boresight=30°

Figure 3.1: Frequency reuse pattern for tri-sectored antennas and $K_f = 3$

In this thesis, a frequency reuse pattern of $1 \times 3 \times 3$ with boresight of 0° is considered (Figure 3.1 (b)).

UE transmission power control

We consider a UE transmission power control depending on the user's QoS target. The power control aims at adapting the UE transmission power as a function of the channel conditions experienced by each UE on each RB and the SINR target (γ_{tg}) required by each UE to achieve its target QoS. Considering that UE k is allocated one RB c and its required QoS is offered with the SINR target γ_{tg}, the UE transmission power control is then expressed as:

$$P^c_{k_{Tx}} = \min\left\{\frac{\gamma_{\text{tg}}.(N + I^c_{eNB})}{\Lambda^c_k \ |h|^2}, P_{max}\right\} \tag{3.1}$$

where Λ^c_k represents the channel conditions of UE k over the RB c and I^c_{eNB} is the total inter-cell interference level received at the eNB on RB c. Of course, the UE transmission power can not exceed its maximum transmission power P_{max}.

Figure 3.2 illustrates the UE transmission power after applying power control while no fading nor shadowing are considered. We notice the variation of the UE transmission power as a function of the users locations. More the users are close to the eNB and/or in the favorite direction of the eNB antenna, best are their channel conditions and less is their transmission power.

3.3 Inter-cell interference estimation models

3.3.1 ICI estimation state of the art

To apply the UE transmission power control, the ICI level that each UE suffers on the RB used for transmission should be estimated. The ICI generated at the eNB on each RB can be estimated by

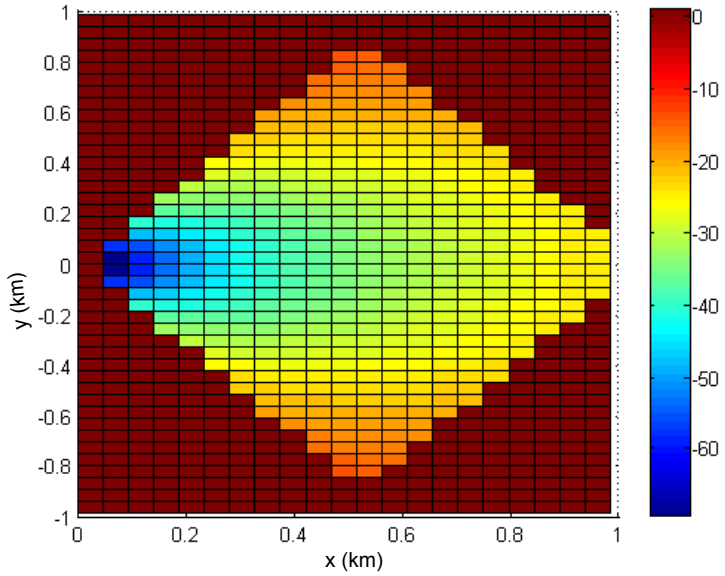

Figure 3.2: UE transmission power in dB as a function of UE locations

the channel conditions over the signal references sent in specific resource elements of each RB [61]. The same idea is used in [62] in case of Rayleigh fading channels. The authors of [63] and [64] propose an analytical model to estimate the inter-cell interference level in uplink considering the collision probability distribution. In [65], the authors propose an analytical model of ICI estimation in uplink based on the collision probability, and considering well known scheduling algorithms such as the round robin scheduling algorithm, the opportunistic scheduling algorithm and the proportional fair scheduling algorithm. The cited methods that we found in the literature do not consider the green LTE networks, where the power control process is applied. However, a reduction of the UE transmission power is directly translated by a reduction of the ICI level. For this purpose, we focus on the ICI level estimation for green LTE networks, while the UE transmission power is controlled as a function of the QoS required by each UE.

3.3.2 ICI estimation model for green uplink LTE networks

The ICI estimation for green uplink LTE networks method should consider the randomness of the interfering UEs and also the randomness of their transmission power. The total ICI level I^c_{eNB} received at the served eNB, while UE k transmits its information in RB c, is defined by the sum of the interference levels received from the random interfering UEs served in the neighboring cells and using the same RB c, as illustrated in Figure 3.3.

Considering the 19 hexagonal cells network, the ICI level can be expressed as :

$$I^c_{eNB} = \sum_{s=2}^{19} I^c_{s,eNB}, \tag{3.2}$$

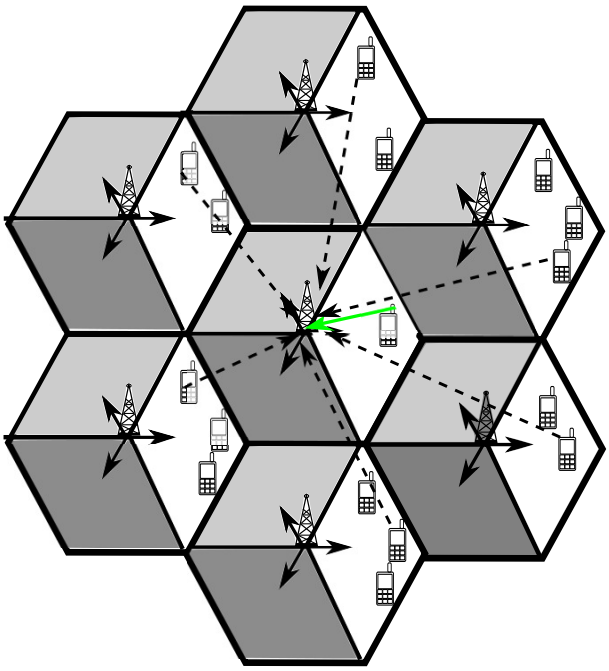

Figure 3.3: First ring of uplink inter-cell interference

where $I^c_{s,eNB}$ is the interference level received at the central eNB, caused by an UE, in the neighboring sector s on RB c. To evaluate $I^c_{s,eNB}$, we should run Monte Carlo simulations that consider all the possible interfering UE locations and transmission powers. To overcome this N-P hard complexity, we propose an easier method that considers that the $I^c_{s,eNB}$ can be represented by the interference caused by only one virtual UE interferer as shown, with the red stars, in Figure 3.4.

Actually, we consider that the contribution of each interfering sector s is equivalent to the power received at the central eNB from a virtual UE interferer v situated at the geographical barycenter of the interfering sector's N_{UE} active UEs and radiating at P_m, where P_m is the median power of $P^c_{k_{Tx}}$, $k = 1, ..., N_{UE}$. It follows that,

$$I^c_{s,eNB_c} = P_m \Lambda^c_v \ |h|^2 \tag{3.3}$$

For this model, we consider one user QoS class. We allocate to the users one RB per time slot, by assuming that they can achieve their target QoS with this RB. Considering a Shannon capacity computation of the user throughput, each user tries to achieve the same signal to interference plus noise ratio γ_{tg}. In order to mitigate the interferences, we reduce the transmission power by applying power control as expressed in relation (3.1). Assuming that all the cells behave the same way, the interference I^c_{eNB} and the updated $P^c_{k_{Tx}}$ are recomputed until convergence, after S iterations, to a stable UE transmission power.
Considering at the first iteration a noise limited network, a quick convergence of the UE transmission power is obtained. Algorithm 3 explains these steps in details.

This method leads to a lower computation complexity. Actually, with Monte Carlo simulations,

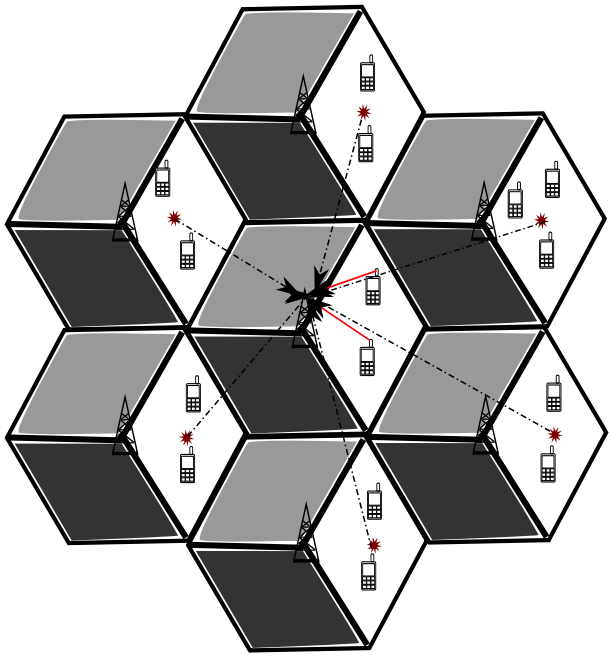

Figure 3.4: First ring uplink inter-cell interference estimation model

many iterations (M_T) are considered to draw the interfering user's positions. In addition, when power control process is applied, additional iterations should be considered to take into account the most UE transmission power values as possible. With the proposed ICI estimation model, the ICI level is given with one formula, without considering all the iterations run with Monte Carlo simulations. For one random draw of N_{UE} active users in each sector, we obtain the estimated ICI level I^c_{eNB} with $\mathcal{O}(S(N_{UE} + N_{eNB}))$ computational complexity. Using the Monte Carlo simulations, M_T additional iterations are considered to randomly choose the interfering user. Then, the ICI level I^c_{eNB} is evaluated with $\mathcal{O}(S(N_{UE} + 1) + SM_T(N_{eNB} - 1))$ computational complexity. However, the proposed ICI estimation model complexity gain is about $\mathcal{O}(SM_T)$ operations.

3.4 ICI estimation model validation

The comparison of the Cumulative Distribution Function (CDF) of the UE stable transmission powers obtained (i) from our proposed model: d_M, and (ii) from Monte Carlo simulations: d_{MC} allows us to evaluate the reliability of the proposed method. This comparison is done by two tests: i) the log ratio test, and ii) the Kullback-Leibler divergence test.

- **The log ratio test** is a simple statistical ratio test, which compares two distributions using the logarithm of the ratio. In our case, the log ratio test Δ is given by:

$$\Delta(x) = \log\left(\frac{\text{Prob}(d_M \leq x)}{\text{Prob}(d_{MC} \leq x)}\right) \tag{3.4}$$

Algorithm 3 Estimating ICI model simulation

Init : $I_{eNB^c} = 0$
Randomly place N_{UE} active users
Compute their barycenter.
for $It = 1$ to S **do**
  for $k = 1$ to N_{UE} **do**
    $P^c_{e_k}(It) = \min\left\{\frac{\gamma_{\text{tg}}\ (N+I^c_{eNB})}{\Lambda^c_k\ |h|^2}, P_{max}\right\}$
  end for
  $P_m = \text{median}[P^c_{k_{Tx}}]$
  $I^c_{eNB} = \sum_{s=2}^{19} P_m\ \Lambda^c_k\ h$: ICI generated by the 18 interfering sectors
end for
for $k = 1$ to N_{UE} **do**
  $P_{S_k} = P^c_{k_{Tx}}(S)$: stable transmission power of user k
end for
$V_S = [P_{S_1} P_{S_2} ... P_{S_{N_{UE}}}]$: stored N_{UE} stable transmission powers

if Δ is less than 1, or close to 0 (ideally) the distributions are similar.

- **The Kullback-Leibler divergence test**, mostly used in information theory, is a non-symmetrical measure of the difference between two probability distributions. It can be used to measure the consistency between d_M and d_{MC}. The result, denoted $KL(x)$, can be expressed as a function of the log ratio test as follows:

$$KL(x) = \text{Prob}(d_M \leq x) * \Delta(x) \tag{3.5}$$

The Kullback-Leibler test, as it is weighted by the CDF, is more representative of the distributions similarities, especially when the distributions are not uniform.
We allocate to each sector a bandwidth $B = 5$ MHz corresponding to $N_{RB} = 25$ RBs. The users are uniformly distributed in each sector. Since each user is allocated only one RB, the maximum number of simultaneously served users is set to $N_{UE} = 25$. Table 3.1 summarizes the most relevant simulation parameters.

In the proposed method of ICI estimation, we have selected the median value for the virtual UE transmission power instead of the mean value in order to achieve more accurate results. This assertion will be illustrated by the analytical validation's results (Section 3.5). Indeed, the mean is a central tendency in statistics, which is reliable only in the presence of symmetrical distributions, whereas the median is still reliable in presence of asymmetrical distributions, since it is considered as a weighted arithmetic average [6–8]. In our case, the distribution of the N_{UE} UE transmission powers follows an asymmetrical distribution, as it is represented on Figure 3.5 with the histogram of the UEs stable transmission powers obtained (after convergence) by Monte Carlo simulations. The asymmetry is caused by the eNB antenna gain pattern and extreme values that correspond to some extreme users positions.
The ICI estimation model's performances are evaluated by comparing the obtained stable transmission

Antenna configuration	Single-Input-Single-Output
Cellular layout Max/ Min UE-eNB distance	Regular network with 19 tri-sector cells. $D = 1.7$ km
Carrier frequency System bandwidth Total number of RB per sector Number of RB per user Number of active users N_{UE}	2.6 GHz $B = 5$ MHz per sector 25 1 25
Rayleigh fading type	uncorrelated fading coefficient h
Offered QoS	Target throughput of 200 kbps ($\gamma_{tg} = 3dB$)

Table 3.1: Simulation parameters for ICI estimation model validation

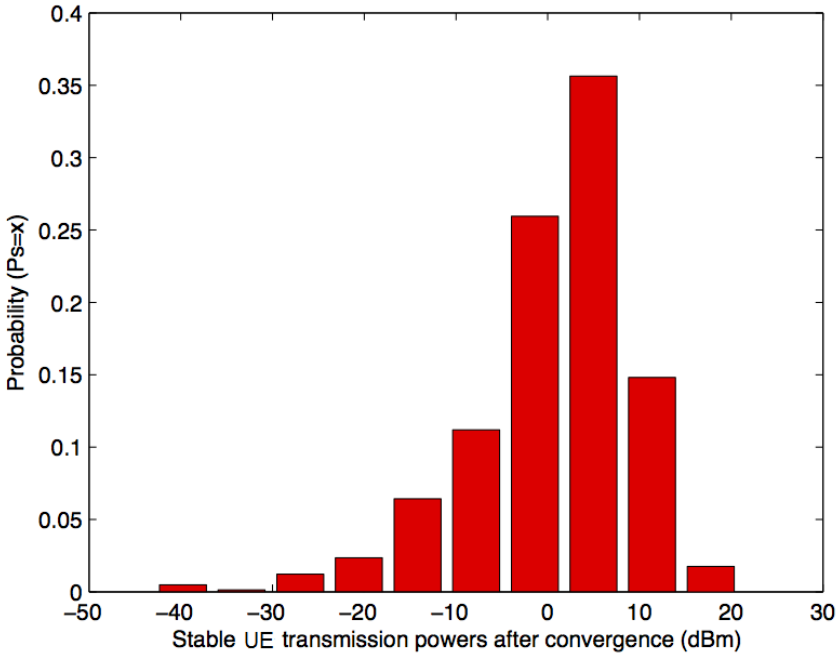

Figure 3.5: Histogram of UE transmission powers after convergence

powers with those issued from Monte Carlo simulations, where the interference caused to each active user in the central cell is computed with M_T random draws of interferers in each interfering sector. To validate our model, we use the log-ratio and Kullback-Leibler tests defined before, and study the method in different and more realistic environments:

(a) PL: Path Loss using only the Okumura Hata model
(b) PL+Fad : Path Loss with Rayleigh fading of $\sigma_f = 1$
(c) PL+Fad+Shad : Path Loss with Rayleigh fading of $\sigma_f = 1$, and shadowing of standard deviation $\sigma_s = 4$ dB

Many draws of Algorithm 3 and Monte Carlo simulations have been considered to obtain more representative results. The number of draws of Algorithm 3 is denoted M and set to 4.10^5. Thanks to adequate initialization of I^c_{eNB}, the stable transmission powers are obtained after less than $S = 5$ iterations.

Figure 3.6 represents the two CDF obtained, after convergence of UE transmission powers, by our

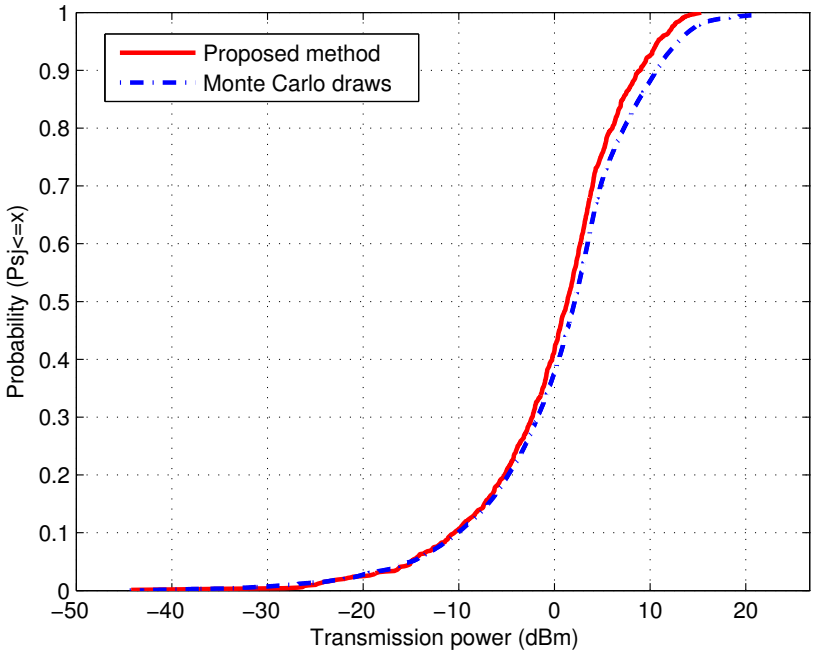

Figure 3.6: CDF of MS transmission powers

proposed method and by Monte Carlo simulations, without fading nor shadowing. Only one RB can satisfy the target throughput. With $\gamma_{\text{tg}} = 3$ dB, the corresponding target throughput per user is about 200 kbps. In this case, less than 2 % of users are unsatisfied[2], and UE transmission powers values vary between -48 dBm and 21 dBm, which respects the standard UE transmission power interval given in [9]. Then, these simulations are extended to a more complex environment in presence of fading and shadowing. Table 3.2 summarizes the most representative results identified by significant probabilities, i.e. UE transmission powers ≥ -30 dBm, obtained by using the log ratio test. The gap between the two CDFs for lower UE transmission powers is larger than the observed one for high transmission powers, which becomes close to zero. Moreover, the complex environment increases this gap. However, the largest value observed is 0.14. Therefore, as it is very lower than 1, the two CDFs can be considered as similar and our model is validated.

The Kullback-Leibler divergence test, as it takes into account the UE transmission power CDF, softens the differences between the results issued from both methods (see Table 3.3) in the lowest transmission powers area. It enhances that most of the time, when UE transmission powers are higher than

[2]an unsatisfied user means that this user is not able to reach its target QoS

UE transmission power (dBm)	Δ σ_f =1, σ_s = 4 dB		
	PL	PL + Fad	PL+Fad+Shad
≤ -30	0.14	0.11	0.122
[-30;-25]	0.048	0.063	0.11
[-25;-20]	0.04	0.009	0.099
[-20;-15]	0.024	0.026	0.09
[-15;-10]	0.022	0.033	0.078
[-1;-5]	0.02	0.024	0.068
[-5;0]	0.03	0.042	0.06
[0;5]	0.043	0.042	0.049
[5;10]	0.026	0.031	0.037
[10;15]	0.014	0.018	0.0 28
[15;21]	0.003	0.0042	0.015

Table 3.2: Δ obtained by Log Ratio test

−15 dBm, the two CDFs are similar. Using the Kullback-Leibler divergence test, we take differ-

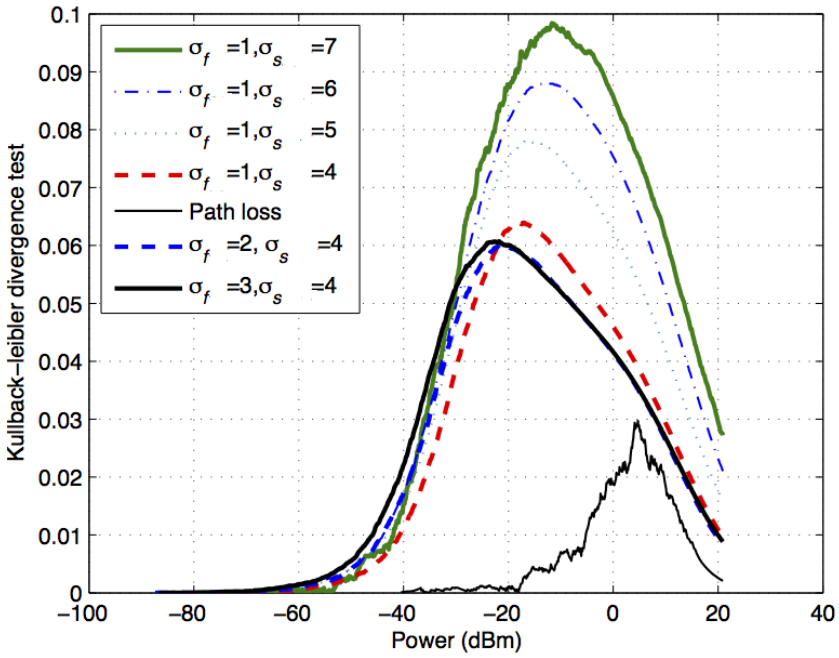

Figure 3.7: Kullback-Leilbler test curves

ent values for shadowing and fast fading parameters. Figure 3.7 summarizes the simulations results curves. As they come from the product of a decreasing function (Δ) and an increasing function (Prob($d_M \leq x$)), all the curves have the same behavior: first they increase, then reach a maximum value (that remains so small that it respects the log ratio validity test) and finally decrease. The max-

UE transmission power (dBm)	KL σ_f =1, σ_s = 4 dB		
	PL	PL + Fad	PL+Fad+shad
$\leq$ -30	0.0016	0.0002	0.024
[-30 ; -25]	0.0028	0.0002	0.04
[-25 ; -20]	0.0012	0.00063	0.057
[-20 ; -15]	0.0027	0.0009	0.064
[-15 ; -10]	0.0019	0.037	0.063
[-10 ; -5]	0.0037	0.049	0.057
[-5 ; 0]	0.0086	0.014	0.052
[0 ; 5]	0.012	0.022	0.044
[5 ; 10]	0.024	0.025	0.035
[10 ; 15]	0.011	0.022	0.027
[15 ; 21]	0.005	0.006	0.014

Table 3.3: Divergence obtained by Kullback-Leibler test results

imum Kullback-Leibler test results in the path loss case is less than 0.03. When the fast fading and the shadowing effects are considered, we observe some fluctuations. The maximum Kullback-Leibler divergence test in presence of fast fading of $\sigma_f = 1$ and shadowing of $\sigma_s = 4$ dB is less than 0.07. Moreover, varying fast fading standard deviation σ_f from 1 to 3 does not influence much. The curves remain nearly identical. On the other hand, varying the shadowing parameter changes the simulation results. Setting σ_f at 1 and varying σ_s from 4 to 7 dB makes the maximum Kullback-Leibler distance increase from 0.06 to 0.1. Nevertheless, the Kullback-Leibler divergence test results remain very small and respect the log ratio validity test. As the variation of shadowing and fading parameters keeps the distributions similarity, the ICI model's validity and robustness against environment variations are confirmed.

3.5 Analytical validation

The ICI estimation model is based on the ICI level caused by a virtual UE located at the barycenter of the interfering sector's active UEs and radiating with a median power P_{med}. In this section, we prove the accuracy of the proposed model when P_{med} is selected instead of the mean power P_{mean}. The analytical validation of the ICI estimation model is investigated based on P_{med} and P_{mean} analytical expressions which are derived in the following subsection, considering a continuous distribution of the UEs in the sectors. Then, the generated ICI level is evaluated when a power control process is applied, and compared to the one obtained when UEs transmission power is set to P_{max}.

3.5.1 Median and mean UEs transmission power analytical determination

In this section, our objective is to determine the analytical expressions of P_{med} and P_{mean}, the median and mean transmission power of the transmitting UEs of a sector.

First, we compute the area A_s of each sector in an hexagonal cell $1 \times 3 \times 3$ network topology where R and R_{min} are respectively the maximum and minimum distance between the eNB and an UE of the considered sector:

$$A_s = \frac{\sqrt{3}}{2} R^2 - \frac{\pi}{3} R_{min}^2 \tag{3.6}$$

The sector can be divided into two sub-areas: in the first one, denoted $A_{\nearrow}$, the UEs can achieve their γ_{tg} with a transmission power lower than P_{max}. In the second sub-area, denoted $A_{P_{max}}$, the UEs transmission power is equal to P_{max} and the achievement of γ_{tg} is not guaranteed. Consequently, if we note $\tau_{\nearrow}$ the proportion of the sector's area where the UEs achieve their γ_{tg} while transmitting at a lower power than P_{max}:

$$\tau_{\nearrow} = \frac{A_{\nearrow}}{A_s}, \tag{3.7}$$

the expression of P_{mean} and P_{med} follows, as an uniform distribution of the UEs in the sector is considered:

$$P_{mean} = \min\left(\frac{A_{\nearrow}}{A_s}, 1\right) \times \bar{P}_{\nearrow} + \left(1 - \min\left(\frac{A_{\nearrow}}{A_s}, 1\right)\right) \times P_{max}, \tag{3.8}$$

where $\bar{P}_{\nearrow}$ denotes the mean UEs transmission power in the section of $A_{\nearrow}$ that is included in the sector, and:

$$P_{med} = \begin{cases} P_{max} & \text{when } \tau_{\nearrow} \leq 0.5 \\ P_{Tx} \text{ such that } F_{P_{Tx}}(p) = 0.5 & \text{when } 0.5 < \tau_{\nearrow} < 1 \\ P_{Tx} \text{ such that } F_{P_{Tx}}(p) \approx 0.5/\left(\frac{A_{\nearrow}}{A_s}\right) & \text{when } \tau_{\nearrow} \geq 1 \end{cases}$$

where $F_{P_{Tx}}$ denotes the cumulative distribution function of the active UEs transmission power in the sector.

When all the UEs of the considered sector belong to $A_{\nearrow}$, which corresponds to the case when $\tau_{\nearrow} \geq 1$, the above determination of P_{med} assumes that these UEs are those of $A_{\nearrow}$ who transmit at the lowest power.

The next step is therefore to express $A_{\nearrow}$. For this purpose, we develop relation (3.1) in order to highlight the individual parameters that determine UE k transmission power as a function of its location in the sector:

$$\begin{aligned} P_{k_{Tx}}(r_k, \theta_k) &= \min\left\{\frac{\gamma_{\text{tg}} \cdot (N + I^c_{eNB})}{\Lambda^c_k \ |h|^2}, P_{max}\right\} \\ &= \min\left\{\beta \ v_k, P_{\max}\right\} \end{aligned} \tag{3.9}$$

with $\beta = \frac{\gamma_{\text{tg}} \cdot (N + I^c_{\text{eNB}})}{G_M \ G_{\text{eNB}}}$, $v_k = \frac{10^{\varphi \theta_k^2} \ h \ r_k^{\gamma}}{K}$, K the path loss constant defined in Section 2.2.3 and the angle θ_k expressed in degree as $\varphi = 1.2/70^2$. The eNB-UE distance r_k, that certifies that an UE is in $A_{\nearrow}$, is such that:

$$\frac{\beta h}{K} \ 10^{\varphi \theta_k^2} \ r_k^{\gamma} \leq P_{max} \tag{3.10}$$

hence,

$$r_k \leq \kappa_{max} 10^{-\frac{\varphi\theta_k^2}{\gamma}} \tag{3.11}$$

where

$$\kappa_{max} = \left(\frac{K\ P_{max}}{\beta h}\right)^{\frac{1}{\gamma}} \tag{3.12}$$

and is deviated by introducing κ_P such that,

$$\kappa_P = \left(\frac{K\ P}{\beta |h|^2}\right)^{\frac{1}{\gamma}} \tag{3.13}$$

Consequently, $A_{\nearrow}$ is determined as follows:

$$\begin{aligned} A_{\nearrow} &= \int_{-\frac{\pi}{3}}^{\frac{\pi}{3}} \int_{R_{min}}^{\kappa_{max} 10^{-\frac{\varphi\theta^2}{\gamma}}} r\ dr\ d\theta \\ &= \frac{\kappa_{max}^2}{2} \omega_{1,\frac{\pi}{3}} - \frac{\pi}{3} R_{min}^2 \end{aligned} \tag{3.14}$$

where $\omega_{1,\frac{\pi}{3}}$ is determined such that:

$$\begin{aligned} \omega_{1,x} &= \int_{-x}^{x} 10^{-\frac{2\varphi}{\gamma}\theta^2} d\theta \\ &= \sqrt{\frac{\pi\gamma}{\varphi Log(100)}} \mathrm{erf}\left(x \sqrt{\frac{\varphi}{\gamma} Log(100)}\right) \end{aligned} \tag{3.15}$$

and $\omega_{1,\frac{\pi}{3}} \approx 1.5$.
As the UEs are uniformly distributed in the network, their probability density function f_{UEs} is constant and:

$$f_{UEs}(r,\theta) = \begin{cases} 1/A_s & \text{when } \tau_{\nearrow} < 1 \\ 1/A_{\nearrow} & \text{when } \tau_{\nearrow} \geq 1 \end{cases}$$

Consequently, the cumulative distribution function of the UEs transmission power is:

$$\begin{aligned} \mathrm{F}_{P_{Tx}}(p) &= \mathrm{Prob}(P_{Tx} \leq p) \\ &= \mathrm{F}_V(\frac{p}{\beta}) \\ &= \iint_{A_{\nearrow}} f_{UEs}(r,\theta)\ r\ dr\ d\theta \\ &= \frac{f_{UEs}}{2} \int_{-\frac{\pi}{3}}^{\frac{\pi}{3}} \left[\kappa_P^2 10^{-\frac{2\varphi\theta^2}{\gamma}} - R_{min}^2\right] d\theta \qquad (3.16) \\ &= \left(\frac{\kappa_P^2}{2} \omega_{1,\frac{\pi}{3}} - \frac{\pi}{3} R_{min}^2\right) f_{UEs} \qquad (3.17) \end{aligned}$$

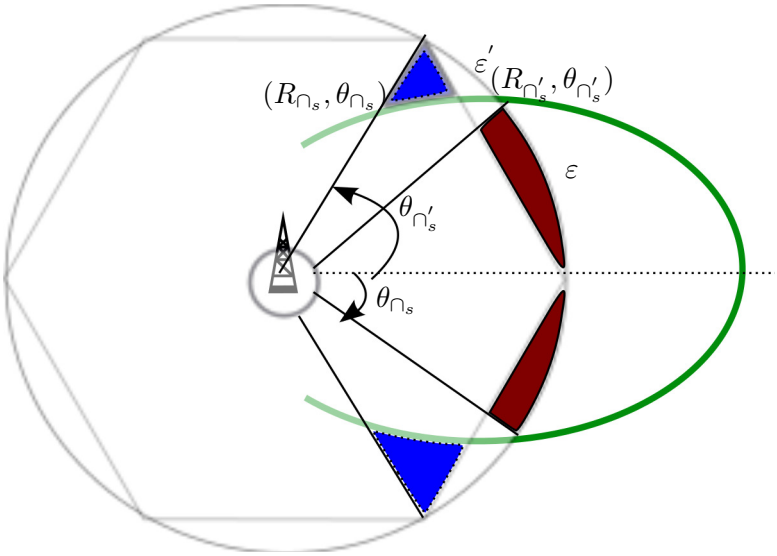

Figure 3.8: Intersection between the sector's limit and the boundary of $A_{\nearrow}$ for $\tau_{\nearrow} \geq 1, R_{\cap_s} < R$

When $\tau_{\nearrow} < 1$, the mean value of the transmission powers of the UEs - in the sector only - in the A_s area is, by definition:

$$\bar{P}_{\nearrow} = \frac{1}{A_{\nearrow}} \int_{-\frac{\pi}{3}}^{\frac{\pi}{3}} \int_{R_{min}}^{\kappa_{max} 10^{-\frac{\varphi\theta^2}{\gamma}}} \frac{\beta h}{K} 10^{\varphi\theta^2} \, r^{\gamma} \, r \, dr \, d\theta \tag{3.18}$$

When $\tau_{\nearrow} \geq 1$, a large proportion of the UEs in the sector transmit at a lower power than P_{max}. But due to the eNB antenna radiation pattern directivity, some of the UEs in the sector can be outside the $A_{\nearrow}$ area.

It is therefore necessary to find the intersection, denoted $\cap_s$, between the sector's limit and the boundary of $A_{\nearrow}$. The set $\cap_s$ contains two points whom polar coordinates are: $\theta_{\cap_s} = \pm\frac{\pi}{3}$ and $R_{\cap_s} = \kappa_{max} 10^{-\varphi\left(\frac{\pi}{3}\right)^2/\gamma}$.
If $R_{\cap_s}$ is higher than R (Figure 3.9), all the UEs in the sector transmit at a lower power than P_{max}. The mean UEs transmission power is then approximated from the computation of the mean UEs transmission power over a third of disk of radius R - without limitation by P_{max}, which leads to a minor overestimation of P_{mean}:

$$P_{mean} = \frac{A_s}{A_o} \int_{-\frac{\pi}{3}}^{\frac{\pi}{3}} \int_{R_{min}}^{R} \frac{1}{A_o} \frac{\beta h}{K} 10^{\varphi\theta^2} r^{\gamma} \, r \, dr \, d\theta \tag{3.19}$$

where

$$A_o = \frac{\pi}{3} \left(R^2 - R_{min}^2\right) \tag{3.20}$$

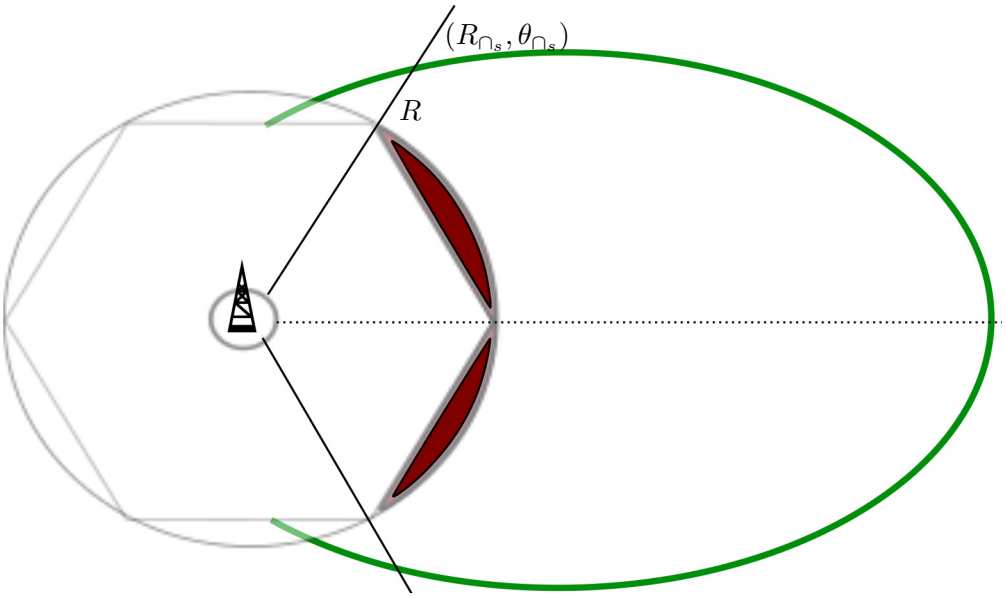

Figure 3.9: Intersection between the sector's limit and the boundary of $A_{\nearrow}$ for $\tau_{\nearrow} \geq 1, R_{\cap_s} > R$

If $R_{\cap_s}$ is lower than R (Figure 3.8), some UEs, in the upper and lower part of the sector, transmit at P_{max}. We denote $\cap_s^{'}$ the intersection between the boundary of $A_{\nearrow}$ and the circle of radius R. Then $\cap_s^{'}$ contains two points whom polar coordinates are: $R_{\cap_s^{'}} = R$ and $\theta_{\cap_s^{'}} = \pm\frac{\gamma}{\varphi}\ \log_{10}\left(\frac{\kappa_{max}}{R}\right)$.

We divide the sector into two parts:

1. the central one is bounded by $-\theta_{\cap_s^{'}} \leq \theta \leq \theta_{\cap_s^{'}}$ and $R_{min} \leq r \leq R$. In this area of surface A_c, the mean UEs transmission power is slightly overestimated by considering the extra-part, denoted ε on Figure 3.8, beyond the sector's limit.
2. the edge one, composed by the lower and upper parts of the sector, is bounded by $\theta < -\theta_{\cap_s^{'}}$ or $\theta > \theta_{\cap_s^{'}}$ and $R_{min} \leq r \leq \kappa_{max} 10^{-\frac{\varphi\theta^2}{\gamma}}$. In this area of surface A_e, the mean UEs transmission power is slightly underestimated because the extreme UEs locations in the sector, denoted ε' on Figure 3.8, are not considered.

Thanks to the eNB antenna radiation pattern's symmetry, the mean UEs transmission power P_{mean} is therefore approximated by:

$$P_{mean} = \frac{2}{A_c + A_e}\left[\int_0^{\theta_{\cap_s^{'}}}\int_{R_{min}}^{R} \frac{\beta h}{K} 10^{\varphi\theta^2} r^{\gamma}\ r\ dr\ d\theta + \int_{\theta_{\cap_s^{'}}}^{\frac{\pi}{3}}\int_{R_{min}}^{\kappa_{max}10^{-\frac{\varphi\theta^2}{\gamma}}} \frac{\beta h}{K} 10^{\varphi\theta^2} r^{\gamma}\ r\ dr\ d\theta\right] \tag{3.21}$$

where

$$A_c = \left(R^2 - R_{min}^2\right)\theta_{\cap_s^{'}}$$

and

$$A_e = \frac{\kappa_{max}^2}{2}\left(\omega_{1,\frac{\pi}{3}} - \omega_{1,\theta_{\cap_s^{'}}}\right) - R_{min}^2\left(\frac{\pi}{3} - \theta_{\cap_s^{'}}\right)$$

Finally, the mean value of the transmission powers of the UEs - in the sector only - is obtained after derivations:

$$P_{mean} = \begin{cases} P_1 & \text{when } \tau_{\nearrow} \leq 1 \\ P_2 & \text{when } \tau_{\nearrow} > 1 \text{ and } R_{\cap_s} \geq R \\ P_3 & \text{when } \tau_{\nearrow} > 1 \text{ and } R_{\cap_s} < R \end{cases}$$

where,

$$P_1 = \frac{1}{A_{\nearrow}} \frac{\beta h}{K(\gamma+2)} \left(\kappa_{max}^{\gamma+2} \, \omega_{1,\frac{\pi}{3}} - R_{min}^{\gamma+2} \, \omega_{2,\frac{\pi}{3}} \right) \tau_{\nearrow} + (1 - \tau_{\nearrow}) \; P_{max}$$

$$P_2 = \frac{1}{A_{\nearrow}} \frac{\beta h}{K(\gamma+2)} \left(\kappa_{max}^{\gamma+2} \, \omega_{1,\frac{\pi}{3}} - R_{min}^{\gamma+2} \, \omega_{2,\frac{\pi}{3}} \right) \tau_{\nearrow} + (1 - \tau_{\nearrow}) \; P_{max}$$

and

$$P_3 = \frac{1}{A_c + A_e} \frac{\beta h}{K(\gamma+2)} \left(\left(R^{\gamma+2} - R_{min}^{\gamma+2} \right) \omega_{2,\theta_{\cap_s'}} + \kappa_{max}^{\gamma+2} \left(\omega_{1,\frac{\pi}{3}} - \omega_{1,\theta_{\cap_s'}} \right) - R_{min}^{\gamma+2} \left(\omega_{2,\frac{\pi}{3}} - \omega_{2,\theta_{\cap_s'}} \right) \right)$$

As for $\omega_{1,x}$, we introduce $\omega_{2,x}$ given with the imaginary error function erfi[3] as:

$$\begin{aligned} \omega_{2,x} &= \int_{-x}^{x} 10^{\varphi\theta^2} d\theta \\ &= \sqrt{\frac{\pi}{\varphi \log_{10}}} \text{erfi}\left(x \sqrt{\varphi \log_{10}} \right) \end{aligned} \tag{3.22}$$

and $\omega_{2,\frac{\pi}{3}} \approx 5.03$.

In the same way, the median value of the transmission powers of the UEs - in the sector only - is obtained after derivations:

$$P_{med} = \begin{cases} P_{max} & \text{when } \tau_{\nearrow} \leq 0.5 \\ \frac{\beta h}{K} \left[\frac{2A_s}{\omega_{1,\frac{\pi}{3}}} \left(0.5 + \frac{\pi R_{min}^2}{3A_s} \right) \right]^{\frac{2}{\gamma}} & \text{when } 0.5 < \tau_{\nearrow} < 1 \\ \frac{\beta h}{K} \left[\frac{2_{\nearrow}}{\omega_{1,\frac{\pi}{3}}} \left(0.5 \frac{A_s}{A_{\nearrow}} + \frac{\pi R_{min}^2}{3A_{\nearrow}} \right) \right]^{\frac{2}{\gamma}} & \text{when } \tau_{\nearrow} \geq 1 \end{cases}$$

Next subsection is dedicated to the results provided by the analytical determination of P_{mean} and P_{med}.

3.5.2 Simulation results

The purpose of this subsection is to check that: 1) the empirical computations of P_{mean} and P_{med}, determined from the N_{UE} UEs transmission powers, are close to their analytical computations issued from the previous subsection, and 2) the use of P_{med} instead of P_{mean} for the virtual interfering UE transmission power leads to a more accurate estimation of the ICI and the UEs stable transmission

[3] erfi is the imaginary error function: $\text{erfi}(z) = -i \, \text{erf}(iz)$

powers. This accuracy is measured by comparison with the results obtained from Monte-Carlo simulations.

To validate the analytical model, we consider the simulation parameters used in the previous section (Table 3.1). The results are given for 10^6 Monte Carlo iterations. For an hexagonal cell of radius $R = 1$ km, the proportion of the sector's area where the UEs achieve their γ_{tg} while transmitting at $P_{e,k} \leq P_{max}$, $\tau_{\nearrow}$ is higher than 1. First, we compare the distributions of the UEs transmission powers obtained when the proposed model and the analytical model are used for the ICI estimation, considering both the virtual point radiating at P_{med} or P_{mean}. Table 3.4 contains the obtained Kullback-Leibler divergence test values. These values vary from 0 to 7.3 10^{-2} independently of the virtual UE transmission power type (P_{med} or P_{mean}). They are small and verify the log ratio validity test. Hence, the P_{mean} and P_{med} analytical expressions derivation is verified, and conformity between the analytical ICI estimation model and the proposed one is proved.

Then, we compare the UEs transmission power distributions when the proposed model and Monte

KL \ $P_{e,k}$ (dBm)	-40	-30	-20	-10	0	10	20
P_{med}	1.7 10^{-5}	3.4 10^{-3}	2.8 10^{-3}	5.6 10^{-3}	1.5 10^{-2}	1.5 10^{-3}	0
P_{mean}	1.4 10^{-3}	1.3 10^{-3}	2.3 10^{-3}	9.5 10^{-3}	7.3 10^{-2}	6.9 10^{-2}	1.7 10^{-2}

Table 3.4: Proposed model vs analytical model UEs transmission power Kullback-Leibler divergence test

Carlo simulations are used for ICI estimation. The Kullback-Leibler divergence test values are illustrated on Figure 3.10. The maximum Kullback-Leibler divergence test value is obtained when the mean power is used and is equal to 17 10^{-2}. This maximum Kullback-Leibler divergence test value is small and respects the log ratio validity test, but the maximum Kullback-Leibler divergence test obtained when a median power is used is less than 5 10^{-2}. The gap between the two curves prove that the ICI estimation model using the median power is more accurate than the one using the mean power.

To enlighten the accuracy of the ICI estimation model using the median power, Figure 3.11 illustrates the ICI levels CDFs. Notice that the curves obtained with Monte Carlo and the proposed method using P_{med} are close. Their levels vary from -130 dBm to -110 dBm. The ICI levels obtained with the proposed method using P_{mean} are higher and vary from -125 dBm to -100 dBm, which corresponds to an average gap of 5 dBm relatively to Monte Carlo simulations. When the power control process is not activated the inter-cell interference is more important and the ICI levels obtained with Monte Carlo simulations vary from -103 dBm to -90 dBm. They confirm that a large amount of ICI can be saved (around 25 dBm), when UE power control can be activated.

The validation of the proposed method of ICI estimation is also verified when $\tau_{\nearrow} \leq 1$ (cell radius $R = 5$ km). The maximum KL divergence test values for UEs transmission powers distributions and for the ICI distributions are smaller than the ones obtained for $\tau_{\nearrow} > 1$. Hence, the proposed model is also validate for $\tau_{\nearrow} \leq 1$.

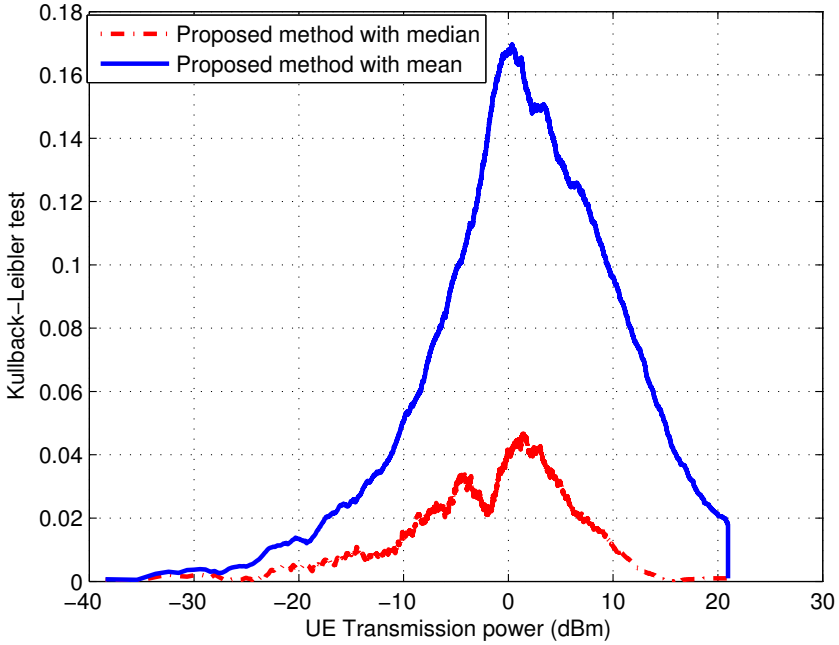

Figure 3.10: Monte Carlo vs Analytical model UEs transmission power Kullback Leiber test for R=1 km

Figure 3.12 and 3.13, respectively, show the controlled UEs transmission powers obtained as a function of the ICI level computation methods for $\tau_{\nearrow} > 1$ and $\tau_{\nearrow} \leq 1$. In both cases, we note that the CDFs of the UEs transmission powers when the ICI is estimated with the proposed model and its analytical expression are close independently of the virtual UE transmission power type. However, the CDF obtained when the virtual UE transmits at P_{med} is closer, and proves that using the median power is more accurate. The UEs transmission power CDFs are lower bounded with the CDF of UEs transmission power computed in noise limited network, and upper bounded with the CDF of the UEs transmission power computed when the ICI is set at its maximum, considering that the power control is not activated for the interferers. For macro cells with a radius $R = 5$ km, the UEs transmission powers vary between -10 dBm and P_{max}. This is due to the path loss, where at a far distance from the eNB, the UEs should transmit at a higher power to achieve their QoS.

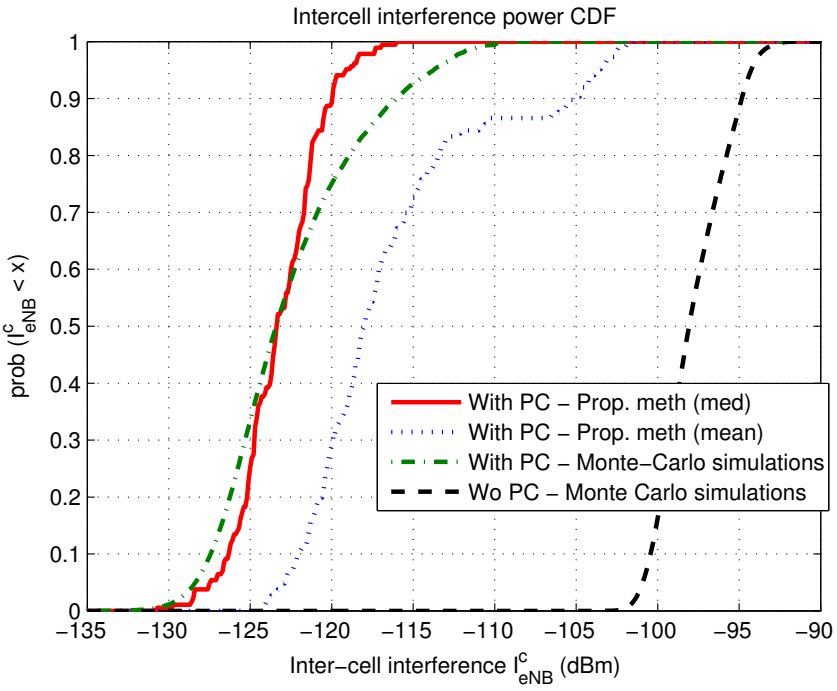

Figure 3.11: ICI cumulative distribution function for R=1 km

3.6 Conclusion

Power control applied on the uplink to the UE transmission power, based on a SINR threshold, drastically reduces the inter-cell interference. This reduction comes at the expense of a higher complexity in the derivation of ICI level. The method we proposed to estimate the inter-cell interference is less heavy and greedy in computation than the classical Monte Carlo method. Actually, it does not drop users in the interfering sectors as Monte Carlo method requires. In this chapter, we have shown that a single virtual UE, situated at the barycenter of each of the concerned interfering sectors, allows us to precisely evaluate the ICI. This virtual UE interferer transmits at the median power of the interfering sector's active UEs, assuming that all neighboring cells behave the same way than the central cell. This equivalent median power creates, in any environment, an inter-cell interference at the central eNB equivalent to that derived with random interfering users obtained from Monte Carlo simulations. An analytical model was also derived to evaluate this virtual UE median power transmission. It allowed an accurate ICI level estimation with an even lower computational complexity, and therefore reduce the planning and evaluation simulators complexity.

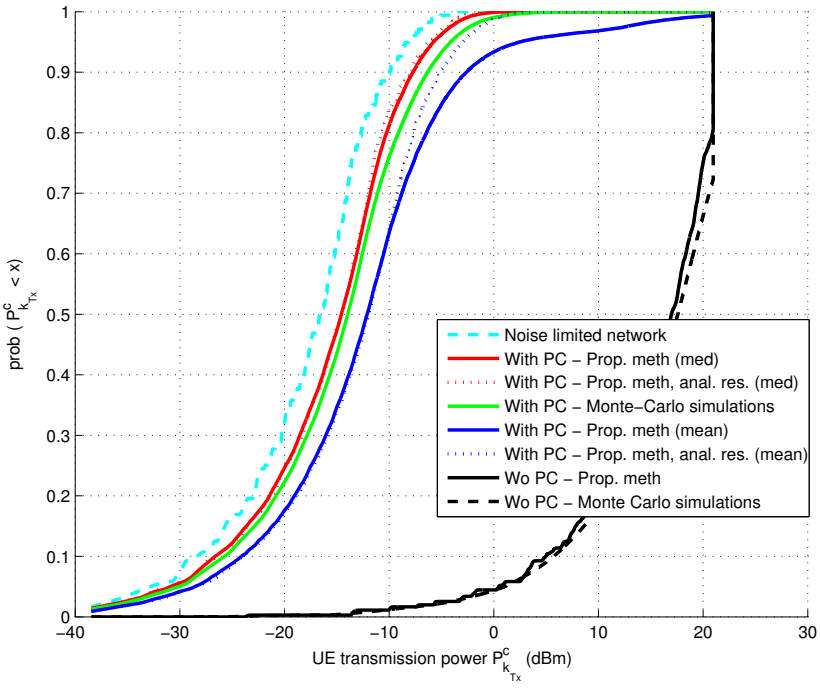

Figure 3.12: UEs transmission power for R=1 km

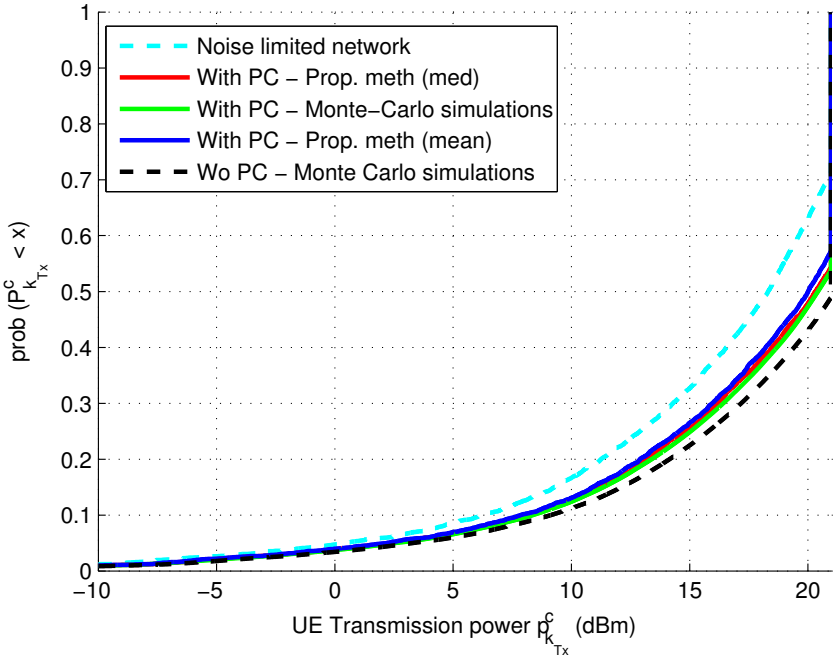

Figure 3.13: UEs transmission power for R=5 km

Chapter 4

Dimensioning outage probability Upper-bound depending on RRM in Uplink LTE networks

Part of this chapter was published in IEEE GLOBECOM 2013[1]

RADIO resource management aims at maximizing the system performances by allocating efficiently the limited number of RBs. This maximization is reached while the number of allocated RBs per cell is adapted with: i) the network's load and ii) the user's required QoS. These two parameters should be considered while determining the maximum number of allocated RBs per cell, corresponding to the allocated bandwidth per cell. Within this framework, the dimensioning outage probability is defined as the probability that a user is not served due to a lack of RBs in the network. In this chapter, we propose an analytical model that estimates the dimensioning outage probability upper bound which helps system planners to evaluate and adapt the allocated bandwidth to each cell. The dimensioning outage probability upper bound is evaluated as a function of the used RB allocation algorithm. This analytical model applies to the cases of single and multiple user's QoS classes and is also extended to the case of MIMO systems.

[1] F.Z. Kaddour, P. Martins, L. Decreusefond, E. Vivier and L. Mroueh, "Outage probability upper's bound in uplink Long Term Evolution networks with multi QoS users classes ", in proceedings of IEEE Global Communications conference (GLOBECOM), Atlanta, USA, December, 2013.

4.1 Introduction

Wireless cell planning aims at providing a proper radio network configuration, given in terms of: network coverage, offered QoS, capacity, deployed equipments, etc. Usually, the cell network planners study the area and create a database with the geographic information. They analyze the behavior of the population in the area and the required QoS. For these reasons, they require techniques to estimate the network configuration and to evaluate the required bandwidth that should be allocated to each cell or sector. Each allocated bandwidth consists of a limited number of RBs. In order to allocate RBs to cell's users, RRM entity takes into account their required QoS and their channel conditions. In this chapter, a user is considered in outage if there is not enough available RBs to serve and satisfy its QoS.

Most cells are considered in theory as hexagonal grids, but in reality and for severals factors, it is not the case. With the help of point processes, that consider the network's spatial distribution as random, we study the statistical behavior of the network configuration. It helps the cell planners to study an average behavior of the network. Our objective is to compute the upper bound of the dimensioning outage probability and to estimate the required bandwidth for the network. This problem was previously studied for the downlink OFDMA network in [66]. Our contribution lies in computing this upper bound in the uplink of LTE networks, considering single and multiple QoS classes according to the RB allocation policy applied by the RRM entity. We consider two RB allocation algorithms: (i) the fair RB allocation algorithm which uniformly allocates RBs to users and (ii) the opportunistic RB allocation algorithm which allocates RBs to the users benefiting from the best channel conditions. We focus on the dimensioning problem that determines the necessary RBs used for transmission in order to achieve the target capacity. The user's throughput is computed by means of the Shannon capacity. However, the considered RB allocation algorithms define the users' selection methodology without specifying the adjacency constraint of the allocated RBs. Then, the proposed analytical model presented in this chapter can be used for dimensioning LTE release 8 and LTE-A networks. In addition, the analytical model is developed for the diversity and multiplexing gains in MIMO systems.
Due to their largest arsenal of results, Poisson point processes are widely used to characterize the statistical behavior over many spatial random realizations of a network. Moreover, they are more tractable and simple to use than other point process models.

In our work, the total required number of RBs is assimilated to a marked Poisson point process. Only the first and second mathematical moments of this marked Poisson point process are necessary to evaluate the upper bound of the dimensioning outage probability.
In Section 4.2 the main assumptions that are used for the computation of the dimensioning outage probability's upper bound are discussed. Dimensioning outage probability upper bound in SISO systems is computed in Section 4.3. It is extended to MIMO systems in Section 4.4. In Section 4.5, the obtained numerical results and the proposed model validation are discussed.

4.2 Assumptions adopted for the computation of the dimensioning outage probability's upper bound

For dimensioning purpose, we are interested in evaluating and computing the upper bound P_{sup} of the dimensioning outage probability P_{out}, that there is not enough available resources N_{RB} in the network to serve and satisfy the QoS required by all the active users.
We define φ_{UE} the set of all active users positions in the cell C with cardinality $\mid \varphi_{UE} \mid = N_{UE}$. The throughput corresponding to the user's required QoS is noted C_0. Then, each user k at position x in the cell C needs $N_k(x)$ RBs to satisfy its target throughput C_0. Consequently, the total number $\mathbb{N}$ of RBs to serve and satisfy all the users in the cell C is:

$$\mathbb{N} = \sum_{k \in \varphi_{UE}} N_k(x)$$

If the necessary number of RBs per cell, $\mathbb{N}$, is higher than the number of available RBs in the cell, N_{RB}, then the system is in outage. The dimensioning outage probability is then expressed as:

$$P_{\text{out}} = Prob\left(\int N d\varphi \geq N_{\text{RB}} \right) \tag{4.1}$$

In this Chapter, the Shannon capacity theorem is used for the throughput computation. If γ_k is the average SINR of the user k over the RBs (by considering average shadowing and fading effects), then its number of required RBs to achieve its target throughput C_0 is expressed as:

$$N_k = \left\lceil \frac{C_0}{\bar{C}_k} \right\rceil \tag{4.2}$$

where $\bar{C}_k = W \log_2(1 + \gamma_k)$ is the average Shannon capacity of the user k in one RB of a bandwidth W. For computation simplicity, we work on the assumptions that:

Assumption 4.1 *The cell C is circular, with radius R and with the eNB at its center. The eNB antenna is assumed to be omnidirectional.*

Assumption 4.2 *Each user is allowed to transmit only if its SINR is higher than a signal to interference plus noise ratio threshold $\gamma_{\min}$. This means that the maximum number of RBs allowed to a UE, is upper bounded by:*

$$N_{\max} = \left\lceil \frac{C_0}{W \log_2(1 + \gamma_{\min})} \right\rceil \tag{4.3}$$

Assumption 4.3 *The power control is not taken into account. Each user k transmits at its maximum power $P_{\max}$ over its whole allocated RBs. In the SC-FDMA technique the total mobile's transmission power is equally shared over the allocated RBs. Then,*

$$P_{k_{Tx}} = \frac{P_{\max}}{N_{\max}} \qquad \forall\ k \in \varphi_{UE}$$

In this chapter, $P_{k_{Tx}}$ is denoted P_t as it is supposed to be constant for all users.

This assumption leads to an under estimation of the user's SINR. Actually, users that will be allocated less than $N_{\max}$ RBs will benefit from a margin in their SINR estimation. Consequently, they will achieve a higher throughput than C_0.
In addition, each user k is marked by the uplink scheduler decision noted z. This decision selects $(z = 1)$ or not $(z = 0)$ the user k to transmit data on RBs, with regards to assumption 4.2. Since the mark z, $z \in \mathbb{Z} = \{0, 1\}$, is independent from one user to another, then the number of allocated RBs $N_k(x, z)$ is considered as a marked Poisson point process.

Assumption 4.4 *User k at position x is served $N_k(x)$ RBs if and only if it is selected by the scheduler. Fair RB allocation and opportunistic RB allocation algorithms are considered.*

These assumptions, which are quite reasonable, are commonly used to simplify the mathematical computation.

4.3 Dimensioning outage probability upper bound in SISO systems

In SISO systems, we consider that the radio channel is affected by shadowing. Hence, we state the following assumptions:

Assumption 4.5 *The channel gain depends on each user's position x and on the shadowing gain g_s equal to $\frac{1}{S}$, where the linear values y of S follow a log-normal distribution with mean μ_s and a standard deviation σ_s as:*

$$p_s(y) = \frac{\xi}{\sigma_s y \sqrt{2\pi}} \exp\left(-\frac{(10\log_{10} y - \mu_s)^2}{2\sigma_s^2}\right) \tag{4.4}$$

where, $\xi = 10/\ln 10$

The analytical model of the dimensioning outage probability upper bound is detailed in the following subsection for single and multiple user's QoS classes.

4.3.1 Single users' QoS class in SISO systems

When the assumptions cited before are considered, the required number of RBs that should be allocated to each user k localized at position x in order to achieve its target throughput C_0, is given as a function of the channel conditions and the RRM decision as follows:

$$N_k(x, y, z) = \left\lceil \frac{C_0}{W \log_2\left(1+\frac{P_t P_L(x)}{\tilde{\eta} y}\right)} \right\rceil z \tag{4.5}$$

$$= \left\lceil \frac{C_0}{W \log_2\left(1+\frac{P_t K}{\tilde{\eta} y \|x\|^{\beta}}\right)} \right\rceil z \tag{4.6}$$

where $P_L(x)$ is the path loss when user k is localized at position x; K and β are respectively the path loss constant and the path loss exponent defined in Section 2; $\tilde{\eta}$ is the sum of the thermal noise N in the considered bandwidth and the average inter-cell interference level received at the eNB in one RB I^c_{eNB}. The marks y and z represent respectively the shadowing and the RRM decision's marks.
Since the marks are independent, $N_k(x, y, z)$ is a Poisson point process on $\mathbb{R}^3$ of intensity $\Lambda(x) \otimes p_s(y)dy \otimes p(z)dz$. We compute the upper bound P_{sup} of the dimensioning outage probability P_{out} for: (i) the fair RB allocation algorithm: $P^{\text{SISO}}_{\text{sup,Fair}}$, and (ii) the opportunistic RB allocation algorithm: $P^{\text{SISO}}_{\text{sup,Opp}}$.

Fair RB allocation algorithm:

The fair RB allocation algorithm allocates RBs to all users, whatever their channel conditions. Hence, the probability that a user will be selected by the scheduler for transmission follows a uniform distribution:

$$p(z) = \frac{1}{N_{\text{UE}}} \tag{4.7}$$

Studying the network behavior statistically, we consider that the number of UEs in the cell N_{UE} can be expressed as:

$$N_{\text{UE}} = \frac{\rho}{\nu}\pi R^2$$

where, ρ and $\frac{1}{\nu}$ are respectively the surface density and service mean time. According to the concentration inequality, we should compute the first and the second moment of the Poisson point process, using the Campbell formula (Theorem 2.1), as:

$$m_N = \int N(x, y, z)\ p_s(y)dy\ p(z)dz\ d\Lambda(x) \tag{4.8}$$

and

$$v_N = \int N^2(x, y, z)\ p_s(y)dy\ p(z)dz\ d\Lambda(x) \tag{4.9}$$

We assume γ_j to be the SINR threshold, j being the user's required number of RBs to achieve its target throughput C_0, with:

$$\gamma_j = 2^{C_0/(jW)} - 1 \quad \text{for } j = 1, \cdots, N_{\max} - 1 \quad \text{and } \gamma_0 = \infty$$

and we define A_j the area which contains the users that require at most j RBs to satisfy their target throughput C_0. The area A_j can be determined as follows:

$$\begin{aligned} A_j &= \int_{C\times\mathbb{R}^+\times Z} \mathbb{1}_{\{y\|x\|^\beta \le P_t K/\tilde{\eta}\gamma_j\}}\ p_s(y)dy\ p(z)dz\ dx \\ &= \int_{C\times\mathbb{R}^+\times Z} p\left(y\|x\|^\beta \le \tilde{\gamma}_j\right) p(z)dz\ dy\ dx \end{aligned} \tag{4.10}$$

where $\tilde{\gamma}_j = \frac{P_t K}{\tilde{\eta}\gamma_j}$.
After a tedious but straightforward integration by parts, detailed in Appendix 4.A.1, we obtain :

$$\boxed{A_j = \frac{\nu}{\rho R^2} \exp\left(2/\zeta + 2\alpha_j/\zeta\right)\Phi(\zeta \ln R - 2/\zeta - \alpha_j) + \frac{\nu}{\rho}\Phi(\alpha_j - \zeta \ln R)} \tag{4.11}$$

with Φ the normal cumulative distribution function[2], and the variables α_j and ζ expressed respectively, as:

$$\alpha_j = \frac{1}{\sigma_s}(10\log_{10}(\tilde{\gamma}_j) - \mu_s)$$

and

$$\zeta = \frac{10\beta}{\sigma_s \ln 10}$$

Then, the first and second moments of $N_k(x, y, z)$ in the fair RB allocation algorithm case can respectively be written as a function of A_j as:

$$m^{\text{SISO}}_{N_{\text{Fair}}} = \frac{\rho}{\nu}\sum_{j=1}^{N_{\max}-1} j(A_j - A_{j-1}) + \frac{\rho}{\nu}N_{\max}(\pi R^2 - A_{N_{\max}-1}) \tag{4.12}$$

and

$$v^{\text{SISO}}_{N_{\text{Fair}}} = \frac{\rho}{\nu}\sum_{j=1}^{N_{\max}-1} j^2(A_j - A_{j-1}) + \frac{\rho}{\nu}N^2_{\max}(\pi R^2 - A_{N_{\max}-1}) \tag{4.13}$$

Using the concentration inequality, the upper bound of the dimensioning outage probability in case of a fair RB allocation algorithm is:

$$Prob\left(\int N d\varphi \geq N_{\text{RB}}\right) \leq \quad P^{\text{SISO}}_{\text{sup,Fair}}$$

where,

$$P^{\text{SISO}}_{\text{sup,Fair}} = \quad \exp\left(-\frac{v^{\text{SISO}}_{N_{\text{Fair}}}}{N^2_{\max}} g\left(\frac{(\alpha-1)m^{\text{SISO}}_{N_{\text{Fair}}} N_{\max}}{v^{\text{SISO}}_{N_{\text{Fair}}}}\right)\right) \tag{4.14}$$

and $g(t) = (1+t)\ln(1+t) - t$.
Using the same methodology, the dimensioning outage probability upper bound in SISO systems using an opportunistic RB allocation algorithm is given in the next paragraph.

Opportunistic RB allocation algorithm:

The opportunistic RB allocation algorithm seeks to maximize the total throughput of the cell C. Hence, it allocates each RB to the user with the highest SINR. Then, the probability of selecting a user depends on its channel conditions, given with the path loss and shadowing effects.

[2]the normal cumulative distribution function is expressed as: $\Phi = \frac{1}{2} + \frac{1}{2}\text{erf}(\frac{x}{\sqrt{2}})$

We assume narrow ring $[\gamma_j, \gamma_{j+1}]$, $\forall\ j = 1, \ldots, N_{max} - 1$ in which the users positions x are considered to as quasi-similar. Consequently, selecting a user with the highest SINR in the range of $\gamma_j \leq \frac{P_t K}{\tilde{\eta} y \|x\|^\beta} \leq \gamma_{j+1}$, means selecting the user with the minimum shadowing coefficient y.
Let $t = \min\{y\}$. Assuming that the shadowing coefficients y are independent from one user to another, the cumulative distribution function of t, $F_T(t)$ can be expressed as:

$$\begin{aligned} F_T(t) &= 1 - (1 - F_y(t))^{\breve{N}_{\mathrm{UE}}} \\ &= 1 - \left(1 - \Phi\left(\frac{10\log_{10}(t) - \mu_s}{\sigma_s}\right)\right)^{\breve{N}_{\mathrm{UE}}} \end{aligned} \tag{4.15}$$

where $\breve{N}_{\mathrm{UE}}$ is the cardinal of the set of users having SINR bounded by γ_j and γ_{j+1}.
Let,

$$A_j = \int_{C\times\mathbb{R}^+\times Z} \mathbb{1}_{\{\min(y)\|x\|^\beta \leq \tilde{\gamma}_j\}} p_s(y)\ dy\ dx\ dz$$

$$\boxed{A_j = 2\pi \int_0^R \left[1 - \left(1 - \Phi\left(\frac{\frac{\tilde{\gamma}_j}{r^\beta} - \mu_s}{\sigma_s}\right)\right)^{\breve{N}_{\mathrm{UE}}}\right] r\ dr} \tag{4.16}$$

Even though relation (4.16) is not a closed formula, the computation of each A_j can be done using a standard mathematical software. Finally, the two first moments of the Poisson point process in case of the opportunistic RB allocation algorithm: $m^{\mathrm{SISO}}_{N_{\mathrm{Opp}}}$ and $v^{\mathrm{SISO}}_{N_{\mathrm{Opp}}}$ are respectively obtained by including the values of A_j (Formula 4.16) in the expression of $m^{\mathrm{SISO}}_{N_{\mathrm{Fair}}}$ and $v^{\mathrm{SISO}}_{N_{\mathrm{Fair}}}$. As well as for the fair RB allocation algorithm, the dimensioning outage probability $P^{\mathrm{SISO}}_{\mathrm{sup,Opp}}$ for the opportunistic RB allocation algorithm can easily be derived from (2.22) by replacing m_N and v_N with their corresponding values.

$$P^{\mathrm{SISO}}_{\mathrm{sup,Opp}} = \exp\left(-\frac{v^{\mathrm{SISO}}_{N_{\mathrm{Opp}}}}{N^2_{\max}} g\left(\frac{(\alpha-1) m^{\mathrm{SISO}}_{N_{\mathrm{Opp}}} N_{\max}}{v^{\mathrm{SISO}}_{N_{\mathrm{Opp}}}}\right)\right) \tag{4.17}$$

The dimensioning outage probability upper bounds given in this subsection only consider one user's QoS class. The following subsection uses these results to evaluate the dimensioning outage probability upper bound in SISO systems in presence of multiple users' QoS classes.

4.3.2 Multiple user's QoS class in SISO systems

We consider in this section users in $\mathbb{L}$ classes of QoS. Each class of QoS requests a throughput C_l with $l = 1, \cdots, \mathbb{L}$. For each class l, $N_k(x, y, z, l)$ the required number of RBs allocated to each user k at position x with shadowing y and scheduler selecting decision z is a Poisson point process of intensity measure $\lambda_l = \Lambda_l(x)dx \otimes p_s(y)dy \otimes p(z)dz$.
Since the Poisson point process of each class l is independent from one class to each another, the point process of the cell, whatever the users QoS classes, is considered as a superposition of the Poisson point processes of all the QoS classes, which is also a Poisson point process, of intensity $\lambda = \sum_{l=1}^{\mathbb{L}} \lambda_l$.
We still consider the assumptions previously mentioned in section 4.2. Then, the maximum number

of RBs allocated to each user of class l is given by:

$$N_{l,\max} = \left\lceil \frac{C_l}{W \log_2(1+\gamma_{\min})} \right\rceil$$

The upper bound of the dimensioning outage probability $P^{\text{SISO}}_{\text{sup,QoS}}$ is then,

$$P^{\text{SISO}}_{\text{sup,QoS}} = \exp\left(-\frac{\hat{v}_N}{\hat{N}^2_{\max}} g\left(\frac{(\alpha-1)\hat{m}_N \hat{N}_{\max}}{\hat{v}_F} \right) \right) \tag{4.18}$$

where, $\hat{N}_{max}$ is the maximum number of RBs allowed in all the QoS classes,

$$\hat{N}_{\max} = \max_k \; N_{k,\max} \tag{4.19}$$

and $\hat{m}_N$ and $\hat{v}_N$ are respectively the first and the second moment of the Poisson point process expressed as:

$$\boxed{\hat{m}_N = \textstyle\sum_{l=1}^{\mathbb{L}} m_{N,l}} \tag{4.20}$$

$$\boxed{\hat{v}_N = \textstyle\sum_{l=1}^{\mathbb{L}} v_{N,l},} \tag{4.21}$$

with $m_{N,l}$ and $v_{N,l}$ the first and second moments of the Poisson point process of each class l. They can be driven from the single user's QoS class in SISO system study as a function of the RB allocation algorithm chosen, as detailed in the previous section.
In the following section, the same methodology as for the point-to-point SISO case is used to derive the dimensioning outage probability upper bound in a MIMO system, as a function of the RRM algorithm.

4.4 Dimensioning outage probability upper bound computation in MIMO systems

In this section, we consider the MIMO system defined in Chapter 2, Section 2.3.2. Let n_t be the number of transmit antennas at the transmitter side (i.e. the UE) and n_r be the number of receive antennas at the receiver side (i.e. the eNB). We assume that the UE experiences the same path loss and the same shadowing over all its antennas. Actually, in MIMO systems, the effect of the fading is more relevant than the shadowing one as when the antennas are sufficiently separated at each device, the fading coefficients can be considered as different over all the paths. Therefore, the following assumption is added to assumptions 4.1, 4.2, 4.3 and 4.4.

Assumption 4.6 *The channel gain depends only on the user's position x and the Rayleigh fast fading effect.*

The shadowing effects are not considered here and the interferences are assumed to be negligible compared to the noise. We denote by **H** the channel matrix containing all the fading coefficients between the transmit and receive antennas.
One of the main advantages of MIMO systems is the possibility to multiplex $\min(n_t, n_r)$ data streams in the same RB. Furthermore, MIMO systems can be used to improve the system's reliability by exploiting the spatial diversity of transmission. In the following, we consider two different MIMO strategies: i) the first one extracts the diversity of a MIMO system, ii) the second one aims to multiplex $\min(n_t, n_r)$ streams on the same RB. For these two strategies, an dimensioning outage probability upper bound is evaluated when using a fair RB allocation algorithm, and then an opportunistic one.

4.4.1 MIMO diversity gain with fair RB allocation algorithm

In the first considered scheme, each UE selects the antenna that experiences the best channel conditions in order to achieve a high data rate and to transmit its data. Hence, the UE chooses the path having the maximal fading magnitude among the $n_t n_r$ possible fading paths, *i.e.*,

$$|h^*|^2 = \max_{1\leq i\leq n_t, 1\leq j\leq n_r} |h_{i,j}|^2.$$

Let $u = |h^*|^2$ be the maximal fading magnitude. Each coefficient $h_{i,j}$ follows a complex Gaussian distribution $h_{i,j} \sim \mathcal{CN}(0,1)$ and has a magnitude $|h_{i,j}|^2$ that is exponentially distributed. Hence, u is the maximal value of $n_t n_r$ random variables that are exponentially distributed and its cumulative distribution function is such that,

$$F_U(u) = (1 - e^{-u})^{n_t n_r}$$

Consequently, the probability distribution function of u is such that,

$$p_U(u) = \frac{dF_U(u)}{du} = n_t n_r (1 - e^{-u})^{n_t n_r - 1}\, e^{-u}$$

The SINR experienced by the UE is then expressed as:

$$\gamma = \frac{P_t K u}{\tilde{\eta}\|x\|^\beta}$$

The number of allocated RBs for each UE k at position x is a Poisson point process marked with the maximum fading coefficient u and the scheduler decision z as:

$$N_k(x, u, z) = \left\lceil \frac{C_0}{W \log_2(1 + \frac{P_t K u}{\tilde{\eta}\|x\|^\beta})} \right\rceil z \tag{4.22}$$

For fair RB allocation algorithm, all UEs are served with equal probability and hence $p(z) = \frac{1}{N_{\text{UE}}}$. Let γ_j be the SINR threshold that allows each UE to achieve its target throughput C_0 with j the number of required RBs by each UE. We define $\gamma_j = 2^{\frac{C_0}{jW}} - 1$ for $j = 1, \ldots, N_{\max} - 1$ and let $\gamma_0 = \infty$.

With assumption 4.2 we obtain:

$$\frac{P_t K u}{\tilde{\eta}\|x\|^\beta} \geq \gamma_{\min} \Rightarrow \frac{\|x\|^\beta}{u} \leq \frac{P_t K}{\gamma_{\min}\tilde{\eta}}$$

and $\frac{P_t K}{\gamma_{\min}\tilde{\eta}} = \tilde{\gamma}_{\min}$.
The area that contains the users which need j RBs are defined as follows:

$$A_j = \int_{C\times\mathbb{R}^+\times[0,1]} \mathbb{1}_{\left\{\frac{\|x\|^\beta}{u}\leq\tilde{\gamma}_j\right\}}\ p_u(u)\ du\ dx\ p(z)\ dz$$

where $\tilde{\gamma}_j = \frac{P_t K}{\gamma_j \tilde{\eta}}$. Then, by considering the polar coordinate system, the areas $A_j\ \forall\ j = 1, \ldots, N_{max} - 1$ can be expressed as:

$$\begin{aligned} A_j &= \frac{1}{N_{\text{UE}}} \int_0^R \int_0^{2\pi} \int_{\frac{r^\beta}{\tilde{\gamma}_j}}^{+\infty} p_u(u) du\ r dr d\theta \\ &= \frac{1}{N_{\text{UE}}} \int_0^R \int_0^{2\pi} \left[1 - F_U\left(\frac{r^\beta}{\tilde{\gamma}_j}\right)\right] r dr d\theta \end{aligned} \tag{4.23}$$

After some simplification,

$$\boxed{A_j = \frac{1}{N_{\text{UE}}}\left[\pi R^2 - 2\pi \int_0^R r\left(1 - e^{-\frac{r^\beta}{\tilde{\gamma}_j}}\right)^{n_t n_r} dr\right]} \tag{4.24}$$

Using the A_j expression, we can compute the first and second moments $m^{\text{MIMO}}_{N_{(\text{Fair,Div})}}$ and $v^{\text{MIMO}}_{N_{(\text{Fair,Div})}}$ of the Poisson point process of the required number of allocated RBs when a fair RB allocation algorithm is used in diversity gain MIMO systems, with the expressions of $m^{\text{SISO}}_{N_{\text{Fair}}}$ and $v^{\text{SISO}}_{N_{\text{Fair}}}$ The corresponding $P^{\text{Div,MIMO}}_{\text{sup,Fair}}$, the dimensioning outage probability upper bound in case of diversity gain in MIMO systems using a fair RB allocation algorithm can, then, be derived from the concentration inequality theorem (2.22)

$$P^{\text{Div,MIMO}}_{\text{sup,Fair}} = \exp\left(-\frac{v^{\text{MIMO}}_{N_{(\text{Fair,Div})}}}{N^2_{\max}} g\left(\frac{(\alpha-1)m^{\text{MIMO}}_{N_{(\text{Fair,Div})}} N_{\max}}{v^{\text{MIMO}}_{N_{(\text{Fair,Div})}}}\right)\right) \tag{4.25}$$

4.4.2 MIMO multiplexing gain with fair RB allocation algorithm

We assume that the channel conditions are not known at the transmitter side. Consequently, the transmission power is equally shared over the n_t antennas. However, the receiver has a full channel knowledge and uses a maximum likelihood optimal decoder. The channel capacity depends on the eigen-values of the matrix $\mathbf{HH}^\dagger$. Let $\mathbf{HH}^\dagger = \mathbf{UDU}^\dagger$ be the eigen-value decomposition of $\mathbf{HH}^\dagger$ where $\mathbf{U}$ is an unitary matrix and D is the diagonal matrix with non zero diagonal terms $\mu_1, \mu_2, \ldots, \mu_m$ entries with $m = \min(n_t, n_r)$ and $\mu_1 \leq \mu_2 \leq \ldots \leq \mu_m$. In this case, the capacity of the MIMO channel

is such that,

$$C = \log_2 \det \left(\mathbf{I}_{n_t} + \frac{P_t K}{n_t \tilde{\eta} \|x\|^\beta} \mathbf{H}\mathbf{H}^\dagger \right)$$

or equivalently,

$$C = \log_2 \prod_{i=1}^{m} \left(1 + \frac{P_t K \mu_i}{n_t \tilde{\eta} \|x\|^\beta} \right)$$

Let C_{tot}, be the total throughput required to transmit the streams on each transmitting antenna. The number of required RBs per UE k at position x to reach C_{tot} is then:

$$N_k(x, \mu, z) = \left\lceil \frac{C_{tot}}{W \log_2(\prod_{i=1}^{m}(1 + \frac{P_t K \mu_i}{n_t \tilde{\eta} \|x\|^\beta}))} \right\rceil z \tag{4.26}$$

For dimensioning stress, we aim at over estimating the number of RBs and for this purpose, we consider the dimensioning over the antenna that needs the highest number of RBs. Since the singular values are ordered, we can find the maximum number of RBs that should be allocated to a UE k to satisfy its target throughput C_{tot} such that:

$$N_k(x, \mu, z) \geq \left\lceil \frac{C_{tot}}{W m \log_2 \left(1 + \frac{P_t K \mu_1}{n_t \tilde{\eta} \|x\|^\beta} \right)} \right\rceil z \tag{4.27}$$

The cumulative distribution function $F_{\mu_1}(\mu)$ of the smallest eigen-value μ_1 is computed for a general case $n_t \times n_r$ MIMO and a special case of 2×2 MIMO systems in the following paragraphs.

General case: $n_t \times n_r$ MIMO system

The entries of the matrix $\mathbf{H}$ follow a Gaussian distribution and the joint distribution of the order eigen-values of the Wishart matrix $\mathbf{H}\mathbf{H}^\dagger$ are known from [67] and are given by:

$$p_{(\mu_1,\ldots,\mu_m)}(\mu_1, \ldots, \mu_m) = k_{n_t,n_r}^{-1} \prod_{i=1}^{m} \mu_i^{|n_t - n_r|} \prod_{i<j} (\mu_i - \mu_j)^2 e^{-\sum_{i=1}^{m} \mu_i}$$

where k_{n_t,n_r} is a normalization constant. The distribution of the smallest eigen-value μ_1 can be deduced by marginalizing over the variables $\mu_2, \ldots, \mu_m$ *i.e.*

$$p_{\mu_1}(\mu_1) = \int_{\mathcal{V}} p(\mu_1, \ldots, \mu_m) d\mu_2 \ldots d\mu_m$$

where $\mathcal{V} = \{0 \leq \mu_1 \leq \ldots \mu_m \leq \infty\}$. The cumulative distributive function can be then deduced as,

$$F_{\mu_1}(\mu) = \int_0^{\mu} p_{\mu_1}(\mu_1) d\mu_1.$$

Then, the areas A_j are:

$$A_j = \int_\theta \int_r \int_z \int_{\mu_1} \mathbb{1}_{\left\{\frac{\|x\|^\beta}{\mu_1} \leq \tilde{\gamma}_j^{\text{MIMO}}\right\}} p_{\mu_1}(\mu_1) d\mu_1 p(z) dz r dr d\theta$$

where $\tilde{\gamma}_j^{\text{MIMO}} = \frac{P_t K}{n_t \gamma_j^{\text{MIMO}}}$ with $\gamma_j^{\text{MIMO}} = 2^{\frac{C_{\text{tot}}}{mjW}} - 1$ and $p(z)$ is the probability that a UE is served, which is equal to $\frac{1}{N_{\text{UE}}}$ for a fair scheduling algorithm. Then,

$$\begin{aligned} A_j &= \frac{1}{N_{\text{UE}}} \int_\theta \int_r \int_{\frac{r^\beta}{\tilde{\gamma}_j^{\text{MIMO}}}}^{+\infty} p_{\mu_1}(\mu_1) d\mu_1 r dr d\theta, \\ &= \frac{1}{N_{\text{UE}}} \int_\theta \int_r \left[1 - F_{\mu_1}\left(\frac{r^\beta}{\tilde{\gamma}_j^{\text{MIMO}}}\right)\right] r dr d\theta \end{aligned}$$

After some mathematical derivations we obtain:

$$\boxed{A_j = \frac{1}{N_{\text{UE}}} \left[\pi R^2 - 2\pi \int_0^R F_{\mu_1}\left(\frac{r^\beta}{\tilde{\gamma}_j^{\text{MIMO}}}\right) r dr\right]} \tag{4.28}$$

Application to the 2×2 MIMO case

We specify our results to the 2×2 MIMO case. In this configuration, two streams can be transmitted simultaneously in each RB. The joint distribution of the eigen-values is such that,

$$p_{(\mu_1,\mu_2)}(\mu_1, \mu_2) = (\mu_1 - \mu_2)^2 e^{-(\mu_1+\mu_2)}$$

The distribution of the smallest eigen-value μ_1 can be deduced by marginalization,

$$p_{\mu_1}(\mu_1) = \int_{\mu_1}^{\infty} p(\mu_1, \mu_2) d\mu_2.$$

After some simplification, this gives,

$$p_{\mu_1}(\mu_1) = 2e^{-2\mu_1}$$

and the cumulative distribution function $F_{\mu_1}(\mu_1)$ is such,

$$F_{\mu_1}(\mu_1) = \int_0^{\mu_1} p_{\mu_1}(x) dx = 1 - e^{-2\mu_1}$$

Then, the areas A_j are:

$$A_j = \int_\theta \int_r \int_z \int_{\mu_1} \mathbb{1}_{\left\{\frac{\|x\|^\beta}{\mu_1} \leq \tilde{\gamma}_j^{\text{MIMO}}\right\}} p_{\mu_1}(\mu_1) d\mu_1 p(z) dz r dr d\theta$$

Then,

$$\begin{aligned} A_j &= \frac{1}{N_{\text{UE}}} \int_\theta \int_r \int_{\frac{r^\beta}{\tilde{\gamma}_j^{\text{MIMO}}}}^{+\infty} p_{\mu_1}(\mu_1) d\mu_1 r dr d\theta, \\ &= \frac{1}{N_{\text{UE}}} \int_\theta \int_r \left[1 - F_{\mu_1} \left(\frac{r^\beta}{\tilde{\gamma}_j^{\text{MIMO}}} \right) \right] r dr d\theta \end{aligned}$$

After some mathematical derivations we obtain:

$$\boxed{A_j = \frac{1}{N_{\text{UE}}} \left[\pi R^2 - 2\pi \int_0^R \left(1 - e^{-2\frac{r^\beta}{\tilde{\gamma}_j^{\text{MIMO}}}} \right) r dr \right]} \tag{4.29}$$

where $\tilde{\gamma}_j^{\text{MIMO}} = \frac{P_t K}{2\gamma_j^{\text{MIMO}}}$ with $\gamma_j^{\text{MIMO}} = 2^{\frac{C_{\text{tot}}}{j2W}} - 1$. Then, the dimensioning outage probability upper bound $P_{\text{sup,Fair}}^{\text{Mux,MIMO}}$ in case of MIMO multiplexing gain using a fair RB allocation algorithm is deduced from the concentration inequality theorem (2.22) as:

$$P_{\text{sup,Fair}}^{\text{Mux,MIMO}} = \exp\left(-\frac{v_{N_{(\text{Fair,Mux})}}^{\text{MIMO}}}{N_{\max}^2} g\left(\frac{(\alpha - 1) m_{N_{(\text{Fair,Mux})}}^{\text{MIMO}} N_{\max}}{v_{N_{(\text{Fair,Mux})}}^{\text{MIMO}}} \right) \right) \tag{4.30}$$

The first and second moments $m_{N_{(\text{Fair,Mux})}}^{\text{MIMO}}$ and $v_{N_{(\text{Fair,Mux})}}^{\text{MIMO}}$ of the considered Poisson point process are computed as a function of the areas A_j, using the expression of $m_{N_{\text{Fair}}}^{\text{SISO}}$ and $v_{N_{\text{Fair}}}^{\text{SISO}}$.

4.4.3 MIMO diversity gain with opportunistic RB allocation algorithm

The opportunistic RB allocation algorithm serves first the user that experiences the best channel conditions over all active users. This algorithm, when combined with the MIMO diversity technique that we described in Subsection 4.4.1, serves the UE, denoted UE k^*, having the best channel magnitude among $N_{\text{UE}} n_t n_r$ random exponentially distributed values, such that:

$$k^* = \arg \max_{1 \le k \le N_{UE}} \left[\max_{1 \le i \le n_t, 1 \le j \le n_r} | h_{i,j}^{(k)} |^2 \right].$$

Then, the cumulative distribution function of the selected UE channel becomes:

$$F_{U^*}(u^*) = (1 - e^{-u^*})^{N_{\text{UE}} n_t n_r}$$

and its probability distribution function is such that,

$$p_{U^*}(u^*) = N_{\text{UE}} n_t n_r (1 - e^{-u^*})^{N_{\text{UE}} n_t n_r - 1} e^{-u^*} \tag{4.31}$$

Similar derivation as in Subsection 4.4.1 can be repeated and the areas A_j become

$$\boxed{A_j = \pi R^2 - 2\pi \int_0^R r \left(1 - e^{-\frac{r^\beta}{\tilde{\gamma}_j}}\right)^{N_{\mathrm{UE}} n_t n_r} dr} \tag{4.32}$$

The corresponding dimensioning outage probability upper bound for diversity gain MIMO systems with an opportunistic RB allocation algorithm $P_{\mathrm{sup,Opp}}^{\mathrm{Div,MIMO}}$ can be deduced by replacing the corresponding first and second moments $m_{N_{\mathrm{Opp}}}^{\mathrm{Div,MIMO}}$ and $v_{N_{\mathrm{Opp}}}^{\mathrm{Div,MIMO}}$ of the Poisson point process, computed as a function of the areas A_j derived from equation (4.32), in the concentration inequality formula as:

$$P_{\mathrm{sup,Opp}}^{\mathrm{Div,MIMO}} = \exp\left(-\frac{v_{N_{\mathrm{Opp}}}^{\mathrm{Div,MIMO}}}{N_{\max}^2} g\left(\frac{(\alpha-1) m_{N_{\mathrm{Opp}}}^{\mathrm{Div,MIMO}} N_{\max}}{v_{N_{\mathrm{Opp}}}^{\mathrm{Div,MIMO}}}\right)\right) \tag{4.33}$$

4.4.4 MIMO multiplexing gain: Opportunistic RB allocation algorithm

As stated in Subsection 4.4.2, a pessimist way of radio-dimensioning is conditioned by considering the worst eigen-value μ_1. The opportunistic RB allocation algorithm selects then among the N_{UE} UEs the UE with the maximal smallest eigen-value μ_1. Let $\mu_1^{(k)}$ define the smallest eigen value of UE k. Then the selected UE k^* is such that,

$$k^* = \arg \max_{1 \le k \le N_{\mathrm{UE}}} \mu_1^{(k)}$$

The cumulative distribution function of $\mu_1^{k^*} = \mu_1^*$ is then such that,

$$F_{\mu_1^*}(\mu^*) = F_{\mu_1}(\mu^*)^{N_{\mathrm{UE}}} = (1 - e^{-2\mu^*})^{N_{\mathrm{UE}}}$$

By replacing the expression of $F_{\mu_1^*}(\mu^*)$ in the area expression A_j we obtain:

$$\begin{aligned} A_j &= 2\pi \int_0^R \int_{\frac{r^\beta}{\tilde{\gamma}_j^{\mathrm{MIMO}}}}^{+\infty} p_{\mu_1^*}(\mu_1^*)\, d\mu_1^*\, r dr, \\ &= 2\pi \int_0^R \left[1 - F_{\mu_1^*}\left(\frac{r^\beta}{\tilde{\gamma}_j^{\mathrm{MIMO}}}\right)\right] r dr. \end{aligned}$$

Then,

$$\boxed{A_j = \pi R^2 - 2\pi \int_0^R \left(1 - e^{-2\frac{r^\beta}{\tilde{\gamma}_j^{\mathrm{MIMO}}}}\right)^{N_{\mathrm{UE}}} r dr} \tag{4.34}$$

Since the areas A_j are computed for multiplexing gains in MIMO systems with opportunistic RB allocation algorithms, the first and second moments $v_{N_{\mathrm{Opp}}}^{\mathrm{Mux,MIMO}}$ and $v_{N_{\mathrm{Opp}}}^{\mathrm{Mux,MIMO}}$ of the Poisson point processes can be computed accordingly. The dimensioning outage probability upper bound $P_{\mathrm{sup,Opp}}^{\mathrm{Mux,MIMO}}$

is then derived from the concentration inequality (2.22) as:

$$P_{\text{sup,Opp}}^{\text{Mux,MIMO}} = \exp\left(-\frac{v_{N_{(\text{Opp,Mux})}}^{\text{MIMO}}}{N_{\max}^2} g\left(\frac{(\alpha-1)m_{N_{(\text{Opp,Mux})}}^{\text{MIMO}} N_{\max}}{v_{N_{(\text{Opp,Mux})}}^{\text{MIMO}}}\right)\right) \tag{4.35}$$

4.5 Validation of the dimensioning outage probability upper bound analytical model

In this section we verify how close is the theoretical upper bound from the dimensioning outage probability obtained by Monte Carlo simulations. Private Mobile Networks (PMN) deployment in LTE technology with microcells of $R = 100$ m radius is considered. To overcome the interference with the LTE cellular network in urban areas, the PMN is operating at a frequency carrier f_c of 800 MHz. For simplicity, we consider that the interference level is not significant compared with the value of thermal noise (i.e. $I_{eNB}^c \ll N$). The mean and standard deviation of the log-normal shadowing are set respectively to $\mu_s = 6$ dB and $\sigma_s = 3$ dB. In case of users with a single QoS class, the surface density of arrivals ρ and the mean time service $\frac{1}{\nu}$ are respectively set to 6 $10^{-4}\text{min}^{-1}\text{m}^{-2}$ and 1 min. We consider different values of target throughputs C_0: 100 kbps, 200 kbps, 300 kbps and 400 kbps. When the minimum signal to interference plus noise ratio $\gamma_{\min}$ is set to 0.2 dB, the corresponding maximum number of RBs that can be allocated to one UE to achieve a target throughput C_0 of 200 kbps is $N_{\max} = 2$.
To validate the multiple users QoS classes dimensioning outage probability upper bound, we consider two user's QoS classes. The request throughput of class 1 and class 2 are respectively set to $C_1 = 150$ kbps and $C_2 = 200$ kbps. The surface density of arrivals of class 1 users is set to $\rho_1 = 4\ 10^{-4}$ min^{-1} m^{-2} with mean service time $\frac{1}{\nu_1} = \frac{1}{2}$ min and the parameters of the class 2 users are $\rho_2 = 2\ 10^{-4}\text{min}^{-1}\text{m}^{-2}$ and $\frac{1}{\nu_2} = 1$ min.

First, the theoretical dimensioning outage probability upper bound is computed according to the obtained formulas. Then, it is compared to the dimensioning outage probability obtained with Monte Carlo simulations when an average number of RBs m_N is available in the network. The validation of the theoretical upper bound is established by the mean of the log ratio test Δ introduced in Chapter 3. We compute the upper bound of the dimensioning outage probability by varying the parameter α, introduced in equation (2.21), from 1.3 to 1.8. These values correspond to a need of 30% to 80% of RBs more than the theoretical average number.

4.5.1 Analytical model validation

In SISO systems, the dimensioning outage probabilities are given in Figures 4.1 and 4.2 with respect to the used RB allocation algorithm. We consider four QoS classes where each one is characterized by its target throughput C_0. From these figures, we note that the analytical upper bound of the dimensioning

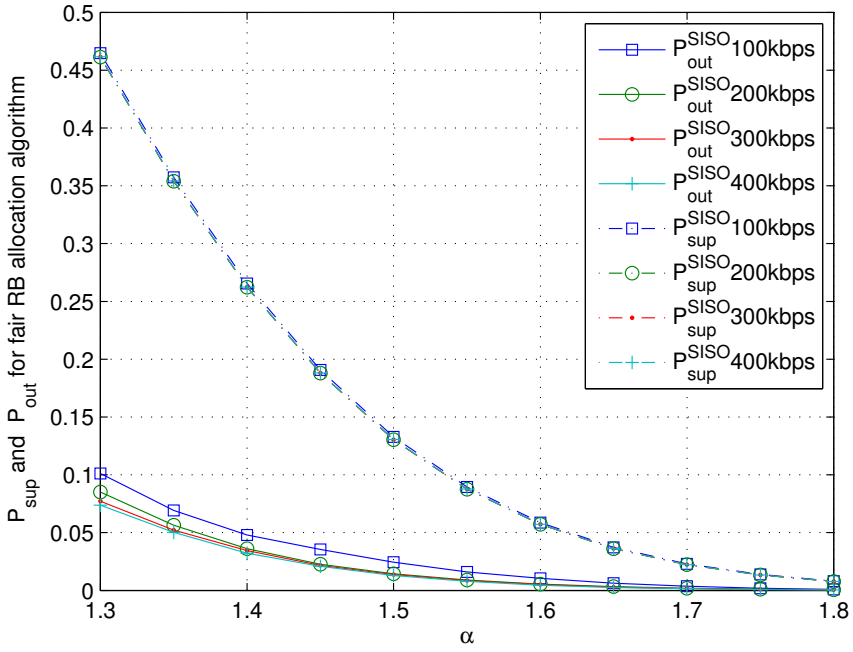

Figure 4.1: Evaluated dimensioning outage probability and dimensioning outage probability upper bound for different target throughputs C_0 in SISO systems with fair RB allocation algorithm

outage probability and the simulated dimensioning outage probability decrease when a larger total bandwidth is assumed. When the fair RB allocation algorithm is used, we note from Figure 4.1 that the dimensioning outage probability upper bounds are almost the same whatever the value of C_0. This is due to the negligible influence of C_0 in $m_{N_{\text{Fair}}}^{\text{SISO}}$ and $v_{N_{\text{Fair}}}^{\text{SISO}}$ expressions and to the same probabilities for all the users to be selected by the scheduler. In addition, with Monte Carlo simulations, the dimensioning outage probability varies from one QoS class to another. The gap between the curves does not exceed 0.03, which is due to the small variation in C_0. The larger dimensioning outage probability is given with the QoS class that requests a target throughput $C_0 = 100$ kbps. In fact, with a low target throughput, the mean shadowing does not affect the average number of RBs per user that will be taken into account for the upper bound computation. This average number is only one RB per UE to achieve C_0, and corresponds to the minimum one that will be allocated to a UE, whatever its radio channel conditions. However, Monte Carlo simulations can generate some users with such shadowing that more RBs will be necessary for the concerned UEs, and leading to outage. For higher throughputs, as the average number of required RBs per UE is higher than one, it better smoothes the shadowing variations over Monte Carlo draws.

In Figure 4.2, we note that the effect of the opportunistic RB allocation algorithm is noticeable in the dimensioning outage probability upper bound computation. The dimensioning outage probability upper bound obtained with $C_0 = 100$ kbps is higher than the other ones. The gap between the dimensioning outage probability obtained with Monte Carlo simulations for $C_0 = 100$ kbps and the

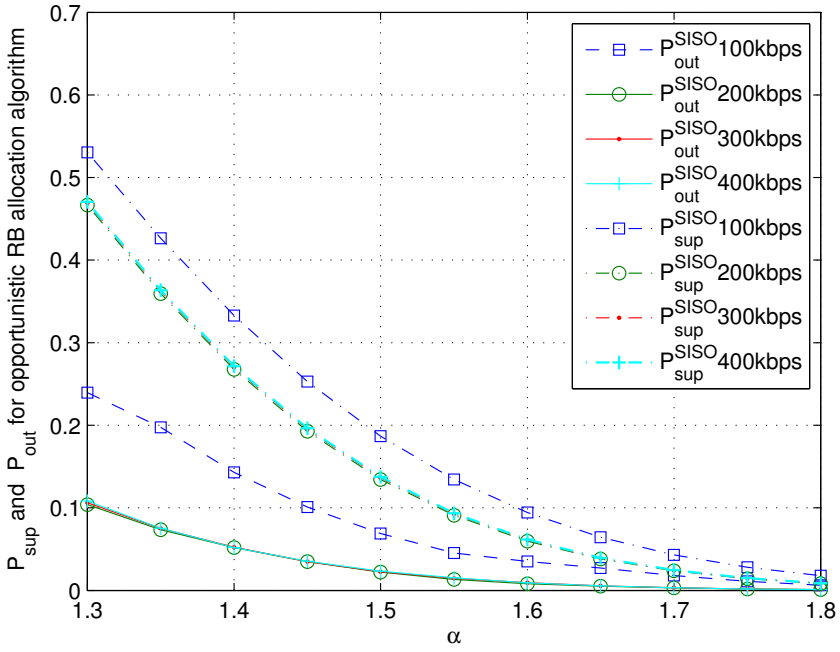

Figure 4.2: Evaluated dimensioning outage probability and dimensioning outage probability upper bound for different target throughputs C_0 in SISO systems with opportunistic RB allocation algorithm

dimensioning outage probabilities obtained with Monte Carlo simulation for the other values is higher than the gap obtained with fair RB allocation algorithm, due to the influence of the target throughput variation in the areas A_j computation and consequently in $m^{\text{SISO}}_{N_{\text{Opp}}}$ and $v^{\text{SISO}}_{N_{\text{Opp}}}$ computations. To evaluate how much the developed analytical model of the dimensioning outage probability upper bound is accurate, Figures 4.3 and 4.4 show the log ratio test values when, respectively, the fair and the opportunistic RB allocation algorithm are used.

We notice that the maximum log ratio $\Delta^{\text{SISO}}_{\text{Fair}}$ and $\Delta^{\text{SISO}}_{\text{Opp}}$, obtained in SISO systems with one QoS class, is about 0.45 whatever the target throughput C_0. Figure 4.5 gives the log ratio test obtained with two user's QoS classes for fair and opportunistic RB allocation algorithms. Since a target throughput C_0 of 150 kbps and 200 kbps are considered, we notice a small variation between the log ratio test obtained in SISO systems for two users QoS classes when using fair or opportunistic RB allocation algorithm.

In MIMO systems only one user's QoS class is considered. In addition to the simulation parameters cited above, a Rayleigh fast fading of standard deviation $\sigma_f = 1$ is considered. Figure 4.6 shows the log ratio test obtained for both MIMO diversity and multiplexing gains when fair and opportunistic RB allocation algorithms are used for a target throughput $C_0 = 300$ kbps. The maximum log ratio test is about 0.42.

Actually, all the log ratio values, obtained in SISO and MIMO systems, are lower than 1 whatever the used RB allocation algorithm, the user's QoS class type and the considered target throughput.

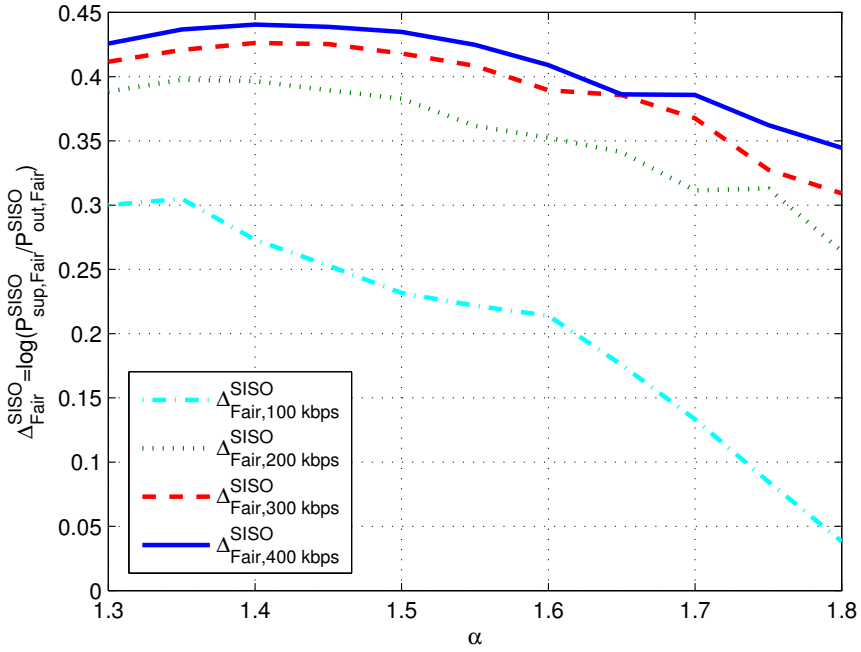

Figure 4.3: Validation of the upper bound dimensioning outage probability (using Log ratio test) for fair RB allocation algorithm

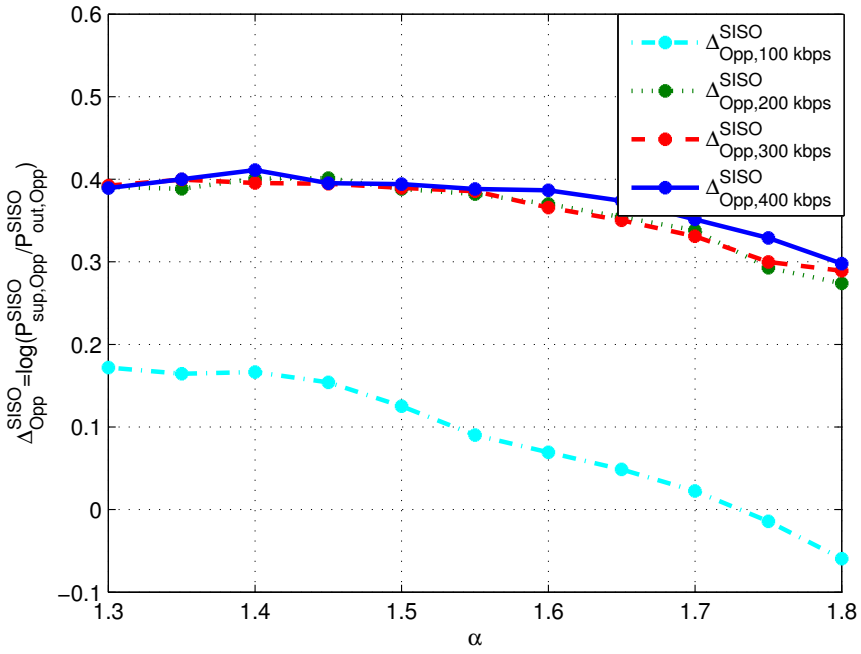

Figure 4.4: Validation of the upper bound dimensioning outage probability (using Log ratio test) for opportunistic RB allocation algorithm

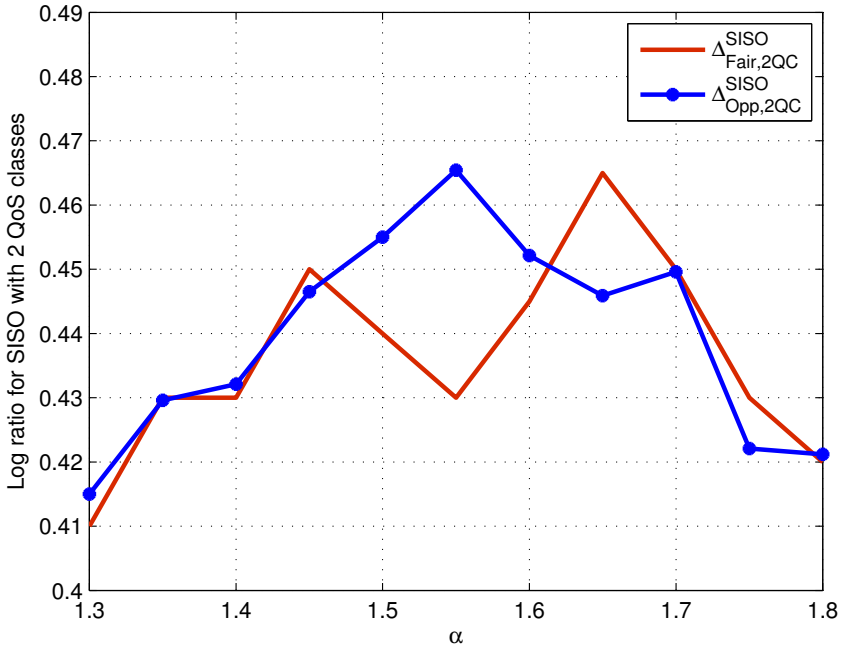

Figure 4.5: Validation of the upper bound dimensioning outage probability (using Log ratio test) for fair and opportunistic RB allocation algorithms with two QoS classes

Therefore, they validate the proposed analytical model of the dimensioning outage probability upper bound, in SISO and MIMO systems, independently of the user's QoS type, the target throughput and the RB allocation algorithm.

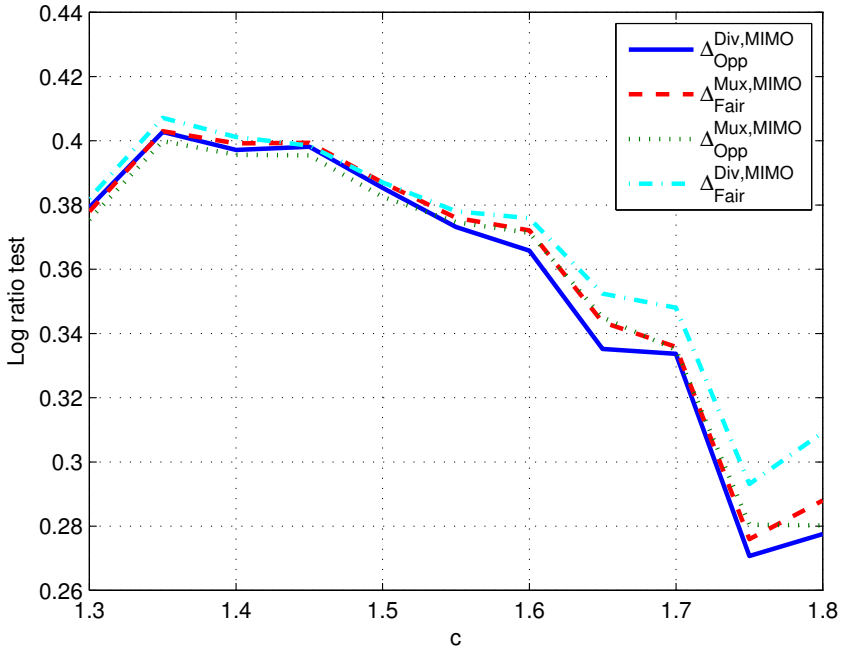

Figure 4.6: Validation of the upper bound dimensioning outage probability (using Log ratio test) in MIMO systems

4.5.2 Bandwidth allocation

The adequate bandwidth B that can be allocated to a cell is then determined using the average number of RBs and the computed dimensioning outage probability upper bound. Figure 4.7 represents the average number of RBs needed by the network as a function of the target throughput C_0, when the fair and opportunistic RB allocation algorithm are used in SISO system for a single user's QoS class. To allocate these average numbers of required RBs values, we propose to associate the nearest LTE standardized bandwidth, varying from 1.4 MHz and 20 MHz, that can be allocated.
Table 4.1 gives the dimensioning outage probability obtained by Monte Carlo simulations. If we allocate these standardized LTE bandwidths, we obtain a dimensioning outage probability for the fair RB allocation algorithm, $P^{SISO}_{out,Fair}$ between 5.2 10^{-2} and 9.1 10^{-6}. If we allocate 5 MHz more, the dimensioning outage probability becomes very small and most of the RBs are not used. To address the RB wastage problem and improve the spectrum use efficiency, we can use the smallest bandwidth $B = 1.4$ MHz as a carrier aggregation component, which allows us to increase the number of RBs per cell by only 6 RBs.

The same methodology is used for MIMO systems. Table 4.2 contains the average number of RBs obtained with the analytical model for diversity and multiplexing gain MIMO systems using fair and opportunistic RB allocation algorithms. To enlighten the MIMO gains, we compare our results with 1×1 diversity gain MIMO system (equivalent to a SISO system that considers only path loss and the fading effect) using a fair RB allocation algorithm. Since MIMO system gains are relevant when

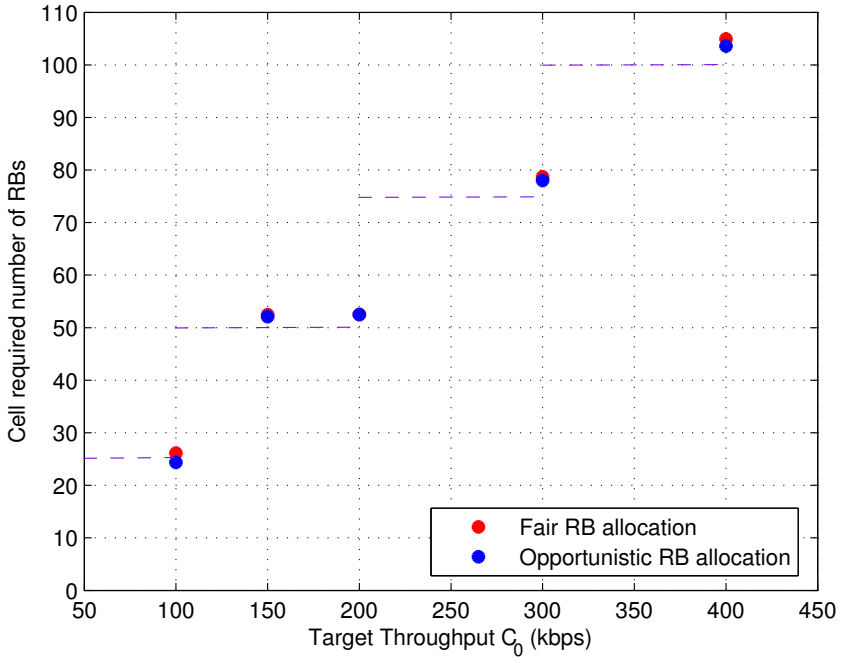

Figure 4.7: Average number of necessary RBs and corresponding total LTE bandwidth for SISO systems with fair RB allocation algorithm

B \ C_0	100	150	200	300	400
5	$6.8\ 10^{-2}$				
10	0	$9.1\ 10^{-6}$	$1.3\ 10^{-5}$		
15	0	0	0	$5.3\ 10^{-2}$	
20	0	0	0	$5.1\ 10^{-4}$	$5.3\ 10^{-2}$

Table 4.1: Dimensioning outage probability computed for different QoS class C_0 (in kbps), using LTE standard bandwidth B (in MHz) in SISO systems with fair RB allocation algorithm

high target throughput is required, we assume in our simulations three QoS classes that request, respectively, a target throughput of 1 Mbps, 3 Mbps and 5 Mbps.

We notice a small variations between the systems required average number of RBs, especially for low target throughput. The variation does not exceed $7\ 10^{-4}$ RBs for $C_0 = 1$ Mbps, and 0.1 RBs for $C_0 = 5$ Mbps. These small variation are due to the negligible influence of the areas A_j to the cell area πR^2.

With the help of these average numbers of RBs, the adequate LTE standardized bandwidth allocation is given. Table 4.3 summarizes the dimensioning outage probabilities obtained with Monte Carlo simulations when the corresponding LTE bandwidths are allocated. For MIMO systems with target throughput $C_0 = 1$ Mbps (i.e. an allocated 5 Mbps LTE bandwidth), they are equal to $6.8\ 10^{-2}$, whatever the system used. This is due to the negligible variation of the required number of RBs

C_0 (Mbps) \ m_N	$m_{N,\text{Fair}}^{\text{SISO}}$	$m_{N,\text{Fair}}^{\text{Div,MIMO}}$	$m_{N,\text{Opp}}^{\text{Div,MIMO}}$	$m_{N,\text{Fair}}^{\text{Mux,MIMO}}$	$m_{N,\text{Opp}}^{\text{Mux,MIMO}}$
1	33.5109	33.5102	33.5102	33.5107	33.5102
3	56.7700	56.7500	56.7000	56.6300	56.6200
5	75.0057	75.0040	74.9800	74.9700	74.9000

Table 4.2: Required average number of RBs in MIMO systems

in Table 4.2. For $C_0 = 3$ Mbps (i.e. an allocated bandwidth $B = 10\ MHz$), the dimensioning outage probability is about 1.1 10^{-2} for SISO and diversity gain MIMO systems, and is null for the multiplexing gain in MIMO system, whatever the RB allocation algorithm used. For 15 MHz bandwidth, corresponding to a target throughput $C_0 = 5$ Mbps, the dimensioning outage probabilities are null for all the systems. It means that the required average number of RBs is more than enough to satisfy and serve all users.

In Table 4.4, the smallest standardized bandwidth $B = 1.4$ MHz is used as a component aggregation

B (MHz) \ P_{out}	$P_{out,\text{Fair}}^{\text{Div,SISO}}$	$P_{out,\text{Fair}}^{\text{Div,MIMO}}$	$P_{out,\text{Opp}}^{\text{Div,MIMO}}$	$P_{out,\text{Fair}}^{\text{Mux,MIMO}}$	$P_{out,\text{Opp}}^{\text{Mux,MIMO}}$
5	6.8 10^{-2}	6.8 10^{-2}	6.8 10^{-2}	6.8 10^{-2}	6.8 10^{-2}
10	1.15 10^{-2}	1.15 10^{-2}	1.10 10^{-2}	0	0
15	0	0	0	0	0

Table 4.3: Dimensioning outage probability in MIMO systems.

in case of C_0 equal to 1 Mbps and 3 Mbps (when the dimensioning outage probabilities are noticeable). This smallest component aggregation leads to a decrease of the dimensioning outage probabilities, for example from 6.8 10^{-2}, before the carrier aggregation, to 0.45 10^{-2} after the carrier aggregation, for $C_0 = 1$ Mbps. Actually, the carrier aggregation decreases the dimensioning outage probabilities whatever the system used to a dimensioning outage probability lower than the one fixed by the operators which is usually about 1%.

Since the allocated bandwidth in case of a target throughout $C_0 = 5$ Mbps leads to a zero dimensioning

(B, CA) (MHz) \ P_{out}	$P_{out,\text{Fair}}^{\text{Div,SISO}}$	$P_{out,\text{Fair}}^{\text{Div,MIMO}}$	$P_{out,\text{Opp}}^{\text{Div,MIMO}}$	$P_{out,\text{Fair}}^{\text{Mux,MIMO}}$	$P_{out,\text{Opp}}^{\text{Mux,MIMO}}$
(5,1.4)	4.5 10^{-3}	4.5 10^{-3}	4.5 10^{-3}	4.5 10^{-3}	4.5 10^{-3}
(10,1.4)	2.4 10^{-3}	2.4 10^{-3}	2.4 10^{-3}	0	0
(10,0)	0.1175	0.1175	0.1152	1.8 10^{-3}	1.3 10^{-3}

Table 4.4: Dimensioning outage probability computed after modifying the allocated bandwidth in MIMO systems.

outage probability, we try to decrease the allocated bandwidth by 33%, to $B = 10$ MHz, corresponding to 50 available RBs. With this reduction, the dimensioning outage probability of SISO and diversity gain MIMO systems increases to 11%, whereas the dimensioning outage probabilities of multiplexing

gain in MIMO systems become on the order of 0.1 %.
These results show that the use of diversity gain MIMO systems, independently of the used RB allocation algorithm, is not sufficient relatively to SISO systems and does not increase significantly the rate when operating in the low SINR regime. Hence, independently of the used RB allocation algorithm, the diversity techniques do not overcome the dimensioning outage situation compared to a classical SISO system. On the contrary, as the multiplexing techniques increase significantly the rate that can be transmitted, and hence decrease the required number of RBs per UE, the dimensioning outage probability decreases significantly compared to the SISO case. We finally note that, although a pessimistic strategy was analytically adopted to estimate the average number of RBs, a significant gain in terms of dimensioning outage probability can be numerically observed. However, this pessimistic strategy gives an over-estimation of the dimensioning outage probability.

4.6 Conclusion

This chapter addressed the radio dimensioning problem of SISO and MIMO LTE uplink networks. We developed an analytical model to evaluate the dimensioning outage probability upper bound and the average number of required RBs per cell, in order to evaluate the adequate bandwidth that should be allocated to the network. The dimensioning outage probability upper bound was evaluated as a function of two RRM strategies: i) fair RB allocation algorithm and ii) opportunistic RB allocation algorithm, considering a single and multiple user's QoS classes. The developed analytical model was based on the stochastic geometry using the Poisson point processes, which helped us to examine the statistical network's behavior. To evaluate how close were the analytical model of the dimensioning outage probability upper bound and the dimensioning outage probability obtained by Monte Carlo simulations, a log ratio test was used. Its values validated the analytical model independently of the used system, the target throughput or the number of user's QoS classes. The dimensioning problem was also extended to MIMO systems. We showed that, in the low SNR regime, when using diversity MIMO techniques, no significant gain on dimensioning outage probability was observed compared to SISO systems. However, the multiplexing gain strategies increased significantly the rate and consequently decreased the dimensioning outage probability.

4.A Appendices

4.A.1 Derivation of area A_j expression in SISO system with fair RB allocation algorithm (Formulas 4.45)

We assume γ_j to be the SINR threshold, j being the user's required number of RBs to achieve its target throughput C_0, with:

$$\gamma_j = 2^{C_0/(jW)} - 1 \quad \text{for } j = 1, \cdots, N_{\max} - 1 \quad \text{and } \gamma_0 = \infty$$

We define A_j the area which contains the users that require at most j RBs to satisfy their target throughput C_0. The area A_j can be determined as follows:

$$\begin{aligned} A_j &= \int_{C\times\mathbb{R}^+\times Z} \mathbb{1}_{\{y\|x\|^\beta \le P_t K/\tilde{\eta}\gamma_j\}}\, p_s(y)dy\; p(z)dz\; dx \\ &= \int_{C\times\mathbb{R}^+\times Z} prob\left(y\|x\|^\beta \le \tilde{\gamma}_j\right) p(z)dz\; dy\; dx \end{aligned} \tag{4.36}$$

where $\tilde{\gamma}_j = \frac{P_t K}{\tilde{\eta}\gamma_j}$.
The probability density function of the shadowing is:

$$p_s(y) = \frac{\xi}{\sigma_s y\sqrt{2\pi}} \exp\left(-\frac{(10\log_{10} y - \mu_s)^2}{2\sigma_s^2}\right) \tag{4.37}$$

where, $\xi = 10/\ln 10$.
The cumulative distribution function of S is then,

$$F_S(y) \quad = \tfrac{1}{2} + \tfrac{1}{2}\mathrm{erf}\left(-\tfrac{(10\log_{10}(y)-\mu_s)^2}{\sqrt{2}\sigma_s}\right) \tag{4.38}$$

It can be expressed using the Q function[3] as:

$$F_S(y) \quad = Q\left(\tfrac{(10\log_{10}(y)-\mu_s)^2}{\sqrt{2}\sigma_s}\right) \tag{4.39}$$

From Formulas 4.36 we obtain:

$$A_j = \frac{1}{N_{\mathrm{UE}}} \int_{x\in C} prob\left(y \le \frac{\tilde{\gamma}}{\|x\|^\beta}\right) dx \tag{4.40}$$

where, $\tilde{\gamma} = \frac{P_t K}{\tilde{\eta}\gamma_j}$ Then,

$$A_j = \quad \tfrac{1}{N_{\mathrm{UE}}} \int_{x\in C} Q\left(\frac{10\log_{10}(\frac{\tilde{\gamma}_j}{\|x\|^\beta}) - \mu_s}{\sigma_s}\right) dx \tag{4.41}$$

$$= \quad \tfrac{1}{N_{\mathrm{UE}}} \int_{x\in C} Q\left(\frac{1}{\sigma_s}10\log_{10}(\tilde{\gamma}_j) - \frac{\mu_s}{\sigma_s} - \frac{\beta}{\sigma_s}10\log_{10}(x)\right) dx \tag{4.42}$$

$$= \quad \tfrac{1}{N_{\mathrm{UE}}} \int_{x\in C} Q\left(\frac{1}{\sigma_s}10\log_{10}(\frac{P_t K}{\tilde{\eta}\gamma_j}) - \frac{\mu_s}{\sigma_s} - \frac{\beta}{\sigma_s}10\log_{10}(x)\right) dx \tag{4.43}$$

$$= \quad \tfrac{1}{N_{\mathrm{UE}}} \int_{\theta=0}^{2\pi}\int_{r=0}^{R} Q\left(\alpha_j - \zeta\ln(r)\right) r dr d\theta \tag{4.44}$$

[3] $Q(x) = \frac{1}{2} + \frac{1}{2}\mathrm{ref}(\frac{x}{\sqrt{2}})$

with: $\alpha = \frac{1}{\sigma_s}\left(10\log_{10}(\frac{P_t K}{\tilde{\eta}\gamma_j}) - \mu_s\right)$, and $\zeta = \frac{\beta 10}{\sigma_s \ln(10)}$.

$$A_j = \frac{1}{N_{\text{UE}}}\left(\frac{1}{4}\exp\left(\frac{2\alpha_j}{\zeta} + \frac{2}{\zeta^2}\right)\text{erf}\left(-\frac{\alpha_j\zeta+\zeta^2\ln(R)-2}{\sqrt{(2)}\zeta}\right) + \frac{R^2}{4} + \frac{R^2}{4}\text{erf}\left(\frac{\alpha_j-\zeta\ln(R)}{\sqrt{2}}\right) + \frac{1}{4}\exp\left(\frac{2\alpha_j}{\zeta} + \frac{2}{\zeta^2}\right)\right)$$

Then, A_j can be expressed with Φ the normal cumulative distribution function[4],

$$\boxed{A_j = \frac{\nu}{\rho R^2}\exp\left(2/\zeta + 2\alpha_j/\zeta\right)\Phi(\zeta\ln R - 2/\zeta - \alpha_j) + \frac{\nu}{\rho}\Phi(\alpha_j - \zeta\ln R)} \tag{4.45}$$

[4]the normal cumulative distribution function is expressed as: $\Phi = \frac{1}{2} + \frac{1}{2}\text{erf}(\frac{x}{\sqrt{2}})$

Chapter 5

Radio resource allocation scheme for green uplink LTE networks

Parts of this chapter were published in IEEE WCNC 2013[1]*, IEEE GREENCOM 2013*[2] *and submitted to IEEE Transactions on Vehicular Technology*[3]

WHEN an adequate frequency bandwidth is determined and allocated to a cell, the RRM entity aims at allocating efficiently the limited radio resources among users. In the uplink of green LTE networks, the radio resources allocation includes two steps: the RBs allocation and an adequate UE transmission power allocation. Each radio resource allocation scheme is based on an utility function which translates the system satisfaction level. In this chapter, the cell capacity maximization is considered. For this purpose, a new radio resource allocation scheme is proposed. It is based on the Opportunistic and Efficient RB Allocation (OEA) algorithm whose objective is to maximize the aggregate throughput while subject to the SC-FDMA constraints. An evolution of the algorithm, named QoS based OEA, providing QoS differentiation, is also proposed. It allocates a given maximum number of RBs to each UE according to the user's QoS requirements. The UE transmission power is adjusted by a channel dependent power control such that the user's QoS

[1]F.Z. Kaddour, M. Pischella, P. Martins, E. Vivier and L. Mroueh, "Opportunistic and Efficient Resource Block Allocation Algorithms for LTE Uplink Networks", in proceedings of IEEE Wireless Communications and Networking Conference (WCNC), Shanghai, China, Apr. 2013.

[2]F.Z. Kaddour, E.Vivier, M. Pischella, L. Mroueh and P. Martins, "Green Opportunistic and Efficient Resource Block Allocation Algorithm for LTE Uplink Networks ", in proceedings of 3rd IEEE GreenComm online conference, October, 2013.

[3]F.Z. Kaddour, E. Vivier, L. Mroueh, M. Pischella and P. Martins, "Green Opportunistic and Efficient Resource Block Allocation Algorithm for LTE Uplink Networks", submitted to IEEE Transactions on Vehicular Technology.

satisfies the previous throughput determined by the RB allocation step. The proposed radio resource allocation scheme is studied in regular and random networks.

5.1 Introduction

Nowadays, in current and next generation mobile networks, the ICT are facing increasing challenges to satisfy the quality of service required by the smart terminals enhanced functionalities. Then the energy consumption of wireless communication networks and the relevant global CO_2 emission show continuous growth for several years. In [68], it has been emphasized that actually the information and communication technology infrastructures consume about 3% of the world-wild energy which causes about 2% of the world CO_2 emissions. Energy costs to the mobile's operators half of the operating expenses [69]. Moreover, improving the energy efficiency is not only beneficial for the global environment, but also makes commercial sense for telecommunication operators supporting sustainable and profitable business. The energy efficiency maximization is reached by maximizing the user's throughput, which is enabled with an adapted RB allocation policy, and minimizing the UE transmission power. Within the framework of radio resource allocation, a number of technical approaches are investigated in the literature.

We focus in this thesis on the radio resource allocation on the uplink 3GPP LTE networks. The relevance of the SC-FDMA on the uplink is that in addition to the OFDMA advantages the PAPR can be decreased by more than 25% compared to the OFDMA technique [70]. This advantage not only leads to the decrease of the equalizer complexity and the cost of the mobile terminal by the same way, but also to the decrease of the UE energy consumption. As saving UE battery life becomes the central concern of the researchers, works on this scope focus on: (i) maximizing the available energy and (ii) minimizing the energy consumption. The available energy can be increased by (a) the battery capacity improvement which is, unfortunately, not sufficient and is limited due to design aspects, and (b) using the surrounding energy sources, such as kinetic, thermal, and solar energy [71].

The UE energy consumption can be minimized by first, optimizing the hardware energy consumption, such as choosing power efficient components and applying power management like performing sleep modes for inactive hardware [72] or the Discontinuous Reception (DRX) in idle mode [73]. The second solution is the adjustment of the UE parameters, like the brightness display and the processor speed for some applications.

In the radio access network, the power consumption reduction is performed by a power control applied on the UE transmission power. However, this could lead to a low signal to interference plus noise ratio and a low individual throughput. Therefore, the power control should take into account the required QoS and the channel conditions that the user experiences. The radio resource allocation decision is made in order to satisfy a system satisfaction level such as the aggregate throughput maximization. In this case, the RB allocation algorithm is based on the channel condition metric. In addition to the user's QoS requirement satisfaction, the proposed strategies and algorithms for allocating RBs to UEs and for determining the UEs transmission power should consider the SC-FDMA adjacency constraint

specific to LTE release 8 network. The SC-FDMA is also characterized by the MCS robustness constraint, as detailed in Section 2.1.4. Due to these two constraints, most RRM algorithms proposed in the literature for the downlink cannot be directly applied to the uplink. Moreover, the packet scheduling occurs every subframe with 1 ms duration [9]. Then, the radio resource allocation schemes shall be simple and efficient. Consequently, the uplink radio resource allocation solution is $S_{RB} \in S$ that maximizes the sum of all individual UE's throughputs $R_k \ \forall \ k = 1, \cdots, N_{UE}$, with S the set of all possible allocations (RB,UE). Then, the uplink RRM problem is expressed as:

$$S_{RB} = \arg \max_{S_{RB} \in S} \left\{ \sum_{k=1}^{N_{UE}} R_k \right\}$$

subject to:

1. Allocating each RB exclusively to one UE,
2. Allocating adjacent RBs to each UE,
3. Using for each UE, the same MCS over all its allocated RBs,
4. Respecting the UE transmission power limitation since the sum of the UE transmission power over its allocated RBs should not exceed P_{max}.

The uplink RRM problem was extensively studied. The optimal solution is given by an exhaustive search (e.g. the branch and bound solution for Binary Integer Programming (BIP) [10] [74]), but at the expense of a high complexity, since this problem is N-P complex. The heuristics proposed in [11] [12] [13] consider the contiguity constraint, but neglect the power control (by setting the UE transmission power at its maximum), the update of the power transmission per RB, and the MCS robustness constraint. These assumptions lead to overestimate the effective final user's throughput and to increase the inter-cell interference and the RB wastage, which consequently decrease the spectral efficiency and the energy efficiency. Detailed state of the art in radio resource allocation schemes is given in Section 5.2.

In this Chapter, an efficient radio resource allocation scheme is proposed. Our algorithm named Opportunistic and Efficient RB Allocation (OEA) algorithm, takes into account the SC-FDMA constraints and the update of the UE transmission power per RB as a function of the number of allocated RBs. This update of the signal to interference plus noise ratio has the benefit of canceling the RB wastage ratio. We suggest a variant of the proposed algorithm, named QoS based OEA, which is adapted to the QoS differentiation. It also maximizes the aggregate throughput, but serves more users while each served user will be allocated no more than the set of RBs required to satisfy its target QoS. The proposed algorithms are compared to the most relevant algorithms found in literature. For fair performance comparison, the final user throughput calculation was established using the MCS mode. The UE transmission power allocation is determined once the RB allocation is performed. The proposed power control depends on the user's QoS target and the channel conditions on the set of allocated RBs. It maintains the user's QoS and reduces the computation complexity compared to joint power and RB allocation algorithms.

The proposed radio resource allocation scheme is detailed in Section 5.3. Section 5.4 gives its computational complexity steps. Its performance analysis is established in a regular and a random network, where the inter-cell interference level considers the average transmission power generated by each RB allocation algorithm. These two performance analysis are given respectively in Section 5.5.1 and Section 5.5.2.

5.2 State of the art

The radio resource management in LTE uplink systems has been addressed in many papers. Usually, the objective of the RRM is to maximize the aggregate throughput. Radio resource allocation includes RBs and power allocation, that can be performed: jointly or separately. The joint allocation of RBs and UEs transmission power is more complex. It can be solved by using game theory, as proposed in [75] for the cognitive radio, or using BIP, by transforming the radio resource allocation problem into a linear optimization problem, as proposed in [74]. The authors consider the RB contiguity and the transmission power minimization as constraints of the linear optimization problem.
The separate allocation of RBs and UEs transmission power is less complex compared to the joint one. First, the UEs transmission power allocation is determined by: i) a power control adjustment according to the target QoS and the channel's conditions (when channel information are available on the allocated RBs), or ii) assuming the UEs transmission power as constant (usually set at P_{max}). In this latter case, the optimal solution for RB allocation is obtained using the BIP. In [10], the branch and bound method is used to solve the BIP. It constitutes a tree that enumerates all the feasible solutions. To decrease the complexity, we can separate the constraints (i.e. the contiguity constraint and the exclusivity of the RB allocation) and fix a lower bound on the objective function which leads to neglect the solutions with low performances.
The RB allocation process must determine, for each user k, the set of allocated RBs $\mathcal{A}_k$, and the number of allocated RBs: $|\mathcal{A}_k|$. The definition of $|\mathcal{A}_k|$ and $\mathcal{A}_k$ is sometimes performed separately. In this case, $|\mathcal{A}_k|$ is determined before the set itself, as it is proposed by the RB grouping algorithms in [11] [76] [77] and [78]. These algorithms constitute Resource Chunks (RC), determined by a fixed number of RBs, and allocate them to UEs. The number of RBs per RC is established by dividing the total number of RBs per the total number of users. The optimal method of this kind of algorithms is proposed in [78]. The authors propose to use the Hungarian algorithm known for its optimality and polynomial complexity. The RC allocation decision is made considering the average channel gain experienced by the UEs over the RCs. In [77], the authors add a fairness factor parameter to the metric computation in order to enable a fair RC allocation among UEs. The RB grouping algorithm proposed in [11] is more opportunistic, as the RCs are allocated to UEs that have the highest metric. In [76], the authors consider multi-class services and take the QoS parameters into account in the metric computation, such as the guaranteed bit rate of the required QoS class and the delay. The drawback of these algorithms is the RCs establishment, as with the multi-user diversity, fairness in the number of allocated RBs does not ensure fairness in throughput.

Joint Allocation	Separate allocation		
	Power control	P_{max}	
	$\mid \mathcal{A}_k \mid$ unknown	$\mid \mathcal{A}_k \mid$ known	$\mid \mathcal{A}_k \mid$ unknown
[74] [75]	OEA QoS based OEA	[11] [76] [77] [78]	[10] [12] [11] [13]

Table 5.1: Summary of the proposed RRM algorithms

When $|\mathcal{A}_k|$ is not determined before the RB allocation itself, the designation of the allocated RBs can be established by a nested approach: allocating one RB (usually, the RB that maximizes the system satisfaction level) and expanding the RB allocation from this RB [11] [12] [13]. The Frequency Domain Packet Scheduling - Largest Metric First (FDPS-LMF), proposed in [11], first searches the pairs (RB,UE) that maximize the metric, and allocates them to the users. If the RBs assigned to a selected user are not adjacent, the algorithm assigns also the in-between RBs to this user. These steps are performed until no RBs are left unallocated or all UEs are served. If some RBs remain free, the algorithm finally keeps them that way. In [12], the authors propose the Recursive Maximum Expansion (RME) algorithm. This algorithm first searches the pair (RB,UE) that maximizes the metric and then expands the RB allocation on the two sides of the selected RB while the considered UE maximizes the metric. These two operations are performed recursively. At the end, the remaining RBs are allocated to the UEs that satisfy the contiguity constraint, at the possible expense of the concerned UEs individual throughput. The Heuristic Localized Gradient Algorithm (HLGA) proposed in [13] is similar to the FDPS-LMF algorithm except for the management of the remaining RBs which is similar to RME algorithm. These allocation policies are based on an opportunistic criterion; nevertheless, RME, FDPS-LMF and HLGA introduce fairness among users by considering in the objective function the proportional fair metric studied in [79], determined for each UE by the ratio between the logarithm of its instantaneous throughput and its average throughput.

Our proposed algorithms: OEA and QoS based OEA algorithms, allocate the UEs transmission power and the RBs separately. The UEs transmission power is determined by a power control adjustment given as a function of the final target throughput and the channel conditions that the users experience over their allocated RBs. Hence, the UEs transmission power allocation is performed after the RB allocation step. In this latter, $|\mathcal{A}_k|$ and $\mathcal{A}_k$ are performed in a nested manner, where the final number of allocated RBs per UE is not known. The RB expansion allocation is performed under the individual user's throughput increase condition which allows an efficient RB allocation. Before each RB expansion allocation, an update of the concerned user's channel conditions is performed, which allows an estimation of the effective user's individual throughput if an additional RB is allocated. This step was neglected in the radio resource management cited earlier, which led to high RB wastage ratio.

Table 5.1 summarizes the state of the art of the radio resource management in LTE networks. It classifies the algorithms as a function of their type of radio resource allocation and the number of RBs to be allocated to each UE. As far as we know, the algorithm we propose is the first heuristic that combines in a separate manner the UEs transmission power and the RBs allocation, without impos-

ing a given number of RBs to be allocated to each UE. However, the performances of the proposed algorithm given in this paper are compared to the one of the algorithms allocating a constant UE transmission power P_{max} and an RB allocation performed in a nested manner where $|\mathcal{A}_k|$ is unknown. For fair comparison while evaluating the energy efficiency and the UE transmission power, a power control step is added at the end of each algorithm.

5.3 Efficient radio resource allocation scheme

The radio resource management can be considered as an assignment problem where the objective is to obtain both the optimal allocation of RBs and the optimal transmission power for each UE. Our objective is to elaborate a low computational complexity efficient radio resource allocation scheme where the allocation of radio resources can be performed in less than one TTI. The efficient radio resource allocation scheme we propose allocates the RBs and the transmission power separately. Since the control of the UE transmission power needs the knowledge of the number of allocated RBs and the channel conditions experienced by the user, the proposed scheme allocates the RBs before the power control (as described in Figure 5.1). The RB allocation entity is channel dependent. It is based on the channel conditions of each UE on each RB. This information is carried by the CQI and is given as an input of the radio resource allocation scheme. Once the RB allocation is performed, the UE transmission power is determined using the power control based on the minimum guaranteed bit rate that each user can reach on its allocated RBs without reducing its throughput.

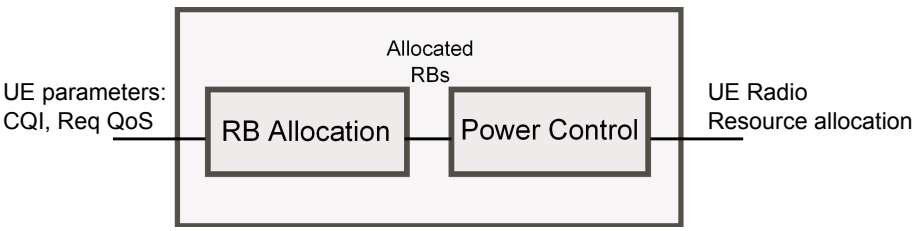

Figure 5.1: Opportunistic and efficient radio resource allocation scheme

5.3.1 Channel dependent RB allocation

The RB allocation process is an optimization problem, where the desired solution is the mapping between a set of users $\mathcal{K}$ and a set of RBs $\mathcal{C}$ that maximizes the target performance. Our objective is the maximization of the aggregate throughput, defined as the sum of all individual throughputs. Then, the RBs allocation can be formulated as:

$$\max \sum_{k \in \mathcal{K}} R_k(t) \tag{5.1}$$

where $R_k(t)$ is the individual throughput of user k at TTI t, over its whole allocated RBs, and subject to the following constraints:

1. The exclusivity of the allocated RBs:

$$\sum_{k \in \mathcal{K}} w_k^c(t) = 1 \quad \forall c \in \mathcal{C}$$

2. The following contiguity constraint:

$$\forall\ k \in \mathcal{K},\ w_k^c(t) = 0\ \forall\ c \geq j+2 \text{ if } w_k^j(t) = 1 \text{ and } w_k^{j+1}(t) = 0$$

3. The MCS robustness:

$$R_k(t) = r_k(t)|\mathcal{A}_k| \tag{5.2}$$

where, $w_k^c(t)$ denotes the RBs allocation for TTI t: $w_k^c(t) = 1$ if the RB c is allocated to user k, otherwise $w_k^c(t) = 0$. The RBs are supposed to be sorted in the increasing order of their carrier frequency, and $r_k(t)$ is the instantaneous rate of user k considering the MCS robustness constraint, expressed as:

$$r_k(t) = \frac{N_{sc}^{RB} N_{symb}^{UL}}{T_s} \min_{c \in \mathcal{A}_k} \delta_k^c(t) \tag{5.3}$$

with T_s being the time slot duration equal to 0.5 ms and $\delta_k^c(t)$ being the number of bits per resource element allocated to UE k over the RB c at TTI t, using the MCS lookup table (Table 2.1) taken from [80] and restricted to the used MCS for a target block error rate of 10%.

Optimal RB allocation

The previous optimization problem can be reformulated as a binary linear optimization problem as it was previously introduced in [10]:

$$\begin{aligned} & \arg\max_{\omega} \ \left(C^T \omega\right) \\ s.t. \quad & A.\omega = 1 \\ & \omega_j \in \{0,1\} \quad 1 \leq j \leq \mathfrak{C}.N_{UE} \end{aligned} \tag{5.4}$$

where, ω is the vector that contains the optimal solution of allocation defined by $\omega_j \in \{0,1\}$ for $1 \leq j \leq \mathfrak{C}.N_{UE}$, $\mathfrak{C}$ being the total number of feasible allocations for one UE, subject to the contiguity constraint and using the branch and bound method. The constraint matrix A is the expansion of $\mathfrak{C}$ to all UEs, subject to both the exclusivity and contiguity constraints. It contains all the possible solutions of allocation. To decrease the matrix A dimension, we can separate it into two parts: firstly enumerate the feasible solutions considering the contiguity constraint, and secondly introduce the exclusivity of the allocation. Therefore, the matrix A dimensions become equal to $(\mathfrak{C}.N_{UE} \times (N_{RB}+N_{UE}))$. The cost matrix C, of dimensions $(\mathfrak{C}.N_{UE} \times 1)$, is obtained from A; it gives the resulting individual throughput for each user in each configuration of allocation. In the cited reference [10], the cost matrix contains the

Shannon capacity corresponding to each allocation, and corresponds to the theoretical upper bound of the capacity.
For fair comparison, in our study, C is built taking into account the standardized MCS settings and considering the MCS robustness constraint. The proposed heuristics use as a metric $\mathcal{M}_x$ the mean effective SINR, experienced over the two time slots that constitute one TTI, by each user k over each RB c: $\mathcal{M}_x(k,c) = \overline{\gamma^{eff}_{(k,c)}}$. The following subsections describe the Opportunistic and Efficient RB Allocation and the QoS based Opportunistic and Efficient RB Allocation algorithms.

Opportunistic and Efficient RB Allocation algorithm (OEA)

The OEA algorithm allocates RBs to a user while its individual throughput is improved. It starts by the user who has the best SINR, when $P_k = P_{max}\ \forall\ k \in \mathcal{K}$. So, the algorithm searches the pair (RB,UE) which maximizes the considered metric. It allocates the RB noted c to UE noted k, and then, it applies the expansion at the two sides of c. The algorithm compares the metric values at the adjacent RBs (left extremity and right extremity) and allocates temporarily the RB with the highest metric to user k. As the UE total transmission power is equally shared over its allocated RBs, its SINR changes as a function of its number of allocated RBs. Then an update of the SINR values is performed before each RB expansion allocation according to the following expression:

$$\overline{\gamma^{\text{eff}}_{(k,c)}} = \overline{\gamma^{\text{eff}}_{(k,c)}} - 10\log(|\mathcal{A}_k| + 1) \quad \forall c \in \mathcal{A}_k \tag{5.5}$$

Using relation (5.2), the potentially new UE individual throughput is computed according to the new effective SINR. The RB allocation is confirmed and the set $\mathcal{A}_k$ updated if and only if the corresponding UE k individual throughput is improved. When the condition is no more satisfied, the algorithm updates the sets $\mathcal{K}$ and $\mathcal{C}$ and repeats the steps cited before, by performing a new search of pair (RB,UE). The algorithm allows the users to be allocated all the RBs that are necessary to increase their individual throughput. It means that, the maximum number of RBs that can be allocated to UE k: $\alpha_{k_{max}}$ is,

$$\alpha_{k_{max}} = N_{RB} \tag{5.6}$$

QoS based Opportunistic and Efficient RB Allocation algorithm (QoS based OEA)

The QoS based OEA algorithm is an RB allocation algorithm based on OEA. The main difference is that the QoS based OEA limits the maximum number of RBs allocated to each UE according to its target QoS. Then, $\alpha_{k_{max}}$ is computed using the following formula:

$$\alpha_{k_{max}} = \left\lceil \frac{R_{target,k}}{r_k(t)} \right\rceil \tag{5.7}$$

where $R_{target,k}$ is the target throughput of user k.
Once the RB allocation is performed, both the channel conditions of each user over each RB of its

allocated set $\mathcal{A}_k$ and $|\mathcal{A}_k|$ are given to the power control entity which allocates the UE transmission power as detailed in next subsection.

5.3.2 Channel dependent UE transmission power allocation

At this step, the UE transmission power is still considered to be set to P_{max}. First, the total throughput $R_k(t)$ achieved by each UE k over all its allocated RBs is computed; it represent the throughput that user k should reach even after the reduction of its power transmission: $P_{e,k}$. To respect this constraint, the power control entity takes into account the minimum SINR level that must be ensured to maintain the use of the same MCS, as follows:

$$P_{e,k} = \frac{P_{\max}}{|\mathcal{A}_k|} \frac{\gamma_{\text{tg}}}{\gamma^{\text{eff}}_{(k,\min)}} \tag{5.8}$$

where γ_{tg} is the SINR target, expressed in dB as:

$$(\gamma_{\text{tg}})_{dB} = (\gamma_{\text{MCS},k})_{dB} + (\Delta_\gamma)_{dB} \tag{5.9}$$

with, $\gamma_{\text{MCS},k}$ being the minimum SINR level required for keeping unchanged the MCS, Δ_γ being a margin, and $\gamma^{\text{eff}}_{(k,\min)}$ being the minimum effective SINR experienced by user k over its whole allocated RBs:

$$\gamma^{\text{eff}}_{(k,\min)} = \min_{c \in \mathcal{A}_k} \gamma^{\text{eff}}_{(k,c)} \tag{5.10}$$

The main steps of the radio resource allocation scheme are given in Algorithm 4 and Algorithm 5. Radio resource allocation scheme proposed, hereafter its performance analysis is presented. Next sections compare the performances of our proposed radio resource allocation scheme with the ones of other well known proposed algorithms for the SC-FDMA technique. The performances are given in terms of computational complexity, aggregate throughput, RB wastage ratio, energy efficiency and energy consumption in both regular and random networks.

5.4 Radio resource allocation computational complexity

The computational complexity evaluation of all the RB allocation algorithm entities is detailed in the following subsections. Assuming that in the worst case, when the target throughput is very high, the QoS based OEA algorithm set a maximum number of allocated RBs allowed to user k: $\alpha_{k_{max}}$ equal to N_{RB}, the computational complexity of QoS based OEA algorithm is upper bounded by the computational complexity of OEA algorithm. The computational complexity of the opportunistic and RME algorithms are considered identical due to the similarity of their RB allocation policy, excepting the used metric. However, the global complexity of the radio resource allocation algorithms should include, in addition, the computational complexity of the power control which is evaluated first.

Algorithm 4 Radio resource allocation algorithm

Inputs: Matrix $\mathcal{M}_x$ of N_{UE} x N_{RB} elements of $\overline{\gamma^{\text{eff}}_{(k,c)}}$.
Set of UE : $\mathcal{K} = \{1, \cdots, k, \cdots, N_{UE}\}$.
Set of RBs : $\mathcal{C} = \{1, \cdots, c, \cdots, N_{RB}\}$.
$\alpha_{k_{max}}$, Δ_γ, γ_{MCS}
Initialization:
$\mathcal{S}_{RB} = \emptyset$, $P_{UE} = \emptyset$
while $\big((\mathcal{C} \neq \emptyset)$ and $(\mathcal{K} \neq \emptyset)\big)$ **do**
1) find $(k, c) = \arg \max_{k \in \mathcal{K}, c \in \mathcal{C}} \mathcal{M}_x$, where $(k, c) \in \mathcal{K} \times \mathcal{C}$
2) assign RB c to UE k:
$\mathcal{S}_{RB} = \mathcal{S}_{RB} \cup \{(c, k)\}$
$\mathcal{A}_k = \mathcal{A}_k \cup \{c\}$
3) remove the RB c from the set $\mathcal{C}$:
$\mathcal{C} = \mathcal{C} \backslash \{c\}$
4) determine the individual throughput:
$R_k(t) = r^c_k(t)$
5) update $\mathcal{M}_x(k, \mathcal{C})$, using (5.5).
6) expand to the adjacent RBs with Algorithm 5.
7) remove UE k from the set $\mathcal{K}$.
8) determine the transmission power $P_{e,k}$ using (5.8):
$P_{UE} = P_{UE} \cup \{P_{e,k}\}$
end while
Outputs: $\mathcal{S}_{RB}$, P_{UE}

Algorithm 5 Allocation expansion to the adjacent RBs

Inputs: k, $\mathcal{C}$, $\mathcal{M}_x(k,\mathcal{C})$, $\mathcal{A}_k$, $R_k(t)$, $\alpha_{k_{max}}$, $\mathcal{S}_{RB}$.
while $|\mathcal{A}_k| < \alpha_{k_{max}}$ **do**
a) select the neighboring RB with the highest metric:
if $\mathcal{M}_x(k, c-1) > \mathcal{M}_x(k, c+1)$ **then**
$c' = \mathcal{A}_k(1)$
else
$c' = \mathcal{A}_k(|\mathcal{A}_k|)$
end if
b) assign conditionally RB c' to UE k by temporarily including c' into $\mathcal{A}_k$.
c) compute the temporary throughput $R_{k_{temp}}$ of UE k with relations (5.2) and (5.3).
if $R_{k_{temp}(t)} > R_k(t)$ **then**
- $\mathcal{S}_{RB} = \mathcal{S}_{RB} \cup \{(c', k)\}$
- $\mathcal{A}_k = \mathcal{A}_k \cup \{c'\}$.
- $\mathcal{C} = \mathcal{C} \backslash \{c'\}$.
- update $\mathcal{M}_x(k, \mathcal{C})$ using (5.5).
else
- break
end if
end while
Output: $\mathcal{S}_{RB}$, $R_k(t)$.

5.4.1 Power control complexity evaluation

The power control entity has to first count the number of allocated RBs to each user which is performed with at least $\mathcal{O}(N_{RB})$ operations, and then to determine the minimum effective SINR experienced by each UE over its whole allocated RBs, with $\mathcal{O}(N_{RB})$ operations. Consequently, these two operations, performed for N_{UE} users, have a $\mathcal{O}(2N_{RB}N_{UE})$ computational complexity. Then the UE transmission power allocation process is done with $\mathcal{O}(2N_{RB}N_{UE} + N_{UE})$ operations.

5.4.2 Radio resource allocation scheme computational complexity

In this section, we compute and compare the computational complexity of the radio resource allocation scheme according to the considered RB allocation algorithms: OEA, FDPS-LMF, HLGA and RME algorithms.

Complexity of the radio resource allocation scheme based on OEA and QoS based OEA algorithm

Step 1) of Algorithm 4 is performed after a linear search on the remaining RBs and users in sets $\mathcal{C}$ and $\mathcal{K}$. At the worst case, each user will be assigned only one RB. Then, the computational complexity of the l^{th} run of this step is upper bounded by $\mathcal{O}((N_{UE}-l)(N_{RB}-l))$. The user's throughput is computed with respect to the MCS robustness (5.2) by looking for the minimum rate in the set $\mathcal{A}_k$. Hence, the computational complexity of steps 4) in Algorithm 4 and step c) in Algorithm 5 is $\mathcal{O}(N_{RB} - l)$. The

user's metric update (steps 5) and d)) is performed before each new RB allocation at the expense of a computational complexity of $\mathcal{O}(N_{RB} - l)$. The RBs allocation expansion must be done as long as $\alpha_{k_{max}}$ is not reached. This parameter $\alpha_{k_{max}}$ depends on the QoS desired by each user and is usually quite low for QoS based OEA. Then, at the worst case represented with OEA ($\alpha_{k_{max}} = N_{RB}$), step 6) will be run $\mathcal{O}(N_{RB} - l)$ times. Both algorithms stop allocating the RBs when all the users are served or when there is no more RB to be allocated. Therefore, l is upper bounded by $\min(N_{RB}, N_{UE})$ and the expression of the proposed algorithms OEA and QoS based OEA complexity $\mathcal{C}_O$ is:

$$\mathcal{C}_O = \sum_{l=0}^{min(N_{RB},N_{UE})} \left[\mathcal{O}((N_{UE} - l).(N_{RB} - l)) + \mathcal{O}(N_{RB} - l) + 2.\mathcal{O}((N_{RB} - l)^2)\right]$$

After some mathematical derivations, and considering the power control computational complexity (step 8 in Algorithm 4) we obtain the following complexity:

$$\mathcal{C}_{O_{N_{UE} \geq N_{RB}}} = \mathcal{O}\left(\frac{N_{RB}^3}{2} + \left(\frac{N_{UE}}{2} - \frac{1}{2}\right) N_{RB}^2 - \frac{N_{UE}}{2} N_{RB}\right) + \mathcal{O}\left(2N_{RB}N_{UE} + N_{UE}\right)$$

$$\mathcal{C}_{O_{N_{UE} \leq N_{RB}}} = \mathcal{O}\left(\frac{N_{UE}^3}{2} + (\frac{1}{2} - \frac{3.N_{RB}}{2})N_{UE}^2\right) + \mathcal{O}\left((2N_{RB}^2 - \frac{3N_{RB}}{2})N_{UE}\right) + \mathcal{O}\left(2N_{RB}N_{UE} + N_{UE}\right)$$

Thus, the computational complexity of OEA and QoS based OEA is polynomial of order 3.

Complexity of the radio resource allocation scheme based on FDPS-LMF and HLGA algorithms

FDPS-LMF and HLGA algorithms both perform a linear search on RBs and users to find the pairs (RB,UE). This step can be done using sorted metrics values and saving the corresponding pairs (RB,UE). The computational complexity of the metrics values sorting is $\mathcal{O}(N_{RB}^2 N_{UE}^2)$ in the worst case. Using the quick sort algorithm [81], the complexity is reduced to $\mathcal{O}(N_{RB}N_{UE}.\log(N_{RB}N_{UE}))$. Then, both algorithms allocate the RBs to the corresponding users considering the contiguity constraint. The complexity for these steps is $\mathcal{O}(N_{UE}N_{RB} - 2)$. The FDPS-LMF stops the RBs allocation at this step, whereas the HLGA allocates the free remaining RBs at the expense of $\mathcal{O}((N_{RB} - 1).(N_{UE} - 1))$ additional operations. Therefore the final complexity for the FDPS-LMF: $\mathcal{C}_F$, and the HLGA: $\mathcal{C}_H$, including the power control computational complexity, are respectively:

$$\mathcal{C}_F = \mathcal{O}\left(N_{RB}N_{UE}.\ln(N_{RB}N_{UE}) + N_{UE}.(N_{RB} - 2)\right) + \mathcal{O}\left(2N_{RB}N_{UE} + N_{UE}\right)$$

and

$$\begin{aligned}\mathcal{C}_H \quad &= \mathcal{O}\left(N_{RB}N_{UE}.\ln(N_{RB}N_{UE}) + N_{UE}.(N_{RB} - 2) + (N_{UE} - 1).(N_{RB} - 1)\right) \\ &+\mathcal{O}\left(2N_{RB}N_{UE} + N_{UE}\right)\end{aligned}$$

Thus the computational complexity of FDPS-LMF and HLGA is in $\mathcal{O}(N^2 \ln(N))$.

Complexity of radio resource allocation scheme based on RME algorithm

The RME algorithm also performs the linear search of the best pair (RB,UE), with a complexity $\mathcal{O}((N_{RB}-l)(N_{UE}-l))$ at the l^{th} run of the algorithm. The complexity of the RME expansion step that recursively finds a new pair (RB,UE) is in $\mathcal{O}((N_{RB}-1).(N_{UE}-1))$ because the updates of $\mathcal{C}$ and $\mathcal{K}$ are not considered. The allocation is done till all users are served or there is no more remaining free RB. The same management method for these remaining free RBs as in HLGA is used. Therefore the computational complexity evaluation of the RME including the computational complexity of the power control: $\mathcal{C}_R$, is :

$$\mathcal{C}_R = \sum_{l=0}^{\min(N_{RB},N_{UE})} \left[\mathcal{O}\left(2(N_{UE}-l)(N_{RB}-l)\right)\right] + \mathcal{O}\left((N_{RB}-1).(N_{UE}-1)\right) + \mathcal{O}\left(2N_{RB}N_{UE}+N_{UE}\right)$$

which can be also expressed as follows:

$$\mathcal{C}_{R_{N_{UE}\geq N_{RB}}} = \mathcal{O}\left(\frac{-N_{RB}^3}{3} + N_{UE}N_{RB}^2 - \frac{2N_{RB}}{3} + (1-N_{UE})\right) + \mathcal{O}\left(2N_{RB}N_{UE}+N_{UE}\right)$$

$$\mathcal{C}_{R_{N_{UE}\leq N_{RB}}} = \mathcal{O}\left(\frac{-N_{UE}^3}{3} + N_{RB}N_{UE}^2 - \frac{2N_{UE}}{3} + (1-N_{RB})\right) + \mathcal{O}\left(2N_{RB}N_{UE}+N_{UE}\right)$$

thus the computational complexity of the RME algorithm is polynomial of order 3.

5.4.3 Comparison of the algorithms complexity

Excepting the optimal solution which is N-P hard, we notice the polynomial form of the computational complexity of each RB allocation algorithm, and hence of the radio resource allocation scheme by the same way. Figure 5.2 shows the required number of operations that the eNB should perform to allocate the radio resources to the N_{UE} users. These results are given when a bandwidth $B = 10$ MHz, corresponding to $N_{RB} = 50$, is allocated to the sector. When the number of users increases, the required number of operations needed to perform the radio resource allocation increases. FDPS-LMF and HLGA are the algorithms that require the lowest computational complexity. In lowly loaded networks, when $N_{UE} < 2N_{RB}$, the required number of operations performed by the RME algorithm is less than the one performed by the OEA algorithm.
The maximum required number of operations to perform the radio resource allocation, whatever the algorithm used when $N_{UE} \leq 200$, is less than 5.10^5 operations. Considering an eNB's processor of 2×34 k million of instructions per second, and 32-bit RISC cores running at 622/700 MHz, the required time of radio resource allocation is given in Table 5.2. The required time is evaluated whatever the RB allocation algorithm for all the LTE standardized bandwidths and a medium loaded network ($N_{UE} = 2N_{RB}$). Note that at most the required time for radio resource allocation never exceeds 4.7 10^{-2} ms. This value is quite reasonable, and enlightens the feasibility of the algorithms' implementation in practical systems.

Alg \ B (MHz)	1.4	3	5	10	15	20
OEA	$8.32\ 10^{-6}$	$1.3\ 10^{-4}$	$6.47\ 10^{-4}$	$5.29\ 10^{-3}$	$3.23\ 10^{-3}$	$4.11\ 10^{-2}$
RME	$1.05\ 10^{-5}$	$1.64\ 10^{-4}$	$7.64\ 10^{-4}$	$6.17\ 10^{-3}$	$2.08\ 10^{-2}$	$4.7\ 10^{-2}$
FDPS-LMF	$1.08\ 10^{-5}$	$9.11\ 10^{-5}$	$3.23\ 10^{-4}$	$1.38\ 10^{-3}$	$3.23\ 10^{-3}$	$6.17\ 10^{-3}$
HLGA	$1.24\ 10^{-5}$	$1.02\ 10^{-4}$	$3.23\ 10^{-4}$	$1.52\ 10^{-3}$	$3.52\ 10^{-3}$	$6.76\ 10^{-3}$

Table 5.2: Time required for radio resource allocation (in milliseconds)

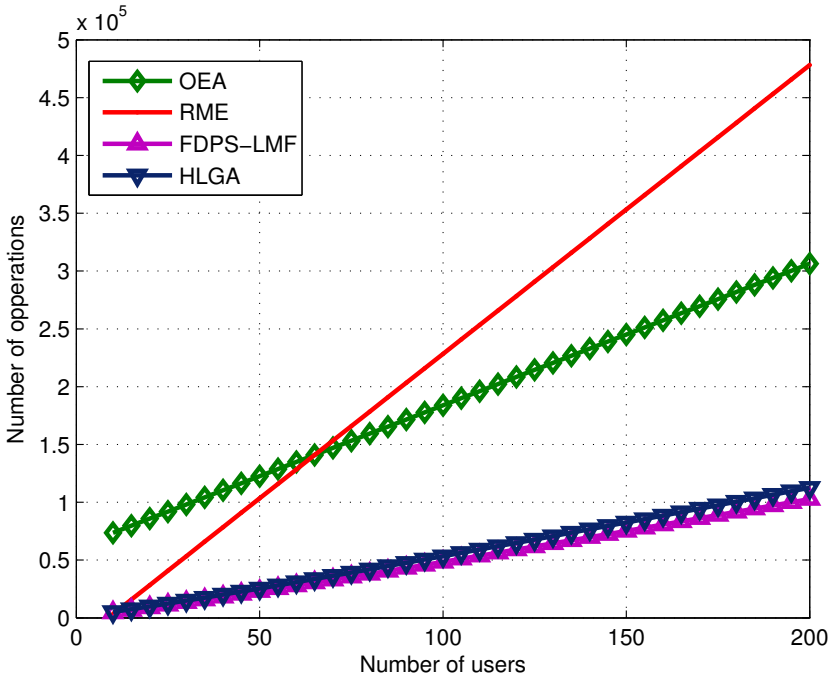

Figure 5.2: Required number of operations for radio resources allocation

5.5 Radio resource allocation scheme performances evaluation

The proposed algorithm performances evaluation are given in regular and random networks. In regular networks, we compare the proposed radio resource allocation scheme based on OEA and QoS based OEA algorithms with: 1) the three proportional fair schedulers cited before (RME, FDPS-LMF and HLGA) and 2) one opportunistic RB allocation algorithm that allocates the RB to the user that experiences the highest SINR, with respect to the contiguity constraint. In addition to these algorithms, a performance comparison with the optimal RB allocation algorithm based on the binary integer programming is done in random networks. The same UE power control process is performed once the RB allocation process is completed by each studied algorithm.
Whatever the network topology used, a $1 \times 3 \times 3$ frequency reuse pattern is used. The simulation parameters are mostly taken from the LTE standards. Each sector is allocated a bandwidth B of 5 MHz, that corresponds to $N_{RB} = 25$ available RBs. The radio resource allocation scheme performances are studied through 1000 TTI, which involves a frequency-time correlated Rayleigh fading used in the SINR computation step. We consider one QoS class of uniformly distributed pedestrian users where a target throughput of 600 kbps is taken into account by the QoS based OEA.

5.5.1 Performances evaluation in regular networks

A regular network composed of 19 hexagonal cells is considered. We focus on radio resource allocation in one sector of the central cell. The inter-cell interference level I_{eNB}^{RB} used in the SINR computation is averaged over Monte Carlo simulations. We compare the performances of the algorithms as a function of the network's load, by varying the number of users per sector from 5 to 80 UEs, which corresponds to a number of UE per number of RBs ratio from 20% to 320%. The simulation parameters, used for the performance evaluation in regular networks, are summarized in Table 5.3.
Figure 5.3 shows the aggregate throughput of one sector of the central cell obtained with the studied

Antenna configuration	Single Input Single Output
Cellular layout Max/ Min UE-eNB distance Frequency reuse pattern	Hexagonal grid,19 tri-sector cells. 500 m/30 m $1 \times 3 \times 3$
Carrier frequency System bandwidth	2.6 GHz $B = 5$ MHz per sector $\Rightarrow N_{RB} = 25$
Rayleigh fading type	frequency-time correlated fading coefficient $h^{(m,n)}$ coef corr $= 0.5$, UE velocity $= 3$ km/h
SINR margin Δ_γ	0.3 dB
MCS setting	QPSK $1/2, 2/3, 3/4$ 16 QAM $1/2, 2/3, 3/4$ 64 QAM $1/2, 2/3, 3/4$

Table 5.3: Simulation parameters in a regular network

algorithms. The aggregate throughput increases when the load of the cell increases. The OEA aggregate throughput is higher than the aggregate throughput of the proportional fair schedulers (RME,

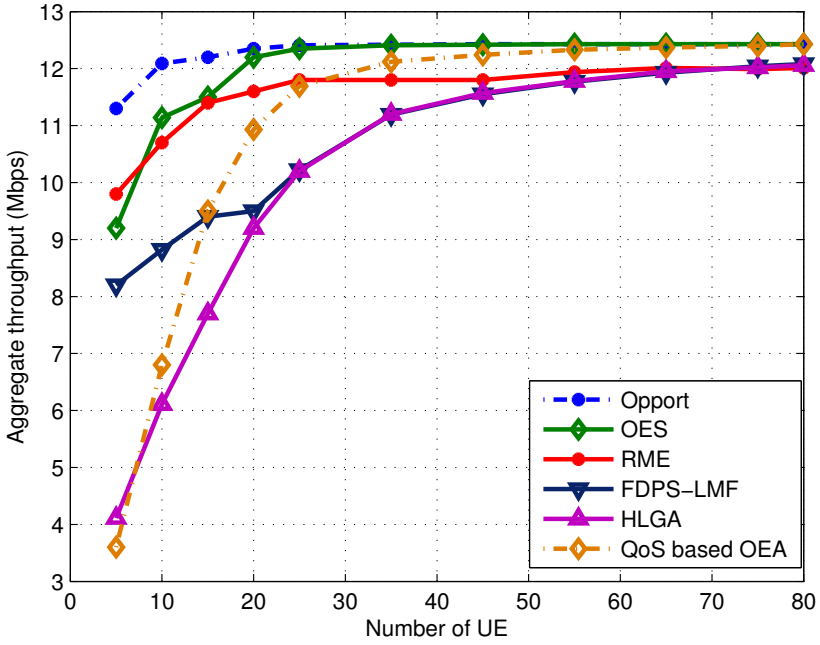

Figure 5.3: Aggregate throughput with N_{RB}=25 in one sector of a regular network

FDPS-LMF and HLGA) and close to the opportunistic one. The aggregate throughput generated by the QoS based OEA increases significantly to be higher than the proportional fair schedulers when $N_{UE} \geq N_{RB}$. At low load, the free RBs management applied by the HLGA decreases the aggregate throughput level compared to FDPS.

When the number of UEs exceeds the number of RBs, both OEA and QoS based OEA offer good performances compared to the RME algorithm: actually, they achieve higher aggregate throughput with less computational complexity. Unlike RME, FDPS-LMF and HLGA algorithms are less complex than our proposed algorithms. However, they achieve a significantly lower aggregate throughput; the gap with OEA varies from more than 200% at low load, to 20% when $N_{UE} = N_{RB}$. It then decreases but is still around 5% when $N_{UE} \geq 2.N_{RB}$. Especially when a large number of RBs are allocated to one UE, the average transmission power per RB is low, which may lead, if no precautions are taken, to a lower SINR per RB than the minimum one required for the most robust MCS, and consequently, to a null resulting throughput.

To enlighten the metrics update benefits, we compute the maximum RB wastage ratio of each algorithm over the simulation duration, that evaluates the number of RBs allocated to users, but with a resulting individual zero throughput. Figure 5.4 shows that OEA and QoS based OEA completely cancel this wastage. The RB wastage ratio of the opportunistic scheduler decreases to cancel when $N_{UE} \geq N_{RB}$. But the RME wastes around 98% of RBs whatever N_{UE}, due to the proportional fair metric, which means that up to 98 RBs out of 100 are allocated to users but do not lead to any data transmission. Considering FDPS-LMF and HLGA algorithms, the RB wastage ratio tends to 40%,

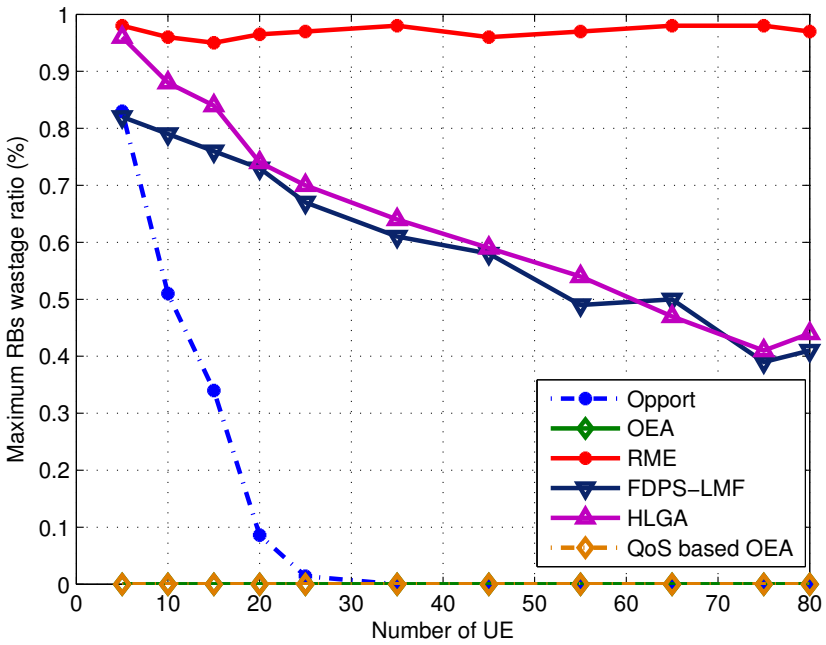

Figure 5.4: Maximum RBs wastage ratio in a regular network

as they compensate the proportional fair metric by their allocation policy. In addition to the high aggregate throughput and the cancellation of RB wastage, the OEA efficiency resides in the number of served users. Actually, the user throughput improvement constraint associated to the MCS robustness limits the number of RBs allocated to each user, hence giving a chance to other users to be served. Figure 5.5 represents the ratio of unallocated RBs. At low load the OEA efficiently uses 10% of the available resources. The ratio of unallocated RBs decreases and is cancelled when N_{UE} increases, under appropriate user radio conditions.

Figure 5.6 and 5.7 represent the energy efficiency of the transmitted data, respectively before and after the power control. The energy efficiency, given in bits per Joule, is defined by the ratio between the users throughput and the corresponding UE transmission power. Before the power control, all the UEs transmit at their maximum power P_{max}. Since the OEA and the QoS based OEA algorithms achieve a higher throughput, then they achieve a higher energy efficiency. They reach respectively 3.5 10^6 and 2.4 10^6 bits/J at low load, while the RME, FDPS-LMF and HLGA do not exceed 0.8 10^6 bits/J. In highly loaded networks, the energy efficiency decreases for the five algorithms to reach 7.5 10^5 bits/J for the OEA algorithm and 7 10^5 bits/J for the QoS based OEA algorithm, 5 10^5 bits/J for both HLGA and FDPS-LMF algorithms and 2 10^5 bits/J for the RME algorithm. Once the power control is applied, the energy efficiency curves increase when the networks load increases. Actually, in case of highly loaded networks, the number of allocated RBs to each UE is low, due to the high number of UEs, which makes the power control more efficient. The number of bits transmitted per Joule achieves 180 Mbits and 170 Mbits for the QoS based OEA and the OEA

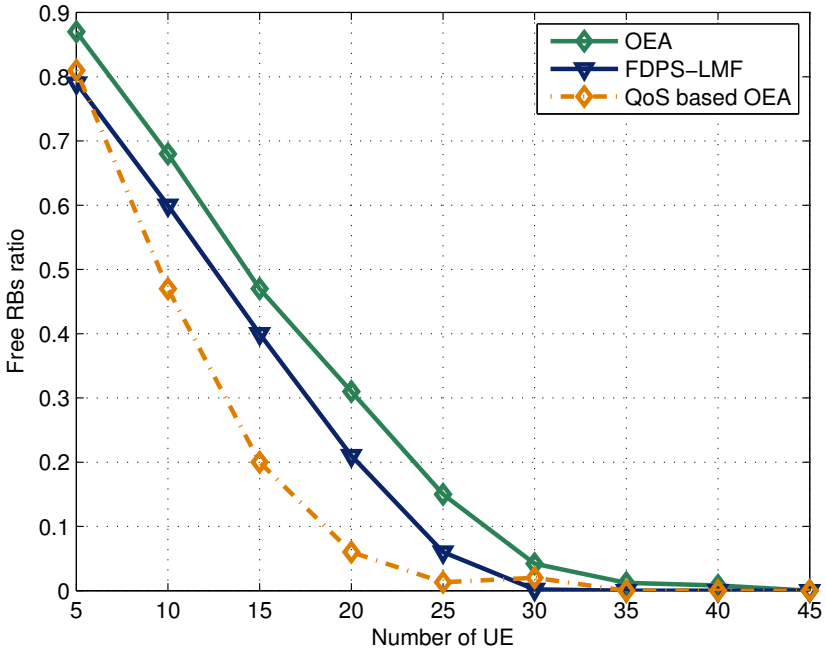

Figure 5.5: Free RBs ratio in a regular network

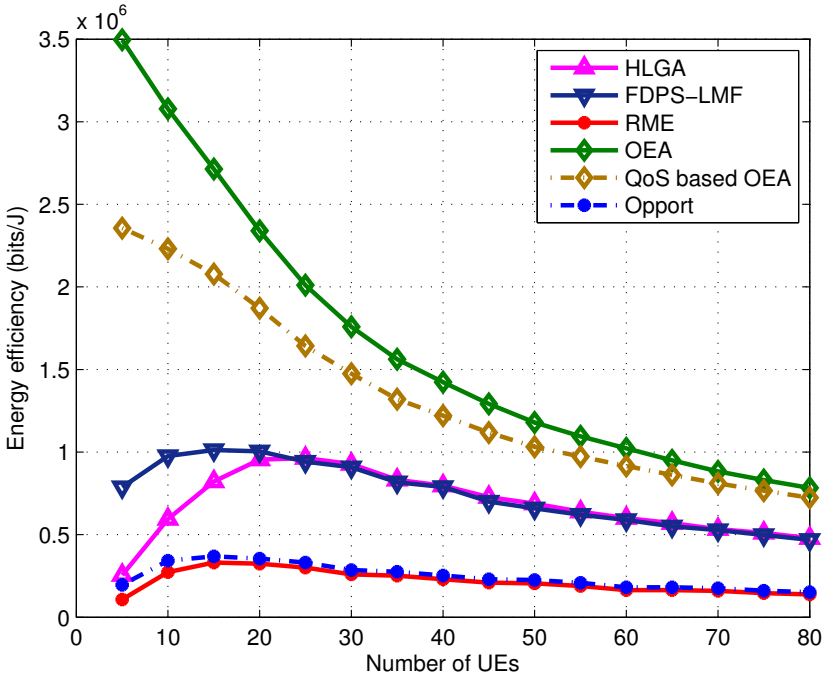

Figure 5.6: Average energy efficiency before power control in a regular network

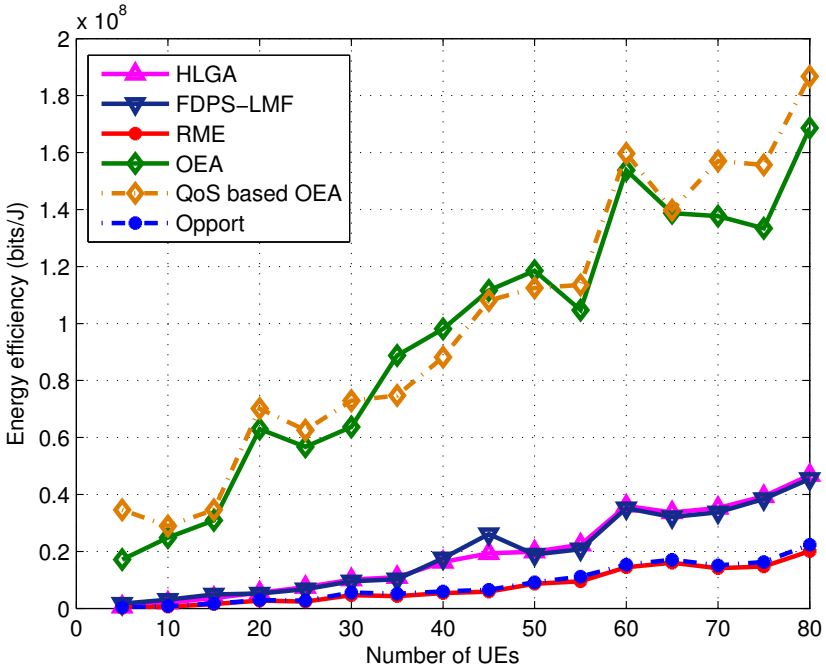

Figure 5.7: Average energy efficiency after power control in a regular network

respectively. The curves are not smoothed as before for the power control curves, because the power allocation depends on the minimum SINR range of the used MCS, which is not linear.

Figure 5.8 shows the average UE transmission power. The thick line corresponds to the UE maximum transmission power set to 21 dBm. The minimum observed UE transmission power is about 17 dBm. We notice that the RME does not decrease a lot the UE transmission power, due to the high number of allocated RBs. The algorithms which allow a lowest UE transmission power are the HLGA, the FDPS-LMF and the QoS based OEA. This large power reduction is explained by the number of RBs allocated to each UE. Actually if $|\mathcal{A}_k|$ is low, $P_{k_{Tx}}$ is high and the power control according to γ_{tg} is more efficient. In Figure 5.9, we represent the ratio of saved energy after power control. The RME algorithm saves only from 2% to 25% of the UE transmission power, depending on the network's load, whereas the QoS based OEA algorithm saves from 28% to 58% of the UE transmission power, which allows it to increase even more the UE battery life.

5.5.2 Performances evaluation in random networks

In this paragraph, the eNBs are represented by an independent homogeneous Poisson point process $\Pi_{eNB} = \{b_1, b_2, \ldots\}$ of intensity λ_{eNB} on $\mathbb{R}^2$. The active users are located according to an independent homogeneous Poisson point process $\Pi_{UE} = \{u_1, u_2, \ldots\}$ of intensity $\lambda_{UE} > \lambda_{eNB}$ on $\mathbb{R}^2$. The superposition of the two Poisson point processes represent our random network in a $D \times D$ square geographical region. Let N_{eNB} be the number of eNBs. Each tri-sectored eNB transmits at a maximum transmission power $(P_{eNB_{max}})_{dBm} =$ 43 dBm per sector. The users are assigned to a sector according

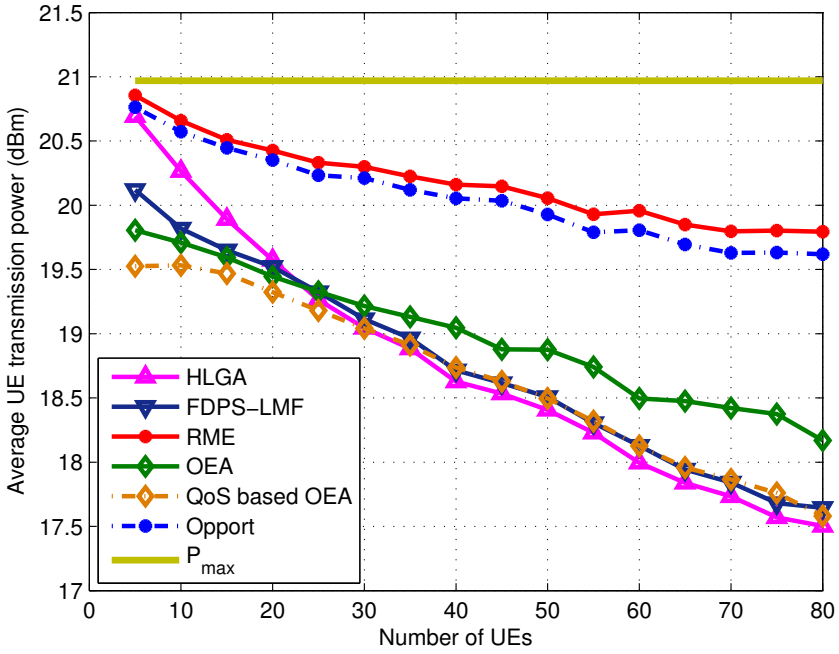

Figure 5.8: Average UE transmission power in a regular network

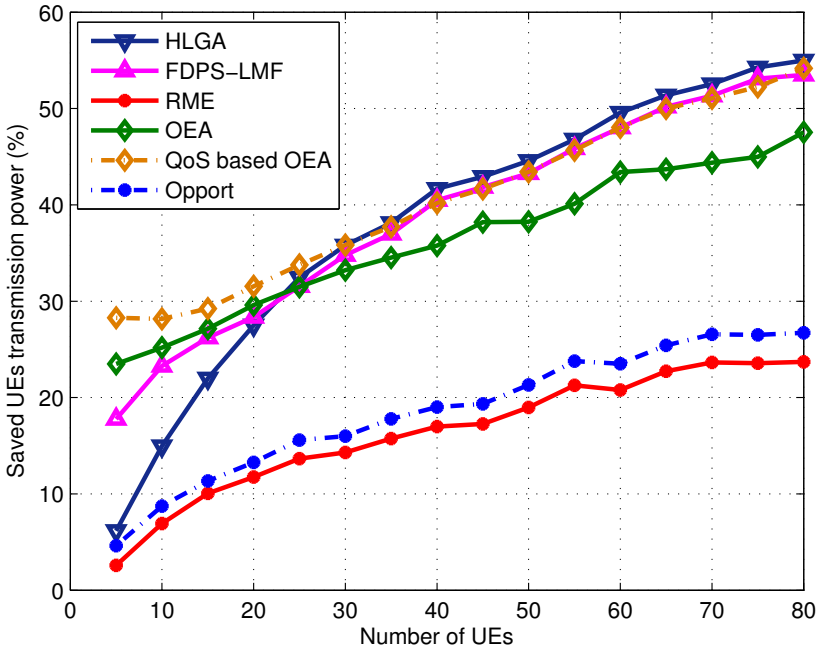

Figure 5.9: Saved power (W) in a regular network

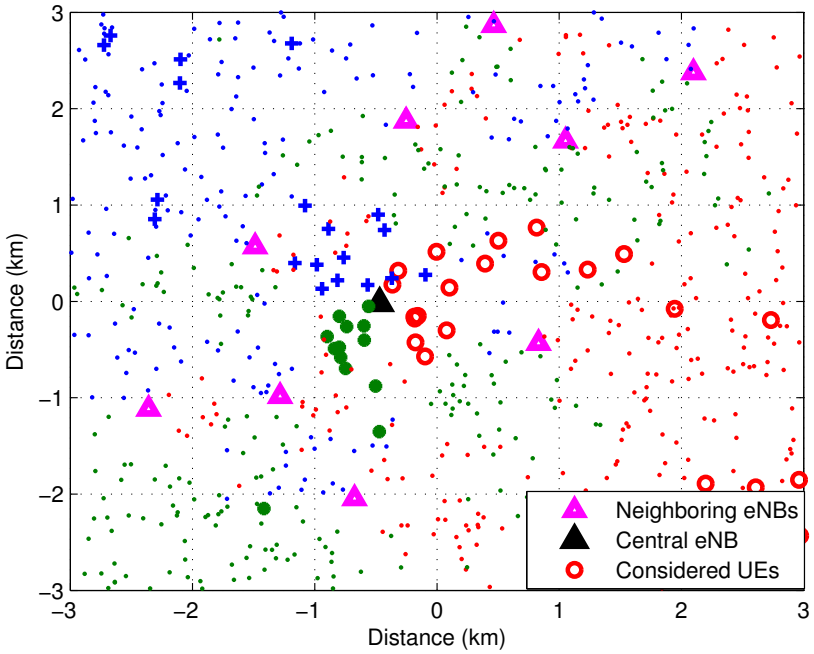

Figure 5.10: Random Network

to their downlink radio channel measurement as shown in Figure 5.10. For this purpose, each UE measures the power received from each sector on the reference signal resource element (Reference Signal Received Power (RSRP)) and selects the sector from which the highest power is received [30]. The RSRP for each UE $u \in \Pi_{UE}$ is computed as:

$$RSRP = P_{eNB_{max}}.G_A(\theta_u)\Lambda_u|A_f|^2 \tag{5.11}$$

The sector we focus on for our RRM is randomly chosen. We denote by $\mathcal{K}$ the subset of Π_{UE} containing N_{UE} users that belong to the considered sector. We compare the performances of the algorithms as a function of the network's load, in lowly and highly loaded networks, by varying the Poisson point process intensity of the users λ_{UE}. Table 5.4 summarizes the simulation parameters. As the metric adopted for OEA algorithms requires the SINR computation, the interference level is estimated, by the method presented in the following subsection.

ICI estimation

We consider the random network described above and focus on the computation of the ICI in one sector. The total ICI level I^c_{eNB}, suffered at each RB of the allocated bandwidth and received by the concerned eNB s, is given by:

$$I^c_{eNB} = \sum_{l \neq s}^{l \in \Pi_{eNB}} I^c_{l,eNB} \tag{5.12}$$

Poisson point process parameters	D = 6 km, $\lambda_{eNB} = 2.10^{-6}\ eNBs/m^2 = 2\ eNB/km^2$ λ_{UE}: $10^{-5} \rightarrow 3.10^{-4}\ users/m^2 = 300\ users/km^2$
Frequency reuse pattern	$1 \times 3 \times 3$
Carrier frequency	2.6 GHz
System bandwidth	$B = 5$ MHz per sector, $N_{RB} = 25$
Rayleigh fading type	frequency-time correlated fading coefficient $h^{m,n}$ coef corr $\alpha = 0.5$, UE velocity $v = 3$ km/h
SINR margin Δ_γ	0.3 dB
MCS settings	QPSK $1/2, 2/3, 3/4$ 16 QAM $1/2, 2/3, 3/4$ 64 QAM $1/2, 2/3, 3/4$

Table 5.4: Simulation Parameters in random network

$R_{s_{Alg}}$ \ N_{UE}	2-5	5-10	10-15	15-20	20-25	25-30	30-35	35-40	40-45	> 45
$R_{s_{OEA}}$	46%	20%	8.9%	6%	4.6%	3%	3%	2.7%	2.3%	2%
$R_{s_{QoS}}$	100%	100%	83%	58%	45%	37%	31%	26%	23%	21%
$R_{s_{Optim}}$	46.4%	19%	8.6%	5.9%	4.5%	3.7%	3%	2.7%	1%	1%
$R_{s_{Opport}}$	70%	63%	48%	46%	39%	32%	29%	24%	20%	18%
$R_{s_{RME}}$	70%	63%	48%	46%	39%	32%	29%	24%	20%	18%
$R_{s_{FDPS}}$	96%	93%	87%	74%	61%	54%	45%	38%	33%	30%
$R_{s_{HLGA}}$	96%	93%	87%	74%	61%	54%	45%	38%	33%	30%

Table 5.5: Ratio of served UEs obtained by each algorithm as a function of N_{UE}

where l belongs to the set of interfering sectors with the concerned eNB s.
Assuming that the random variables $I^c_{l,eNB}$ follow the same law and are independent and identically distributed, the central limit theorem can be invoked and the ICI level modeled as a Gaussian random process. Since, in uplink, the total UE transmission power is equally shared over the whole allocated RBs, then $I^c_{l,eNB}$ depends on the average transmission power per RB: P_{RB}, as determined by the following formula:

$$I^c_{l,eNB} = P_{RB_{Alg}}.\Lambda_{l,eNB}.|h|^2 \tag{5.13}$$

The average transmission power per RB: $P_{RB_{Alg}}$, depends on the considered RB allocation algorithm. Then, the average transmission power per RB is defined as:

$$P_{RB_{Alg}} = P_{max}.\frac{R_{s_{Alg}}.N_{UE}}{N_{RB}} \tag{5.14}$$

with $R_{s_{Alg}}$ the average ratio of served UEs obtained by each studied RB allocation algorithm. To ensure a correct evaluation of the ICI level and by the way a correct computation of $R_{s_{Alg}}$, we simulate the different algorithms included in our study in a noise limited network, when no power control is activated. Assuming $N_{RB} = 25$, we obtain the values for $R_{s_{Alg}}$ that are summarized in Table 5.5, as a function of N_{UE}.
The average UE transmission power per RB being estimated, Monte Carlo simulations determine for

each realization of the UE Poisson point process of intensity λ_{UE}:

1. The ICI cdf corresponding to each RB allocation algorithm, as illustrated in Figure 5.11 for $\lambda_{UE} = 2.10^{-5}$.
2. The ICI CDF parameters as a function of λ_{UE}, as listed in Table 5.6. Actually, the ICI distribution follows a Gaussian distribution with mean μ and standard deviation σ.

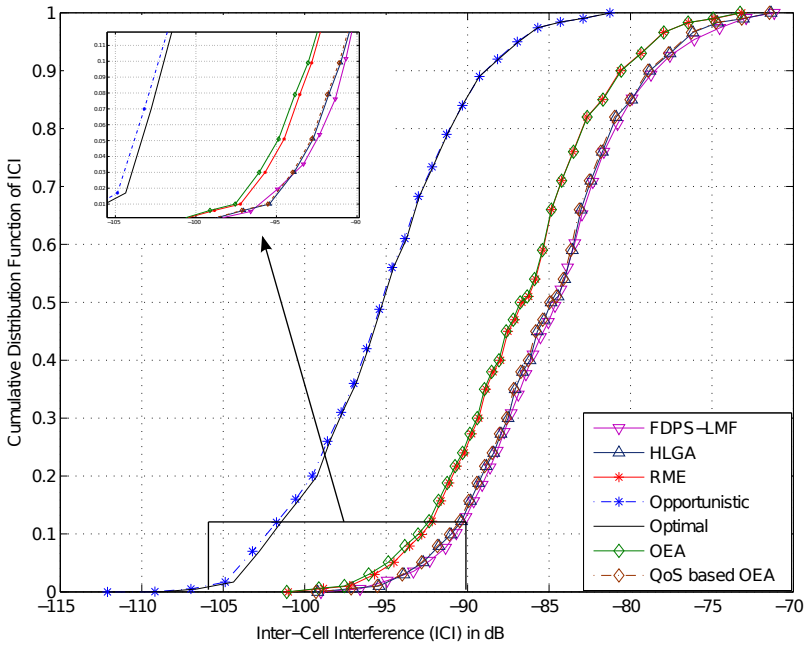

Figure 5.11: CDF of ICI suffered on one RB, generated by each algorithm for $\lambda_{UE} = 2.10^{-5}$ in a random network

From Figure 5.11, we notice the impact of the RB allocation algorithm on the ICI level distribution. We can classify the seven algorithms in three classes according to their generated ICI level. The first class consists of OEA and the optimal RB allocation algorithm as they have almost the same generated ICI level and the lowest one. The RME and the opportunistic algorithms form the second class, they generate about 5 dB more of ICI than the first class. Finally, QoS based OEA, HLGA and FDPS-LMF algorithms generate the most important ICI level, due to the number of RBs that are allocated to each UE. Actually, allocating a few number of RBs to one UE is reflected in a high average power per RB and a high generated inter-cell interference I_{RB}.
Table 5.6 summarizes the distributions parameters, obtained with Monte Carlo simulations, as a function of the network's load. The χ^2 test shows that the ICI distribution can be estimated with a normal distribution with a confidence interval greater that 99%. It should be noticed that the ICI is slightly overestimated as power control is not taken into account.

Algo / λ_{UE}	FDPS-LMF		HLGA		RME		Opportunistic		Optimal		OEA		QoS based OEA	
	μ	σ	μ	σ	μ	σ	μ	σ	μ	σ	μ	σ	μ	σ
10^{-5}	-89.17	4.51	-89.51	4.51	-90.59	4.52	-90.59	4.52	-92.89	4.49	-92.86	4.49	-88.98	4.53
2.10^{-5}	-86.53	4.81	-86.51	4.81	-88.18	4.79	-88.18	4.80	-92.02	4.51	-91.93	4.54	-86.34	4.89
3.10^{-5}	-84.58	5.31	-84.58	5.30	-86.44	5.30	-86.44	5.30	-91.83	5.17	-91.66	5.17	-84.50	5.33
5.10^{-5}	-82.61	5.48	-82.61	5.48	-84.89	5.45	84.89	5.46	-92.50	5.13	-91.96	4.94	-83.09	5.37
9.10^{-5}	-81.05	5.52	-80.95	5.53	-83.14	5.53	−83.15	5.53	-92.42	5.48	-89.76	6.11	-82.38	5.44
2.10^{-4}	-80.13	5.71	-79.99	5.71	-82.33	5.71	-82.34	5.71	-94.70	5.59	-91.59	5.59	-81.68	5.71

Table 5.6: Parameter of the ICI distributions generated by each RB allocation algorithm (μ and σ in dB)

Performance evaluation

As in regular networks, the radio resource allocation scheme simulations in random networks are run on MATLAB. For the optimal RB allocation algorithm the bintprog function of the optimization toolbox is used to solve the binary integer programming [82]. This function, based on the branch and bound algorithm, avoids the enumeration of large classes of bad solutions and only lists potentially good solutions [83]. However, the algorithm searches for an optimal solution by solving series of linear programming relaxation problems, in which the binary integer variables indicating each RB allocation are replaced by fuzzy values varying in the unit interval. But the maximum number of iterations that the linear programming relaxation entity performs to find the optimal solution is limited. Beyond this limit, it is considered that the optimal allocation decision can not be given in one TTI, and the allocation is not performed. We notice from our simulations that this is the case when N_{UE} exceeds 40. Thus, we use a least-squares sense polynomial approximation of the results obtained for low values of N_{UE}, in order to estimate the values when the BIP RB allocation can not be performed.

Figure 5.12 shows the aggregate throughput in the considered sector, averaged on 1000 TTI simulations, as a function of λ_{UE}. For the optimal, opportunistic and OEA algorithms, the aggregate throughput increases when the number of users in the cell increases, unlike the proportional fair algorithms FDPS-LMF, HLGA and RME. Actually, the latter ones aim at maximizing the aggregate throughput while minimizing the variation between the users throughputs. When the number of users increases, the probability that some users experience bad radio conditions increases. In such situations, they can not even use the most robust MCS. As proportional fair algorithms serve in priority users experiencing bad radio conditions, that leads to a decrease of the aggregate throughput. The aggregate throughput obtained by the OEA algorithm is close to the one obtained with the optimal algorithm in the range $10^{-5} \leq \lambda_{UE} \leq 3\ 10^{-5}$, and then they both reach 9.3 Mbps in a highly loaded network. The aggregate throughput of the QoS based OEA algorithm is close to the opportunistic one and they both achieve up to 9 Mbps. The target throughput for the QoS based OEA is set to 600 kbps which explains the relatively low value of the aggregate throughput in a low loaded network.

Figure 5.13 represents the ratio between the number of served users and the number of active users in the considered sector. The total number of active users is given with the RSRP decision and it also includes the UEs with bad radio conditions that can not reach the minimum SINR value of

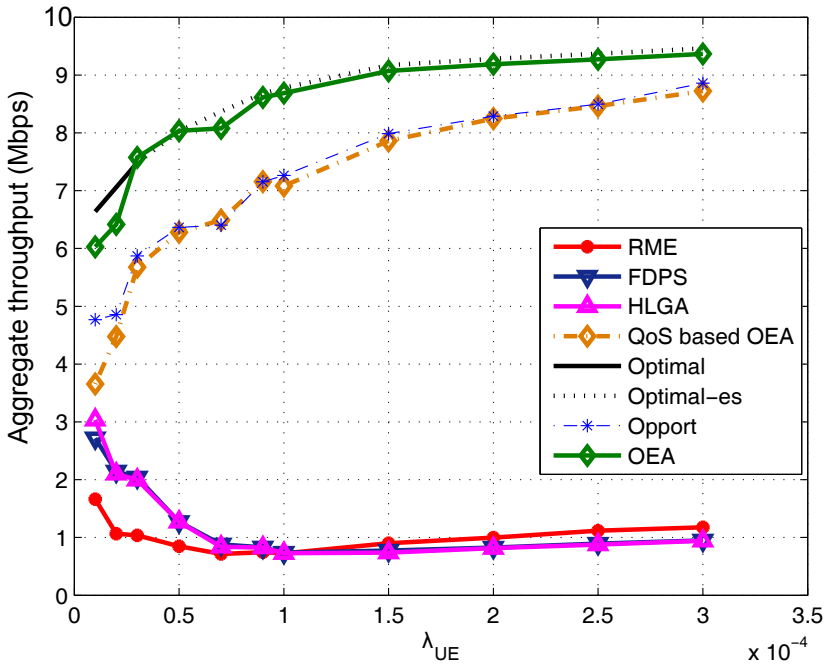

Figure 5.12: Aggregate throughput in the concerned sector of a random network

the most robust MCS. The RME algorithm allocates a large number of RBs to the best UE, which explains the low ratio of served UEs. The OEA algorithm serves 60% of the active UEs at low load. Then, it serves less and less proportion of users while the number of active users increases, to achieve 7% at high load. The OEA algorithm performances are close to the optimal algorithm ones where they reach 68% of served UEs at low load. The algorithms serving more UEs and ensuring a good ratio of served UEs are the FDPS-LMF and the HLGA when $\lambda_{UE} \leq 3\ 10^{-5}$, and the QoS based OEA when $\lambda_{UE} > 3\ 10^{-5}$. They reach respectively 92% and 85% of served UEs in low loaded network. From these results, we identify the need of the radio admission controller before the radio resource allocation, that selects only users with channel conditions that allow them to transmit their data, at least with the most robust MCS. In addition, the QoS based OEA algorithm shows all its interest, since it maximizes the proportion of served users as soon as the network's load exceeds $\lambda_{UE} = 4\ 10^{-5}$.

In Figure 5.14, we evaluate the ratio of wasted RBs. For $10^{-5} \leq \lambda_{UE} \leq 7\ 10^{-5}$, the RME wastes more RBs than the FDPS-LMF and the HLGA, and achieves 78% of wasted RBs. Then, the wastage ratio decreases to reach 65%. The FDPS-LMF and the HLGA have almost similar RB wastage ratios, except in low loaded networks, where the FDPS-LMF RB wastage ratio only reaches 25% instead of 35% for HLGA, due to the remaining RBs allocation policy. The opportunistic algorithm has a low RB wastage ratio at low load (about 5% for $10^{-5} \leq \lambda_{UE} \leq 5\ 10^{-5}$); it is then cancelled due to the users channel conditions diversity. Even at low load, OEA and QoS based OEA algorithms present no wasted RBs, thanks to the update of the SINR performed before each new RB allocation. In the same

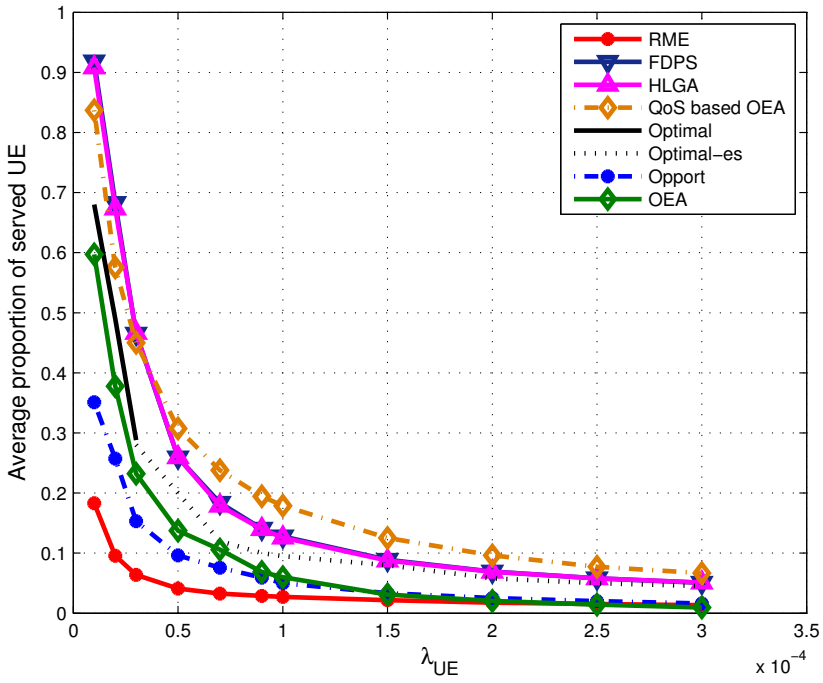

Figure 5.13: Average proportion of served UEs in a random network

way, the optimal algorithm cancels the RB wastage ratio whatever the intensity of users in the network.

The served users achieving an individual zero throughput are considered as unsatisfied users. Then the behavior of the ratio of unsatisfied users is similar to the ratio of wasted RBs. The fairness criteria, in terms of throughput, is given as a function of the users intensity per area unit in Figure 5.15. It measures the variation of the individual throughput between satisfied users, as defined in [14] and is expressed as:

$$F_{Alg} = \frac{\left(\sum_{k=1}^{N_{UE}} R_k(\Delta T)\right)^2}{\left(N_{UE} \sum_{k=1}^{N_{UE}} R_k(\Delta T)^2\right)} \tag{5.15}$$

We consider a short term fairness criteria, where ΔT is equal to 1 ms. The higher F_{Alg} is, the more the algorithm is fair. In Figure 5.15, we notice that the least fair algorithms are the opportunistic, OEA and optimal algorithms. As we consider one class of QoS users with a target throughput of 600 kbps, the QoS based OEA algorithm is more fair than the OEA algorithm. However, FDPS-LMF, HLGA and RME algorithms are the most fair algorithms, due to the use of the proportional fair metric. It must be noticed that their high number of unsatisfied users, with zero throughput, improves also their fairness sensation.

At low load, the algorithms that allocate a low number of RBs per user without RB wastage let more free RBs. In Figure 5.16, we represent the ratio of unused RBs. We note that the RME and

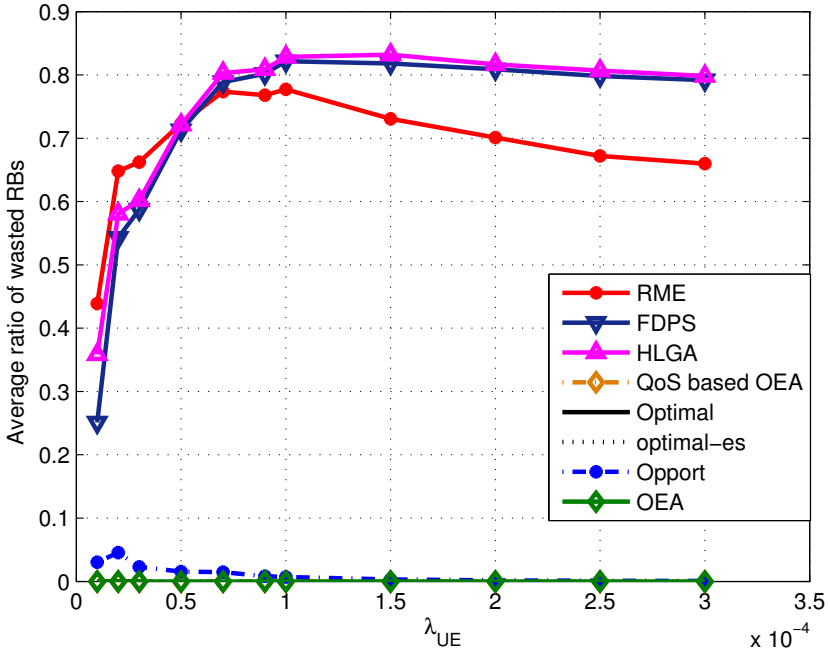

Figure 5.14: Average ratio of wastage RBs in a random network

the HLGA use N_{RB} RBs by allocating at the end of their allocation algorithm the remaining RBs to the users satisfying the contiguity constraints. The FDPS-LMF lets up to 24% of RBs free at low load. Whatever the network's load, the maximum ratio of unused RBs is achieved by the QoS based OEA algorithm. These free RBs could be used in a cooperative network to mitigate the interference generated by highly interfering UEs.

The average energy efficiency obtained by the different algorithms when all the UEs transmit at P_{max} is presented in Figure 5.17. Whatever the RB allocation algorithm used, the obtained average energy efficiency curves decrease when the intensity of users per area unit increases. The algorithm that maximizes the average energy efficiency is the optimal one. The OEA and QoS based OEA algorithms have almost the same behavior and the obtained average energy efficiency is close to the one obtained by the optimal algorithm. The FDPS-LMF and the HLGA algorithms achieve a lower energy efficiency. At $\lambda_{UE} = 3.5\ 10^{-3}$, the HLGA algorithm obtains a lower average energy efficiency than the FDPS-LMF algorithm, due to the lower reached throughput caused by the allocation of the remaining RBs. The algorithms that achieve the lowest average energy efficiency are the opportunistic and the RME algorithms. After the power control we proposed, the behavior of the average energy efficiency curves changes. We notice from Figure 5.18 that: i) the curves are not smoothed as before for the power control, which is due to the nonlinearity of the throughput computation (i.e. the use of the MCS table for the throughput computation), and ii) the average energy efficiency tends to increase when the intensity of users per area unit increases due to the power allocation efficiency when the number of allocated RBs to each user is low. The maximum average energy efficiency is achieved by

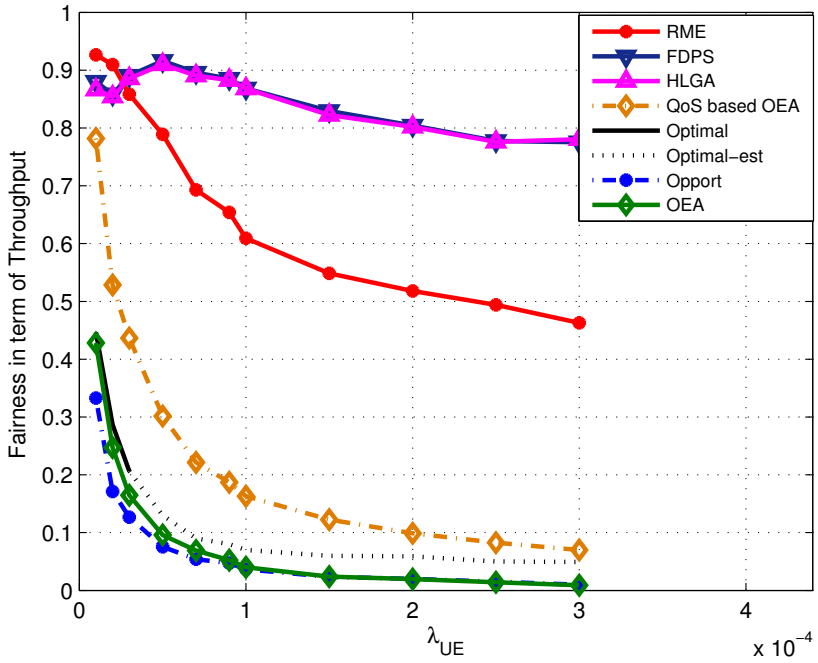

Figure 5.15: Fairness among users in terms of throughput in a random network

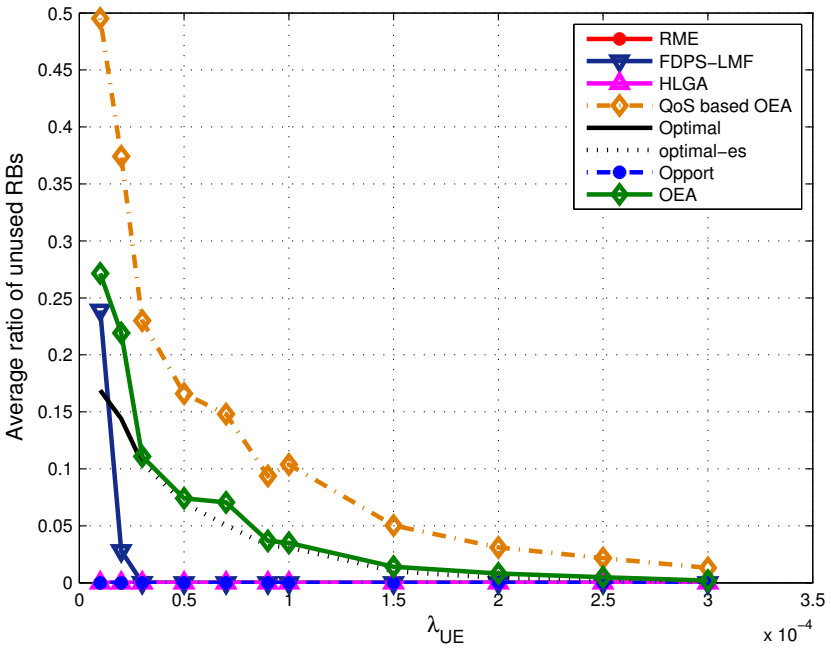

Figure 5.16: Average ratio of unused RBs in a random network

the QoS based OEA algorithm and it reaches 10^{12} bits/J. Finally, the average UE transmission power

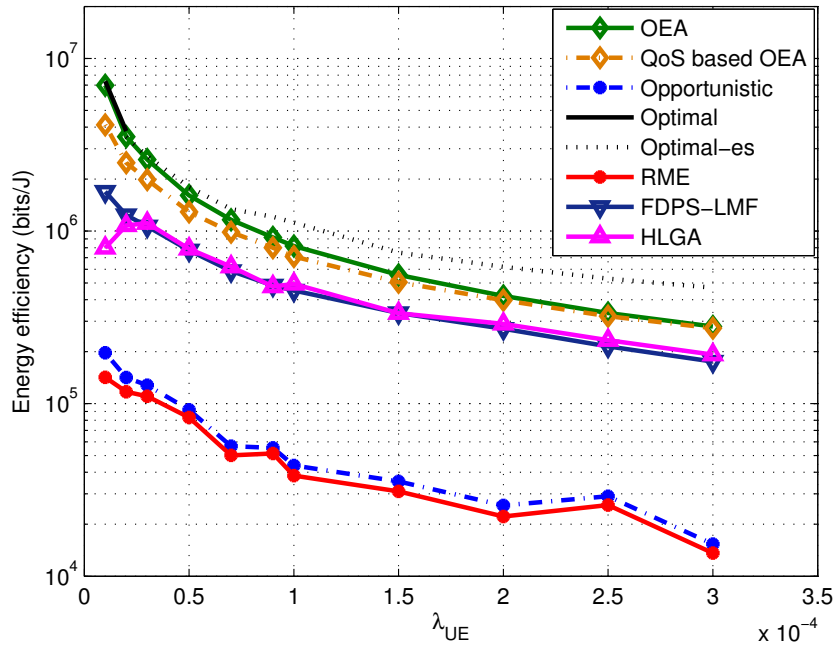

Figure 5.17: Energy efficiency of the UEs in a random network, before the power allocation

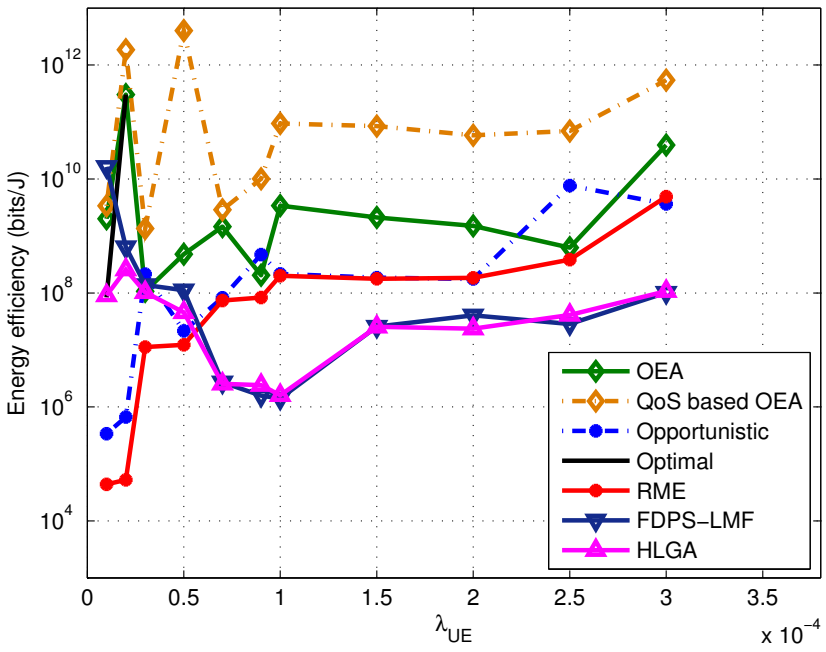

Figure 5.18: Energy efficiency of the UEs in a random network, after the power allocation

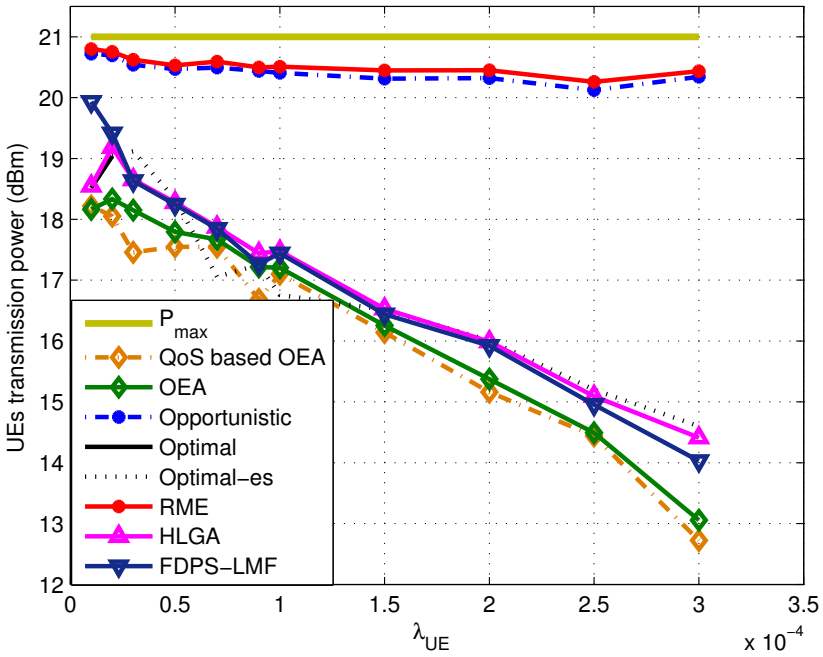

Figure 5.19: Average UEs transmission power in one TTI, in a random network

after power control is given in Figure 5.19. It varies between 12 dBm and P_{max} = 21 dBm, and is compliant with the standards [9]. The algorithms that allocate the highest average UE transmission power are the RME and the Opportunistic algorithms, because they allocate the highest number of RBs per UE. It must be noticed that the maximum transmission power of the unsatisfied users increases the average transmission power obtained by each algorithm. As expected from the average energy efficiency results, the algorithms that allocate the lowest average UE transmission power are the OEA and QoS based OEA algorithms. In low loaded networks, the average saved transmission power is about 50% when OEA, QoS based OEA, FDPS-LMF or the optimal algorithms are used. On the contrary, the opportunistic and the RME algorithms save less than 5% of consumed power. In highly loaded networks, the average rate of saved UE transmission power increases whatever the radio resource allocation algorithm. It reaches around 10% for the opportunistic and the RME algorithms, when it achieves more than 80% when the OEA and the QoS based OEA algorithms are adopted.

5.6 OEA based radio resource allocation algorithm for LTE-A networks

Since the OEA and QoS based OEA algorithms consider the contiguity constraint imposed in LTE release 8 uplink air interface, they can not be directly used in LTE-A networks. To overcome this limitation, we adapt them to the LTE-A uplink air interface, which only imposes the MCS robustness constraint. Hence, the LTE-A adapted version of OEA algorithm steps are summarized in Algo-

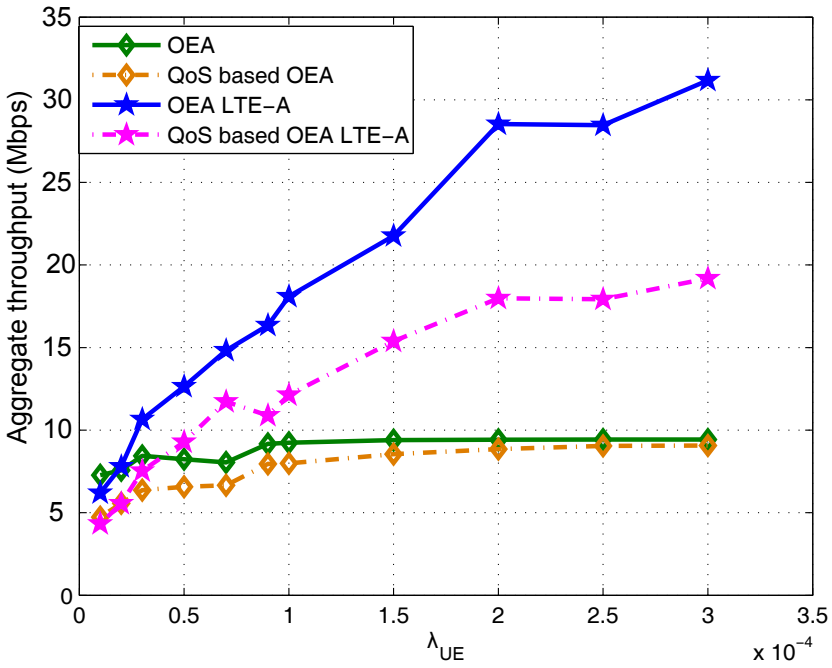

Figure 5.20: Aggregate throughput in a concerned sector of a random LTE and LTE-A networks

rithm 6. These adapted algorithms are compared with their classical versions in terms of aggregate throughput. The comparison is given on Figure 5.20 over 1000 TTI for a random network, where the same simulation parameters as those cited in Table 5.4 are considered.

At low load, the aggregate throughputs are almost similar, with a small advantage for the OEA algorithm and its adapted version for LTE-A networks. When the number of users increases, the aggregate throughput increases, independently of the radio resource algorithm. Once λ_{UE} exceeds 0.3 10^{-4}, the aggregate throughput noticeably increases in LTE-A networks, as it achieves more than 30 Mbps, where it does not exceed 10 Mbps in LTE. The same observation is given for the QoS differentiation algorithms. The QoS based OEA adapted for LTE-A networks achieves 20 Mbps in highly loaded networks when it converges to the one obtained with OEA algorithm in LTE. Hence, when the RB contiguity constraint is removed, the aggregated throughput of the sector can be tripled. This improvement is due to the users channel diversity.

Algorithm 6 Radio resource allocation algorithm for LTE-A networks

Inputs: Matrix $\mathcal{M}_x$ of N_{UE} x N_{RB} elements of $\overline{\gamma^{\text{eff}}_{(k,c)}}$.
Set of UE : $\mathcal{K} = \{1, \cdots, k, \cdots, N_{UE}\}$.
Set of RBs : $\mathcal{C} = \{1, \cdots, c, \cdots, N_{RB}\}$.
$\alpha_{k_{max}}$, Δ_γ, γ_{MCS}
Initialization:
$\mathcal{S}_{RB} = \emptyset$, $P_{UE} = \emptyset$
while $\big((\mathcal{C} \neq \emptyset)$ and $(\mathcal{K} \neq \emptyset)\big)$ **do**
1) find $(k, c) = \arg \max_{k \in \mathcal{K}, c \in \mathcal{C}} \mathcal{M}_x$, where $(k, c) \in \mathcal{K} \times \mathcal{C}$
2) assign RB c to UE k:
$\mathcal{S}_{RB} = \mathcal{S}_{RB} \cup \{(c, k)\}$
$\mathcal{A}_k = \mathcal{A}_k \cup \{c\}$
3) remove the RB c from the set $\mathcal{C}$:
$\mathcal{C} = \mathcal{C} \backslash \{c\}$
4) determine the individual throughput:
$R_k(t) = r^c_k(t)$
5) update $\mathcal{M}_x(k, \mathcal{C})$, using (5.5).
6) extend the RB allocation of UE k.
while $|\mathcal{A}_k| < \alpha_{k_{max}}$ **do**
a) find $(k, c') = \arg \max_{k \in \mathcal{K}, c' \in \mathcal{C}} \mathcal{M}_x$, where $(k, c') \in \mathcal{K} \times \mathcal{C}$
b) assign conditionally RB c' to UE k by temporarily including c' into $\mathcal{A}_k$.
c) compute the temporary throughput $R_{k_{temp}}$ of UE k with relations (5.2) and (5.3).
if $R_{k_{temp}(t)} > R_k(t)$ **then**
- $\mathcal{S}_{RB} = \mathcal{S}_{RB} \cup \{(c', k)\}$
- $\mathcal{A}_k = \mathcal{A}_k \cup \{c'\}$.
- $\mathcal{C} = \mathcal{C} \backslash \{c'\}$.
- update $\mathcal{M}_x(k, \mathcal{C})$ using (5.5).
else
- break
end if
end while
7) remove UE k from the set $\mathcal{K}$.
8) determine the transmission power $P_{e,k}$ using (5.8):
$P_{UE} = P_{UE} \cup \{P_{e,k}\}$
end while
Outputs: $\mathcal{S}_{RB}$, P_{UE}

5.7 Conclusion

In this Chapter, a new radio resource allocation scheme for uplink LTE release 8 networks, respecting the SC-FDMA constraints, was presented. It determines the UE transmission power after the determination of the set of RBs allocated for transmission. This scheme has the benefits of adapting the UE transmission power as a function of the user's channel conditions over its whole allocated RBs, and maintaining all the individual throughputs as before the power reduction. This new radio resource allocation scheme is declined in two opportunistic and efficient versions: 1) a definitely opportunistic one, and 2) an adapted to QoS differentiation one. The achieved aggregate throughputs are close to the one achieved by the optimal RB allocation algorithm. As the optimal algorithm, they cancel the RBs wastage; but in addition, they increase each served user's energy efficiency thanks to the power control and the individual throughput increase constraint applied for the RB expansion allocation. The resulting saved UE transmission power increases the UE battery life and generates less inter-cell interference. In cooperative networks, the remaining free RBs could be allocated to the neighboring users generating a high inter-cell interference. The computational complexity and the number of necessary operations evaluation proved the hardware implementation feasibility of the proposed radio resource scheme and its possibility to be run in less than the scheduling frequency. To adapt the proposed radio resource allocation scheme for LTE-A networks, the RB contiguity constraint was removed from the RB allocation algorithm. By this way, we proved that with a small modification of the algorithm we can adapt the proposed radio resource allocation logarithm to the LTE-A networks and maximize the network's aggregate throughput by exploiting the user's channel diversity.

Chapter 6

RB allocation in MU-MIMO uplink LTE networks

Part of this chapter was published in IEEE PIMRC 2013[1]

IN this chapter, we consider the RB allocation problem in the uplink of a multi-user MIMO LTE network. In the MU-MIMO context, the aggregate throughput in the cell does not depend only on the RB allocation algorithm but also on the MU-MIMO transceiver's design. For this reason, we focus first on the transceiver structure design and then we show how to extend the OEA algorithm presented in Chapter 5 to the multi-user context with respect to SC-FDMA constraints. The proposed transceiver structure is based on the use of an adequate encoder at the transmitter side, to take advantage of the multiple transmit antenna diversity, and a combination of a joint zero forcing (ZF) and a maximum likelihood (ML) decoder at the receiver side. The evaluated throughput performances of the proposed transceiver in a scheduling uplink LTE context outperform the ones of other well known decoders.

[1]L. Mroueh, E. Vivier, F.Z. Kaddour, M. Pischella and P. Martins, "Combined ZF and ML Decoder for Uplink Scheduling in Multi-User MIMO LTE Networks ", in proceedings of IEEE International Symposium on Personal, Indoor and Mobile Radio Communications (PIMRC), London, UK, September, 2013.

6.1 Introduction and Motivations

We consider N_s UEs, having n_t transmit antennas each, want to communicate with an eNB having n_r receive antennas. One of the main advantages of MU-MIMO systems deployment in cellular network is to increase the system reliability and the total data throughput in the cell. On one hand, the use of multiple transmit antennas at both sides provides a diversity gain that can be extracted using appropriate transceiver schemes. On the other hand, the use of multiple antennas at the eNB offers the possibility to multiple UEs to transmit simultaneously on a same RB. The MU-MIMO multiplexing over a single RB in the MU-MIMO uplink channel have been widely studied in the literature where different scheduling strategies are proposed in [84] [85] and references therein. Most of these strategies aim at maximizing the total aggregate throughput by choosing an appropriate combination of simultaneously transmitting UEs on the considered RB. However, to the best of our knowledge, few works address the case of a MU-MIMO uplink resource allocation in the entire LTE bandwidth. Actually, an exhaustive search (under the LTE SC-FDMA constraints) for the combination of simultaneously transmitting UEs with maximal throughput at each RB of the LTE bandwidth becomes non feasible when extended to several RBs. While scheduling strategies aim to offer the highest possible data throughput, robust transceivers design aims to offer the possibility to spatially multiplex different UEs data streams and to offer to each UE a reliable individual throughput by exploiting the transmit and the receive diversity. Low complexity linear decoders such as ZF or Minimum Mean Square Error (MMSE) [84] decode independently each of the transmitted data streams and lead to a loss in the transmit diversity. The ML decoder offers both gains in diversity and multiplexing gain, but this comes at the expense of a high decoding complexity at the eNB side [86].
This Chapter proposes a robust MU-MIMO uplink transceiver design that is based on the use of an adequate space time code at the UE and a combination of multi-user ZF and ML decoder at the eNB. Section 6.2 provides the MIMO an MU-MIMO background material and details the MIMO space coding. The proposed uplink spatial multiplexing transceiver is presented in Section 6.3. The RB allocation based on OEA algorithm in uplink MU-MIMO LTE networks is given in Section 6.4. The performances evaluation of the proposed transceiver and the use of the OEA algorithm in MU-MIMO, studied in a regular network, are shown in Section 6.5.

6.2 Background materials

The MU-MIMO system introduced in Section 2.3.3 is considered. In LTE systems, UEs can be equipped by $n_t = 1$ or $n_t = 2$ antennas, and the eNB can have up to $n_r = 4$ antennas. Let $\mathbf{x}_k \in \mathbb{C}^{n_t \times 1}$ denote the transmitted vector of a UE k characterized by its position (r_k, θ_k) such that $\mathbb{E}[\mathbf{x}_k \mathbf{x}_k^{\dagger}] = \mathbf{I}_{n_t}$. Let N_s be the number of simultaneously active UEs in each RB. At the eNB, the received signal vector $\mathbf{y}_{\text{eNB}} \in \mathbb{C}^{n_r \times 1}$ depends on the wireless channel variations and is given by,

$$\mathbf{y}_{\text{eNB}} = \sum_{n=1}^{K} \sqrt{P^m_{k_{Tx}} \Lambda_k}\, \mathbf{H}_k \mathbf{x}_\mathbf{k} + \mathbf{z} + \mathbf{I}, \tag{6.1}$$

where the channel matrix $\mathbf{H}_k \in \mathbb{C}^{[n_r \times n_t]}$ contains the fading coefficients $h_{i,j}^{(k)}$ between the antenna j of UE k and the antenna i of the eNB, $\mathbf{z} \in \mathbb{C}^{n_r \times 1}$ is the additive noise vector and $\mathbf{I} \in \mathbb{C}^{n_r \times 1}$ represents the intercell interference coming from 18 UEs in the neighboring interfering cells.
In the following, we consider the statistical inter-cell interference I_{inter} received at the eNB. We denote by $\mathbf{\Sigma} = \left(N_0 + I_{\text{inter}}\right) \mathbf{I}_4$ the covariance matrix of the noise plus inter-cell interference vector received by the eNB. In addition, we note T the number of time slots over which an elementary information signal is transmitted.
We first recall some basis on the MIMO space coding in order to fully exploit the spatial diversity and multiplexing gains. Two different configurations are considered: the 2×1 MISO system and the 2×2 MIMO system. Then, in the multi-user context, we review the multi-user linear ZF decoder used to cancel the multi-user interference.

6.2.1 Preliminaries on MIMO coding

We consider a MIMO system as depicted in Figure 6.1.
Let $\mathbf{H}^{[n_r \times n_t]}$ be the $n_r \times n_t$ channel matrix and let $\mathbf{X} \in \mathbb{C}^{n_t \times T}$ be the transmitted space time code

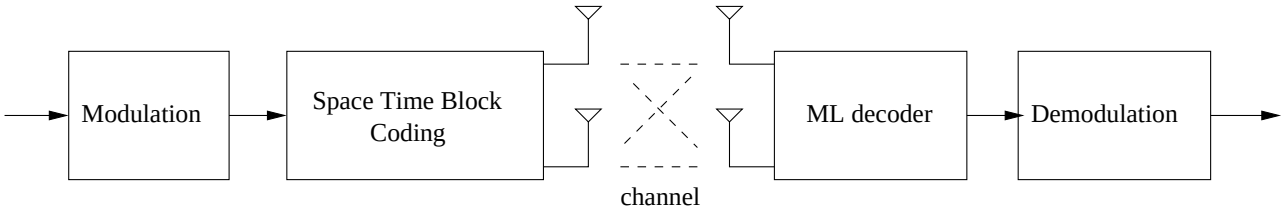

Figure 6.1: MIMO system: Space Time coding at the encoder and Maximum Likelihood at the decoder

matrix that belongs to a codebook $\mathcal{X}_p$ such that

$$\text{Tr}\left[\mathbb{E}[\mathbf{X}\mathbf{X}^{\dagger}]\right] = T.$$

The received signal is,

$$\mathbf{Y}^{[n_r \times T]} = \sqrt{\frac{P_{k_{Tx}}^{m} \Lambda_k}{n_t}} \mathbf{H}_k^{[n_r \times n_t]} \mathbf{X}_k^{[n_t \times T]} + (\mathbf{z}^{[n_r \times T]} + \mathbf{i}^{[n_r \times T]}).$$

where Λ_k is the attenuation factor induced by the path loss, the shadowing and the antenna gains, $(\mathbf{z} + \mathbf{i})$ is the additive noise plus interference vector with covariance matrix $\mathbf{\Sigma}$. One of the main characteristics of MIMO systems is that one can multiplex $\min(n_t, n_r)$ different symbols during one channel use. The space time code structure contains then s different symbols with $s = \min(n_t, n_r)T$. Moreover, the different symbols can be conveyed from the transmitter side to the receiver side using $n_t n_r$ different paths which correspond to the diversity gain. The space time coding scheme should ensure that the $\min(n_t, n_r)$ information symbols are coded onto the different antennas in such a way that each information symbol is transmitted through the $n_t n_r$ different paths. At the receiver side,

the informations are decoded using a ML decoder that searches the matrix $\hat{\mathbf{X}}$ in the family of space time codes that minimizes the following distance,

$$\hat{\mathbf{X}} = \arg \min_{\mathbf{C} \in \mathcal{X}_p} \mathrm{Tr}[(\mathbf{Y} - \mathbf{\Sigma}^{-1/2}\mathbf{HC})(\mathbf{Y} - \mathbf{\Sigma}^{-1/2}\mathbf{HC})^{\dagger}]$$

Exhaustive research among all the possible space time codewords can be performed. Algorithm with less complexity such as sphere decoder [87] and Schnorr Euchner [88] are used in practice.

Diagonal Algebraic Space Time Block (DAST) coding for 2×1 MISO system

For a 2×1 MISO system, the transmission is performed over two channels use where it is assumed that the channel remains the same. The multiplexing gain is equal to 1, meaning that one symbol can be transmitted over one channel use. Let s_1 and s_2 denote the information symbols transmitted during the two channels use. The structure of the DAST code is

$$\mathbf{X} = \frac{1}{\sqrt{5}} \begin{bmatrix} x_0 & 0 \\ 0 & \sigma(x_0) \end{bmatrix}$$

where $x_0 = \alpha(s_1 + \theta s_2)$ and $\sigma(x_0) = \bar{\alpha}(s_1 + \bar{\theta} s_2)$ with $\theta = \frac{1+\sqrt{5}}{2}$, $\bar{\theta} = \frac{1-\sqrt{5}}{2}$, $\alpha = 1 + i - i\theta$ and $\bar{\alpha} = 1 + i - i\bar{\theta}$. The main characteristics of this code is that it achieves the full diversity of the MISO code $d = 2$ and the full multiplexing gain of 1 as the symbol rate is equal to 1. An intuitive interpretation on the diversity gain can be given by observing that in this DAST coding structure, symbol s_1 (respectively s_2) is transmitted over the first fading path in the first channel use and on the second fading path in the second channel use. The DAST code transforms the MISO channel into two parallel channels for which the capacity of the channel is,

$$C_{\mathrm{MISO}} = \frac{1}{2} \sum_{i=1}^{2} \log_2(1 + \frac{P^m_{k_{Tx}}}{N_0 + I_{inter}} \Lambda |h_i|^2) \leq \log_2 \left(1 + \frac{P^m_{k_{Tx}}}{2(N_0 + I_{inter})} A\Big(|h_1|^2 + |h_2|^2\Big)\right)$$

The effective SINR required to decode information on each channel use is then,

$$\gamma_{\mathrm{eff}} = 2^{C_{\mathrm{MISO}}} - 1$$

which is slightly less than the SINR of an equivalent MISO channel.

Golden code for 2×2 MIMO system

In a 2×2 MIMO system, the transmission is performed over two time slots where it is assumed that the channel remains the same. The multiplexing gain is equal to 2 meaning that two symbols can be transmitted at once over one channel use. Let s_1, s_2, s_3 and s_4 denote information symbols

transmitted during the two channels use. In [89], the Golden code structure is given as:

$$\boldsymbol{\mathcal{G}} = \frac{1}{\sqrt{5}} \begin{bmatrix} x_1 & \sigma(x_2) \\ ix_2 & \sigma(x_1) \end{bmatrix}$$

where $x_1 = \alpha(s_1 + \theta s_2)$, $\sigma(x_1) = \bar{\alpha}(s_1 + \bar{\theta} s_2)$, $x_2 = \alpha(s_3 + \theta s_4)$ and $\sigma(x_2) = \bar{\alpha}(s_3 + \bar{\theta} s_4)$. The main characteristics of this code is that it achieves the full diversity of the MIMO code $d = 4$ and the full multiplexing gain of 2 as the symbol rate is equal to 2. An intuitive interpretation of the diversity gain can be given by observing that in this Golden code structure, symbol s_1 (respectively s_2, s_3 and s_4) is transmitted over the fading path $h_{1,1}$ and $h_{2,1}$ in the first channel use and on the fading paths $h_{1,2}$ and $h_{2,2}$ in the second channel use. The effective SINR of the MIMO system required to decode one data stream using the Golden code is then,

$$\gamma_{\text{eff}} = 2^{\frac{1}{2} C_{\text{MIMO}}} - 1$$

where

$$C_{\text{MIMO}} = \log_2 \det(\mathbf{I}_{n_r} + \frac{P^m_{k_{Tx}}}{(N_0 + I_{inter})} A \mathbf{H}\mathbf{H}^\dagger).$$

6.2.2 Preliminaries on multi-user linear ZF decoder

For the uplink MU-MIMO channel in (6.1), the multi-user linear ZF decoding removes the multi-user interference coming from the others $(N_s - 1)$ UEs. For example, in order to decode UE 1 information, one can find a matrix $\mathbf{V}_1$ that is simultaneously orthogonal to $\mathbf{H}_2, \mathbf{H}_3, \ldots, \mathbf{H}_{N_s}$ *i.e.* $\mathbf{V}_1\mathbf{H}_2 = \ldots = \mathbf{V}_1\mathbf{H}_{N_s} = 0$ or equivalently $\mathbf{H}_2^\dagger \mathbf{V}_1^\dagger = \ldots \mathbf{H}_{N_s} s^\dagger \mathbf{V}_1^\dagger = 0$. The solution of this problem is

$$\mathbf{V}_1^\dagger \perp (\mathbf{H}_2^\dagger, \mathbf{H}_3^\dagger \ldots \mathbf{H}_{N_s}^\dagger) \Leftrightarrow \mathbf{V}_1^\dagger \subseteq \ker(\boldsymbol{\mathcal{H}}).$$

where

$$\boldsymbol{\mathcal{H}} = \begin{bmatrix} \mathbf{H}_2^{\dagger[n_t \times n_r]} \\ \mathbf{H}_3^{\dagger[n_t \times n_r]} \\ \vdots \\ \mathbf{H}_{N_s}^{\dagger[n_t \times n_r]} \end{bmatrix}$$

having $(N_s - 1)n_t$ rows and n_r columns. Its kernel space has a maximal dimensionality of $\min(n_r - (N_s - 1)n_t; 0)$. The matrix $\mathbf{V}_1^\dagger$ has therefore n_r rows and $\min(n_r - (N_s - 1)n_t; 0)$ columns. Hence, $\mathbf{V}_1$ has $\min(n_r - (N_s - 1)n_t; 0)$ rows and n_r columns. The same procedure can be repeated for all the other $(N_s - 1)$ UEs.

6.3 Uplink Spatial Multiplexing Transceiver

One of the main advantages of using MU-MIMO systems is the possibility to schedule different UEs in the same RB using spatial division multiple access techniques. In the following, some information theory basics from [86] [90] on the capacity region and the spatial multiplexing gain region will be first presented. Then, we describe the proposed transceiver structure and we derive the resulting SINR required to decode each UE's data stream.

6.3.1 Multiplexing region of the MU-MIMO uplink channel

As mentioned in Chapter 2, the multiplexing region defines the maximal number of streams that can be decoded simultaneously at the eNB. Over a RE, let $N_{u,p}$ be the number of potential UEs among the total number N_{UE} of UEs, and r_k with $1 \leq k \leq N_s$ be the number of streams submitted by a UE k over a RE. Then, the multiplexing region $\mathcal{R}$ is defined as $\mathcal{R} = \left\{r_k \in \mathbb{N} : r_k \leq \min(n_t, n_r) \text{ and } r_{tot} = \sum_k r_k \leq \min(n_r, N_{u,p} n_t)\right\}$. The $\min(n_r, N_{u,p} n_t)$ transmitted streams can be simultaneously decoded at the eNB side using suboptimal linear decoders (such as ZF or MMSE decoder) or other optimal decoders such as the ML decoder. Although the ML decoder improves the theoretical total throughput compared to linear precoding schemes, this comes at the expense of an increased complexity at the receiver side. In the following, the structure of the proposed transceiver is described.

6.3.2 Combined multi-user ZF and ML decoder

At the eNB, we propose to use a multi-user ZF decoder that *only* removes the multi-user interferences, followed by a ML decoder that jointly decodes the encoded data streams. Unlike the classical ZF decoder, the proposed combination of multi-user ZF and ML decoders can extract the multi-antenna transmit diversity for each UE when an adequate space time code is used at the transmitter side. The received signal in (6.1) is first equalized using a multi-user ZF decoder for each UE k in order to

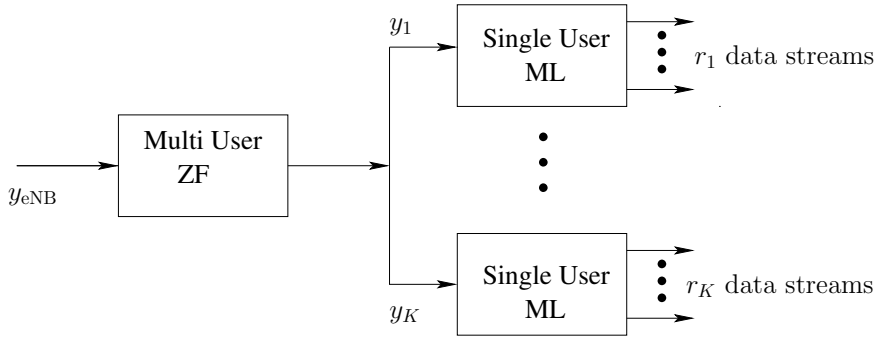

Figure 6.2: Combined ZF and ML decoder: Multi-user ZF removes the multi-user interference. The single-user ML decoder jointly decode the r_i data streams of each user such that $r_i \leq \min(n_t, n_r)$ and $\sum_{i=1}^{K} r_i = \min(n_r, K n_t)$.

cancel the multi-user interference coming from the other $(N_s - 1)$ UEs. For this purpose, the received

signal is projected in a similar way as in [91] onto the *orthonormal* space spanned by $\mathbf{V}_k$ such that: $\mathbf{V}_k\mathbf{H}_i = 0$, $\forall i \neq k$. These orthogonality constraints consume $(N_s - 1)n_t$ degrees of freedom and the matrix $\mathbf{V}_k$, that spans the kernel space of $\mathbf{H}_{\text{conc},k}$ formed by the concatenated matrices $\mathbf{H}_i$ $(\forall i \neq k)$, has therefore $\min(n_r - (N_s - 1)n_t, 0)$ rows and n_r columns. The structure of this decoder will be detailed later in Subsections 6.3.3 and 6.3.4 for different MU-MIMO configurations.

6.3.3 Transceiver schemes for UEs with $n_t = 1$

In this case, the maximal number of streams that can be transmitted by each UE k is $r_{\max,k} = 1$ and $r_{tot} = 4$. This means that at most four users can transmit information simultaneously on a given RE.

Case $N_s = 1$

In this case, the MU-MIMO channel is equivalent to a 1×4 SIMO system. The 4×1 received vector at the eNB is

$$\mathbf{y} = \sqrt{P^m_{k_{Tx}}\Lambda_1}\mathbf{h}_1^{[4\times1]}x_1 + (\mathbf{z} + \mathbf{i})^{[4\times1]} \tag{6.2}$$

The SINR over a RE is then,

$$\gamma_1^{(m,n)} = \frac{P^m_{k_{Tx}}\Lambda_1\|\mathbf{h}_1\|^2}{N_0 + I_{inter}}$$

Case $N_s = 2$

In this case, each UE transmits only one data stream using QAM constellation symbols. The 4×1 received vector at the eNB is

$$\mathbf{y}_{\text{eNB}} = \sqrt{P^m_{k_{Tx}}\Lambda_1}\mathbf{h}_1^{[4\times1]}x_1 + \sqrt{P^m_{k_{Tx}}\Lambda_2}\mathbf{h}_2^{[4\times1]}x_2 + (\mathbf{z} + \mathbf{i})^{[4\times1]} \tag{6.3}$$

In order to decode UE 1 information, the received signal is equalized using the precoder

$$\mathbf{V}_1^{\dagger} \in \mathbb{C}^{[4\times3]} \subseteq \ker\left(\left[\ \mathbf{h}_2^{\dagger[1\times4]}\ \right]\right)$$

The projection of $\mathbf{y}_{\text{eNB}}$ over $\mathbf{V}_1$ gives:

$$\mathbf{y}_{e,1}^{3\times1} = \sqrt{P^m_{k_{Tx}}\Lambda_1}\mathbf{V}_1^{[3\times4]}\mathbf{y}^{[4\times1]} \in \mathbb{C}^{3\times1}.$$

The equivalent channel model for UE 1 is then,

$$\mathbf{y}_{e,1}^{3\times1} = \sqrt{P^m_{k_{Tx}}\Lambda_1}\mathbf{g}_1^{[3\times1]}x_1 + \mathbf{n}_1^{[3\times1]}$$

with $\mathbf{g}_1^{[3\times1]} = \mathbf{V}_1^{[3\times4]}\mathbf{h}_1^{[4\times1]}$ a 3×1 Gaussian vector and $\mathbf{n}_1^{[3\times1]} = \mathbf{V}_1^{[3\times4]}(\mathbf{z} + \mathbf{i})^{[4\times1]}$ a Gaussian vector with covariance matrix $(N_0 + I_{\text{inter}})\,\mathbf{I}_3$ since $\mathbf{V}_1$ is a unitary matrix. Using the equivalent system model, it can be deduced that the MU-ZF decomposes the MU-MIMO into two parallel 1×3 MISO

channels as shown in Figure 6.3.

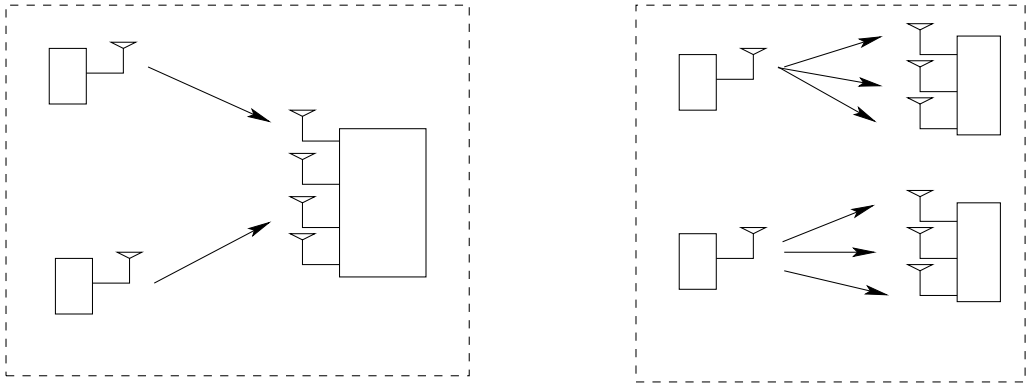

Figure 6.3: The linear ZF precoder decomposes the multi-user uplink MIMO channel into two parallel SIMO 1×3 channels that do not interfere. The receive diversity is equal to 3: Virtual SIMO reception.

Case $N_s = 3$

The number of data streams is also limited to 1 in this case. The 4×1 received vector at the eNB is,

$$\mathbf{y}_{\text{eNB}} = \sqrt{P^m_{k_{Tx}} \Lambda_1} \mathbf{h}_1^{[4\times1]} x_1 + \sqrt{P^m_{k_{Tx}} \Lambda_2} \mathbf{h}_2^{[4\times1]} x_2 + \sqrt{P^m_{k_{TX}} \Lambda_3} \mathbf{h}_3^{[4\times1]} x_3 + (\mathbf{z} + \mathbf{i})^{[4\times1]} \tag{6.4}$$

In order to decode UE 1 information, the received signal is equalized using the precoder

$$\mathbf{V}_1^{\dagger} \subseteq \ker \left(\begin{bmatrix} \mathbf{h}_2^{\dagger[1\times4]} \\ \mathbf{h}_3^{\dagger[1\times4]} \end{bmatrix} \right)$$

and $\mathbf{V}_1 \in \mathbb{C}^{2\times4}$. The projection of $\mathbf{y}_{\text{eNB}}$ over $\mathbf{V}_1$ gives:

$$\mathbf{y}_{e,1}^{2\times1} = \sqrt{P^m_{k_{Tx}} \Lambda_1} \mathbf{V}_1^{[2\times4]} \mathbf{y}^{[4\times1]} \in \mathbb{C}^{2\times1}.$$

The equivalent channel model for UE 1 is then,

$$\mathbf{y}_{e,1}^{2\times1} = \sqrt{P^m_{k_{Tx}} \Lambda_1} \mathbf{g}_1^{[2\times1]} x_1 + \mathbf{n}_1^{[2\times1]}$$

with $\mathbf{g}_1^{[2\times1]} = \mathbf{V}_1^{[2\times4]} \mathbf{h}_1^{[4\times1]}$ a 2×1 Gaussian vector and $\mathbf{n}_1^{[2\times1]} = \mathbf{V}_1^{[2\times4]} (\mathbf{z} + \mathbf{i})^{[4\times1]}$ is a Gaussian vector with covariance matrix $(N_0 + I_{\text{inter}}) \mathbf{I}_2$ since $\mathbf{V}_1$ is a unitary matrix. Using the equivalent system model, it can be deduced that the MU-ZF decomposes the MU-MIMO into three parallel 1×2 MISO channels as shown in Figure 6.4.

For UE 1, the SINR over a RE (m, n) is then,

$$\gamma_1^{(m,n)} = \frac{P^m_{k_{Tx}} \Lambda_1 \|\mathbf{g}_1\|^2}{N_0 + I_{inter}}.$$

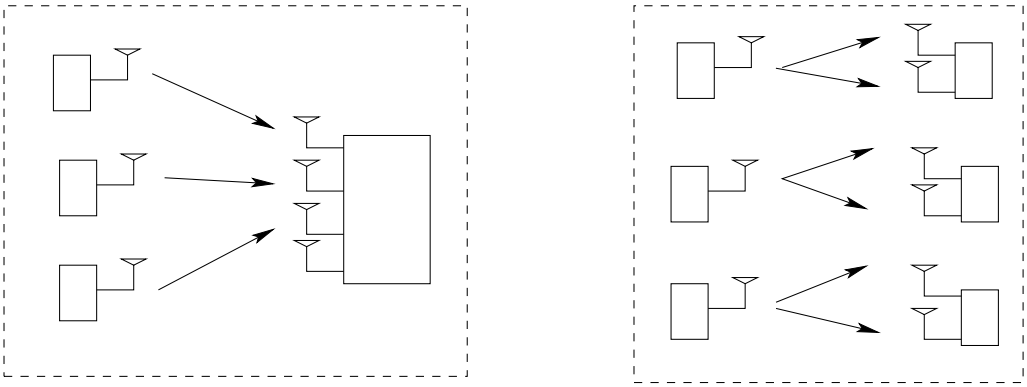

Figure 6.4: The linear ZF precoder decomposes the multi-user uplink MIMO channel into three parallel SIMO 1×2 channels that do not interfere. The receive diversity is equal to 2: Virtual SIMO reception.

Case $N_s = 4$

The 4×1 received vector at the eNB is then,

$$\mathbf{y} = \sqrt{P^m_{k_{Tx}} \Lambda_1} \mathbf{h}_1^{[4\times1]} x_1 + \sqrt{P^m_{k_{Tx}} \Lambda_2} \mathbf{h}_2^{[4\times1]} x_2 + \sqrt{P^m_{k_{Tx}} \Lambda_3} \mathbf{h}_3^{[4\times1]} x_3 + \sqrt{P^m_{k_{Tx}} \Lambda_4} \mathbf{h}_4^{[4\times1]} x_4 + (\mathbf{z}+\mathbf{i})^{[4\times1]} \quad (6.5)$$

In order to decoder the information submitted by UE 1, the received signal should be projected on the orthonormal space $\mathbf{v}_1$ that is simultaneously orthogonal to $\mathbf{h}_2, \mathbf{h}_3$ and $\mathbf{h}_4$. This means that:

$$\mathbf{v}_1^{\dagger} \subseteq \ker\Big(\begin{bmatrix} \mathbf{h}_2^{\dagger[1\times4]} \\ \mathbf{h}_3^{\dagger[1\times4]} \\ \mathbf{h}_4^{\dagger[1\times4]} \end{bmatrix} \Big).$$

and implies that $\mathbf{v}_1$ is a 1×4 vector. Then,

$$y_{e,1} = \mathbf{v}_1^{[1\times4]} \mathbf{y}^{[4\times1]} = \sqrt{P^m_{k_{Tx}} \Lambda_1}\ \mathbf{v}_1^{[1\times4]} \mathbf{h}_1^{[4\times1]} x_1 + \mathbf{v}_1^{[1\times4]} (\mathbf{z}+\mathbf{i})$$

Let $g_1 = \mathbf{v}_1^{[1\times4]} \mathbf{h}_1^{[4\times1]}$ and $n_1 = \mathbf{v}_1^{[1\times4]} (\mathbf{z}+\mathbf{i})^{[4\times1]}$. then,

$$y_{e,1} = \sqrt{P^m_{k_{Tx}} \Lambda_1} g_1 x_1 + n_1 \quad (6.6)$$

The projection of the Gaussian vector $\mathbf{h}_1$ onto an orthonormal vector $\mathbf{v}_1$ results in a complex Gaussian variable g_1. The information of a UE k (with $1 \leq k \leq N_s$) is then decoded over each RE at the eNB with an SINR of

$$\gamma_k^{(m,n)} = P^m_{k_{Tx}} \frac{\Lambda_k |g_1|^2}{N_0 + I_{\text{inter}}}.$$

The same procedure should be applied to decode information of UE 2, UE 3 and UE 4. Using the equivalent system model, it can be deduced that the MU-ZF decomposes the MU-MIMO into four parallel 1×1 SISO channels as shown in Figure 6.5.

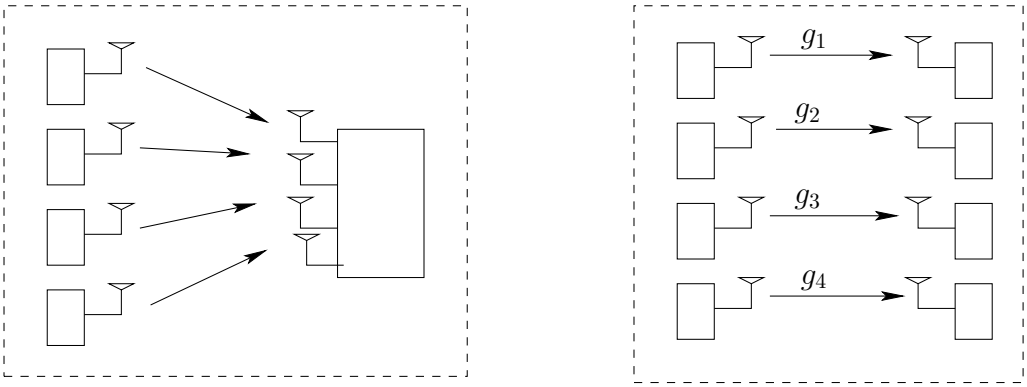

Figure 6.5: The linear ZF precoder decomposes the multi-user uplink MIMO channel into four parallel SISO 1×1 channels that do not interfere.

6.3.4 Transmission scheme for UEs with $n_t = 2$

In this case, the maximal number of data streams transmitted per each UE is limited to $\min(n_t, n_r) = 2$, the total number of data streams should not exceed $\min(n_r, N_{u,p} n_t) = 4$ and N_s varies from 1 to 4 as detailed hereafter.

Case $N_s = 1$

The MU-MIMO uplink channel is equivalent to a 2×4 MIMO channel. The two transmitted data streams can be jointly encoded using a full diversity optimal space-time code such as the Golden code [89]. At the eNB, each of the two UE streams is decoded over each RE with an SINR

$$\gamma_k^{(m,n)} = 2^{\frac{1}{2} C_{\text{MIMO}}} - 1, \tag{6.7}$$

where

$$C_{\text{MIMO}} = \log_2 \left| \mathbf{I}_4 + \frac{1}{n_t} \frac{P^m_{k_{Tx}}}{\left(N_0 + I_{\text{inter}}\right)} \Lambda_k \mathbf{H}_k \mathbf{H}_k^{\dagger} \right|.$$

Case $N_s = 2$

As for $N_s = 1$ case, each UE transmits two data streams that can be jointly encoded using the Golden code to extract the full transmit diversity. At the eNB, the ZF equalizer $\mathbf{V}_k \in \mathbb{C}^{2\times 4}$ for UE k removes the multi-user interference and is followed by a ML decoder. The 4×1 received signal during $T = 2$ slots at the eNB is then,

$$\mathbf{y}_{\text{eNB}}^{[4\times T]} = \sqrt{\frac{P^m_{k_{Tx}}}{2} \Lambda_1}\, \mathbf{H}_1^{[4\times 2]} \mathbf{X}_1^{[2\times T]} + \sqrt{\frac{P^m_{k_{Tx}}}{2} \Lambda_2}\, \mathbf{H}_2^{[4\times 2]} \mathbf{X}_2^{[2\times T]} + (\mathbf{Z} + \mathbf{I})^{[4\times T]}$$

The decoder of UE 1 should satisfy:

$$\mathbf{V}_1^{\dagger} \subseteq \ker \left(\left[\begin{array}{c} \mathbf{H}_2^{\dagger[2\times 4]} \end{array} \right] \right)$$

Hence $\mathbf{V}_1$ has dimensions 2×4. The equivalent received signal is then,

$$y_{e,1}^{[2\times T]} = \mathbf{V}_1^{[2\times 4]}\mathbf{y}^{[4\times 1]} = \sqrt{\frac{P_{k_{Tx}}^m}{2}\Lambda_1}\,\mathbf{G}_1^{[2\times 2]}\mathbf{X}_1^{[2\times T]} + \mathbf{n}_1,$$

where $\mathbf{G}_1^{[2\times 2]} = \mathbf{V}_1^{[2\times 4]}\mathbf{H}_1^{[4\times 2]}$. This implies that the information of UE 1 can be decoded over a 2×2 MIMO system with full diversity and full rate coding scheme. Using the equivalent system model, it can be deduced that the MU-ZF decomposes the MU-MIMO into two parallel 2×2 SISO channels as shown in Figure 6.6.

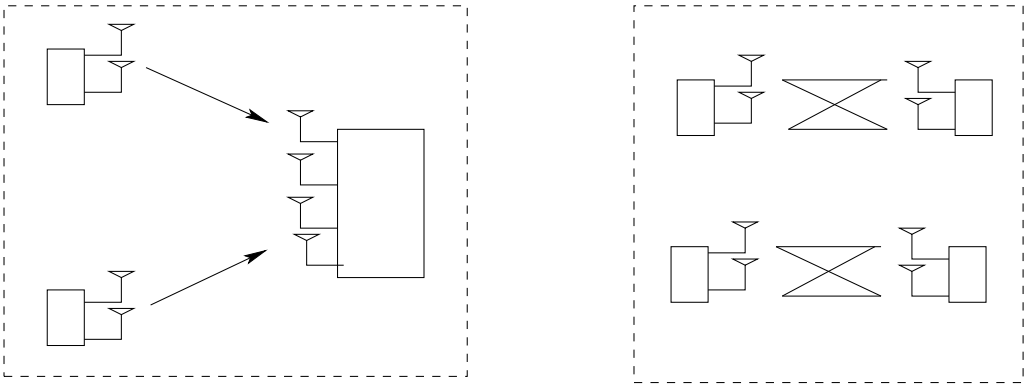

Figure 6.6: The linear ZF precoder decomposes the multi-user uplink MIMO channel into two parallel MIMO 2×2 channels that do not interfere.

Over each RE, the SINR obtained at the eNB after MU-ZF equalization is established for each data stream using (6.7) where

$$C_1^{\text{MIMO}} = \log_2 \det\left(\mathbf{I}_2 + \frac{P_{k_{Tx}}^m \Lambda_1}{2(N_0 + I_{inter})}\mathbf{G}_1\mathbf{G}_1^{\dagger}\right).$$

Case $N_s = 3$

The first UE transmits two data streams and the two others transmit only one each. For the first UE, the full transmit diversity can be obtained as previously via the Golden code. The two other UEs can also benefit from the full transmit diversity by using an optimal MISO space time coding scheme such as an Alamouti [92] or a DAST [93] code that encodes each UE's data over two consecutive time slots. The DAST code is more adapted as, at each time slot, it activates only one of the two transmit antennas, at the opposite of the Alamouti code that activates both antennas. This diagonal code structure makes the ZF equalization feasible for the three simultaneously transmitting UEs. The 4×1

received vector at the eNB during $T = 4$ time slots is,

$$\begin{aligned}\mathbf{y}_{\text{eNB}}^{[4\times T]} &= \sqrt{\frac{P_{k_{Tx}}^m}{2}\Lambda_1}\,\mathbf{H}_1^{[4\times 2]}\mathbf{X}_1^{[2\times T]} + \sqrt{P_{k_{Tx}}^m\Lambda_2}\,\mathbf{H}_2^{[4\times 2]}\mathbf{X}_2^{[2\times T]} \\ &\quad + \sqrt{P_{k_{Tx}}^m\Lambda_3}\,\mathbf{H}_3^{[4\times 2]}\mathbf{X}_3^{[2\times T]} + (\mathbf{Z}+\mathbf{I})^{[4\times T]}\end{aligned}$$

where $\mathbf{X}_1$ contains two imbricated Golden codes such that;

$$\mathbf{X}_1 = \frac{1}{\sqrt{5}}\begin{bmatrix} a_1 & b_1 & \sigma(c_1) & \sigma(d_1) \\ \iota c_1 & \iota d_1 & \sigma(a_1) & \sigma(b_1)\end{bmatrix}$$

$\mathbf{X}_2$ and $\mathbf{X}_3$ are DAST codes such that;

$$\mathbf{X}_2 = \frac{1}{\sqrt{5}}\begin{bmatrix} a_2 & 0 & b_2 & 0 \\ 0 & \sigma(a_2) & 0 & \sigma(b_2)\end{bmatrix}$$

and

$$\mathbf{X}_3 = \frac{1}{\sqrt{5}}\begin{bmatrix} a_3 & 0 & b_3 & 0 \\ 0 & \sigma(a_3) & 0 & \sigma(b_3)\end{bmatrix}.$$

In a similar way as the previous case, the DAST code permits to turn off one antenna at each time slot while still taking advantage of the MISO gain in term of diversity. In the first time slot, the decoder of the UE 1 information consists first to find the kernel $\mathbf{V}_{1:c1}$ of the space composed by the first columns of $\mathbf{H}_2$ and $\mathbf{H}_3$ which have 2×4 dimensions. The equivalent channel model at the first time slot is then,

$$\mathbf{y}_{e,1}^{[2\times 1]}(1) = \sqrt{\frac{P_{k_{Tx}}^m}{2}\Lambda_1}\mathbf{G}_1^{[2\times 2]}\mathbf{x}_{1:c1} + \mathbf{n}_1(1)$$

where $\mathbf{G}_{1:c1} = \mathbf{V}_{1:c1}^{[2\times 4]}\mathbf{H}_1^{[4\times 2]}$. The kernel space of the space composed by the second columns of $\mathbf{H}_2$ and $\mathbf{H}_3$ is denoted by $\mathbf{V}_{1:c2}^{[2\times 4]}$ in the following and the equivalent MIMO matrix $\mathbf{G}_{1:c2} = \mathbf{V}_{1:c2}^{[2\times 4]}\mathbf{H}_1^{[4\times 2]}$.

The same procedure can be repeated to time slot 2, 3 and 4. This gives:

$$\mathbf{y}_{e,1}^{[2\times 1]}(1) = \sqrt{\frac{P_{k_{Tx}}^m}{2}\Lambda_1}\mathbf{G}_{1:c1}^{[2\times 2]}\mathbf{x}_{1:c1}^{[2\times 1]} + \mathbf{n}_1(1) \tag{6.8}$$

$$\mathbf{y}_{e,1}^{[2\times 1]}(2) = \sqrt{\frac{P_{k_{Tx}}^m}{2}\Lambda_1}\mathbf{G}_{1:c2}^{[2\times 2]}\mathbf{x}_{1:c2}^{[2\times 1]} + \mathbf{n}_1(2) \tag{6.9}$$

$$\mathbf{y}_{e,1}^{[2\times 1]}(3) = \sqrt{\frac{P_{k_{Tx}}^m}{2}\Lambda_1}\mathbf{G}_{1:c1}^{[2\times 2]}\mathbf{x}_{1:c3}^{[2\times 1]} + \mathbf{n}_1(3) \tag{6.10}$$

$$\mathbf{y}_{e,1}^{[2\times 1]}(4) = \sqrt{\frac{P_{k_{Tx}}^m}{2}\Lambda_1}\mathbf{G}_{1:c2}^{[2\times 2]}\mathbf{x}_{1:c4}^{[2\times 1]} + \mathbf{n}_1(4) \tag{6.11}$$

The first Golden code can be formed from slots 1 and 3 in (6.8) and (6.10), the second from (6.9) and (6.11). This implies that the information of UE 1 can be decoded over a 2×2 MIMO system with

full diversity and full rate coding scheme. The capacity of the 2×2 MIMO system is

$$C_1^{(m,n)} = \frac{1}{2}\sum_{i=1}^{2} \log_2 \det \left(\mathbf{I}_2 + \frac{P_{k_{Tx}}^m \Lambda_1}{2(N_0 + I_{inter})} \mathbf{G}_{1:ci} \mathbf{G}_{1:ci}^{\dagger} \right)$$

The SINR over each RE required to decode each data stream is then,

$$\gamma_1^{(m,n)} = 2^{\frac{1}{2}C_1^{(m,n)}} - 1$$

For UE 2 and UE 3, the decoder $\mathbf{V}_2$ and $\mathbf{V}_3$ are the same as in the previous case. By repeating similar steps, it can be deduced that the information of UE 2 and UE 3 can be respectively decoded on an equivalent two parallel SISO channel with diversity equal to 2 and a multiplexing gain of 1. The capacity of this parallel channel is,

$$C_{\text{MISO}} = \frac{1}{2}\left(\log_2 \left(1 + \frac{P_{k_{Tx}}^m \Lambda_1}{N_0 + I_{inter}} |g_2(1)|^2 \right) + \log_2 \left(1 + \frac{P_{k_{Tx}}^m \Lambda_1}{N_0 + I_{inter}} |g_2(2)|^2 \right) \right).$$

The SINR over the RE is,

$$\gamma_2^{(m,n)} = 2^{C_{\text{MISO}}} - 1.$$

Using the equivalent channel model, we can deduce that the MU-ZF decomposes the channel into two parallel MISO 2×1 channels and one 2×2 MIMO channel as shown in Figure 6.7.

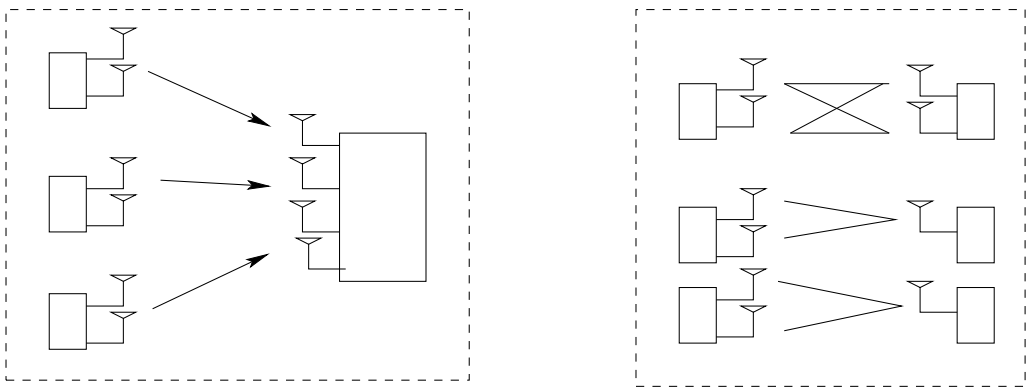

Figure 6.7: The linear ZF precoder decomposes the multi-user uplink MIMO channel into two parallel MISO 2×1 channels and one 2×2 MIMO channel that do not interfere.

Case $N_s = 4$

Only one stream is transmitted by each UE. As in the previous case of $N_s = 3$, the full transmit diversity can be also achieved here using the previously defined DAST coding scheme. The 4×1

received vector at the eNB is then,

$$\begin{aligned}\mathbf{y}_{\text{eNB}}^{[4\times T]} &= \sqrt{P_{k_{Tx}}^{m}\Lambda_1}\,\mathbf{H}_1^{[4\times 2]}\mathbf{X}_1^{[2\times T]} + \sqrt{P_{k_{Tx}}^{m}\Lambda_2}\,\mathbf{H}_2^{[4\times 2]}\mathbf{X}_2^{[2\times T]} \\ &\quad + \sqrt{P_{k_{Tx}}^{m}\Lambda_3}\,\mathbf{H}_3^{[4\times 2]}\mathbf{X}_3^{[2\times T]} + \sqrt{P_{k_{Tx}}^{m}\Lambda_4}\,\mathbf{H}_4^{[4\times 2]}\mathbf{X}_4^{[2\times T]} + (\mathbf{Z}+\mathbf{I})^{[4\times T]}\end{aligned}$$

In order to decode the information submitted by UE 1, the received signal should be projected on the orthonormal space $\mathbf{V}_1$ that is simultaneously orthogonal to $\mathbf{H}_2, \mathbf{H}_3$ and $\mathbf{H}_4$. This means that:

$$\mathbf{V}_1^{\dagger} \subseteq \ker\Big(\begin{bmatrix}\mathbf{H}_2^{\dagger[2\times 4]} \\ \mathbf{H}_3^{\dagger[2\times 4]} \\ \mathbf{H}_4^{\dagger[2\times 4]}\end{bmatrix}\Big).$$

Without DAST coding, the only possible solution is the zero matrix as the dimensionality of the kernel space is $\min(4-3\times 2;0)=0$. When using a DAST code, the received signal at the first time slot is:

$$\begin{aligned}\mathbf{y}^{[4\times 1]}(1) &= \sqrt{P_{k_{Tx}}^{m}\Lambda_1}\,\mathbf{H}_1^{[4\times 2]}\begin{bmatrix}x_1\\0\end{bmatrix} + \sqrt{P_{k_{Tx}}^{m}\Lambda_2}\,\mathbf{H}_2^{[4\times 2]}\begin{bmatrix}x_2\\0\end{bmatrix} \\ &\quad + \sqrt{P_{k_{Tx}}^{m}\Lambda_3}\,\mathbf{H}_3^{[4\times 2]}\begin{bmatrix}x_3\\0\end{bmatrix} + \sqrt{P_{k_{Tx}}^{m}\Lambda_4}\,\mathbf{H}_4^{[4\times 2]}\begin{bmatrix}x_4\\0\end{bmatrix} + (\mathbf{Z} \\ &\quad +\mathbf{I})_{1:c1}^{[4\times 1]}\end{aligned} \tag{6.12}$$

It can be easily seen from (6.12), that the 4×1 received signal at the eNB comes only from the first antenna of each UE. The first column of each 4×2 matrix $\mathbf{H}_i$, which we denote in the following by $\mathbf{h}_{i:c1}$, contributes to the received signal. The equivalent model can be then written as:

$$\begin{aligned}\mathbf{y}_1^{[4\times 1]}(1) &= \sqrt{P_{k_{Tx}}^{m}\Lambda_1}\,\mathbf{h}_{1:c1}^{[4\times 1]}x_1 + \sqrt{P_{k_{Tx}}^{m}\Lambda_2}\,\mathbf{h}_{2:c1}^{[4\times 1]}x_2 \\ &\quad + \sqrt{P_{k_{Tx}}^{m}\Lambda_3}\,\mathbf{h}_{3:c1}^{[4\times 1]}x_3 + \sqrt{P_{k_{Tx}}^{m}\Lambda_4}\,\mathbf{h}_{4:c1}^{[4\times 1]}x_4 + (\mathbf{Z}+\mathbf{I})_{1:c1}^{[4\times 1]}\end{aligned} \tag{6.13}$$

The channel models in (6.13) is equivalent to the one in (6.5). The same procedure can be used to separate UEs information. For example, to find x_1 of UE 1 we need to project the received signal $\mathbf{y}$ on the Kernel $\mathbf{v}_{1:c1}^{[1\times 4]}$ of the space that contains the first columns of each matrix $\mathbf{H}_i$ with $i=2,3,4$. Finally, the projection of $\mathbf{y}(1)$ on $\mathbf{v}_{1:c1}$ gives:

$$\mathbf{y}_{e,1}(1) = \sqrt{P_{k_{Tx}}^{m}\Lambda_1}\,g_1(1)x_1 + n_1(1) \tag{6.14}$$

where $g_1(1) = \mathbf{v}_{1:c1}^{[1\times 4]}\mathbf{h}_{1:c1}^{[4\times 1]}$.

The received signal at the second time slot is:

$$\begin{aligned}\mathbf{y}^{[4\times1]}(2) &= \sqrt{P^m_{k_{Tx}}\Lambda_1}\,\mathbf{H}_1^{[4\times2]}\begin{bmatrix}0\\ \sigma(x_1)\end{bmatrix}+\sqrt{P^m_{k_{Tx}}\Lambda_2}\,\mathbf{H}_2^{[4\times2]}\begin{bmatrix}0\\ \sigma(x_2)\end{bmatrix}\\ &+\sqrt{P^m_{k_{Tx}}\Lambda_3}\,\mathbf{H}_3^{[4\times2]}\begin{bmatrix}0\\ \sigma(x_3)\end{bmatrix}+\sqrt{P^m_{k_{Tx}}\Lambda_4}\,\mathbf{H}_4^{[4\times2]}\begin{bmatrix}0\\ \sigma(x_4)\end{bmatrix}\\ &+(\mathbf{Z}+\mathbf{I})^{[4\times1]}_{1:c2}\end{aligned} \tag{6.15}$$

Similarly, it can be seen from (6.15), that the 4×1 received signal at the eNB comes only from the second antenna of each UE. The second column of each 4×2 matrix $\mathbf{H}_i$, which we denote in the following by $\mathbf{h}_{i:c2}$ contributes to the received signal. The equivalent model can be then written as:

$$\begin{aligned}\mathbf{y}^{[4\times1]}(2) &= \sqrt{P^m_{k_{Tx}}\Lambda_1}\,\mathbf{h}^{[4\times1]}_{1:c2}\sigma(x_1)+\sqrt{P^m_{k_{Tx}}\Lambda_2}\,\mathbf{h}^{[4\times1]}_{2:c2}\sigma(x_2)\\ &+\sqrt{P^m_{k_{Tx}}\Lambda_3}\,\mathbf{h}^{[4\times1]}_{3:c2}\sigma(x_3)+\sqrt{P^m_{k_{Tx}}\Lambda_4}\,\mathbf{h}^{[4\times1]}_{4:c2}\sigma(x_4)+(\mathbf{Z}+\mathbf{I})^{[4\times1]}_{1:c2}\end{aligned} \tag{6.16}$$

Similarly, the channel model in (6.16) is equivalent to the one in (6.5). The same procedure can be used to separate UEs information. To find $\sigma(x_1)$ of UE 1 we need to project the received signal $\mathbf{y}$ on the Kernel $\mathbf{v}^{[1\times4]}_{1:c2}$ of the space that contains the second columns of each matrix $\mathbf{H}_i$ with $i=2,3,4$. Finally, the projection of $\mathbf{y}(2)$ on $\mathbf{v}_{1:c2}$ gives:

$$\mathbf{y}_{e,1}(2)=\sqrt{P^m_{k_{Tx}}\Lambda_1}\,g_1(2)\sigma(x_1)+n_1(2) \tag{6.17}$$

where $g_1(2)=\mathbf{v}^{[1\times4]}_{1:c2}\mathbf{h}^{[4\times1]}_{1:c2}$.

From (6.14) and (6.17) and using the fact that $g_1(1)$ and $g_1(2)$ are Gaussian variable such that $\mathbb{E}\left[g_1(1)g_1(2)\right]=\mathbb{E}\left[\mathbf{v}_{1:c1}\mathbf{h}_{1:c1}\mathbf{h}^{\dagger}_{1:c2}\mathbf{v}^{\dagger}_{1:c2}\right]=0$, it can be deduced that the information of UE 1 can be decoded over a set of two parallel independent channels, which is equivalent in term of its error probability to a 2×1 MISO system. The capacity of 2 parallel SISO channel is,

$$C_{\text{MISO}}=\frac{1}{2}\left(\log_2\left(1+\frac{P^m_{k_{Tx}}\Lambda_1}{N_0+I_{inter}}|g_1(1)|^2\right)+\log_2\left(1+\frac{P^m_{k_{Tx}}\Lambda_1}{N_0+I_{inter}}|g_1(2)|^2\right)\right).$$

The SINR over the RE is,

$$\gamma_1^{(m,n)}=2^{C_{\text{MISO}}}-1.$$

Using the equivalent channel model, we can deduce that the MU-ZF decomposes the channel into four parallel MISO 2×1 channels in Figure 6.8.

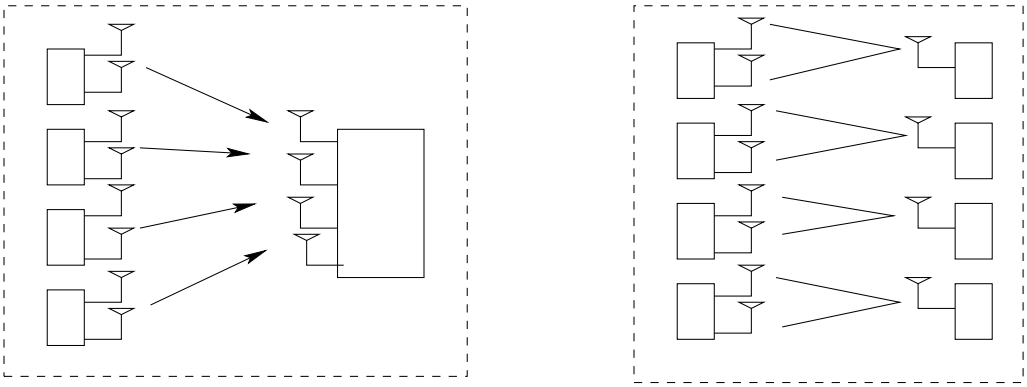

Figure 6.8: The linear ZF precoder decomposes the multi-user uplink MIMO channel into four parallel MISO 1×2 channels that do not interfere. The transmit diversity is equal to 2: Virtual MISO.

6.4 RB Allocation in the Uplink of Multi-User MIMO LTE Networks

Based on the above transceiver structure, we present different strategies for multi-user allocation over one single RB. Then, we show how it can be extended to the whole LTE bandwidth under the SC-FDMA constraints. We note that these RB allocation strategies are independent of the transceiver.

6.4.1 Multi-user allocation strategies over one RB

As stated in Section 6.3, over each RB, a maximal number of $1 \leq N_s \leq 4$ UEs can be selected to simultaneously transmit. For a given RB, different strategies can be used to select these N_s UEs among a total number $N_{u,p}$ of potential UEs, as detailed in the following:

One RB random allocation

The random pairing strategy selects a maximal number $N_s = \min(n_r, N_{u,p})$ of randomly chosen UEs, to simultaneously transmit, independently of the wireless channel propagation conditions.

One RB opportunistic allocation with maximal metric

All the potential UEs are sorted according to their CQI defined by their effective SINR received at the eNB when each UE is assumed to be the only transmitting UE. The eNB scheduler selects then N_s UEs that are adequately chosen among the best CQI UEs in order to maximize a predefined metric ($\mathcal{M}_{\text{rate}}$ or $\mathcal{M}_{\text{UE}}$). The metric $\mathcal{M}_{\text{rate}}$ aims at maximizing the RB capacity: the scheduler chooses among the $\min(n_r, N_{u,p})$ best CQI UEs, $N_s \leq \min(n_r, N_{u,p})$ UEs having the maximal aggregate throughput. The metric $\mathcal{M}_{\text{UE}}$ aims at maximizing the number of simultaneously transmitting UEs per RB: the scheduler chooses, the maximal number $\min(n_r, N_{u,p})$ of best CQI UEs independently of their aggregate throughput.

One RB opportunistic allocation with maximal orthogonality

All the potential UEs are also sorted here in function of their CQI. The maximal orthogonal (Orth) strategy searches, among a predefined number of best CQI UEs, the set $\mathcal{A}$ of semi-orthogonal UEs. The semi-orthogonality is defined with respect to a threshold angle between fading vectors for $n_t = 1$ and a threshold chordal distance between the fading matrices for $n_t = 2$ [94]. This semi-orthogonality is studied for fading vectors or matrices corresponding to the fading coefficients on the 6^{th} subcarrier of the considered RB. This assumption holds since the coherence bandwidth is much larger than the RB bandwidth and the values of the correlated frequency fading coefficients do not change significantly within one RB from its center to its extremities. Then, the scheduler selects, for simultaneous transmission, the N_s UEs within $\mathcal{A}$, that maximize $\mathcal{M}_{\text{rate}}$ or $\mathcal{M}_{\text{UE}}$.

6.4.2 Extension to the whole LTE bandwidth

We extend here the one RB multi-user allocation strategies to the whole LTE bandwidth, with respect to the localized SC-FDMA constraints.

Random matching scheduling (RMS) algorithm

The Random Matching Scheduling (RMS) extends the one RB random allocation strategy to the whole LTE bandwidth. First, the number of RBs allocated per UE: $N_{\text{RB},u}$, is computed depending on the total number N_{UE} of UEs in the cell,

$$N_{\text{RB},u} = \min\left(\left\lceil \frac{n_r \times N_{\text{RB}}}{N_{UE}} \right\rceil, 1\right).$$

Then, the RBs are allocated in the ascending order by choosing, every $N_{\text{RB},u}$ RBs, N_s new randomly selected UEs.

Central opportunistic scheduling (COS) algorithm

The Central Opportunistic Scheduling (COS) algorithm extends the one RB opportunistic allocation to the whole LTE bandwidth. It recursively selects a central (UE, RB) pair. The first pair corresponds to the (UE, RB) pair that maximizes the CQI over all the UEs and RBs. For this central RB, N_s UEs are selected according to one of the pre-defined metrics. Then, the COS algorithm extends the allocation to the adjacent RBs while the central UE remains among the N_s selected UEs. If this condition is not satisfied, the algorithm searches for a new central (RB, UE) pair that maximizes the CQI over all the other remaining potential UEs and the non allocated RBs. The procedure is repeated until no more RBs or UEs are available. The main steps of this algorithm are summarized in Algorithm 7. An individual Rate Increase (RI) condition similar to the OEA algorithm can be added to the COS. It consists in checking that the new allocated adjacent RB increases the individual rate of each UE. In this case, a search for a new central (RB, UE) pair will be activated as soon as the

Algorithm 7 Central opportunistic scheduling-COS algorithm

1: Select a first central (RB, UE) pair with a maximum CQI.
2: **repeat**
3: Select N_s UEs for this central RB according to one of the pre-defined metrics.
4: **while** the central UE is among the N_s selected UEs on the adjacent RB **do**
5: Extend the allocation to the adjacent RBs
6: **end while**.
7: Search for a new central (RB, UE) pair with a maximum CQI.
8: **until** no more RBs or UEs are available.

individual throughput increase (RI) condition is not satisfied by the central UE. For the other UEs, the scheduler allocates this RB only to the UEs satisfying this RI condition.

6.5 Performance evaluation

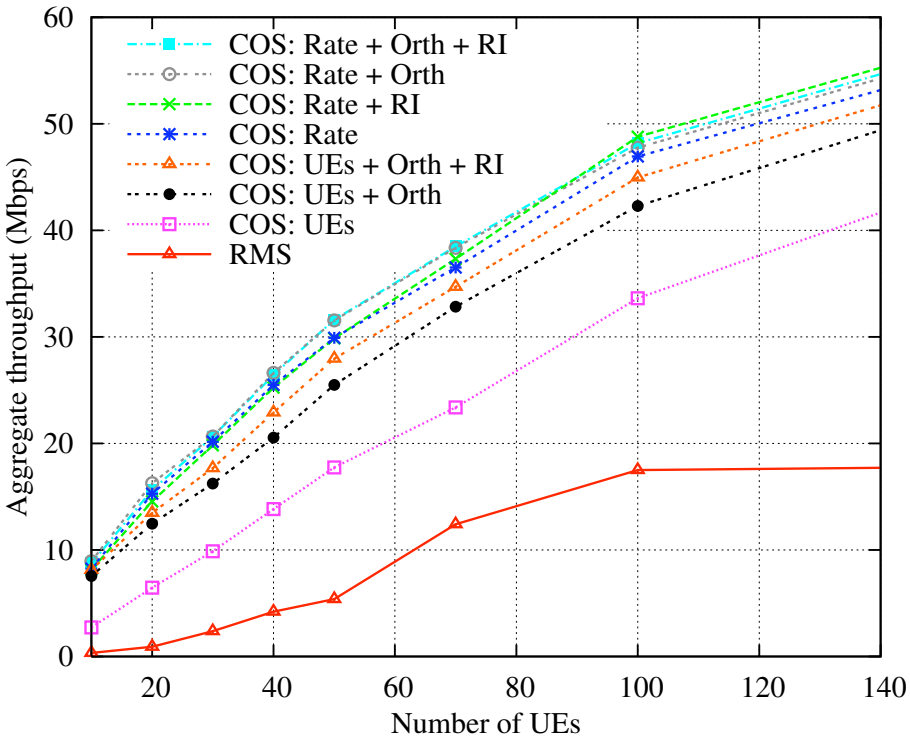

Figure 6.9: Aggregate throughput in the cell for RMS and COS algorithms using the combined multi-user ZF-ML decoder with $n_t = 1$

In this section, we compare the performances of these algorithms in a regular network. Each sector is allocated a 5 MHz bandwidth. The inter-cell interference is estimated considering a highly loaded network where each RB of the interfering cell is shared by four simultaneously transmitting UEs. Simulations show that $\mathbf{i}_{\text{inter}}$ can be generated by a Gaussian distribution with mean value $I_{\text{inter}} = -124$ dBW and standard deviation 0.9 dB.

For RMS and COS algorithms using the combined ZF-ML decoder with $n_t = 1$, Figure 6.9 and 6.10 illustrate the performances of respectively $\mathcal{M}_{\text{rate}}$ and $\mathcal{M}_{\text{UE}}$ (referred as Rate and UE in the figures) by giving respectively the aggregate throughput and the percentage of served UEs in the cell. The impact of the additional optional constraints: Orthogonality (Orth) and/or rate increase (RI), is also depicted.

As expected for Figure 6.9, the $\mathcal{M}_{\text{rate}}$ metric leads to higher capacity than the $\mathcal{M}_{UE}$ metric. However, the gap between $\mathcal{M}_{\text{UE}}$ and $\mathcal{M}_{\text{rate}}$ set of curves can be significantly reduced when adopting the Orth constraint and, to a lesser extent, the RI constraint. The RMS algorithm becomes rate-limited when the number of UEs in the cell exceeds $n_r \times N_{\text{RB}}$, as beyond this limit only one RB is allocated to each randomly chosen UE.

Figure 6.10 shows the limit of $\mathcal{M}_{\text{UE}}$ in COS algorithms without Orth and RI constraints. Actually, $\mathcal{M}_{\text{UE}}$ selects the four best CQI UEs for the best RB. Then, as the fading coefficients are correlated from one RB to its neighbors, it is more probable that the 4 selected UEs will remain the best CQI UEs on a consequent number of contiguous RBs if no additional constraint is imposed. This explains the relatively bad fairness among UEs when Orth and RI constraints are not considered. We note that the COS algorithm which associates $\mathcal{M}_{\text{UE}}$, Orth and RI constraints presents a good tradeoff between fairness and aggregate throughput.

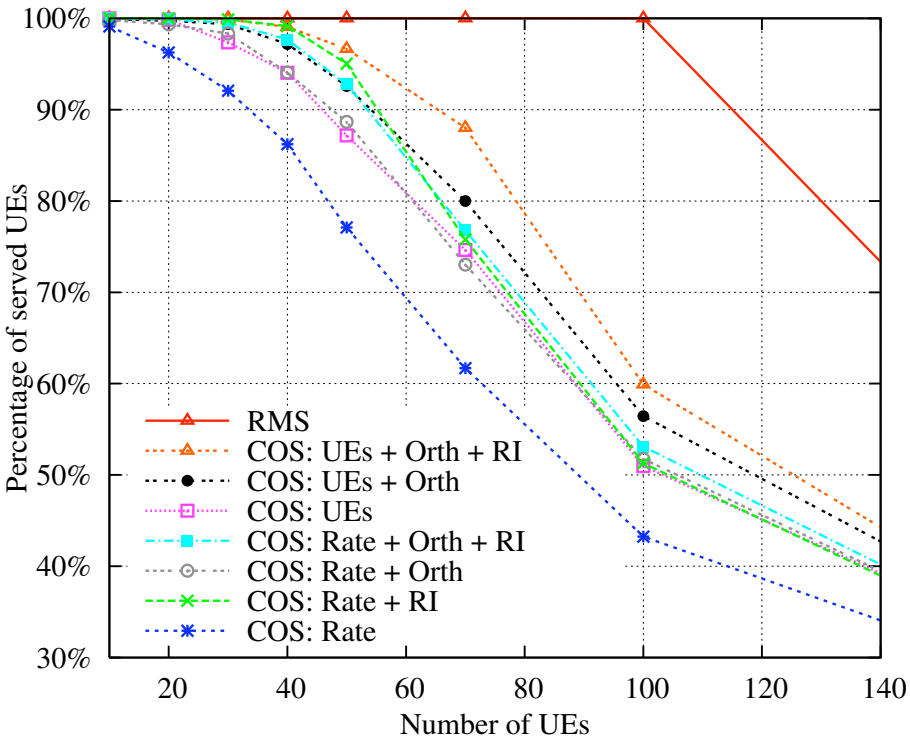

Figure 6.10: Percentage of served UEs in the cell for RMS and COS algorithms using the combined multi-user ZF-ML decoder with $n_t = 1$

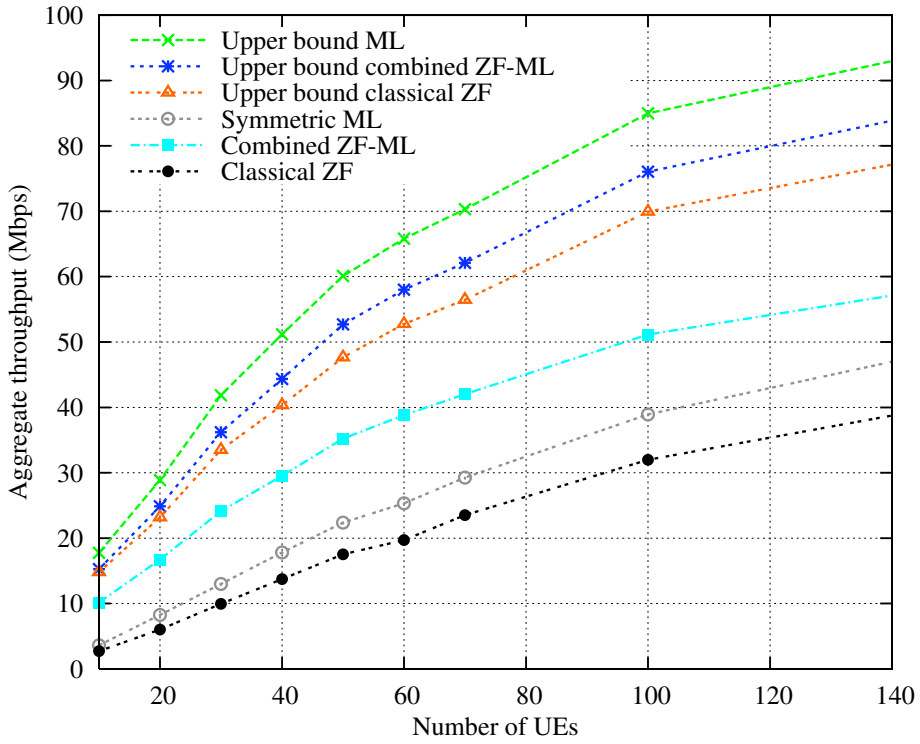

Figure 6.11: Comparison of the combined ZF-ML decoder, the classical ZF decoder and the symmetric ML decoder for $n_t = 2$

The rate performance of the combined ZF-ML decoder, the classical ZF decoder and the symmetric ML are compared in Figure 6.11 for $n_t = 2$ and using $\mathcal{M}_{\text{rate}}$ metric with Orth and RI constraints. The upper bound of each decoder is obtained when no MCS constraint is considered, and underlines the theoretical good performances of ML decoder towards the other decoders. In the LTE context, the ML decoder attributes the corresponding MCS to each UE by searching for a feasible $\mathcal{J}$-tuple of rate in the uplink MU-MIMO capacity region defined in (2.15). To limit this search complexity, we assume a symmetric ML decoder for which, at each RB, all the UEs have the same MCS. Consequently, at each RB, the N_s selected UEs should adjust their individual throughputs to the minimal one imposed by the capacity region.

The classical ZF decodes independently the two data streams of one single UE and attributes to this UE the minimal MCS of both data streams. Hence, the total rate provided by this decoder, in Figure 6.11, is 40% lower than the one of combined ZF-ML.

Finally, as seen from Figure 6.9 and 6.11, a second antenna transmitter per UE increases the aggregate throughput, but at the expense of the number of served UEs.

6.6 Conclusion

In this chapter, we proposed a robust transceiver for multi-user MIMO scheduling in the uplink of LTE networks. This transceiver is based on the use of an adequate space time encoder at the UE and a combined multi-user ZF-ML decoder at the eNB. The rate performances of this transceiver were evaluated in a LTE context when using a proposed central opportunistic scheduling (COS) algorithm. We showed that a tradeoff between the number of served UEs and the cell total throughput is provided when the COS maximizes the number of orthogonal served UEs per RB, conditioned by their individual throughput increase. Finally, as a consequence of the LTE MCS constraint, the combined ZF-ML decoder rate outperformed the symmetric ML and classical ZF decoders rates.

Conclusion and Perspectives

THIS thesis has studied a distributed radio resource management in the uplink of green LTE networks, aiming to allocate radio resources to users with respect to their QoS requirements in order to maximize the networks capacity. For this purpose, a channel dependent radio resource allocation scheme was adopted.

A new ICI estimation model adapted to the UE power control process was first elaborated to estimate the ICI level received at a given eNB from interfering UEs located in the neighboring sectors and that are transmitting on the same RB. We showed that the ICI level generated by a virtual UE located at the barycenter of the active user's interfering sector and radiating at a median power of the UEs transmission power gives a good estimation of the statistical ICI level. This model was validated by numerical results using the statistical log ratio and Kullback-Leibler tests, and analytically where an analytical expression of the median and mean of the UEs transmission power was derived. Then, we considered the radio resource dimensioning problem within one cell to determine, with respect to its radio channel conditions, the average number of RBs required by a UE to achieve a given QoS. If the total number of RBs in the network was not sufficient to satisfy the UE's QoS, UE was classified in outage. For dimensioning stress, an analytical model of the dimensioning outage probability upper bound was proposed. This dimensioning outage probability was established according to the networks configuration, by considering a statistical behavior of UEs and the offered QoS. An upper-bound on the dimensioning outage probability upper bound was developed, considering the RRM strategies, for single and multiple user's QoS class in SISO systems and for diversity and multiplexing gain in MIMO systems. Fair and opportunistic RB allocation algorithms were considered. A comparison with the realistic dimensioning outage probability obtained from Monte Carlo simulations was given and the model validation was proved using the statistical log ratio test. From these results an adequate bandwidth was allocated to the cells. With carrier aggregation technique, a small additional LTE bandwidth was used as a carrier component to decrease the dimensioning outage probability.

Finally, the management of the limited radio resource was investigated. We proposed a new radio resource allocation scheme (referred as OEA in this thesis) that allocates efficiently the RBs to UEs while minimizing the UEs power consumption. The proposed RB allocation algorithm was developed in the context of LTE release 8 and hence it respects the SC-FDMA constraints. This algorithm was also adapted to the uplink of LTE-A networks where the OFDMA technique is adopted. In both cases, the achieved aggregate throughput obtained with the OEA algorithm is close to the one

achieved by the optimal RB allocation algorithm. However, the complexity of the OEA algorithm has low computational complexity compared to other well known RB allocation algorithms in literature. Furthermore, this algorithm minimizes the RB wastage and increases UEs energy efficiency thanks to the power control and the individual throughput increase constraint applied for RB expansion allocation. The resulting saved UE transmission power increases the UE battery life and generates less inter-cell interference. An extension of the radio resource allocation scheme to MU-MIMO systems was also investigated, using a new transceiver that combined ZF and ML decoders.

The proposed methods and algorithms proposed in this thesis should be complemented by additional studies. We hereunder provide first steps insights into open issues that have not been addressed in the thesis, and that could be studied in a future work:

- The ICI estimation model was proposed for green LTE network when a single RB is allocated to each UE. Since in SC-FDMA technique, the UE transmission power is equally shared over the allocated RBs, the median power of the virtual point should consider the UE average transmission power per RB, by considering the number of RBs allocated to each UE, in a multiple RB allocation case.
- In the framework of LTE networks dimensioning, the dimensioning outage probability upper bound developed for diversity and multiplexing gain of MIMO systems, when an opportunistic RB allocation algorithm is used, considers a pessimist policy by dimensioning over the path that requires the highest number of RBs. For further improvement, the real UE required number of RBs should be computed, by considering the channel condition of each antenna independently. For this purpose, successive interference cancellation methods can be used to evaluate the UEs required number of RBs that satisfies their QoS without wasting RBs.
- The results obtained with the OEA and QoS based OEA algorithm were close to the optimal one. Their low computational complexity proves the LTE hardware implementation. Using these algorithms in cooperative networks can improve the network's coverage and manage the ICI by allocating the unused RBs to users that are in outage in the neighboring cells or generating a high ICI level. The complexity of applying these algorithms in cooperative networks, and the overhead exchange between the eNBs should be evaluated.
- The study given in MU-MIMO systems should consider the power control process applied in green LTE networks and the transceiver structure should be adapted to reduce the total consumed power especially when multiple radio resources are allocated to a single UE.

Appendix A

Correlated fast fading

Assume $h(t,\tau)$ the time varying channel response at a Dirac impulse and $\mathbb{H}$ the linear operator that describe the channel. The wireless fast fading can be characterized by two function. The first is the delay-Doppler spreading function $S_{\mathbb{H}}(\nu,\tau)$ defined as Fourier transform $(t \to \nu)$ of $h(t,\tau)$, where ν denote the Doppler spread caused by the movement of the transmitters, receivers and scatterers generated as detailed in section A.1. The second is the time varying transfert function $L_{\mathbb{H}}(t,f)$ defined as a Fourier transform $(\tau \to f)$ of $h(h(t,\tau))$. The relatonship between these system function is given by,

$$L_{\mathbb{H}}(t,f) = \int_{\tau} h(t,\tau)e^{-j2\pi f\tau}d\tau, \tag{A.1}$$

$$S_{\mathbb{H}}(\nu,\tau) = \int_{\nu} h(t,\tau)e^{-j2\pi\nu t}dt, \tag{A.2}$$

$$L_{\mathbb{H}}(t,f) = \int_{\tau}\int_{\nu} S_{\mathbb{H}}(\nu,\tau)e^{j2\pi(\nu t-\tau f)}d\nu d\tau. \tag{A.3}$$

and is summarized in Figure A.1.

A.1 Generating a frequency correlated Rayleigh fading

This method generate only frequency correlated fast fading coefficients. Since different paths are of different lengths, a single impulse sent from the transmitter will result in multiple copies being received at different times.
The effects of scatterers in discrete delay ranges are grouped together into individual "taps" with the same delay; each tap represents a single beam. Each taps has a gain which varies in time according

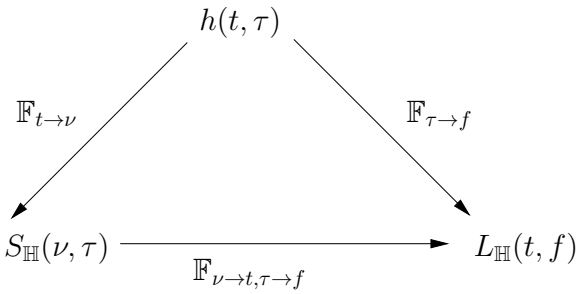

Figure A.1: Relationship between the channel transfer function [1].

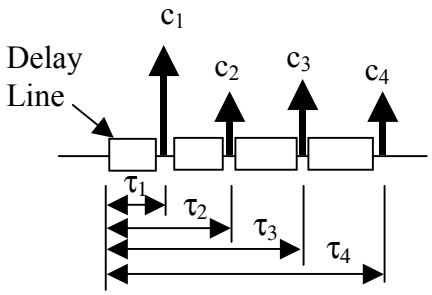

Figure A.2: Tapped Delay Line Model

to the standard narrowband channel statistics. The taps are usually assumed to be uncorrelated from each other. Therefore, the channel is modeled as a linear filter with a time-variant finite impulse response as follows:

$$h(t,\tau) = \sum_{i=1}^{N} c_i(t)\delta(\tau - \tau_i) \tag{A.4}$$

This model represents the channel by a delay line with N taps (figure A.2). The mean relative powers of the taps are specified by the power delay profile (PDP) for the channel, defined as the variation of mean power in the channel with delay,

$$P(\tau) = \frac{\mathbb{E}[\mid h(t,\tau \mid^2]}{2} \tag{A.5}$$

If we look at the Fourier transform of the power delay profile, we can obtain the frequency dependence of the channel characteristics. The frequency bandwidth for which the channel characteristics remain similar is called coherence bandwidth. A useful approximation to the coherence time for the classical channel is then:

$$T_c = \frac{9}{16\pi\nu}, \qquad \text{for 0.5 factor of correlation} \tag{A.6}$$

ν represent the Doppler spread [1] and its value is twice the maximum Doppler shift f_D:

$$\nu = 2 \times f_D \tag{A.7}$$

and f_D is calculated as :

$$f_D = \frac{f \times v \cos\theta}{c} \qquad \text{set } \theta = 0 \text{ for the maximum Doppler spread} \tag{A.8}$$

where v is the mobile velocity, θ is the angle that antenna LOS or incident wave makes with user's direction of movement and c is the speed of light. Thus, if the transmitter, receiver, or the intermediate objects move very fast, the Doppler spread is large and the coherence time is small, i.e., the channel changes fast.

A.2 Generating a time-frequency correlated Rayleigh fading

Usually, the Linear Varying Time (LVT) channel model is studied under the Wide Sense Stationary and Uncorrelated Scattering (WSSUS) assumption. This property assume that the channel is wide sense stationary in time and uncorrelated in delay (τ). It implies that the time varying-transfert function $L_{\mathbb{H}}(t, f)$ is wide-sense stationary in both time and frequency, and the spreading function $S_{\mathbb{H}}(\nu, \tau)$ is uncorrelated in delay τ and in Doppler ν,

$$\mathbb{E}[L_{\mathbb{H}}(t, f)L^*_{\mathbb{H}}(t', f')] = R_{\mathbb{H}}(t - t', f - f'), \tag{A.9}$$

$$\mathbb{E}[S_{\mathbb{H}}(\nu, \tau)S^*_{\mathbb{H}}(\nu', \tau')] = C_{\mathbb{H}}(\nu, \tau)\delta(\tau - \tau')\delta(\nu - \nu'). \tag{A.10}$$

The function $R_{\mathbb{H}}(t, f)$ is referred to as the channel time-frequency correlation function, and $C_{\mathbb{H}}(\nu, \tau)$ the scattering function. These two function are related by the 2-D Fourier transform, such that,

$$R_{\mathbb{H}}(\Delta t, \Delta f) = \int_\tau \int_\nu C_{\mathbb{H}}(\nu, \tau) e^{j2\pi\nu\Delta t} e^{-j2\pi\tau\Delta f} d\tau d\nu. \tag{A.11}$$

[1] The power delay profile gives the statistical power distribution of the channel over time for a signal transmitted for just an instant. Similarly, Doppler power spectrum gives the statistical power distribution of the channel for a signal transmitted at just one frequency f. The Doppler power spectrum is non-zero for $(f - \nu, f + \nu)$, where ν is the maximum Doppler spread or Doppler spread

Appendix B

Gaussian distribution of the coefficients

We review here the main properties of the Gaussian distribution of the fading coefficients used in this thesis.

B.1 Complex Gaussian Variable

Let X be a complex Gaussian variable $X \sim \mathcal{CN}(0, \sigma)$ with mean equal to 0 and variance σ. The probability distribution function (pdf) of X is such that,

$$p_X(x) = \frac{1}{\sqrt{2\pi\sigma^2}} e^{-\frac{|x|^2}{2\sigma^2}}.$$

Let $\rho = |x|$ be the absolute value of the complex Gaussian variable X and θ be its argument such that $X = \rho e^{j\theta}$. Let $u = \rho^2$, then u follows an exponential distribution such that:

$$p_U(u) = e^{-u},$$

and θ is uniformly distributed such that:

$$p_\theta(\theta) = \frac{1}{2\pi}.$$

B.2 Gaussian complex vectors

Let $\mathbf{x}$ be a vectors with n complex Gaussian and identically and independently distributed (i.i.d) components $X_1, \ldots, X_n \sim \mathcal{CN}(0, \sigma)$, such that:

$$\mathbf{x} = \begin{pmatrix} X_1 \\ X_2 \\ \vdots \\ X_n \end{pmatrix}.$$

The joint distribution of $(X_1, \ldots, X_n)$ is such,

$$p_X(x) = p_{(X_1,\ldots,X_n)}(x_1, \ldots, x_n) = \prod_{i=1}^{n} p_{X_i}(x_i) = \frac{1}{(\sqrt{2\pi\sigma^2})^n} e^{-\frac{|x_1|^2+\ldots+|x_n|^2}{2\sigma^2}}.$$

Define ρ the norm of the vector $\mathbf{x}$ such that $\rho = \|\mathbf{x}\|$ and $u = \rho^2$. Then, $u = |x_1|^2 + \ldots + |x_n|^2$ follows a chi-sqaure distribution with $2n$ degrees of freedom such that:

$$p_U(u) = \frac{1}{2^n(n-1)!} x^{(n-1)} e^{-\frac{x}{2}}$$

Let $\mathbf{R}$ be a $m \times n$ unitary matrix ($m \leq n$)such that $\mathbf{R}\mathbf{R}^\dagger = \mathbf{I}_m$, then $\mathbf{R}\mathbf{x}$ is also a Gaussian variable with m i.i.d. complex Gaussian components.

B.3 Complex Gaussian Matrix

Let $\mathbf{H} \in \mathbb{C}^{n_r \times n_t}$ a complex matrix having components that follow a Gaussian distribution. Let $p = \min(n_t, n_r)$ be the rank of this matrix. Then the joint distribution of the $p = \min(n_t, n_r)$ non zero ordered eigen-values $(\mu_1 \leq \mu_2 \leq \cdots \leq \mu_p)$ of the Wishart matrix $\mathbf{H}\mathbf{H}^\dagger$ are known from [67] and are given by,

$$p_{(\mu_1,\ldots,\mu_p)}(\mu_1, \ldots, \mu_p) = k_{n_t,n_r}^{-1} \prod_{i=1}^{m} \mu_i^{|n_t - n_r|} \prod_{i<j} (\mu_i - \mu_j)^2 e^{-\sum_{i=1}^{m} \mu_i}$$

where k_{n_t,n_r} is a normalization constant.

Bibliography

[1] L. Mroueh, "On space time coding design and multiuser multiplexing gain over selective channel," Ph.D. dissertation, Telecom Paristech, December 2009.

[2] M. Jar and G. Fettweis, "Throughput maximization for LTE uplink via resource allocation," in *proceedings of IEEE International Symposium on Wireless Communication Systems (ISWCS)*, 2012, pp. 146–150.

[3] *Evolved Universal Terrestrial Radio Access (E-UTRA); Base Station (BS) radio transmission and reception (Release 11)*, 3GPP TS 36.104, V11.5.0 Std., July 2013.

[4] *IEEE 802.20 Working Group on Mobile Broadband Wireless Access, Proposed Text for the SCM Evaluation Process*, Std., January 2005.

[5] Y. Okumura, E. Ohmori, and K. Fukuda, "Field strength and its variability in VHF and UHF land-mobile radio service," *Review of the Electrical communication Laboratory*, pp. 825–873, 1968.

[6] A. Papoulis and S. U. Pillai, *Probability, Random Variables and Stochastic Processes.* McGraw-Hill, 2002.

[7] A. Marazzi and C. Ruffieux, "The truncated mean of an asymmetric distribution," *Computational Statistics & Data Analysis*, vol. 32, pp. 79–100, 1999.

[8] M. S. Kumar, "Median as a weighted arithmetic mean of all sample observations," *proceedings of Economics Bulletin*, vol. 3, pp. 1–6, 2004.

[9] *Evolved Universal Terrestrial Radio Access (E-UTRA); User Equipment (UE) radio transmission and reception*, 3GPP TS 36.101, V10.3.0 Std., June 2011.

[10] I. Wong, O. Oteri, and W. Mccoy, "Optimal resource allocation in uplink SC-FDMA systems," *IEEE Transaction on Wireless Communications*, vol. 8, no. 5, pp. 2161 –2165, May 2009.

[11] S.-B. Lee, L. Pefkianakis, A. Meyerson, S. Xu, and S. Lu, "Proportional fair frequency-domain packet scheduling for 3gpp LTE uplink," in *UCLA TR-090001*, 2009.

[12] L. Á. M. R. de Temiño, G. Berardinelli, S. Frattasi, and P. E. Mogensen, "Channel-aware scheduling algorithms for SC-FDMA in LTE uplink," in *Proceedings of IEEE Personal, Indoor and Mobile Radio Communications (PIMRC)*, 2008.

[13] M. Al-Rawi, R. Jantti, J. Torsner, and M. Sagfors, "Opportunistic uplink scheduling for 3G LTE systems," in *proceedings of Innovations in Information Technology*, 2007.

[14] C. Wengerter, J. Ohlhorst, and A. von Elbwart, "Fairness and throughput analysis for generalized proportional fair frequency scheduling in OFDMA," in *proceedings of IEEE Vehicular Technology Conference (VTC)*, vol. 3, Stockholm, Sweden, 2005.

[15] *Requirements for Evolved UTRA (E-UTRA) and Evolved UTRAN (E-UTRAN)*, 3GPP TR 25.913, V9.0.0 Std., December 2009.

[16] *3GPP System Architecture Evolution: Report on Technical Options and Conclusions*, 3GPP TR 23.882, V8.0.0 Std., September 2008.

[17] M. Salah, "Comparative performance study of LTE uplink schedulers," Master's thesis, Queen's University, Ontario, Canada, April 2011.

[18] F. Shamshad, U. Javed, S. Saleem, and Q. ul Islam, "Physical layer aspects of 3GPP's Long Term Evolution (LTE)," *Advances in Computer Science and its Applications (ACSA)*, vol. 2, no. 1, pp. 287 –294, 2012.

[19] F. Khan, *LTE for 4G Mobile Broadband- Air Interface Technologies and Performance*. Cambridge University Press, 2009.

[20] IXIA, "SC-FDMA Single Carrier FDMA in LTE," IXIA, November 2009.

[21] X. Lagrange, "Principe de la transmission OFDM- utilisation dans les systèmes cellulaires," Techniques de l'ingénieur, Mai 2012.

[22] H. G. Myung and D. Goodman, *Single Carrier FDMA: A New Air Interface for Long Term Evolution*. Wiley, 2008.

[23] S. Sesia, I. Toufik, and M. Baker, *LTE - The UMTS Long Term Evolution: From Theory to Practice*, 2nd ed. Wiley, 2011.

[24] *Evolved Universal Terrestrial Radio Access (E-UTRA); Physical channels and modulation*, 3GPP TS 36.211, V8.6.0 Std., March 2009.

[25] 3GPP, "Carrier Aggregation explained," 3GPP. [Online]. Available: http://www.3gpp.org/technologies/keywords-acronyms/101-carrier-aggregation-explained

[26] *IEEE Standard for Local and Metropolitan area networks part 16: Air Interface for Fixed Broadband Wireless Access Systems*, IEEE Std 802.16-2001, Std., March 2001.

[27] T.-T. Tran, Y. Shin, and O.-S. Shin, "Overview of enabling technologies for 3GPP LTE-advanced," *EURASIP Journal on Wireless Communications and Networking*, vol. 2012, no. 1, p. 54, 2012. [Online]. Available: http://jwcn.eurasipjournals.com/content/2012/1/54

[28] S. Tripathi, V. Kulkarni, and A. kuma, "LTE E-UTRAN and its access side protocols," Radisys, September 2011.

[29] *Policy and Charging Control Architecture*, 3GPP TR 23.203 Std., March 2010.

[30] *Evolved Universal Terrestrial Radio Access (E-UTRA) and Evolved Universal Terrestrial Radio Access Network (E-UTRAN); Overall description; Stage 2*, 3GPP TS 36.300 Std., December 2010.

[31] IXIA, "Quality of Service (QoS) and policy management in mobile data networks, validating service quality to ensure subscriber Quality of Experience (QoE)," IXIA, july 2011.

[32] *Technical Specification Group Radio Access Network; User Equipment (UE) radio transmission and reception (TDD)*, 3GPP TS 25.102, V9.1.0 Std., March 2010.

[33] L. Song and J. Shen, *Evolved Cellular Network Planning and Optimization for UMTS and LTE*. Taylor & Francis Group, 2011.

[34] K. Ramadas and R. Jain, "Wimax system evaluation methodology," *Technical report*, January 2007.

[35] C. Lengoumbi, "Modélision d'un canal large bande," Telecom Paristech intern repport, 2005.

[36] D. Tse and P. Viswanath, *Fundamentals of Wireless Communication*. Upper Saddle River, NJ, USA: Cambridge University Press, 2005.

[37] E. Telatar, "Capacity of multi-antenna gaussian channels," *European Transactions on Telecommunications*, vol. 10, no. 6, pp. 585–595, 1999.

[38] H. ElSawy, E. Hossain, and M. Haenggi, "Stochastic geometry for modeling, analysis, and design of multi-tier and cognitive cellular wireless networks: A Survey," *IEEE Communications Surveys Tutorials*, vol. 15, no. 3, pp. 996–1019, 2013.

[39] F. Baccelli, M. Klein, M. Lebourges, and S. Zuyev, "Stochastic geometry and architecture of communication networks," *Telecommunication Systems*, vol. 7, pp. 209–227, 1995.

[40] F. Baccelli, B. Blaszczyszyn, and P. Muhlethaler, "An aloha protocol for multihop mobile wireless networks information theory," *IEEE Transactions on Information Theory*, vol. 52, no. 2, pp. 421–436, 2006.

[41] ——, "Stochastic analysis of spatial and opportunistic aloha," *IEEE JSAC, special issue on Stochastic Geometry and Random Graphs for Wireless Networks*, vol. 27, no. 7, pp. 1105 – 1119, September 2009.

[42] F. Baccelli and B. Blaszczyszyn, "A new phase transition for local delays in MANETs," *IEEE INFOCOM*, 2010.

[43] B. Blaszczyszyn and P. Muhlethaler, "Stochastic analysis of non-slotted aloha in wireless Ad-Hoc networks," in *IEEE INFOCOM*, San Diego, USA, 2010, pp. 1 – 9.

[44] A. Hunter, J. Andrews, and S. P. Weber, "Capacity scaling of Ad-Hoc networks with spatial diversity," in *proceedings of IEEE International Symposium on Information Theory (ISIT)*, 2007, pp. 1446–1450.

[45] T. T. Vu, "Spartial models for cellular network planning," Ph.D. dissertation, Telecom Paristech, 2012.

[46] P. Robert, *Statistic networks and queues*. Springer-Verlag, Berlin and Heidelberg GmbH & C, 2003.

[47] L. Wu, "A new modified logarithmic Sobolev inequality for Poisson point processes and several applications," *Probability Theory and Related Fields*, vol. 118, no. 3, pp. 427–438, 2000.

[48] C. Houdré and N. Privault, "Concentration and deviation inequalities in infinite dimensions via covariance representations," *Bernoulli*, pp. 697–720, 2002.

[49] L. Decreusefond, E. Ferraz, P. Martins, and T. T. Vu, "Robust methods for LTE and WiMAX dimensioning," in *Performance Evaluation Methodologies and Tools (VALUETOOLS), 2012 6th International Conference on*, Oct 2012, pp. 74–82.

[50] J. Heyman, "Intercell interference management in an OFDM-based downlink," Ph.D. dissertation, Linköpings universitet, 2006.

[51] Alcatel, "OFDM with interference control for improved HSDPA coverage," 3GPP TSG-RAN WG1 N37, R1-040572, 2004.

[52] D. Gang, Z. Ting, and Z. P. X. Ning, "A dowlink radio resource allocation algorithm based on inter-cell interference mitigation for multi-cell OFDMA system," in *proceedings of Communication and Networking in China*, Beijing, China, 2006.

[53] M. Pischella and J.-C. Belfiore, "Optimal power allocation for downlink cooperative cellular networks," in *proceedings of IEEE Vehicular Technology Conference (VTC)*, April 2007, pp. 2864–2868.

[54] J. Lafuente-Martinez, A. Hernandez-Solana, I. Guio, and A. Valdovinos, "Radio resource strategies for uplink inter-cell interference fluctuation reduction in SC-FDMA cellular systems," in *proceedings of IEEE Wireless Communications and Networking Conference (WCNC)*, March 2011, pp. 185–190.

[55] L. Cao, L. Zhong, H. Lei, Y. Wang, Y. Chang, and D. Yang, "Uplink power control for an SC-FDMA mobile cellular system," in *proceedings of IEEE Vehicular Technology Conference (VTC)*, September 2008, pp. 1 –5.

[56] F. Calabrese, M. Anas, C. Rosa, P. Mogensen, and K. Pedersen, "Performance of a radio resource allocation algorithm for UTRAN LTE uplink," in *proceedings of IEEE Vehicular Technology Conference (VTC)*, April 2007, pp. 2895–2899.

[57] Nortel, "Adaptive fractional frequency reuse," 3GPP TSG-RAN WG1 N44bis, R1-060905, 2006.

[58] D. Liang, S. Zhu, W. Liu, and W. Wang, "A frequency reuse partitioning scheme with successive interference cancellation for OFDMA uplink transmission," in *proceedings of IEEE Personal, Indoor and Mobile Radio Communications (PIMRC)*, 2009, pp. 1362–1366.

[59] A. Simonsson and A. Furuskar, "Uplink power control in LTE - overview and performance, subtitle: Principles and benefits of utilizing rather than compensating for SINR variations," in *proceedings of IEEE Vehicular Technology Conference (VTC)*, 2008, pp. 1–5.

[60] M. Maqbool, M. Coupechoux, and P. Godlewski, "Comparison of various frequency reuse patterns for WiMAX networks with adaptive beamforming," in *proceedings of IEEE Vehicular Technology Conference (VTC)*, 2008, pp. 2582–2586.

[61] S. Coleri, M. Ergen, A. Puri, and A. Bahai, "Channel estimation techniques based on pilot arrangement in OFDM systems," *proceedings of IEEE Transactions on Broadcasting*, vol. 48, no. 3, pp. 223–229, September 2002.

[62] S. Yameogo, J. Palicot, and L. Cariou, "Mobile radio channels' estimation for SC-FDMA systems by means of adequate noise and inter-carrier interference filtering in a transformed domain," in *proceedings of IEEE GLOBECOM Workshops*, December 2010, pp. 1302–1306.

[63] I. Viering, A. Klein, M. Ivrlac, M. Castaneda, and J. Nossek, "On uplink intercell interference in a cellular system," in *proceedings of IEEE International Conference onCommunications (ICC)*, vol. 5, June 2006, pp. 2095–2100.

[64] S. Elayoubi and O. Ben Haddada, "Uplink intercell interference and capacity in 3G LTE systems," in *proceedings of IEEE International Conference on Networks (ICON)*, november 2007, pp. 537–541.

[65] H. Tabassum, F. Yilmaz, Z. Dawy, and M.-S. Alouini, "A framework for uplink intercell interference modeling with channel-based scheduling," *IEEE Transactions on Wireless Communications*, vol. 12, pp. 206–217, 2013.

[66] L. Decreusefond, E. Ferraz, and P. Martins, "Upper bound of loss probability for the dimensioning of OFDMA systems with multi class randomly located users," in *proceedings of Workshop on Spatial Stochastic Models for Wireless Networks (SPASWIN)*, Seoul, South Korea, June 2009.

[67] J. Muirhead, *Aspects of Multivariate Statistical Theory*. John Wiley & Sons Inc, 1982.

[68] e Mobility European Technology Platform, *proceedings of International Workshop on Green Wireless 2008 (W-GREEN)*, September 2008. [Online]. Available: http://www.cwc.oulu.fi/workshops/W-Green2008.pdf

[69] Ericsson, *Ericsson Press Release*, June 2008. [Online]. Available: http://www.ericsson.com/ericsson/press

[70] H. G. Myung, "Single carrier orthogonal multiple access technique for broadband wireless communications," Ph.D. dissertation, Polytechnic university, 2007.

[71] A. Joseph, "Energy harvesting projects," *IEEE transaction on Pervasive Computing*, vol. 4, no. 1, pp. 69–71, 2005.

[72] A. Lioumpas and A. Alexiou, "Uplink scheduling for Machine-to-Machine communications in LTE-based cellular systems," in *proceedings of IEEE GLOBECOM Workshops*, 2011, pp. 353–357.

[73] S. Fowler, "Study on power saving based on radio frame in LTE wireless communication system using DRX," in *proceedings of IEEE GLOBECOM Workshops*, 2011, pp. 1062–1066.

[74] F. I. Sokmen and T. Girici, "Uplink resource allocation algorithms for Single-Carrier FDMA systems," in *Wireless Conference*, 2010, pp. 339–345.

[75] M. Canales, J. Gallego, and R. Ciria, "Distributed channel allocation and power control in cognitive radio networks using game theory," in *proceedings of IEEE Vehicular Technology Conference (VTC Fall)*, September 2011, pp. 1 –5.

[76] O. Delgado and B. Jaumard, "Scheduling and resource allocation for multiclass services in LTE uplink systems," in *proceedings of IEEE Wireless and Mobile Computing, Networking and Communications (WiMob)*, October 2010, pp. 355 –360.

[77] J.-H. Noh and S.-J. Oh, "Distributed SC-FDMA resource allocation algorithm based on the hungarian method," in *proceedings of IEEE Vehicular Technology Conference (VTC)*, Anchorage, Alaska, USA, September 2009.

[78] O. Nwamadi, X. Zhu, and A. Nandi, "Dynamic subcarrier allocation for single carrier-FDMA systems," in *proceedings of European Signal Processing Conference (EUSIPCO)*, Lausanne, Switzerland, August 2008.

[79] A. L. Stolyar, "On the asymptotic optimality of the gradient scheduling algorithm for multiuser throughput allocation," *Operations Research*, vol. 53, no. 1, pp. 12–25, 2005.

[80] M. Jar and G. Fettweis, "Throughput maximization for LTE uplink via resource allocation," in *proceedings of IEEE International Symposium on Wireless Communication Systems (ISWCS)*, August 2012.

[81] R. Sedgewick and P. Flajolet, *An introduction to the analysis of algorithms.* Addison-Wesley-Longman, 1996.

[82] MATLAB, "bintprog: optimization toolbox," Help MATLAB, 2008. [Online]. Available: http://203.64.187.42/98-sum/LP-98-SUM/matlab-bintprog.pdf

[83] V. T. Paschos, *Concepts of Combinatorial Optimization.* Wiley, August 2010.

[84] Y. Hara, L. Brunel, and K. Oshima, "Spatial scheduling with interference cancellation in multiuser MIMO systems," vol. 57, no. 9, pp. 893–905, March 2008.

[85] Y. Zhang, C. Ji, Y. Liu, W. Malik, D. Brien, and D. Edwards, "A low complexity scheduling algorithm for uplink MU-MIMO systems," vol. 7, no. 7, pp. 2486–2491, July 2008.

[86] D. Tse, P. Viswanath, and L. Zheng, "Diversity-multiplexing tradeoff in multiple access channels," no. 2, pp. 1859–1874, September 2004.

[87] E. Viterbo and J. Boutros, "A universal lattice code decoder for fading channels," vol. 45, no. 5, 1999, pp. 1639–1642.

[88] E. Agrell, T. Eriksson, A. Vardy, and K. Zeger, "Closest point search in lattices," *IEEE Transactions on Information Theory*, vol. 48, no. 8, pp. 2201–2214, 2002.

[89] J. C. Belfiore, G. Rekaya, and E. Viterbo, "The golden code: a 2×2 full-rate space-time code with non-vanishing determinants," vol. 51, no. 4, pp. 1432–1436, April 2005.

[90] T. Cover and J. A. Thomas, *Elements of Information Theory, 2nd Edition.* John Wiley & Sons, 2006.

[91] J. Lee and N. Jindal, "High SNR analysis for MIMO broadcast channels: Dirty paper coding versus linear precoding," vol. 53, no. 2, pp. 4787–4792, December 2007.

[92] S. Alamouti, "A simple transmit diversity technique for wireless communications," vol. 16, no. 8, pp. 1451–1458, October 1998.

[93] M. Damen, K. Abed-Meraim, and J. Belfiore, "Diagonal algebraic space-time block codes," vol. 48, no. 3, pp. 628–636, March 2002.

[94] T. Yoo, N. Jindal, and A. Goldsmith, "Multi-antenna downlink channels with limited feedback and user selection," vol. 25, no. 7, pp. 1478–1491, September 2007.